Carla Sofia Pinheiro Vitorino

LIPID NANOPARTICLES AND PERMEATION ENHANCEMENT FOR TRANSDERMAL DRUG DELIVERY

Tese de Doutoramento na área científica de Farmácia, especialidade de Tecnologia Farmacêutica
e apresentada à Faculdade de Farmácia da Universidade de Coimbra.

2013

UNIVERSIDADE DE COIMBRA

Lipid nanoparticles and permeation enhancement for transdermal drug delivery

Carla Sofia Pinheiro Vitorino

Faculdade de Farmácia, Universidade de Coimbra, 2013

Tese apresentada à Universidade de Coimbra para apreciação nas provas de Doutoramento em Farmácia, especialidade de Tecnologia Farmacêutica

Trabalho desenvolvido sob orientação científica do Professor Doutor João José Martins Simões de Sousa do Laboratório de Tecnologia Farmacêutica da Faculdade de Farmácia da Universidade de Coimbra e do Professor Doutor Alberto António Caria Canelas Pais do Departamento de Química da Faculdade de Ciências e Tecnologia da Universidade de Coimbra.

Acknowledgements

I would also like to direct a special thanks to my colleagues and friends from Department of Chemistry, Andreia Jorge, Carmen Móran, Filipe Antunes, João Almeida, Luís Alves, Sandra Nunes, Tânia Firmino, and Telma Encarnação, for the fruitful discussions and scientific contribution, allied to the good moments shared. I express a special thanks to my lab colleagues and my friends from FFUC, Ana Fortuna, Ana Santos, Ana Serralheiro, Amélia Vieira, Carla Varela, Daniela Gonçalves, Dulce Bento, Fátima Pina, Filipa Lebre, Ivo Múrias, Joana Almeida, Marisa Gaspar, Marlene Lopes, Raquel Teixeira, Rita Figueiras, Sandra Jesus, Sérgio Silva, Susana Simões, for the great moments we have shared, including all the "scientific" seminars, their support and collaboration throughout this journey. To my lab colleagues of FFUL Professor Ana Matos, Giuliana Manchini, Joana Marto, Rui Lopes, Sara Raposo, thank you for friendship during the times spent in the FFUL.

Finally, I thank my parents, brother and sister-in-law for their love, patience, support and for instilling in me confidence and a drive for pursuing strength to conclude this step of my life.

"A ciência será sempre um busca e jamais uma descoberta.

É uma viagem, nunca uma chegada."

Karl Popper

Table of contents

Chapter 1

General introduction

Chapter 2

Methods for lipid nanoparticles production, characterization and optimization

Chapter 3

Optimization of solid lipid nanoparticles by solvent emulsification-evaporation

Chapter 4

Optimization of co-encapsulating nanostructured lipid carriers by high pressure homogenization: *in vitro, in silico* **and cellular viability approaches**

Chapter 5

Development and validation of a rapid reversed-phase HPLC method for the simultaneous analysis of olanzapine and simvastatin in nanostructured lipid carriers

Chapter 6

Nanostructured lipid carriers characterization based on physicochemical, rheological and mechanical properties

Chapter 7

Passive and active strategies for transdermal delivery using co-encapsulating nanostructured lipid carriers: *in vitro vs. in vivo* studies

Chapter 8

Concluding remarks

Appendix 1

Method revalidation

Method validation for the determination of olanzapine and simvastatin in rat plasma by liquid chromatography - tandem mass spectrometry (LC-MS/MS)

Abbreviations & Symbols

AFM   Atomic force microscopy

AL   Area per lipid

CLSM Confocal laser scanning microscopy

DL   Drug loading

DLS   Dynamic light scattering

DPPC Dipalmitoylphosphatidylcholine

EE   Entrapment efficiency

EMA   European Medicines Agency

ESI   Electrospray ionization interface

FDA   US Food and Drug Administration

GRAS Generally regarded as safe

HLQ   High limit of quantification

HPLC High performance liquid chromatography

ICH   International Conference on Harmonization

IS   Internal standard

LB   Lamellar bodies

LC-MS/MS   Liquid chromatography tandem mass spectrometry

LD   Limit of detection

LLOQ Lower limit of quantification

LQ   Limit of quantification

MD   Molecular dynamics

MP   Mercury porosimetry

MRM   Multiple-reaction monitoring

msd   Mean square displacement

MTT   3-(4,5-dimethylthiazol-2-yl)-2,5-diphenyltetrazolium bromide

NLC   Nanostructured lipid carriers

OL   Olanzapine

PI   Polydispersity index

QC	Quality control
rdf	Radial distribution function
RSD	Relative standard deviation
SB	Stratum basale
SC	Stratum corneum
Scd	Deuterium order parameter
SEM	Scanning electron microscopy
SG	Stratum granulosum
SL	Stratum lucidum
SLN	Solid lipid nanoparticles
SS	Stratum spinosum
SV	Simvastatin
SVA	Simvastatin acid
TDDS	Transdermal drug delivery system
TEM	Transmission electron microscopy
TEWL	Transepidermal water loss
TPA	Texture profile analysis
VE	Viable epidermis
ZP	Zeta potential

Abstract

The main challenge in transdermal drug delivery is to overcome the barrier of the stratum corneum (SC), the outermost layer of the skin. Many approaches have been used to enhance the penetration of drugs through this layer, covering passive and active methods or the combination of both. This work aimed at developing a transdermal delivery system for the simultaneous administration of olanzapine and simvastatin.

In order to fulfill the main goal, the potential combination of lipid nanoparticles and chemical enhancers was addressed, in what concerns passive strategies. Additionally, the active microneedle-mediated delivery of nanoparticles into the skin was investigated as an alternative to potentiate drug transport. Lipid nanoparticles, comprising solid lipid nanoparticles (SLN) and nanostructured lipid carriers (NLC) were prepared by the solvent emulsification-evaporation (SE/E) and high pressure homogenization (HPH) methods. Full factorial designs, 2^k, were conducted to rationalize and optimize formulation composition, production conditions and application. The combined effect of lipid nanoparticles and chemical enhancers was investigated by *in vitro*, *in silico* and cellular viability methodologies. The formulations were assessed in a joint *in vitro*/*in vivo* approach.

As a result of the reduced solubility of olanzapine in the solid lipid, tripalmitin, NLC were selected for co-encapsulation. For NLC production, the HPH technique was chosen, since it allowed a higher drug loading, a more sustained release, better permeation rate, in conjunction with the ability to scale up, avoidance of organic solvents and shorter production times.

The *in vitro* skin experiments showed that the external medium in the NLC dispersion strongly influenced permeation. Olanzapine exhibited a higher permeation than simvastatin. Moreover, it was also seen that the use of NLC determined a synergistic effect with the selected permeation enhancers, ethanol and limonene, thus promoting marked flux enhancement ratios, relative to the drugs in solution. The further gelation of the formulation led to a reduction roughly by half in the flow rate. A correlation between enhancer positioning in a lipid bilayer and enhancement effect was suggested from both molecular dynamics studies and experimental results.

The study of the interaction of limonene, ethanol and Carbopol Ultrez® 10NF as gelling agent with the NLC dispersion covering rheological, mechanical and physicochemical properties, suggested that the developed formulation was suitable for transdermal administration. Additionally, the optimal formulation was not considered irritant.

As a proof-of-concept of the above findings, *in vivo* transdermal administration to rats were conducted, which resulted in steady-state levels reached after 10 h and maintained for 48 h. The NLC dispersions displayed a better *in vivo* performance than hydrogels, which was consistent with the *in vitro* results. These differences were, however, negligible in the flux values, supporting the use of hydrogel as final, more convenient, formulation. Skin perforation promoted by the microneedles device only slightly increased the permeation rate. This emphasized that the formulation itself determined the main driving force for skin permeation.

Overall, these findings highlight the NLC-based formulations as promising for the development of a clinical transdermal system, covering an innovative therapeutic approach.

Resumo

O principal desafio na administração transdérmica de fármacos consiste em transpor a camada córnea, a mais externa da pele.

Têm sido desenvolvidas diferentes estratégias para promover a penetração de fármacos através desta barreira, as quais incluem métodos passivos, activos ou uma combinação de ambos. O presente trabalho teve como objectivo o desenvolvimento de um sistema transdérmico para a administração simultânea de olanzapina e sinvastatina.

De forma a atingir este objectivo, foi abordada como estratégia passiva a combinação de nanopartículas lipídicas com promotores químicos de penetração. Por seu lado, a administração de nanopartículas recorrendo a microagulhas enquanto método activo foi avaliada como estratégia alternativa para potenciar o transporte de fármacos através da pele.

As nanopartículas lipídicas, compreendendo as nanopartículas lipídicas sólidas (SLN) e os transportadores lipídicos nanoestruturados (NLC), foram preparadas pelos métodos de emulsificação-evaporação do solvente (SE/E) e homogeneização a alta pressão (HPH). Recorreu-se a planeamentos factoriais, do tipo 2^k, para racionalizar e optimizar a composição das formulações, condições de produção e respectiva aplicação. O efeito combinado das nanopartículas lipídicas e promotores químicos foi investigado recorrendo a metodologias *in vitro*, *in silico* e estudos de viabilidade celular. As formulações foram adicionalmente avaliadas numa abordagem combinada *in vitro*/*in vivo*.

Como resultado da reduzida solubilidade da olanzapina no lípido sólido, tripalmitina, foram utilizadas NLC para a co-encapsulação. A técnica HPH a quente foi seleccionada para a produção das NLC, uma vez que permitiu uma maior capacidade de carga de fármaco, uma libertação mais sustentada, uma melhor permeação, evitar o recurso a solventes orgânicos e tempos de produção mais curtos, apresentando também a possibilidade de transposição de escala.

Os ensaios *in vitro* demonstraram que o meio externo da dispersão NLC influenciou marcadamente a permeação. Verificou-se também um efeito sinérgico entre as NLC e os promotores químicos seleccionados, etanol e limoneno, evidenciado pelas acentuadas razões

de permeação, em comparação com soluções de referência. A olanzapina apresentou uma permeação superior à sinvastatina, resultados que foram confirmados nos ensaios *in vivo* referidos mais adiante. A posterior gelificação do sistema levou a uma redução para cerca de metade nos fluxos de permeação. As simulações de dinâmica molecular e os resultados experimentais permitiram estabelecer uma correlação entre o posicionamento dos promotores químicos (terpenos) numa bicamada lipídica e o seu efeito de intensificação na permeação. O estudo da interacção entre o limoneno, o etanol e o Carbopol Ultrez ® 10NF, como gelificante, com a dispersão de NLC, abrangendo as propriedades reológicas, mecânicas e físico-químicas, sugeriu que a formulação desenvolvida era adequada para administração transdérmica. Verificou-se, também, não ser irritante.

Para a avaliação da eficácia do conceito acima desenvolvido, foram conduzidos ensaios *in vivo* em ratos, cuja administração transdérmica permitiu atingir o estado estacionário após 10 horas, mantendo-o durante 48 h. As dispersões de NLC caracterizaram-se por um melhor desempenho, *in vivo,* comparativamente aos hidrogéis, em concordância com os resultados *in vitro*. Estas diferenças foram, no entanto, mitigadas nos valores de fluxo, justificando a utilização de hidrogel como formulação final. A perfuração da pele promovida pelo dispositivo de microagulhas apenas aumentou ligeiramente a velocidade de permeação. Estes resultados corroboraram que a formulação, por si só, constitui a principal força motriz para a permeação de fármacos através da pele.

Em geral, estes resultados indicam as formulações baseadas em NLC como promissoras para o desenvolvimento de um sistema transdérmico clínico, abrangendo uma abordagem terapêutica inovadora.

Palavras-chave Coencapsulação, nanopartículas lipídicas sólidas, transportadores lipídicos nanoestruturados, planeamento factorial, promotores de permeação, dinâmica molecular, farmacocinética, administração transdérmica

Chapter 1

General introduction

1.1 Scope

Over time, the skin has become an important route for drug delivery encompassing topical, regional or systemic effects. The present work focuses on the pharmaceutical development of a transdermal drug delivery system (TDDS), i.e., a product intended to deliver a drug through the skin in order to attain the bloodstream. The advantages of transdermal delivery include providing a noninvasive, painless and convenient means of drug administration, avoidance of possible infection and compliance issues related to injections, steadier and sustained drug levels over a prolonged period of time, reduced side effects associated with peaks and troughs in drug plasma concentration, avoidance of the liver first-pass metabolism and other variables associated with the GI tract (pH, gastric emptying), as such providing an alternative route when oral dosing is not possible (unconscious or nauseated patients), and the ease of dose termination when adverse effects occurs [1].

Nevertheless, the skin constitutes an excellent natural barrier, which limits the number of drugs able to cross its external layer, the stratum corneum, in sufficient quantities to reach a therapeutic plasma concentration. This explains why ca. 30 years since the approval by FDA of the first transdermal patch, the Alza's Transderm Scop® (scopolamine) to treat motion sickness, only approximately 20 drugs or drug combinations have been marketed in the United States and European Union [2].

In Portugal, there are currently 39 different presentations of TDDS approved, spanning 14 molecules [3], which represents an annual turnover of about 52.4 million

euros, or about 1% in unit and 2.7% in value of the total ambulatory market (Figure 1.1) [4].
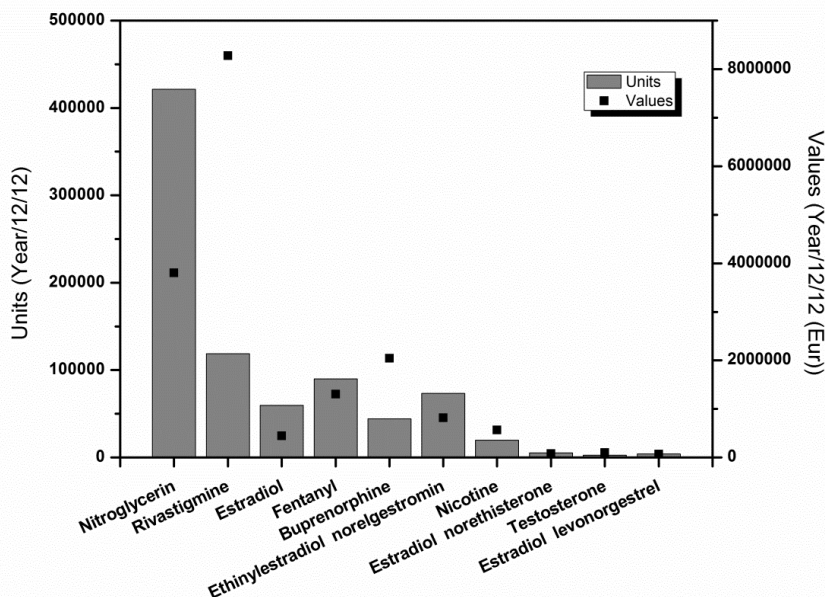
Figure 1.1 Transdermal market trends in Portugal, reporting IMS Health data in value and units, from MAT December, 2012 [4].

Taking into account the TDDS market, for the period between May 2011 and May 2012 the brand (original) medicines occupied a market share of 93,5% and the generics 6,5% (in value). Considering the previous period, between May 2010 and May 2011, the market share values suffered no change, which may indicate that this TDDS market is relatively stable and protected from the entry of generics [5].

Facing a declining output from innovative pharmaceutical research, before starting the development process of a new product, a careful analysis of the market is crucial in order to identify relevant needs. Thus, a problem must first be identified for which a solution with a discernible benefit can be found.

The above market trends indicate that TDDS are limited to some drugs/therapeutic areas, such as nitroglycerin for cardiovascular disorders, rivastigmine for Alzheimer's disease, fentanyl for pain management, estradiol and testosterone for hormone replacement, ethinylestradiol/norelgestromin for female contraception and nicotine for smoking cessation.

We have explored a new therapeutic area, the antipsychotic market, where non-compliance represents a crucial issue that affects most therapeutics, and selected olanzapine as a model drug, with the purpose of combining improvement over an existing therapy, and providing a solution to a problem with an existing drug [6].

Olanzapine belongs to a class of second generation derivative antipsychotic agents, the so-called atypical antipsychotics. Atypical antipsychotics have greater affinity for

serotonin 5-HT2A receptors than for dopamine D2 receptors, causing fewer extrapyramidal symptoms and improving negative symptoms in contrast to classical antipsychotics, such as haloperidol [7]. Olanzapine is indicated for the treatment of schizophrenia and moderate to severe manic episodes. In patients whose manic episodes have responded to olanzapine treatment, it is indicated for the prevention of recurrence in patients with bipolar disorder [8]. It should be noted that schizophrenia affects about 24 million people worldwide, presenting a high prevalence due to chronicity [9]. Currently, olanzapine is administered orally or by injection, being commercially available in tablet and intramuscular form, administered once daily. Thus, a potential benefit of transdermal administration of olanzapine is the improvement of patient compliance, in particular for this population, which is known for having problems with adherence to medication. It should be stressed that poor compliance is the leading cause for relapse and re-hospitalization among schizophrenia patients [6]. Despite the effective benefits as a therapeutic antipsychotic, the long-term use of olanzapine has been limited by its substantial, un-wanted effects on metabolism that result in weight gain and increase in insulin resistance and lipid metabolism [10]. The alterations in the lipid profile can contribute to the increase in cardiovascular mortality that has been observed among patients with schizophrenia since the availability of the atypical antipsychotic medications [11-14]. Besides, metabolic syndrome and other cardiovascular risk factors are also highly prevalent in people with schizophrenia, which are attributable in part to the unhealthy lifestyle, including poor diet and sedentary behavior [15].

All these aspects support the association with simvastatin, belonging to the class of statins, in order to prevent dyslipidemia and cardiovascular risk [16, 17]. Additionally, co-administration of two drugs to treat chronic conditions further reinforces compliance problems, in particular if transdermally delivered. Naturally, to be addressed for transdermal administration, both drugs should also gather adequate physicochemical and pharmacokinetic properties, which will be discussed below in this chapter.

The administration of both drugs was based on a nanoparticulate system that allowed co-encapsulation. The enhancement of drug transdermal absorption was further explored in an innovative combination of different passive and active methodologies.

The system uses thus nanotechnology to address a therapeutic issue, increasing the value of the co-encapsulated drugs in a clearly differentiated approach.

1.2 Skin

1.2.1 Function

The skin is the largest organ of the human body, covering about 1.7 m^2 and accounting for more than 10% of the total body mass of an average person [1, 18].

Numerous functions have been attributed to the skin. As the human integument, it establishes the interface between body and external environment, ensuring a protective barrier against chemical, mechanical, microbial, physical, and ultraviolet (UV) radiation injuries, and preventing the loss of moisture and body nutrients [18-20]. Besides limiting the entrance of xenobiotics, it constitutes a physical barrier for the penetration of microorganisms. The production of the "acid mantle" (pH~5) by the sebaceous and sweat glands, the presence of a thin film on the skin surface comprised of sebum, corneocyte debris and residual material from sweat, the low surface water content, the resident microflora, and surface-deposited antimicrobial lipids contribute additionally to the antimicrobial protection [21, 22].

The skin also serves important metabolic, immunological and sensorial functions. It has an important role in the metabolism of melanin, vitamin D, lipids, collagen and keratin. Additionally, it presents immunological activity, as it contains Langerhans cells [23, 24]. The skin also provides sensory information, such as pressure, pain and temperature, since it encloses nerve endings and receptors [18].

Furthermore, its role in assuring the homeostasis of the body should be stressed, not only in terms of the maintenance of the respective composition and excretory functions, but also in blood pressure control and thermoregulation [18, 24].

1.2.2 Structure

To properly assess and rationalize the ability of a drug to be delivered transdermally, an understanding of the fundamental aspects of skin anatomy and physiology is of crucial importance and will be firstly discussed in this chapter.

Essentially, the skin consists of four layers: the stratum corneum (nonviable epidermis), the remaining layers of the epidermis (viable epidermis), dermis, and subcutaneous tissues (hypodermis). A number of appendages are also associated with the skin, comprising hair follicles, apocrine and eccrine sweat glands, and nails (Figure 1.2) [24].
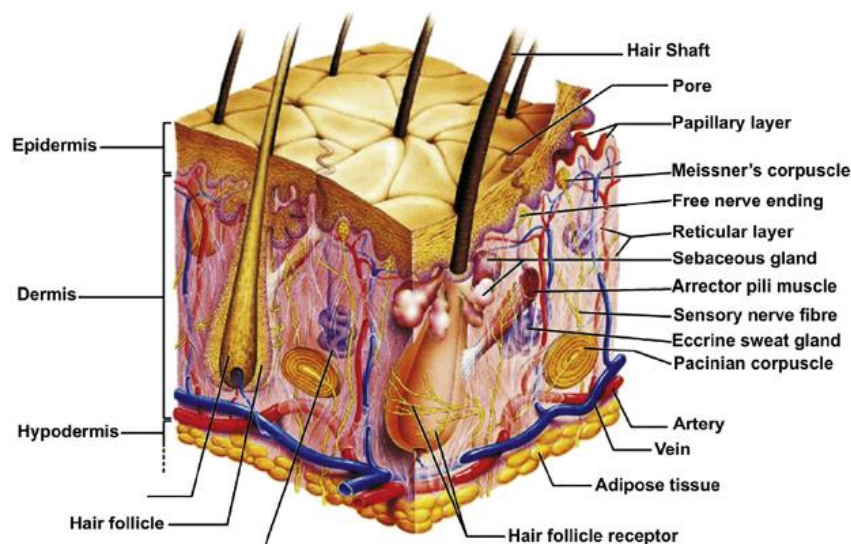
Figure 1.2 Schematic representation of the skin layers and appendage. From reference [25].

Although the large surface area would indicate that the skin is as a suitable pathway for drug delivery, from a permeation point of view skin represents a challenge due to its outermost layer, the SC, which determines the formidable barrier described above. The qualification for this is the unique physicochemical composition and architecture of the SC. Therefore, the structure of this layer will be discussed in more detail. The other layers and appendages present important functions, constituting target sites for drug delivery.

Epidermis

The epidermis is a dynamic multilayered region, with a thickness ranging from ca. 0.06 mm on the eyelids to 0.8 mm on the soles of the feet and on the palms of the hands [18]. The epidermis is avascular, composed by keratinocytes (95% of cells) that undergoes constant proliferation, differentiation, and keratinization, being responsible for the constant physiological renewal of the skin. Each layer is known to represent a different level of cellular or epidermal differentiation [1]. Thus, the structure and composition of the keratinocytes change during their migration from the stratum basale, through the stratum spinosum, stratum granulosum, and the stratum lucidum up to the outermost SC. During their maturation process, keratinocytes synthesize and express numerous different protein and lipids [26]. On reaching the SC, cells become enucleated (corneocytes) and flattened, being usually referred as nonviable epidermis, in contradistinction to the lower epidermal layers (viable epidermis) [18, 27]. Interspersed among the keratinocytes in the viable epidermis, another population   exists (accounting

for the remaining 5% [28] of cells), but do not participate in the process of keratinization. These include the melanocytes, Merkel cells (tactile epithelioid cells), and Langerhans cells (intraepidermal macrophages) [29]. In addition to the structured cellular components of skin, various skin appendages, such as hair, sweat and sebaceous glands exist as specializations of the epidermis. The epidermis also possesses many enzymes capable of metabolizing topically applied compounds, which are also involved in the physiological keratinocyte maturation and desquamation process, formation of natural moisturizing factor (NMF) and general homeostasis [23, 30, 31].

The stratum basale (SB), also referred as the stratum germinativum or basal layer, is a single layer of columnar cells, presenting a high nucleo-cytoplasmic ratio, attached to the basement membrane via hemidesmosomes (proteinaceous anchors). Desmosomes interconnect the keratin of adjacent and overlying cells, thereby ensuring the structural integrity of the skin. It is the only layer of the epidermis composed of keratinocytes able to undergo cell division (stem cells) [32]. It also contains the melanocytes, Langerhans cells, and Merkel cells.

Melanocytes are dendritic cells that synthesize melanin, a high molecular weight polymer that provide the pigmentation of the skin, hair, and eyes. Melanin is packaged in subcellular organelles, called melanosomes and transported to the neighboring basal keratinocytes [28]. The main function of melanin is to afford protection of the skin by absorbing potentially harmful UV radiation, thus minimizing the liberation of free-radicals in the basal layer [18].

Langerhans are bone marrow-derived dendritic cells and the major antigen presenting cells in the skin [28]. They are activated by the binding of antigen to the cell surface, then migrating from the epidermis to the dermis and on to the regional lymph nodes, where they sensitize T cells to generate an immunological response [18].

Merkel cells are associated with the nerve endings and are concentrated in the touch-sensitive sites of the body, such as the fingertips and lips, being associated to sensorial perception [18, 22, 33].

The stratum spinosum (SS) is composed of two to six rows of keratinocytes immediately above the basal layer. Their morphology changes from columnar to polygonal, and possess an enlarged cytoplasm containing a higher number of keratin filaments (tonofilaments) and organelles when compared with the SB. Beyond the typical cell organelles observed in SB, the presence of Odland bodies, lipid-enriched lamellar bodies (LB) is also evident in this layer. The increase in protein and lipid synthesis denotes the dual aspect of epidermal differentiation [18, 32]

The stratum granulosum (SG), also known as granular layer is composed by keratinocytes at a different level of differentiation. They contain intracellular keratohyalin

granules, composed by keratin, as well as profillagrin, loricrin and a cysteine-rich protein. The fillagrin subunits of profillagrin are important as matrix molecules to promote the aggregation and alignment of the keratin filaments [32]. The rise in the protein synthesis is accompanied by an increased lipogenesis, as evidenced by the large numbers of LB, which are believed to be the precursors of the intercellular lipid lamellae of the SC [34]. The LB also contain hydrolytic enzymes, such as the SC chymotryptic enzyme, a serine protease which has been associated with the desquamation process [35]. As the cells ascend in the SG, the LB are extruded to the intercellular domains (Figure 1.3) [18].
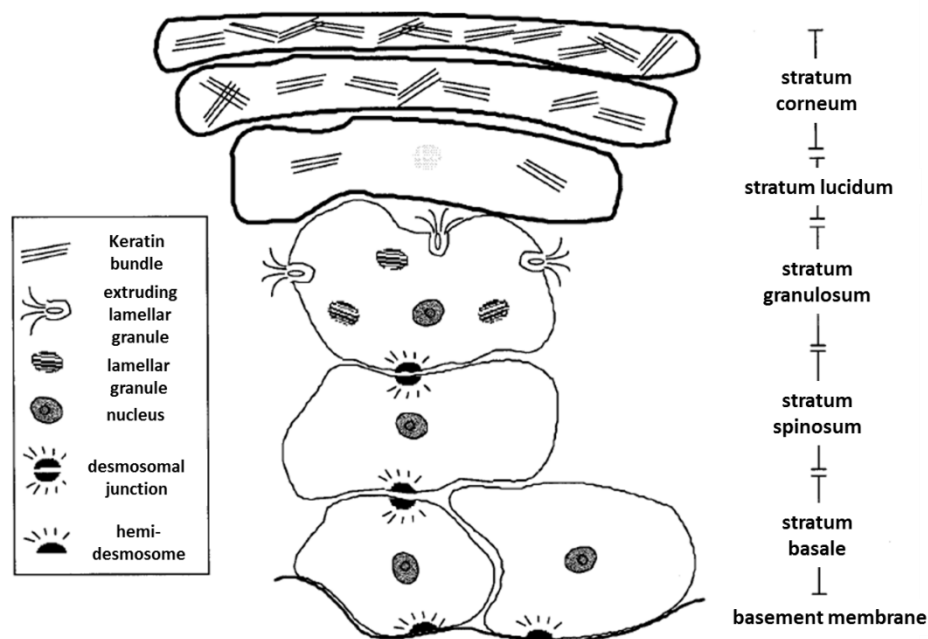
Figure 1.3 Schematic representation of epidermal differentiation. Major events include extrusion of lamellar bodies, loss of nucleus, and increasing amount of keratin in the stratum corneum. From reference [24].

In the stratum lucidum (SL), a layer present in the palms and soles where the skin is particularly thick, the cell nucleus and other organelles disintegrate, keratinization increases, and cells become flattened and compact [18].

Stratum corneum: a key role

The stratum corneum, also known as horny layer, is the outermost layer of the skin, consisting of 10-15 cells in depth, which corresponds to 10-20 μm cell layers of high density (1.4 g/cm^3 in the dry state) with low hydration (10-20% in comparison to ca. 70% in viable epidermis). The SC has been described as a brick wall-like structure, in which the corneocytes represent the "bricks", embedding in a "mortar" of the intercellular lipids,

interlinked by desmosomes (Figure 1.4a) [36]. The corneocytes are flat and elongated cells, usually up to 50 µm in length and 1.5 µm thick, devoid of nucleus, and composed of about 70-80% keratin and 20% lipid within a cornified cell envelope (~10 nm thick) [18]. The cornified cell envelope is a protein/lipid polymer structure formed just below the cytoplasmic membrane, surrounding the exterior of the corneocytes. It consists of two parts: a protein envelope and a lipid envelope (Figure 1.4b). The protein envelope is thought to contribute to the biomechanical properties (e.g., impact resistance) of the cornified envelope, as a result of the cross-linking of specialized structural proteins, mainly involucrin and loricrin, by both disulfide bonds and N-(γ-glutamyl) lysine isopeptide bonds formed by transaminases [37].
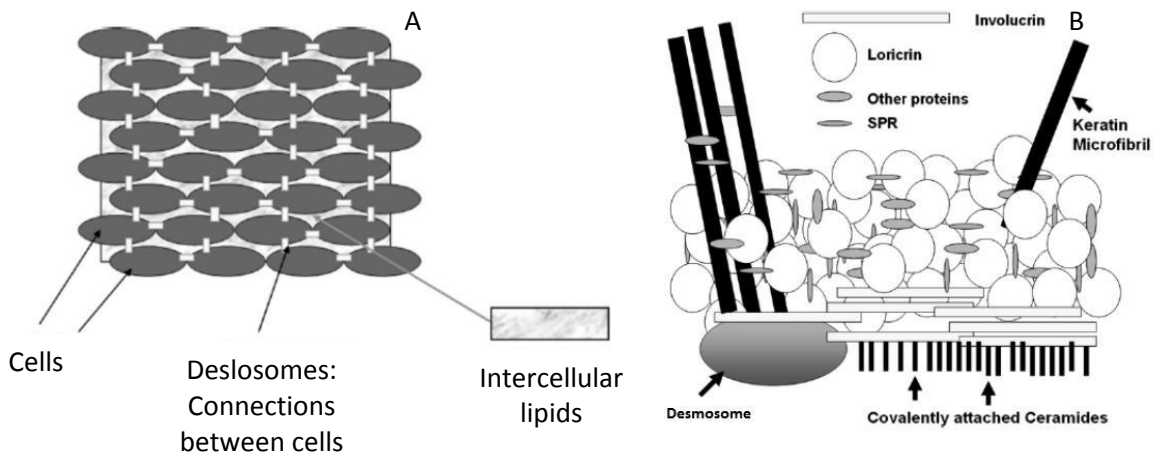
Figure 1.4 Schematic representation of (A) the "bricks and mortar" model for human stratum corneum, with the corneocyte "bricks", the intercellular lipid "mortar", and the corneodesmosomes connecting the corneocytes, and (B) the corneocyte envelope. From reference [38].

The lipid envelope comprises ω-hydroxyceramides covalently bound to the protein matrix of the cornified envelope [39, 40]. There are indications that it is essential in the assembly of the intercellular lipid lamellae, thus providing the structure and barrier function of the SC [41].

The unique composition of the SC intercellular lipids and their particular organization as multiple stacked membrane layers within a continuous lipid domain is critical to the permeability barrier function of the SC. The major components of the lipid domains are ceramides, cholesterol, free fatty acids, cholesterol esters, and cholesterol sulfate, whose contents vary between individuals and with the anatomical site [18, 42, 43]. Ceramides, the most abundant lipids in SC, consist of a sphingoid base (sphingosine, dihydrosphingosine, phytosphingosine, or 6-hydroxy-sphingosine), linked via an amide bond to a fatty acid (nonhydroxy, α-hydroxy, or ester-linked ω-hydroxy) [44]. Both

variations in the fatty acid carbon chain and the sphingoid base architecture result in a large number of ceramide subclasses, with a wide variation in chain length distribution, as depicted in Figure 1.5.
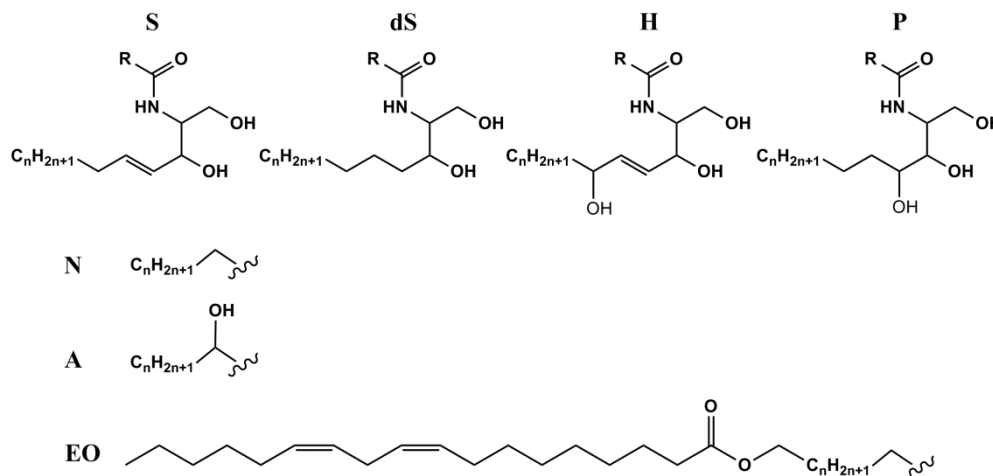
Figure 1.5 Ceramides structure. Four possible sphingosine related chains (S, sphingosine; dS, dihydrosphingosine; H, 6-hydroxysphingosine; P, phyto-sphingosine) are linked via an amide bond to either of three different fatty acid, R (N, nonhydroxy fatty acid; A, α-hydroxy fatty acid; EO, esterified ω-hydroxy fatty acid) resulting in 12 different ceramides subclasses [44].

Another important lipid class in stratum corneum is cholesterol, the second most abundant, which is crucial for promoting the intermixing of different lipid species [32]. On the other hand, cholesterol sulfate, in spite of being present in small amounts (typically 2–5% w/w), plays an important role in the SC desquamation process [26, 45].

Free fatty acids have also been identified among the intercellular lipid, and consist of long chain saturated free fatty acids, especially lignoceric acid (C24) and hexacosanoic acid (C26), and trace amounts of very long-chain (C32-C36) saturated and monounsaturated free fatty acids [46].

Hitherto, several models for the structural organization of lipids have been suggested. These include the "sandwich model" proposed by Bouwstra et al, in which a long periodicity phase, consisting of three regions (a central liquid crystalline layer surrounded by two crystalline gel phases in an orthorhombic arrangement on both sides) was identified [47] or the 'single gel phase' model propounded by Norlén [48], which suggests a lipid arrangement in a single coherent gel phase with no boundaries. However, there is no consensus about the existence of a single, general, model for lipid packing.

Thus, the impermeable character of the cornified envelope, together with the highly structured lipid lamellae that are oriented parallel to the corneocyte cells, defines a very densely packed structure in the SC, important to consider as main barrier for drug penetration.

Dermis

Beneath the epidermis, separated by a thin basement membrane, is the dermis, a layer of about 2-5 mm in thickness, composed of dense irregular connective tissue. It consists of collagen fibrils that provide support, and elastic connective tissue that ensures elasticity and flexibility, embedded in an amorphous ground substance of mucopolysaccharides. Predominant cell types of the dermis are fibroblasts, responsible for the synthesis and renewal of the components of the connective tissue, mast cells, and macrophages involved in immune and inflammatory response. As a result of its structure, dermis affords low resistance to drug permeation. Nevertheless, the transport of very lipophilic drugs to the deeper tissues may be compromised, due to the increased hydration degree [18, 23].

It provides a highly vascularized network that ensures the removal of the permeant molecules from the dermo-epidermal junction to the bloodstream, thus allowing a concentration gradient between the applied formulation on the skin surface and the dermis. Lymph vessels within the dermis can also remove permeated molecules from the skin, which is particularly important in the case of large molecules. Moreover, it plays a crucial role in the physiological temperature maintenance and in tissue nutrition and metabolic changes. It also contains sensory nerves (free nerve endings and end corpuscles), including Pacinian corpuscles that sense vibration and Meissner corpuscles, responsible for tactile and pressure sensations [28].

Besides, a number of appendages are originated within the dermis, such as the hair follicles and associated sebaceous glands, eccrine and apocrine sweat glands.

Hypodermis

Beneath the dermis is a layer of loose connective tissue, commonly known as the hypodermis or subcutaneous tissue. It is composed of lipocytes, arranged into fat lobules with interconnecting collagen and elastin fibers [28]. Its primary functions are protection against physical shock, heat insulation, and energy storage. Blood vessels and nerves are supplied to the skin via the hypodermis. It also aids in binding the skin to the underlying fascia and skeletal muscle [24].

Appendages

The hair follicles are distributed across the entire skin surface with the exception of the soles of the feet, the palms of the hands and the lips, representing a fractional area of about 1/1000 of the total skin surface. The sebaceous gland associated with each hair follicle secretes sebum, which is composed of free fatty acids, triglycerides, and waxes. Sebum ensures protection and lubricates the skin, also maintaining the skin surface at a pH value of about 5. A smooth muscle, the erector pilorum, attaches the follicle to the dermal tissue, enabling hair to respond to fear or cold. Eccrine glands, present a fractional area of about 1 in 10,000 of the total body surface, and secrete sweat in response to exercise, high environmental temperature, as well as emotional stress. The apocrine glands are limited to specific body regions (axillae, nipples, and anogenital area), being about ten times the size of the eccrine glands [18, 24].

1.3 Percutaneous absorption

According to what was mentioned above, the process of drug absorption from a transdermal drug delivery system into the systemic circulation may be regarded as a passage through consecutive skin layers. Thus, it starts with the release of the permeant from the dosage form, followed by penetration into the SC. It diffuses through the lipophilic SC at a rate determined by its diffusivity within this layer, then partitioning to the more aqueous epidermal environment of viable epidermis (VE). Finally, it is absorbed by the capillaries in the dermis, also hydrophilic in nature.

From what was exposed, the first limiting step is the drug partitioning into the SC, which may be, to a certain extent, modulated by the release from the vehicle. On the other hand, all these steps are highly dependent on the solubility and diffusivity of the permeant within each environment. Release of the permeant from the vehicle and uptake into the lipophilic SC is dependent on the relative solubility in each part, and hence the vehicle-SC partition coefficient. In turn, the diffusion coefficient or the speed at which the permeant moves within each environment is dependent on both the permeant properties and factors related to the environment, such as its viscosity and tortuosity, i.e. diffusional path length [18, 49].

Despite of the heterogeneity of the skin barrier, steady-state permeation or flux (J) of a drug through the SC can be simplistically described by Fick's first law of diffusion

$$J = \frac{dQ}{dt} = \frac{DKC_0}{h} \tag{1.1}$$

where Q is the drug amount permeating a certain unit area of skin, D is the diffusion coefficient of the permeant in the skin, K is the partition coefficient between the stratum

corneum and the vehicle, C_0 is the applied concentration of permeant, and h the diffusional path length. The mechanism of drug penetration can be primarily considered driven by passive diffusion and, thus, dependent on the concentration gradient.

1.3.1 Routes of drug penetration

The transport of drug through the skin may be carried out through three potential pathways: sweat ducts, hair follicles and associated sebaceous glands (*transappendageal route*), or across the continuous stratum corneum (*transepidermal route*) (Figure 1.6). In what regards the latter, two particular pathways through intact SC may exist: the intercellular lipid route between the corneocytes (*intercellular*) and the transcellular route through the corneocytes and interleaving lipids (*transcellular*) [50, 51].
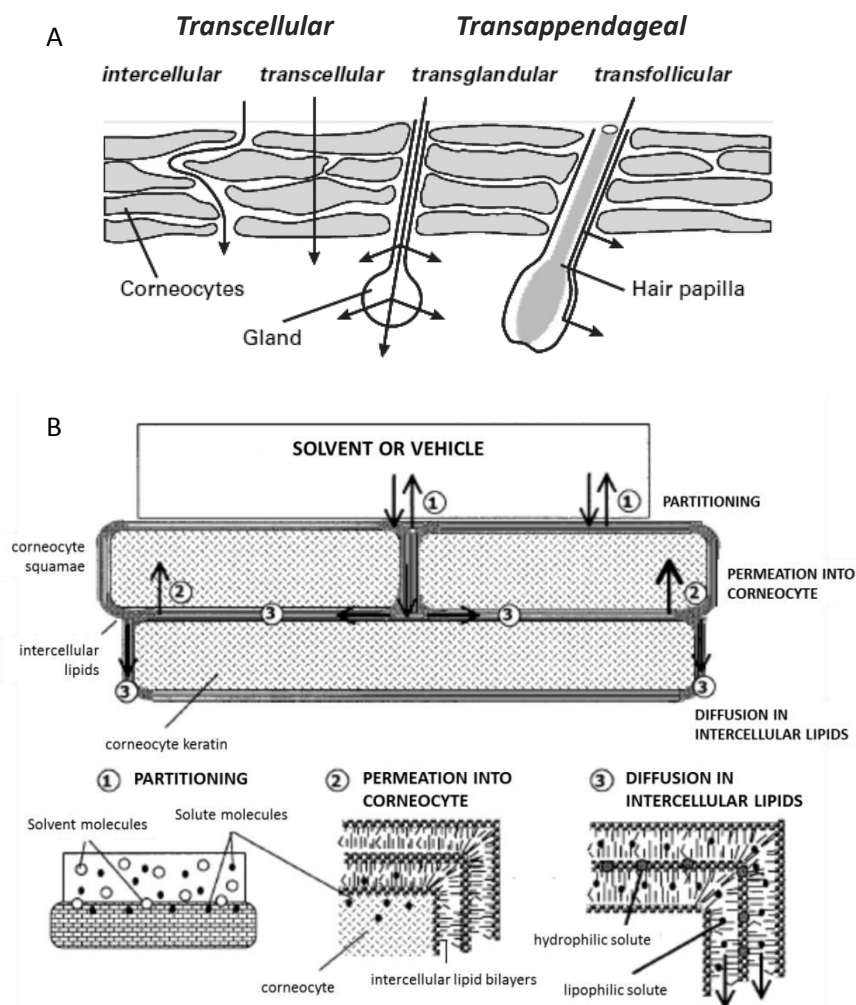
Figure 1.6 (A) Schematic representation of the possible penetration pathways through the SC (from reference [50]); (B) Partitioning and diffusion processes involved in drug penetration through the stratum corneum (from reference [49]).

It should be noted that these pathways are not mutually exclusive, that is, a drug may use more than one penetration route, which will be dependent on its physicochemical properties.

The transcellular route has been regarded as a polar route through the SC, since the corneocytes contain an intracellular keratin matrix that is relatively hydrated and, thus, polar in nature. Therefore, permeation requires consecutive partitioning between this polar environment and the lipophilic domains involving the corneocytes [18, 49]. This a preferential route for hydrophilic compounds, despite the need of the permeant to cross the intercellular lipids, in order to jump from one corneocyte to another [52].

Although this is the more direct route, the transport is predominantly carried out by the intercellular route, which provides the only continuous route through the SC [50]. In this case, the diffusional path length is much longer than the simple thickness of the SC (10-15 µm), since the intercellular domains are highly tortuous, and may be in excess of 150 µm. Within intercellular spaces, a diffusing molecule has to cross a variety of lipophilic (via lipid core) and hydrophilic (via polar head groups) domains of the structured lipids [49, 53].

Despite the appendages (glands and hair follicles) have been considered as low resistance shunts, their contribution was primarily estimated to be small, since they represent only 0.1-1% of the total skin surface area [54]. However, it is suggested that the appendageal route dominates during the lag phase of the diffusional process [18]. In recent years, there has been renewed interest in targeting follicular delivery through colloidal-based formulation approaches [29].

1.4 Factors affecting drug permeation

Physiological factors

Skin permeability may be affected by a large number of physiological factors. This includes age, anatomical site, ethnicity, gender and some skin disorders.

Intrinsic aging leads the epidermis to become thinner and the corneocytes less adherent to one another, although the SC thickness has been shown not to significantly change [55]. It is also reported that the lipid composition suffers alterations with age, with decreased levels of all major lipid species, particularly for ceramides. Additionally, the dermis becomes atrophic and relatively acellular and avascular. The reduced hydration levels and lipid content of ageing skin may be responsible for a demonstrated reduction in skin permeability with hydrophilic compounds [49, 56]. Moreover, the skin barrier

function in young children is significantly reduced, which may lead to an increased permeability [57].

Skin permeability may also vary with anatomical site. Several studies have revealed that distinct anatomic skin sites possess different morphologic and functional characteristics. These regional variations induce skin barrier function alterations in the following order: genitals (more permeable)>head and neck>trunk>arm and leg (less permeable).

Some differences have been reported across ethnic groups, although inconsistent, suggesting that ethnic differences are much less profound than interindividual differences within ethnic groups [43].

Concerning gender, only slight or no differences in the epidermal barrier have been reported as determined by basal transepidermal water loss (TEWL) between male and female skin [18, 58, 59].

The state of the skin (normal, abraded, or diseased) may also influence permeation. A number of common skin disorders, such as eczema (dermatitis), psoriasis, ichthyosis, and acne vulgaris may compromise barrier function. Skin infections that manifest eruptions at the skin surface, e.g. impetigo, *Herpes simplex* and fungal infections can also temporarily reduce the barrier [18, 25].

Properties of the drug

The capacity of a drug to enter the skin depends on its ability to penetrate, consecutively, the hydrophobic and hydrophilic domains of the skin. From Equation (1.1), ideal physicochemical properties of a molecule to penetrate and permeate through the SC can be extracted. These include [51, 60] a high, but balanced partition coefficient (K). Thus, a log P(o/w) comprised between 1 and 3 is pointed as optimal, since drugs that are too hydrophilic are unable to partition from the vehicle into the SC. On the other hand, very lipophilic drugs will be retained in intercellular SC lipids, and will not partition to the more aqueous viable epidermis, thus limiting their skin permeation rate. Additionally, ionized species of a drug has also a lower permeability coefficient than its respective unionized species, as the log P of ionized species is lower [53]. A low molecular weight is also desirable, since the size of the permeant will influence the diffusivity (D) within the SC. An inverse relationship between permeant size and skin permeation has been reported. As a general rule, permeants selected for transdermal delivery tend to be less than 500 Da, when D tends to be high. It should also possess an adequate lipid solubility (high diffusion coefficient, D), but also reasonable aqueous solubility (> 1mg/mL) (high donor concentration, C_v, in order to ensure a high

concentration gradient, the driving force for diffusion) to maximize flux. Finally, a low melting point (<200 °C) is also a good characteristic, since it correlates with good solubility of the drug in the intercellular SC lipid domain.

In addition to these specific physicochemical properties, drug candidates should be characterized by a high therapeutic potency (deliverable dose ideally below 20 mg/day), poor oral bioavailability and short biological half-live, in order to take maximal advantage of a transdermal administration. The drug should also not be irritant to the skin nor stimulate an immune reaction in the skin [61, 62].

Properties of the vehicle

The successful development of a transdermal drug delivery system relies on the application of the skin permeation fundamentals to the design of an appropriate formulation. The latter assumes particular importance, since the vehicle may profoundly influence the drug release mechanism from a formulation (by modulating the vehicle/SC partition coefficient), alter the skin barrier properties (by SC modification/circumvention), or simply promoting an increase of the drug solubility in the SC. The effects upon the SC may range from the interaction with SC intrinsic elements, including the intercellular lipid lamellae and protein components, or promoting SC hydration by an occlusive effect [49, 63]. Methods to enhance skin permeation are discussed in detail below.

1.5   Permeation enhancement

Under normal circumstances, due to barrier properties of the skin, transport from simple vehicles will often be insufficient to achieve therapeutic drug concentrations at the site of action [64]. In order to overcome this limitation, a number of techniques have been developed aiming at increase the range of penetrants and the rate of transdermal delivery. Strategies to achieve penetration enhancement can be categorized as passive and active, ranging from simple occlusion and formulation optimization, to the use of chemical and physical methods or combinations of both (Figure 1.7). These rely on two main approaches: increasing skin permeability and/or providing a driving force acting on drug [25].
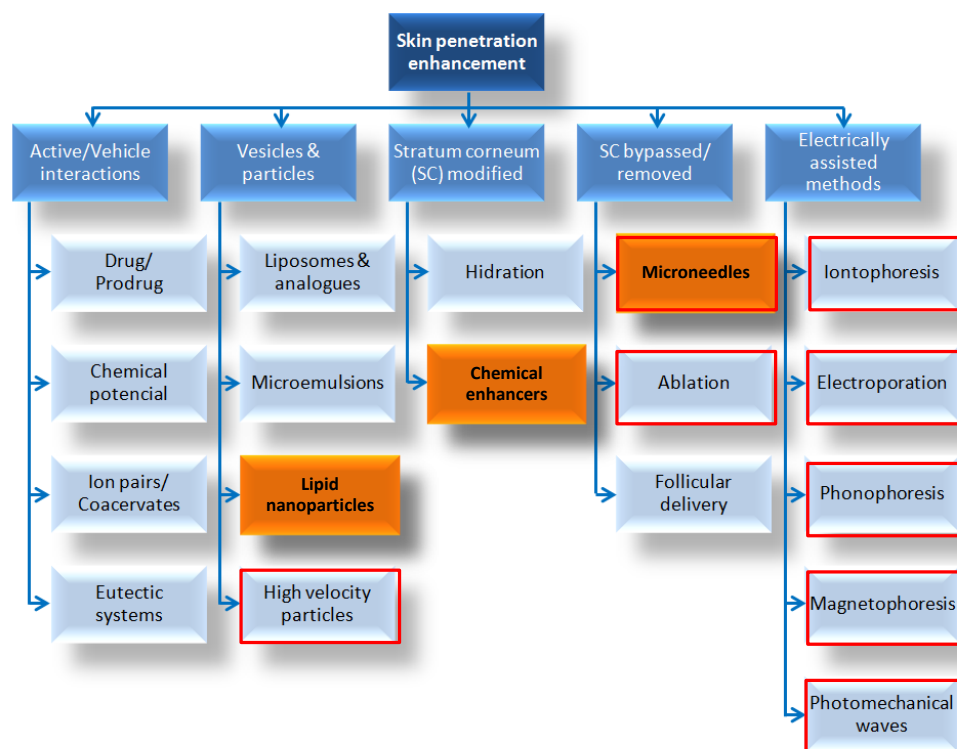
Figure 1.7 Passive and active (indicated by the red solid line) methods to facilitate penetration of drugs through the skin. Adapted from reference [51].   Highlight (orange background) is given to the strategies considered in the present work. The mechanisms by which compounds permeate the skin through these approaches are discussed later in this chapter.

1.5.1 Passive methods

Passive penetration enhancement can be achieved by formulation manipulation, increasing the thermodynamic activity of the drug in formulations (e.g., supersaturated and nanocarrier systems), drug modification, and/or by using chemical penetration enhancers (CPE) that interact with skin constituents to promote drug flux [60].

Supersaturated systems

Supersaturation is a state reached when the amount of drug dissolved in a matrix exceeds its equilibrium solubility. Supersaturated formulations allow an increased driving force by increasing the concentration of the drug in the vehicle. However, since the thermodynamic activity of supersaturated systems is higher than that of saturated systems, they are inherently unstable, thus compromising long-term stability. The use of mixed cosolvent systems (e.g., mixtures of propylene glycol and water), with antinucleant polymers to inhibit or retard crystallization [65], or the induction of *in situ* changes in drug

concentration with solvent evaporation [66] are some of the strategies employed to produce supersaturated systems and avoid stability problems [60, 61].

Drug modification

Other approaches to increase drug delivery through the skin rely on chemical modification of a poorly penetrating drug into a pharmacologically inactive prodrug, which readily penetrates the skin, as a result of the increase in lipophilicity [67].

The ion-pair formation and the use of eutectic mixtures are other examples of drug modification. Ion pairs are defined as neutral species formed only by electrostatic attraction between oppositely charged ions, which exhibit sufficient lipophilicity to dissolve in the SC [60]. The ion pair diffuses subsequently to the aqueous viable epidermis, where dissociation into the charged species occurs, before diffusing onwards [51].

Eutectic mixtures take advantage of a reduction in the melting point of a permeant, which will have a direct effect on its solubility in skin and thus should increase skin permeability [68].

Chemical penetration enhancers

Chemical penetration enhancers (CPE) are pharmacologically inactive compounds that may temporarily diminish the barrier of the skin, by affecting drug partition and diffusion into the skin, thus interacting with the SC constituents [67]. Several substances have been identified as drug penetration enhancers. However, safety issues constitute the major concern that limits their clinical use. Therefore, there is an attempt to identify new CPE that are classified as GRAS (generally recognized as safe). Ideal properties of a chemical enhancer are depicted in Table 1.1.

Table 1.1 Properties of an ideal chemical penetration enhancer [69].

Ideal chemical penetration enhancer
• Pharmacologically inert.
• Nonallergenic, nonirritating, and nontoxic.
• Rapid onset of effect with a predictable duration of activity.
• After removal of the enhancer, the SC should immediately and completely recover its normal barrier property.
• The barrier function of the skin should decrease in one direction only; loss of endogenous materials should not occur.
• Physically and chemically compatible with drugs and excipients in the dosage form; readily incorporated into the delivery system.
• Cosmetically acceptable when applied to the skin.
• Inexpensive, odorless, tasteless, colorless.

CPE are believed to affect permeation via one or more of three main mechanisms, relying on the lipid-protein-partitioning theory of skin penetration enhancement [70]. This concept comprises lipid bilayer interaction (intercellular route), protein modification (intracellular route), and partitioning promotion effects [51]. Therefore, enhancers can [71] modify the intercellular lipid domains, reducing the barrier resistance of the lipid bilayers, and thus, augmenting diffusivity in the SC. Multiple actions are described regarding interaction of the CPE within the intercellular lipid domain (Figure 1.8A).
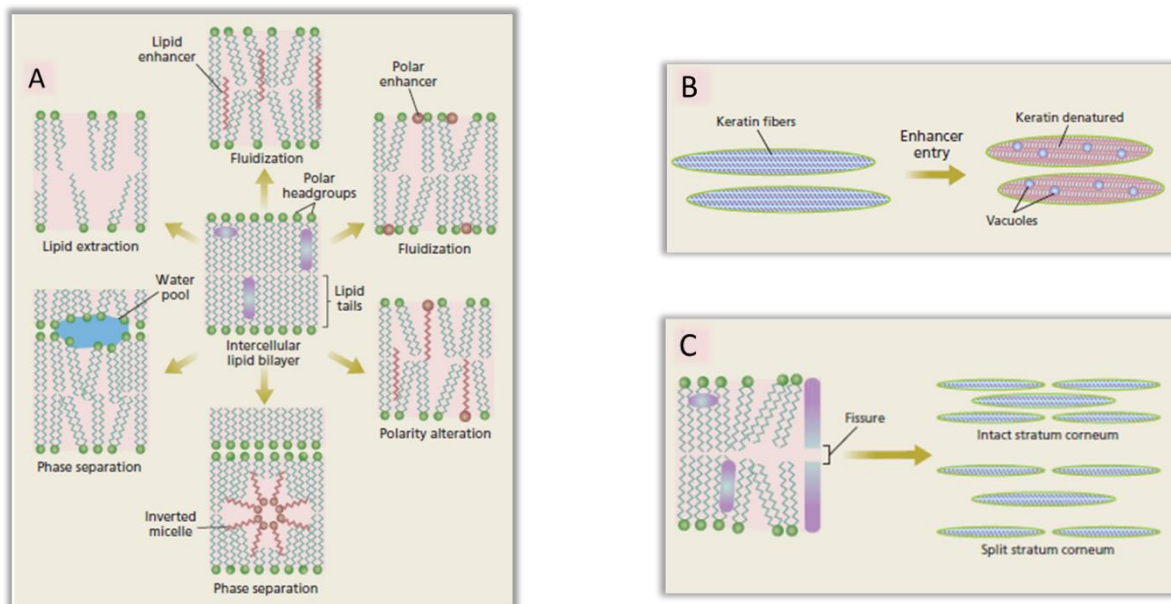
Figure 1.8 Modes of action of CPE with the intercellular lipids (A), desmosomes and protein structures (B), and with corneocytes. From reference [72].

Thus, they may interact with the lipid polar headgroups by establishing H-bonding and/or ionic forces and causing alteration in the hydration spheres of the lipid bilayers, or insert between the hydrophobic lipid tails (e.g. terpenes). As a result, they are able to disturb the lipid packing, thus increasing lipid fluidity and promoting drug permeation. On

the other hand, perturbation in the lipid order may arise when the enhancer forms pools in the skin, as a result of its structure (polar head and long saturated alkyl chain, e.g., oleic acid), allowing the permeant to diffuse faster either through them or through the defects between the pools and the structured lipids [60, 73]. Some CPE may also cause lipid extraction (e.g., ethanol).

They can also act on SC proteins, such as intracellular keratin, causing its denaturation or modification of its conformation, which leads to swelling and increased hydration (Figure 1.8C); or, by interacting with desmosomes, responsible for the maintenance of cohesion between corneocytes (Figure 1.8B).

In some cases, they alter the partitioning of the drug or of a co-solvent into the skin, by promoting modifications in the solvent nature (aqueous domain) of the stratum corneum. Solvents such as propyleneglycol, ethanol, and Transcutol® (diethylene glycol monoethyl ether) are believed to act in this way [74].

CPE may also indirectly increase the thermodynamic activity of the vehicle or promote the solubilization of the permeant in the formulation [71].

Nanocarrier systems

Nanocarrier systems including, liposomes and derivatives, microemulsions, nanoemulsions, polymer and lipid nanoparticles have deserved increasingly attention in the delivery of drugs to the skin. Particular emphasis will be given to lipid nanoparticles.

Lipid nanoparticles

Solid lipid nanoparticles (SLN), considered the first generation of lipid nanoparticles, were introduced in 1991 as an alternative carrier system to emulsions, liposomes and polymeric nanoparticles [75]. SLN are colloidal carriers, with sizes typically ranging from 40 to 1000 nm, derived from o/w emulsions, in which the liquid lipid (oil) was replaced by biodegradable and biocompatible solid lipids (0.1-30% w/w), that is, lipids that are in the solid state at both room and body temperatures, and stabilized by aqueous emulsifiers (0.5-5%) solution. Solid lipids can vary from pure lipids or a mixture of lipid compounds, encompassing triglycerides, partial glycerides, fatty acids, and waxes. On the other hand, the emulsifiers, including a large variety of non-ionic and ionic surfactants, are chosen depending on the administration route, being often used in association, in order to prevent particle agglomeration more efficiently [76].

At the turn of the millennium, a second generation of lipid nanoparticles, consisting of a matrix composed of a blend of solid and liquid lipids (oils), led to the creation of the

concept of nanostructured lipid carriers (NLC) [77]. NLC were introduced to overcome some potential limitations of the SLN, such as low drug loading and drug expulsion during storage [78]. These problems are a consequence of the SLN crystalline matrix (pure solid lipid or a mixture of solid lipids) and of the occurrence of polymorphic transitions, respectively [79-81]. Lipids molecules are known to exhibit polymorphism, that is, presenting different three-dimensional structures (polymorphic forms): unstable α, metastable β′, and as the most stable the β modification [82]. After preparation, at least a part of the lipid particle crystallizes in a higher energy modification (α and β' polymorphic forms). During storage, rearrangement of the crystal lattice might occur evolving to a more thermodynamically stable configuration (β form), which corresponds to a lower free energy state and, consequently, to a highly ordered system, with less imperfections on the crystal lattice of the lipids [83]. This transformation leads to the expulsion of the drug and contributes also to the instability of the system. The drug expulsion as a consequence of the crystallisation process led to the development of NLC, in which the matrix remains solid, but not crystalline [84]. In the NLC, the incorporation of a liquid lipid in the solid matrix creates a less ordered structure. This characteristic makes them able to accommodate higher amounts of drug, which can be located not only between the fatty acid chains and the lipid layers, but also in imperfections of the lipid matrix (Figure 1.9). Additionally, the solubility of the drug in oils is usually higher than in solid lipids [78, 79, 85, 86].
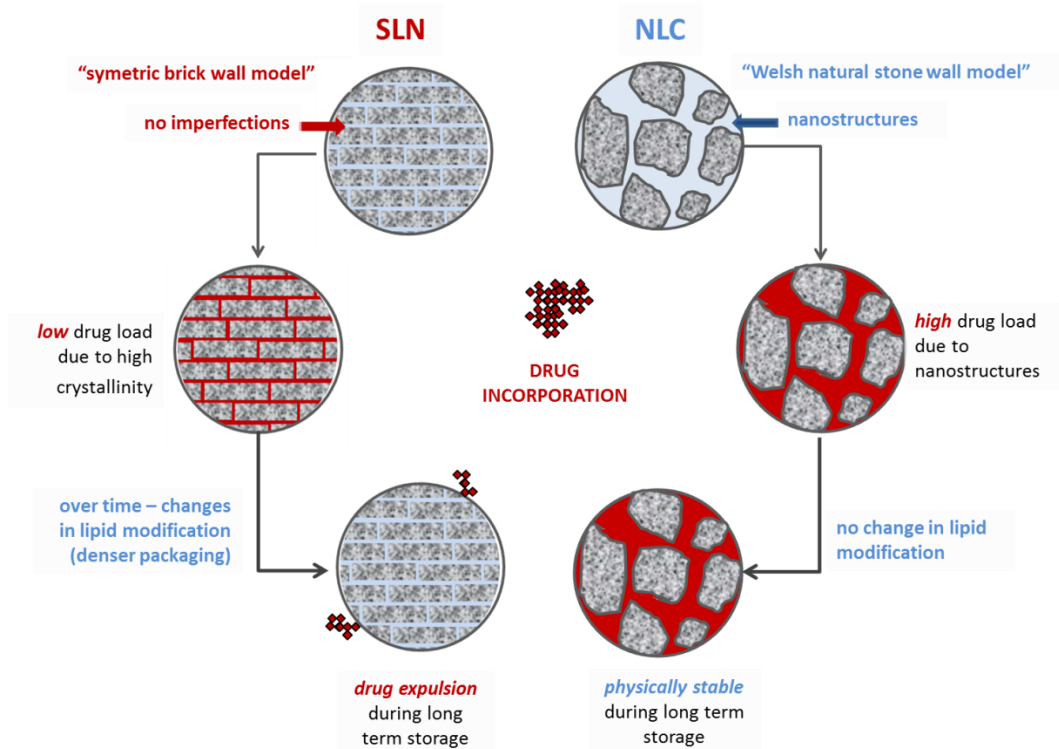
Figure 1.9 Difference between an SLN and NLC lipid matrix structure. Adapted from [87].

Several mechanisms of drug incorporation have been considered for these nanocarriers. For the SLN, three models can be applied: SLN type I or the homogenous matrix of solid solution, in which the drug is molecularly dispersed in the particle matrix, SLN type II or the drug enriched shell and SLN type III or drug enriched core models, where the drug is concentrated in the particle shell and core, respectively. For NLC, also three types are described: NLC type I or the imperfect model, with many imperfections in the matrix which are able to accommodate the drug, being created when small amounts of the liquid lipids are employed, NLC type II or the structureless/amorphous model, which is created when mixing special lipids which avoid the occurrence of crystallization , and NLC type III or the multiple O/F/W model, which is characterized by small oil nanocompartments dispersed in the solid lipid matrix. This can be obtained when the liquid lipids are incorporated in the solid matrix, exceeding the respective solubility. These particles are able to accommodate higher amounts of drug, in particular drugs more soluble in the liquid than in the solid lipids.[82, 84] Thus, either the composition or the method of production contribute to obtain different types/structures of lipid nanocarriers, which therefore result in different performances in terms of drug loading and release.

The nature of lipid nanoparticles confers them distinct advantages over conventional carriers (emulsions, liposomes, and polymer nanoparticles), such as an excellent tolerability, resulting from the generally recognized as safe (GRAS) status of the excipients employed. Thus, there is a reduced danger of acute and chronic toxicity, improved physical stability, protection of incorporated labile drugs from degradation, low cost, possibility to modulate drug release due to the solid nature of the lipid matrix, drug targeting, feasibility of scaling-up, cost-effective production method, and relatively low cost of excipients [80, 86, 88-92]. Moreover, their unique properties such as reduced size, combined with a large surface area and high drug loading are attractive for a potential improvement in the performance of pharmaceuticals, in particular for transdermal delivery [93, 94].

1.6 Active strategies

Active methods involve the use of external energy to act as driving force and/or to reduce the barrier function of the SC, which allows expanding the range of permeants to deliver through the skin. These manipulations include the application of various forms of energy (e.g., heat, electrical, magnetic), or breaching, reducing, or weakening the SC barrier by mechanical means [1]. Focus will be given to electrically assisted and mechanical methods. However, other technologies, such as magnetophoresis, which

involves the application of a magnetic field, to enhance the driving force on a penetrant [95], photomechanical waves [96, 97], or thermal ablation [98] to increase the "permeabilization" of the SC have also been investigated.

Electrical assisted methods

Iontophoresis is a noninvasive method that involves the application of a small electric current to drive ionic molecules across the skin. It is particularly effective for ionic and polar drugs such as peptides, which are very poorly absorbed by the skin under normal conditions [99]. The technology employs the use of two electrodes immersed in a solution containing the drug compound. The application of a potential difference (voltage) across the electrodes results in the motion of drug molecules, in the form of charged ions, which travel from the electrodes into the skin [100]. Transdermal drug transport enhancement by iontophoresis is promoted by three main mechanisms: electrorepulsion of charged solutes by the electrode, electroosmotic effects on unionized, polar species, and permeabilization of the skin by the electric current [61, 99].

Electroporation involves the application of high voltage (>50V) pulses to the skin, lasting for a period in the microsecond-millisecond range, and leading to the creation of aqueous pores or pathways through the SC. The pores formed are small (<10nm), transient (from microseconds to seconds), sparse (0.1% of surface area), and congregated in discrete local transport regions. This technique also expands the range of drugs (small to macromolecules, lipophilic or hydrophilic, charged or neutral molecules) which can be delivered transdermally [99, 101].

Sonophoresis is used to describe enhanced transdermal delivery following application of ultrasound energy to the skin. Low-frequency ultrasound (<100 kHz, usually 20 kHz) is reported to disrupt the lipid bilayer of SC through several phenomena: cavitation, which leads to generation and oscillation of gas bubbles form small hydrophilic channels through the SC, combined with thermal effects (temperature increase), induction of convective transport and mechanical effects (occurrence of stresses due to pressure variation induced by ultrasound) [102]. This technique has been employed in the enhancement of the delivery of drugs, macromolecules, oligonucleotides, DNA and vaccines [103].

Mechanical methods

The microneedles technique uses small micron-sized needles as a mechanical approach to breach the SC, creating microchannels through the skin, so as to deliver a drug at a predetermined depth [104]. Microfabrication techniques have been developed

for silicon, metal, biodegradable polymers, and sugar-based microneedle arrays, having solid and hollow bores with different geometries and sizes. There are four general approaches of transdermal delivery by microneedles: (a) hollow microneedles, whereby a drug in solution is active and passively delivered through the bore of the microneedle ("poke and flow" approach), (b) solid microneedles to pierce the skin, following by application of a patch to diffuse drug through the skin ("poke and patch" approach), (c) biodegradable polymeric microneedles, containing the drug encapsulated (dissolving or porous microneedles), allowing a controlled drug release by dissolution or diffusion from the pores into the skin ("poke and release" approach), and (d) drug coated microneedles, inserting them into the skin for subsequent release through hydration of the coating ("coat and poke" approach) [25, 105]. Microneedles have been used to deliver drugs, proteins, and particles across skin in a simple, painless and minimally invasive manner, since they do not penetrate up to the papillary dermis where nerve endings are located [104]. However, important issues concerning safety and difficulty in self-administration can be pointed as disadvantages, which may delaying the introduction of microneedles in the market [106].

Needleless jet injectors arise as a painless technique, alternative to conventional needle injection, that enable to overcome the SC barrier, in this case by propel powders or liquids at high velocity into skin. It has been particularly employed in the transdermal delivery of proteins and peptides [107].

Other mechanical techniques, such as microdermabrasion or tape stripping may enhance penetration by reducing the thickness of the SC barrier, whereas stretching or flexing can lead to a general weakening of the barrier [99, 108].

Recent combinational techniques

In order to make the transport through the skin more effective, combinations among several strategies have been investigated. This has involved the association of passive with active methods, such as CPE-iontophoresis [109], SLN-iontophoresis [110], CPE-electroporation [111], CPE-sonophoresis [112], and between active technologies, e.g., microneedles-iontophoresis [113], microneedles-sonophoresis [114], microneedles-electroporation [115], or electroporation-iontophoresis [116].

1.7 Development of the transdermal formulation

The development of a transdermal pharmaceutical formulation may range from an aerosol spray, a semisolid or self-adhesive patch (reservoir, matrix, drug-in-adhesive or microreservoir). Whatever the dosage form, important technological concerns must be

undertaken throughout the pharmaceutical development, including compatibility, stability, acceptability, as well the bioavailability in order to ensure the therapeutic outcome. That implies an optimization of the applied formulation focused on the improvement of release and permeation through the skin [74]. Accordingly, the composition of the vehicle and the active substances deserves special emphasis, especially because a close contact with the skin is often accompanied by possible risks of adverse reactions. Furthermore, the lack of precision related to the variability of the amount of drug delivered through the skin as a result of the epidermis thickness, as well as to a possible mechanical removal of the applied formulation must be equated [82]. In order to overcome the above-mentioned issues, better solutions have still to be found.

1.7.1 Drug and formulation strategies

Drug characteristics

Olanzapine (OL), chemically a thienobenzodiazepine described as 2-methyl-4-(4-methyl-1-piperazinyl)-10H-thieno[2,3-b][1,5] benzodiazepine [117] (Figure 1.11a) is a second-generation antipsychotic drug used for the treatment of schizophrenia, bipolar mania and associated agitation [7]. Although it is more effective than other first-line second-generation drugs, the long-term use of olanzapine has been limited by its substantial, un-wanted effects on metabolism that result, among others, in weight gain and development of dyslipidemia, as above referred (it increases the levels of triglycerides and low-density lipoprotein cholesterol, LDL-C, and decreases high-density lipoprotein cholesterol, HDL-C) [10, 118], which leads to an increased cardiovascular risk [11, 119]. This calls for the need of a close monitoring of patients on olanzapine treatment so that, if these adverse events arise, the maintenance of the therapy may be evaluated [120]. In order to mitigate some of these unwanted effects, the treatment with statins, such as simvastatin, might be required [121, 122].

Simvastatin (SV), chemically butanoic acid, 2,2-dimethyl-,1,2,3,7,8,8a-hexahydro-3,7-dimethyl-8-[2-(tetrahydro-4-hydroxy-6-oxo-2H-pyran-2-yl)ethyl]-1-naphthalenyl ester, [1S-[1α,3α,7β,8β(2S*,4S*),8aβ]] [117] (Figure 1.10b), is the lactone prodrug that is hydrolyzed *in vivo*, in the liver and non-hepatic tissues, to the corresponding β-hydroxy acid (simvastatin acid, SVA, Figure 1.10b) [123, 124]. The latter is a potent inhibitor of the enzyme 3-hydroxy-3-methylglutaryl coenzyme A reductase, involved in the cholesterol synthesis. This inhibition is mainly responsible for reducing LDL-C levels, but simvastatin has also been shown to reduce the levels of triglycerides and increase the levels of HDL-C. SV is also reported as effective in the reduction of the morbidity and mortality associated to the coronary heart disease [16].
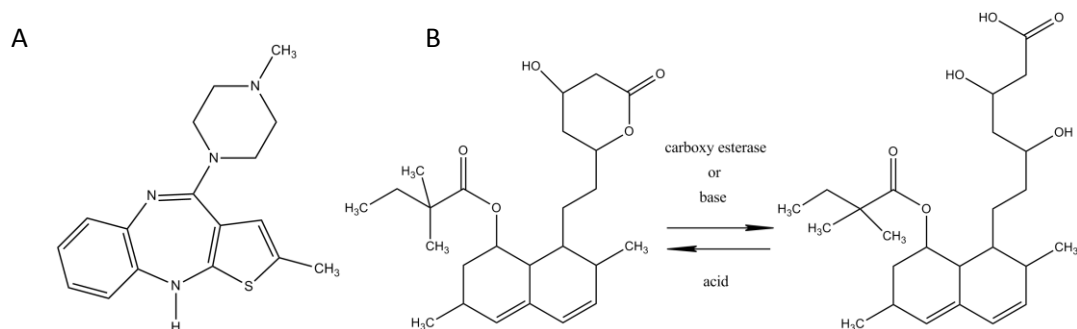
Figure 1.10 Chemical structures of (A) olanzapine and (B) simvastatin (left), the prodrug as inactive lactone form with simvastatin acid (right), the respective active β-hydroxy acid form. Note that simvastatin is rapidly absorbed from the gastrointestinal tract after oral administration, but undergoes extensive first-pass metabolism in the liver, which is responsible for its low oral bioavailability [125].

Lipid nanoparticles for the coencapsulation of OL and SV arise as a promising approach in a transdermal drug delivery system (TDDS). Moreover, the complementarity between the therapeutics and the advantage that clearly results in the improvement of treatment compliance, a reduction in the time of production and the challenge stemming from the simultaneous incorporation of drugs with different lipophilicity into the same colloidal carrier, are also appealing factors from a nanotechnological point of view.

In addition, both drugs gather properties that make them suitable as candidates for transdermal delivery (Table 1.2).

Table 1.2 Physicochemical and pharmacokinetic properties of olanzapine and simvastatin.

Drug	Olanzapine	Simvastatin
Molecular weight	312.433	418.566
Log P/Lipophilicity	2.8[a]	4.7[b]
Aqueous solubility	3–5 µg/mL[c]	30 µg/mL[d]
Melting point	195°C[d]	135-138°C[d]
Daily oral dose	5-10 mg/day[e]	10-40 mg/day[f]
Half-life	33 h[g]	2 h[h]
Bioavailability	60%[g]	5%[h]

[a] Ref. [126], [b] Ref.[127], [c] Ref. [128], [d] Ref. [129], [e] Ref. [130], [f] Ref. [131], [g] Ref. [132], [h] Ref. [125].

Lipid nanoparticles

SLN and NLC as colloidal systems claim several advantages for improving penetration of drugs through the skin. These include their chemical similarity to skin lipids, stemming from the common hydrophobic character, the existence of a solid matrix, and the biocompatibility, which makes these carriers suitable for long-term controlled-release skin administration. Moreover, as a result of the small particle size, a high specific surface area for drug absorption through the skin is made available, thereby providing a larger efficacy as a delivery system [133]. Additionally, the adhesion of lipid nanoparticles to the skin leads to the formation of a film, and subsequently, to an occlusive effect with the reduction in transepidermal water loss [134, 135]. The resulting hydration of the SC could be also related to a reduction of corneocyte packing and a widening of the inter-corneocyte gaps, hence facilitating drug penetration into deeper skin strata (Figure 1.11) [135-137].
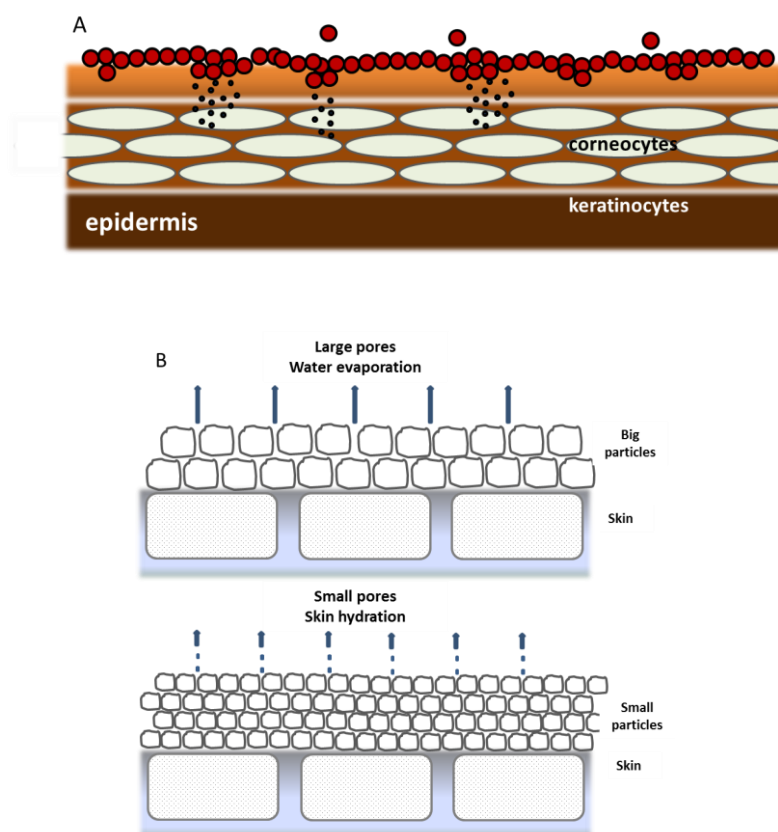
Figure 1.12 Transdermal administration of lipid nanoparticles. (A) When in contact with the skin, lipid nanoparticles create a thin film with very narrow interspaces between the particles. Adapted from [87]. (B) This film hinders water evaporation, leading to an occlusive effect, and subsequently, to increased skin hydration, resulting in drug penetration-increasing effects. Adapted from [82].

Ethanol and terpenes

The use of chemical permeation enhancers has long been shown to increase the diffusivity and/or the solubility of the drugs by reversibly disordering or 'fluidizing' the lipid structure of the SC, thus reducing the barrier resistance of the skin [25, 71, 138]. Bearing this in mind, terpenes and ethanol as co-solvent were subsequently incorporated in a lipid nanoparticles formulation so as to maximize permeation, by combining the occlusive and adhesive properties of the latter with the skin permeability alterations promoted by the chemical enhancers.

Skin perforation

A further alternative that is probed in this work is the perforation of the SC by a microneedle roller device (Dermaroller[®]). Microneedles can transiently create micropathways that help lipid nanoparticles and drugs to bypass the SC, the major rate limiting barrier for transdermal delivery, thus facilitating their permeation into the viable epidermis.[25, 139]

Different approaches are thus sequentially addressed, attempting to assess the respective influence in the simultaneous drugs permeation.

References

1. Brown, M.B., G.P. Martin, S.A. Jones, and F.K. Akomeah, Dermal and Transdermal Drug Delivery Systems: Current and Future Prospects. Drug Delivery, 2006. 13(3): p. 175-187.

2.Watkinson, A.C., Transdermal and Topical Drug Delivery Today, in Transdermal and Topical Drug Delivery2011, John Wiley & Sons, Inc. p. 357-366.

3. Infomed. Available from: http://www.infarmed.pt/infomed/lista.php, accessed on 21/03/2013.

4. IMS Health Data, December 2012.

5. Apifarma – Associação Portuguesa da Indústria Farmacêutica. Relatório "Características do Mercado" Available from: http://www.apifarma.pt/estudos/IndicadoresMF/Paginas/default.aspx, accessed on 10/08/2011.

6. Masand, P.S. and M. Narasimhan, Improving adherence to antipsychotic pharmacotherapy. Curr Clin Pharmacol, 2006. 1(1): p. 47-56.

7. Kantrowitz, J.T. and L. Citrome, Olanzapine: review of safety 2008. Expert Opinion on Drug Safety, 2008. 7(6): p. 761-769.

8. Summary of Product Characteristics. Available from: http://www.ema.europa.eu/ema/index.jsp?curl=pages/medicines/human/medicines/000115/human_med_001189.jsp&mid=WC0b01ac058001d124, accessed on 25/03/2013.

9.   Schizophrenia.   Available   from: http://www.who.int/mental_health/management/schizophrenia/en/, accessed on 04/04/2013.

10. Lieberman, J.A., T.S. Stroup, J.P. McEvoy, M.S. Swartz, R.A. Rosenheck, D.O. Perkins, R.S.E. Keefe, S.M. Davis, C.E. Davis, B.D. Lebowitz, J. Severe, and J.K. Hsiao, Effectiveness of Antipsychotic Drugs in Patients with Chronic Schizophrenia. New England Journal of Medicine, 2005. 353(12): p. 1209-1223.

11. Saha, S., D. Chant, and J. McGrath, A systematic review of mortality in schizophrenia: Is the differential mortality gap worsening over time? Archives of General Psychiatry, 2007. 64(10): p. 1123-1131.

12. Basu, D. and M. Aggarwal, Mortality in patients with schizophrenia. The Lancet, 2009. 374(9701): p. 1591.

13. Healy, D., J. Le Noury, M. Harris, M. Butt, S. Linden, C. Whitaker, L. Zou, and A.P. Roberts, Mortality in schizophrenia and related psychoses: data from two cohorts, 1875–1924 and 1994–2010. BMJ Open, 2012. 2(5).

14. De Hert, M., V. Schreurs, K. Sweers, D. Van Eyck, L. Hanssens, S. Šinko, M. Wampers, A. Scheen, J. Peuskens, and R. van Winkel, Typical and atypical antipsychotics differentially affect long-term incidence rates of the metabolic syndrome in first-episode patients with schizophrenia: A retrospective chart review. Schizophrenia Research, 2008. 101(1–3): p. 295-303.

15. De Hert, M., V. Schreurs, V. Davy, and V.W. Ruud, Metabolic syndrome in people with schizophrenia: a review. World Psychiatry, 2009. 8(1): p. 15-22.

16. Kolovou, G.D., I. Vasiliadis, K. Anagnostopoulou, and D.V. Cokkinos, Simvastatin: Two Decades in a Circle. Cardiovascular Therapeutics, 2008. 26(2): p. 166-178.

17. Pedersen, T.R. and J.A. Tobert, Simvastatin: a review. Expert Opinion on Pharmacotherapy, 2004. 5(12): p. 2583-2596.

18. Benson, H.A.E., Skin Structure, Function, and Permeation, in Transdermal and Topical Drug Delivery2011, John Wiley & Sons, Inc. p. 1-22.

19. Desai, P., R.R. Patlolla, and M. Singh, Interaction of nanoparticles and cell-penetrating peptides with skin for transdermal drug delivery. Molecular Membrane Biology, 2010. 27(7): p. 247-259.

20. Elias, P.M., Stratum corneum defensive functions: an integrated view. J Invest Dermatol, 2005. 125(2): p. 183-200.

21. Elias, P.M., The skin barrier as an innate immune element. Semin Immunopathol, 2007. 29(1): p. 3-14.

22. Chilcott, R.P., Cutaneous Anatomy and Function, in Principles and Practice of Skin Toxicology2008, John Wiley & Sons, Ltd. p. 1-16.

23. Riviere, J.E., Dermal Absorption Models in Toxicology and Pharmacology2005: Taylor & Francis.

24. Kenneth, W. and R. Michael, The Structure and Function of Skin, in Dermatological and Transdermal Formulations2002, Informa Healthcare.

25. Alexander, A., S. Dwivedi, Ajazuddin, T.K. Giri, S. Saraf, S. Saraf, and D.K. Tripathi, Approaches for breaking the barriers of drug permeation through transdermal drug delivery. Journal of Controlled Release, 2012. 164(1): p. 26-40.

26. Bouwstra, J.A. and M. Ponec, The skin barrier in healthy and diseased state. Biochimica et Biophysica Acta (BBA) - Biomembranes, 2006. 1758(12): p. 2080-2095.

27. Madison, K.C., Barrier function of the skin: "la raison d'etre" of the epidermis. J Invest Dermatol, 2003. 121(2): p. 231-41.

28. Lai-Cheong, J.E. and J.A. McGrath, Structure and function of skin, hair and nails. Medicine, 2009. 37(5): p. 223-226.

29. Prow, T.W., J.E. Grice, L.L. Lin, R. Faye, M. Butler, W. Becker, E.M.T. Wurm, C. Yoong, T.A. Robertson, H.P. Soyer, and M.S. Roberts, Nanoparticles and microparticles for skin drug delivery. Advanced Drug Delivery Reviews, 2011. 63(6): p. 470-491.

30. Zeeuwen, P.L.J.M., Epidermal differentiation: The role of proteases and their inhibitors. European Journal of Cell Biology, 2004. 83(11–12): p. 761-773.

31. Hachem, J.P., M.Q. Man, D. Crumrine, Y. Uchida, B.E. Brown, V. Rogiers, D. Roseeuw, K.R. Feingold, and P.M. Elias, Sustained serine proteases activity by prolonged increase in pH leads to degradation of lipid processing enzymes and profound alterations of barrier function and stratum corneum integrity. J Invest Dermatol, 2005. 125(3): p. 510-20.

32. Menon, G.K., New insights into skin structure: scratching the surface. Advanced Drug Delivery Reviews, 2002. 54, Supplement(0): p. S3-S17.

33. Tachibana, T. and T. Nawa, Recent progress in studies on Merkel cell biology. Anatomical Science International, 2002. 77(1): p. 26-33.

34. Landmann, L., The epidermal permeability barrier. Anatomy and Embryology, 1988. 178(1): p. 1-13.

35. Egelrud, T., Purification and preliminary characterization of stratum corneum chymotryptic enzyme: a proteinase that may be involved in desquamation. J Invest Dermatol, 1993. 101(2): p. 200-4.

36. Elias, P.M., Epidermal lipids, barrier function, and desquamation. J Invest Dermatol, 1983. 80: p. 44s-49s.

37. Nemes, Z. and P.M. Steinert, Bricks and mortar of the epidermal barrier. Exp Mol Med, 1999. 31(1): p. 5-19.

38. Wickett, R.R. and M.O. Visscher, Structure and function of the epidermal barrier. American Journal of Infection Control, 2006. 34(10, Supplement): p. S98-S110.

39. Lazo, N.D., J.G. Meine, and D.T. Downing, Lipids are covalently attached to rigid corneocyte protein envelopes existing predominantly as beta-sheets: a solid-state nuclear magnetic resonance study. J Invest Dermatol, 1995. 105(2): p. 296-300.

40. Behne, M., Y. Uchida, T. Seki, P.O. de Montellano, P.M. Elias, and W.M. Holleran, Omega-hydroxyceramides are required for corneocyte lipid envelope (CLE) formation and normal epidermal permeability barrier function. J Invest Dermatol, 2000. 114(1): p. 185-92.

41. Coderch, L., O. Lopez, A. de la Maza, and J.L. Parra, Ceramides and skin function. Am J Clin Dermatol, 2003. 4(2): p. 107-29.

42. Masukawa, Y., H. Narita, E. Shimizu, N. Kondo, Y. Sugai, T. Oba, R. Homma, J. Ishikawa, Y. Takagi, T. Kitahara, Y. Takema, and K. Kita, Characterization of overall ceramide species in human stratum corneum. Journal of Lipid Research, 2008. 49(7): p. 1466-1476.

43. Darlenski, R. and J.W. Fluhr, Influence of skin type, race, sex, and anatomic location on epidermal barrier function. Clinics in Dermatology, 2012. 30(3): p. 269-273.

44. van Smeden, J., L. Hoppel, R. van der Heijden, T. Hankemeier, R.J. Vreeken, and J.A. Bouwstra, LC/MS analysis of stratum corneum lipids: ceramide profiling and discovery. J Lipid Res, 2011. 52(6): p. 1211-21.

45. Sato, J., M. Denda, J. Nakanishi, J. Nomura, and J. Koyama, Cholesterol sulfate inhibits proteases that are involved in desquamation of stratum corneum. J Invest Dermatol, 1998. 111(2): p. 189-93.

46. Norlen, L., I. Nicander, A. Lundsjo, T. Cronholm, and B. Forslind, A new HPLC-based method for the quantitative analysis of inner stratum corneum lipids with special reference to the free fatty acid fraction. Arch Dermatol Res, 1998. 290(9): p. 508-16.

47. Bouwstra, J.A., P.L. Honeywell-Nguyen, G.S. Gooris, and M. Ponec, Structure of the skin barrier and its modulation by vesicular formulations. Progress in Lipid Research, 2003. 42(1): p. 1-36.

48. Norlen, L., Skin barrier structure and function: the single gel phase model. J Invest Dermatol, 2001. 117(4): p. 830-6.

49. Walters, K.A., Dermatological and Transdermal Formulations2002: Taylor & Francis.

50. Trommer, H. and R.H.H. Neubert, Overcoming the Stratum Corneum: The Modulation of Skin Penetration. Skin Pharmacology and Physiology, 2006. 19(2): p. 106-121.

51. Barry, B.W., Novel mechanisms and devices to enable successful transdermal drug delivery. European Journal of Pharmaceutical Sciences, 2001. 14(2): p. 101-114.

52. Bolzinger, M.-A., S. Briançon, J. Pelletier, and Y. Chevalier, Penetration of drugs through skin, a complex rate-controlling membrane. Current Opinion in Colloid & Interface Science, 2012. 17(3): p. 156-165.

53. Hadgraft, J., Skin deep. European Journal of Pharmaceutics and Biopharmaceutics, 2004. 58(2): p. 291-299.

54. Moser, K., K. Kriwet, A. Naik, Y.N. Kalia, and R.H. Guy, Passive skin penetration enhancement and its quantification in vitro. European Journal of Pharmaceutics and Biopharmaceutics, 2001. 52(2): p. 103-112.

55. Batisse, D., R. Bazin, and T. Baldeweck, Influence of age on the wrinkling capacities of skin. Skin Research and Technology, 2002. 8(3): p. 148-154.

56. Roskos, K., H. Maibach, and R. Guy, The effect of aging on percutaneous absorption in man. Journal of Pharmacokinetics and Biopharmaceutics, 1989. 17(6): p. 617-630.

57. Giusti, F., A. Martella, L. Bertoni, and S. Seidenari, Skin Barrier, Hydration, and pH of the Skin of Infants Under 2 Years of Age. Pediatric Dermatology, 2001. 18(2): p. 93-96.

58. Cua, A.B., K.P. Wilhelm, and H.I. Maibach, Frictional properties of human skin: relation to age, sex and anatomical region, stratum corneum hydration and transepidermal water loss. Br J Dermatol, 1990. 123(4): p. 473-9.

59. Tupker, R.A., P.J. Coenraads, J. Pinnagoda, and J.P. Nater, Baseline transepidermal water loss (TEWL) as a prediction of susceptibility to sodium lauryl sulphate. Contact Dermatitis, 1989. 20(4): p. 265-9.

60. Lane, M.E., P. Santos, A.C. Watkinson, and J. Hadgraft, Passive Skin Permeation Enhancement, in Transdermal and Topical Drug Delivery2011, John Wiley & Sons, Inc. p. 23-42.

61. Naik, A., Y.N. Kalia, and R.H. Guy, Transdermal drug delivery: overcoming the skin's barrier function. Pharmaceutical Science & Technology Today, 2000. 3(9): p. 318-326.

62. Finnin, B., K.A. Walters, and T.J. Franz, In Vitro Skin Permeation Methodology, in Transdermal and Topical Drug Delivery2011, John Wiley & Sons, Inc. p. 85-108.

63. Vitorino, C., J. Almeida, L.M. Gonçalves, A.J. Almeida, J.J. Sousa, and A.A.C.C. Pais, Co-encapsulating nanostructured lipid carriers for transdermal application: From experimental design to the molecular detail. Journal of Controlled Release, 2013. 167(3): p. 301-314.

64. Adrian, D., G. Robert, H. Jonathan, P. Mark, and W. Kenneth, Formulation Strategies for Modulating Skin Permeation, in Dermatological and Transdermal Formulations2002, CRC Press.

65. Pellett, M.A., S. Castellano, J. Hadgraft, and A.F. Davis, The penetration of supersaturated solutions of piroxicam across silicone membranes and human skin in vitro. Journal of Controlled Release, 1997. 46(3): p. 205-214.

66. Morgan, T.M., H.M.M. O'Sullivan, B.L. Reed, and B.C. Finnin, Transdermal delivery of estradiol in postmenopausal women with a novel topical aerosol. Journal of Pharmaceutical Sciences, 1998. 87(10): p. 1226-1228.

67. Marjukka Suhonen, T., J. A. Bouwstra, and A. Urtti, Chemical enhancement of percutaneous absorption in relation to stratum corneum structural alterations. Journal of Controlled Release, 1999. 59(2): p. 149-161.

68. Stott, P.W., A.C. Williams, and B.W. Barry, Transdermal delivery from eutectic systems: enhanced permeation of a model drug, ibuprofen. Journal of Controlled Release, 1998. 50(1–3): p. 297-308.

69. Finnin, B.C. and T.M. Morgan, Transdermal penetration enhancers: Applications, limitations, and potential. Journal of Pharmaceutical Sciences, 1999. 88(10): p. 955-958.

70. Barry, B.W., Lipid-Protein-Partitioning theory of skin penetration enhancement. Journal of Controlled Release, 1991. 15(3): p. 237-248.

71. Williams, A.C. and B.W. Barry, Penetration enhancers. Advanced Drug Delivery Reviews, 2004. 56(5): p. 603-618.

72. Barry, B.W., Breaching the skin's barrier to drugs. Nature Biotechnology, 2004. 22(2): p. 165-167.

73. Ongpipattanakul, B., R.R. Burnette, R.O. Potts, and M.L. Francoeur, Evidence that oleic acid exists in a separate phase within stratum corneum lipids. Pharm Res, 1991. 8(3): p. 350-4.

74. Hadgraft, J., Passive enhancement strategies in topical and transdermal drug delivery. International Journal of Pharmaceutics, 1999. 184(1): p. 1-6.

75. Lucks, S. and R. Müller, Medication vehicles made of solid lipid particles (solid lipid nanospheres-SLN), 1991, MEDAC Gesellschaft für klinische spezial präparate GmbH (Fehlandtstrasse 3, Hamburg, D-20354, DE).

76. Mäder, K. and W. Mehnert, eds. 1 - Solid Lipid Nanoparticles—Concepts, Procedures, and Physicochemical Aspects, Lipospheres in drug targets and delivery: approaches, methods, and applications. ed. C. Nastruzzi2004, CRC Press. 1 - 22.

77. Lipid particles based on matrix comprising solid and liquid lipid, useful in diagnostics and for controlled release of active agents, especially pharmaceuticals, 2000.

78. Pardeike, J., A. Hommoss, and R.H. Müller, Lipid nanoparticles (SLN, NLC) in cosmetic and pharmaceutical dermal products. International Journal of Pharmaceutics, 2009. 366(1-2): p. 170-184.

79. Müller, R.H., M. Radtke, and S.A. Wissing, Solid lipid nanoparticles (SLN) and nanostructured lipid carriers (NLC) in cosmetic and dermatological preparations. Advanced Drug Delivery Reviews, 2002. 54(Supplement 1): p. S131-S155.

80. Wissing, S.A., O. Kayser, and R.H. Müller, Solid lipid nanoparticles for parenteral drug delivery. Advanced Drug Delivery Reviews, 2004. 56(9): p. 1257-1272.

81. Rawat, M., D. Singh, S. Saraf, and S. Saraf, Nanocarriers: Promising Vehicle for Bioactive Drugs. Biological & Pharmaceutical Bulletin, 2006. 29(9): p. 1790-1798.

82. Thassu, D., Nanoparticulate drug delivery systems. Drugs and the pharmaceutical sciences, 1662007, New York [u.a.]: Informa Healthcare. Chapter 14: 213-233.

83. Mehnert, W. and K. Mäder, Solid lipid nanoparticles: Production, characterization and applications. Advanced Drug Delivery Reviews, 2001. 47(2-3): p. 165-196.

84. Müller, R.H., M. Radtke, and S.A. Wissing, Nanostructured lipid matrices for improved microencapsulation of drugs. International Journal of Pharmaceutics, 2002. 242(1-2): p. 121-128.

85. Teeranachaideekul, V., E.B. Souto, V.B. Junyaprasert, and R.H. Müller, Cetyl palmitate-based NLC for topical delivery of Coenzyme Q10 - Development, physicochemical characterization and in vitro release studies. European Journal of Pharmaceutics and Biopharmaceutics, 2007. 67(1): p. 141-148.

86. Muchow, M., P. Maincent, and R.H. Müller, Lipid Nanoparticles with a Solid Matrix (SLN®, NLC®, LDC®) for Oral Drug Delivery. Drug Development and Industrial Pharmacy, 2008. 34(12): p. 1394 - 1405.

87. Müller, R.H., R. Shegokar, and C.M. Keck, 20 Years of Lipid Nanoparticles (SLN and NLC): Present State of Development and Industrial Applications. Curr Drug Discov Technol, 2011.

88. Venkateswarlu, V. and K. Manjunath, Preparation, characterization and in vitro release kinetics of clozapine solid lipid nanoparticles. Journal of Controlled Release, 2004. 95(3): p. 627-638.

89. zur Mühlen, A., C. Schwarz, and W. Mehnert, Solid lipid nanoparticles (SLN) for controlled drug delivery - Drug release and release mechanism. European Journal of Pharmaceutics and Biopharmaceutics, 1998. 45(2): p. 149-155.

90. Souto, E.B., S.A. Wissing, C.M. Barbosa, and R.H. Müller, Development of a controlled release formulation based on SLN and NLC for topical clotrimazole delivery. International Journal of Pharmaceutics, 2004. 278(1): p. 71-77.

91. Müller, R.H., D. Rühl, S. Runge, K. Schulze-Forster, and W. Mehnert, Cytotoxicity of Solid Lipid Nanoparticles as a Function of the Lipid Matrix and the Surfactant. Pharmaceutical Research, 1997. 14(4): p. 458-462.

92. Wong, H.L., R. Bendayan, A.M. Rauth, Y. Li, and X.Y. Wu, Chemotherapy with anticancer drugs encapsulated in solid lipid nanoparticles. Advanced Drug Delivery Reviews, 2007. 59(6): p. 491-504.

93. Bhaskar, K., C.K. Mohan, M. Lingam, S.J. Mohan, V. Venkateswarlu, Y.M. Rao, J. Anbu, and V. Ravichandran, Development of SLN and NLC Enriched Hydrogels for Transdermal Delivery of Nitrendipine: In Vitro and In Vivo Characteristics. Drug Development and Industrial Pharmacy, 2009. 35(1): p. 98-113.

94. Joshi, M. and V. Patravale, Nanostructured lipid carrier (NLC) based gel of celecoxib. International Journal of Pharmaceutics, 2008. 346(1–2): p. 124-132.

95. Murthy, S.N., S.M. Sammeta, and C. Bowers, Magnetophoresis for enhancing transdermal drug delivery: Mechanistic studies and patch design. Journal of Controlled Release, 2010. 148(2): p. 197-203.

96. Doukas, A.G. and N. Kollias, Transdermal drug delivery with a pressure wave. Advanced Drug Delivery Reviews, 2004. 56(5): p. 559-579.

97. Sá, G.F.F., C. Serpa, and L.G. Arnaut, Stratum corneum permeabilization with photoacoustic waves generated by piezophotonic materials. Journal of Controlled Release, 2013. 167(3): p. 290-300.

98. Arora, A., M.R. Prausnitz, and S. Mitragotri, Micro-scale devices for transdermal drug delivery. International Journal of Pharmaceutics, 2008. 364(2): p. 227-236.

99. Grice, J.E., T.W. Prow, M.A.F. Kendall, and M.S. Roberts, Electrical and Physical Methods of Skin Penetration Enhancement, in Transdermal and Topical Drug Delivery2011, John Wiley & Sons, Inc. p. 43-65.

100. Guy, R.H., Y.N. Kalia, M.B. Delgado-Charro, V. Merino, A. López, and D. Marro, Iontophoresis: electrorepulsion and electroosmosis. Journal of Controlled Release, 2000. 64(1–3): p. 129-132.

101. Denet, A.-R., R. Vanbever, and V. Préat, Skin electroporation for transdermal and topical delivery. Advanced Drug Delivery Reviews, 2004. 56(5): p. 659-674.

102. Joshi, A. and J. Raje, Sonicated transdermal drug transport. Journal of Controlled Release, 2002. 83(1): p. 13-22.

103. Smith, N.B., Perspectives on transdermal ultrasound mediated drug delivery. International Journal of Nanomedicine, 2007. 2(4): p. 585-594.

104. Tanner, T. and R. Marks, Delivering drugs by the transdermal route: review and comment. Skin Research and Technology, 2008. 14(3): p. 249-260.

105. van der Maaden, K., W. Jiskoot, and J. Bouwstra, Microneedle technologies for (trans)dermal drug and vaccine delivery. Journal of Controlled Release, 2012. 161(2): p. 645-655.

106. Liu, S., M.-n. Jin, Y.-s. Quan, F. Kamiyama, H. Katsumi, T. Sakane, and A. Yamamoto, The development and characteristics of novel microneedle arrays fabricated from hyaluronic acid, and their application in the transdermal delivery of insulin. Journal of Controlled Release, 2012. 161(3): p. 933-941.

107. Benson, H.A.E. and S. Namjoshi, Proteins and peptides: Strategies for delivery to and across the skin. Journal of Pharmaceutical Sciences, 2008. 97(9): p. 3591-3610.

108. Prausnitz, M.R. and R. Langer, Transdermal drug delivery. Nat Biotechnol, 2008. 26(11): p. 1261-8.

109. Nair, V.B. and R. Panchagnula, The effect of pretreatment with terpenes on transdermal iontophoretic delivery of arginine vasopressin. Il Farmaco, 2004. 59(7): p. 575-581.

110. Liu, W., M. Hu, W. Liu, C. Xue, H. Xu, and X. Yang, Investigation of the carbopol gel of solid lipid nanoparticles for the transdermal iontophoretic delivery of triamcinolone acetonide acetate. International Journal of Pharmaceutics, 2008. 364(1): p. 135-141.

111. Tokudome, Y. and K. Sugibayashi, Mechanism of the synergic effects of calcium chloride and electroporation on the in vitro enhanced skin permeation of drugs. Journal of Controlled Release, 2004. 95(2): p. 267-274.

112. Seto, J.E., B.E. Polat, R.F.V. Lopez, D. Blankschtein, and R. Langer, Effects of ultrasound and sodium lauryl sulfate on the transdermal delivery of hydrophilic permeants: Comparative in vitro studies with full-thickness and split-thickness pig and human skin. Journal of Controlled Release, 2010. 145(1): p. 26-32.

113. Qin, G., Y. Gao, Y. Wu, S. Zhang, Y. Qiu, F. Li, and B. Xu, Simultaneous basal-bolus delivery of fast-acting insulin and its significance in diabetes management. Nanomedicine: Nanotechnology, Biology and Medicine, 2012. 8(2): p. 221-227.

114. Chen, B., J. Wei, and C. Iliescu, Sonophoretic enhanced microneedles array (SEMA)—Improving the efficiency of transdermal drug delivery. Sensors and Actuators B: Chemical, 2010. 145(1): p. 54-60.

115. Wong, T.-W., C.-H. Chen, C.-C. Huang, C.-D. Lin, and S.-W. Hui, Painless electroporation with a new needle-free microelectrode array to enhance transdermal drug delivery. Journal of Controlled Release, 2006. 110(3): p. 557-565.

116. Tokumoto, S., N. Higo, and K. Sugibayashi, Effect of electroporation and pH on the iontophoretic transdermal delivery of human insulin. International Journal of Pharmaceutics, 2006. 326(1–2): p. 13-19.

117. NIST, NIST Standard Reference Database 69: NIST Chemistry WebBook. 2011.

118. McEvoy, J.P., J.M. Meyer, D.C. Goff, H.A. Nasrallah, S.M. Davis, L. Sullivan, H.Y. Meltzer, J. Hsiao, T. Scott Stroup, and J.A. Lieberman, Prevalence of the metabolic syndrome in patients with schizophrenia: Baseline results from the Clinical Antipsychotic Trials of Intervention

Effectiveness (CATIE) schizophrenia trial and comparison with national estimates from NHANES III. Schizophrenia Research, 2005. 80(1): p. 19-32.

119. Capasso, R.M., T.W. Lineberry, J.M. Bostwick, P.A. Decker, and J. St. Sauver, Mortality in schizophrenia and schizoaffective disorder: An Olmsted County, Minnesota cohort: 1950–2005. Schizophrenia Research, 2008. 98(1): p. 287-294.

120. Meyer, J.M., V.G. Davis, D.C. Goff, J.P. McEvoy, H.A. Nasrallah, S.M. Davis, R.A. Rosenheck, G.L. Daumit, J. Hsiao, M.S. Swartz, T.S. Stroup, and J.A. Lieberman, Change in metabolic syndrome parameters with antipsychotic treatment in the CATIE Schizophrenia Trial: Prospective data from phase 1. Schizophrenia Research, 2008. 101(1): p. 273-286.

121. Ballantyne, C.M., A.G. Olsson, T.J. Cook, M.F. Mercuri, T.R. Pedersen, J. Kjekshus, and f.t.S.S.S.S. Group, Influence of Low High-Density Lipoprotein Cholesterol and Elevated Triglyceride on Coronary Heart Disease Events and Response to Simvastatin Therapy in 4S. Circulation, 2001. 104(25): p. 3046-3051.

122. Heart Protection Study Collaborative, G., Effects on 11-year mortality and morbidity of lowering LDL cholesterol with simvastatin for about 5 years in 20?536 high-risk individuals: a randomised controlled trial. The Lancet, 2011. 378(9808): p. 2013-2020.

123. Ertürk, S., A. Önal, and S. Müge Çetin, Analytical methods for the quantitative determination of 3-hydroxy-3-methylglutaryl coenzyme A reductase inhibitors in biological samples. Journal of Chromatography B, 2003. 793(2): p. 193-205.

124. Yang, D.-J. and L.S. Hwang, Study on the conversion of three natural statins from lactone forms to their corresponding hydroxy acid forms and their determination in Pu-Erh tea. Journal of Chromatography A, 2006. 1119(1–2): p. 277-284.

125. Schachter, M., Chemical, pharmacokinetic and pharmacodynamic properties of statins: an update. Fundamental & Clinical Pharmacology, 2005. 19(1): p. 117-125.

126. Olanzapine - Compound summary. Available from: http://pubchem.ncbi.nlm.nih.gov/summary/summary.cgi?cid=4585, accessed on 16/05/2013.

127. Simvastatin - Compound Summary. Available from: http://pubchem.ncbi.nlm.nih.gov/summary/summary.cgi?cid=54454&loc=ec_rcs, accessed on 16/05/2013.

128. Patel, R.B., M.R. Patel, K.K. Bhatt, and B.G. Patel, Development and validation of an HPTLC method for determination of olanzapine in formulations. J AOAC Int, 2010. 93(3): p. 811-9.

129. Moffat, A.C., D. Osselton, B. Widdop, and E.G.C. Clarke, Clarke's analysis of drugs and poisons: in pharmaceuticals, body fluids and postmortem material2004: Pharmaceutical Press.

130. RCM Zyprexa. Available from: http://www.ema.europa.eu/docs/en_GB/document_library/EPAR_-_Product_Information/human/000115/WC500055207.pdf, accessed on 16/05/2013.

131. Zocor RCM. Available from: http://www.infarmed.pt/infomed/download_ficheiro.php?med_id=9475&tipo_doc=rcm, accessed on 16/05/2013.

132. Mauri, M.C., L.S. Volonteri, A. Colasanti, A. Fiorentini, I.F. De Gaspari, and S.R. Bareggi, Clinical Pharmacokinetics of Atypical Antipsychotics: A Critical Review of the Relationship Between Plasma Concentrations and Clinical Response. Clinical Pharmacokinetics, 2007. 46(5): p. 359-388.

133. Muller, R.H. and C.M. Keck, Challenges and solutions for the delivery of biotech drugs - a review of drug nanocrystal technology and lipid nanoparticles. Journal of Biotechnology, 2004. 113(1-3): p. 151-170.

134. Jenning, V., M. Schäfer-Korting, and S. Gohla, Vitamin A-loaded solid lipid nanoparticles for topical use: drug release properties. Journal of Controlled Release, 2000. 66(2–3): p. 115-126.

135. Müller, R.H., R.D. Petersen, A. Hommoss, and J. Pardeike, Nanostructured lipid carriers (NLC) in cosmetic dermal products. Advanced Drug Delivery Reviews, 2007. 59(6): p. 522-530.

136. Sanna, V., G. Caria, and A. Mariani, Effect of lipid nanoparticles containing fatty alcohols having different chain length on the ex vivo skin permeability of Econazole nitrate. Powder Technology, 2010. 201(1): p. 32-36.

137. Puglia, C. and F. Bonina, Lipid nanoparticles as novel delivery systems for cosmetics and dermal pharmaceuticals. Expert Opinion on Drug Delivery, 2012. 9(4): p. 429-441.

138. Heather, A.E.B., Transdermal Drug Delivery: Penetration Enhancement Techniques. Current Drug Delivery, 2005. 2(1): p. 23-33.

139. Prausnitz, M.R., Microneedles for transdermal drug delivery. Advanced Drug Delivery Reviews, 2004. 56(5): p. 581-587.

Chapter 2

Methods for lipid nanoparticles production, characterization and optimization

In this chapter, a brief introduction to most of the methods and techniques used in this study is presented. Further details, including practical considerations about the actual procedures are provided in the specific methods and results sections along the thesis.

For convenience, the methods were divided into nine sections, encompassing the different stages of the work, and ranging from the experimental to the simulation part. The former comprises a comprehensive description of the preparation methods of lipid nanoparticles carried out, a technical description of the methods used for the lipid nanoparticles characterization, including particle size analysis, zeta potential, drug incorporation measurements, morphological and crystallinity characterization techniques, such as high-resolution microscopy (scanning electron microscopy, transmission electron microscopy and atomic force microscopy), differential scanning calorimetry and attenuated total reflectance infrared spectroscopy, respectively. Experimental design was a technique omnipresent throughout the study and is addressed in the perspective of its importance for the screening and optimization procedures. A short introduction to rheological and texture analysis, and to the methods for studying *in vitro* and *in vivo* percutaneous absorption, stability and cytotoxicity is provided. Some general aspects of molecular dynamics simulation are, finally described.

2.1 Production

Numerous methodologies for lipid nanoparticles production are described in the literature, including high pressure homogenization [1-3], via microemulsion [4, 5], solvent

emulsification-evaporation [6, 7] or diffusion [8-10], w/o/w double emulsion [11, 12], phase inversion [13-15] and high shear homogenization [16] and/or ultrasonication techniques [17]. Other approaches have been developed as described elsewhere [18].

The lipid nanoparticles addressed in this work were produced by two different methods: a modified solvent emulsification-evaporation method, combined with high shear homogenization and ultrasonication, and hot HPH. For this reason, these techniques will be described in more detail in what follows.

2.1.1 Solvent emulsification-evaporation

The solvent emulsification-evaporation is a method similar to the production of polymeric nanoparticles by solvent evaporation in o/w emulsions. The lipid is previously dissolved in a water immiscible organic solvent (e.g. chloroform, or methylene chloride) and the organic solution is dispersed in aqueous surfactant phase, in order to obtain an o/w emulsion. The solvent is then removed by evaporation and a solid lipid nanoparticle dispersion is formed [6, 19, 20].

The emulsification step was supported by the ultrasonication technique, followed by high shear homogenization (**Figure 2.1**). Both are dispersing techniques also employed in the preparation of lipid nanoparticles.
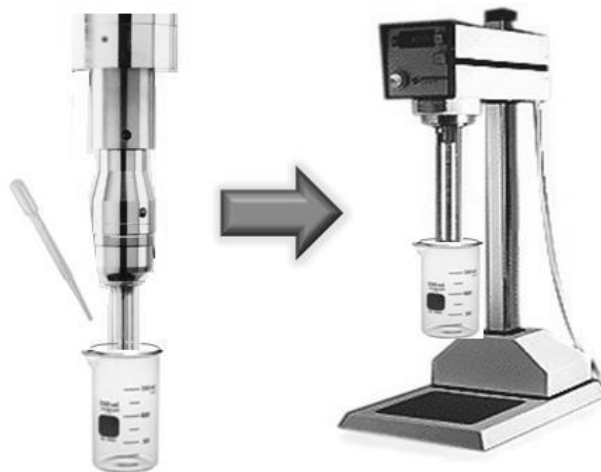
Figure 2.1 Schematic representation of the two main steps in the modified solvent emulsification-evaporation method for lipid nanoparticles production [21].

Ultrasonication is based on the mechanism of cavitation through which high frequency sound waves propagate into liquid media, resulting in cavitation bubbles which generate high shear forces to reduce droplet size (Figure 2.2). On the other hand, the implosion of the cavitation bubbles cause intensive shock waves in the surrounding

medium, resulting in the formation of liquid jets of high velocity leading to the reduction of droplet size to nanoscale [18].
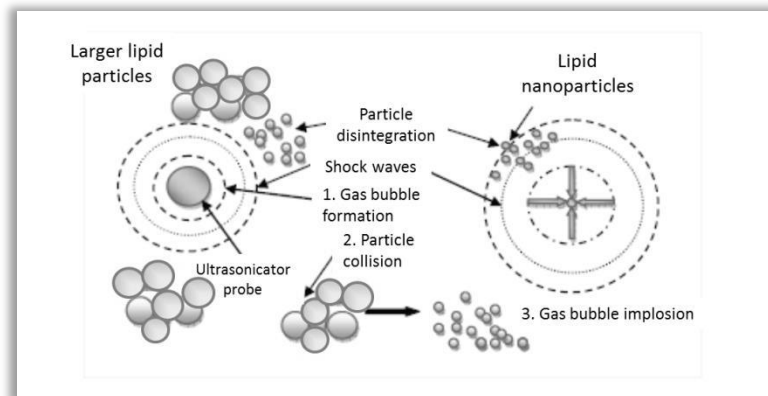
Figure 2.2 Mechanism of formation of lipid nanoparticles by the ultrasonication technique. Adapted from [18].

High shear homogenization takes advantage of high shear rates performed by high speed rotor homogenizers. Centrifugal force drives the dispersion to the periphery of the workhead and subjects it to mechanical shear in the precision gap between the rotor and stator. This is followed by an intense hydraulic shear, which allows to reduce droplet size [22].

The main advantage of this procedure is that it avoids thermal stress. The use of organic solvents and some ultrasonication probe metal contamination arises as potential drawbacks [19]. The low dispersion efficiency attributed to high shear homogenization and ultrasonication [23] can be overcome by combining the two different homogenization methods.

2.1.2 Hot high pressure homogenization

HPH is a technique broadly used in several research areas, including the pharmaceutical, for example, in the production of parenteral emulsions [24]. The already established HPH large-scale production lines allows to overcome the lack of scaling up associated to some nanoparticle production methods, being also a simple and very cost-effective technique [20, 25].

Additionally, HPH leads to a product relatively homogeneous in size, that is, possessing a higher physical stability of the aqueous dispersion [20].

High pressure homogenizers functions as follows: a pump pushes a liquid (the hot pre-emulsion, as referred below) with high pressure (100–2000 bar) through a constricted passageway called the gap region (in the range of a few microns). The fluid

accelerates on a very short distance to a very high velocity (over 1000 Km/h), leaves the gap region and enters the exit region flowing in the direction of the impact ring. After passing through this region, the fluid exits through the outlet (**Figure 2.3**) [26-28].
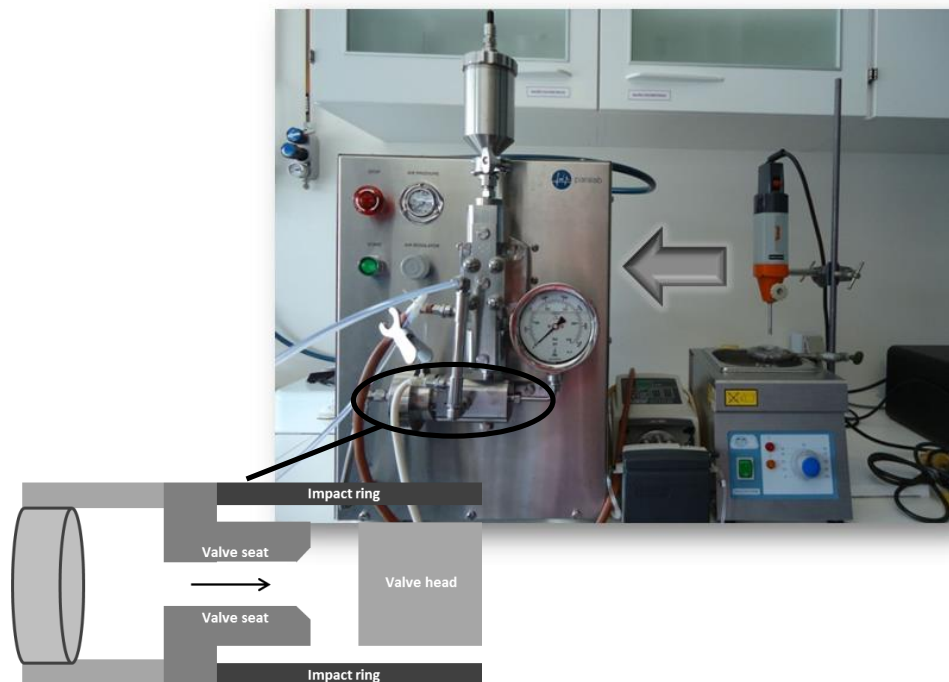
Figure 2.3 Schematic representation of the hot HPH technique (at right) [29]. The homogenizing valve of the homogenizer (at left) consists of three main regions, namely, the inlet region (also referred to as the entrance region), the gap and the exit region (also called the impact region or the impingement zone). Adapted from reference [28].

The mechanism for HPH-action is not thoroughly clear, but includes high-pressure gradients/rapid decompression (the pressure begins at a high value and remains high until the flow enters the gap region, where the pressure falls very quickly), turbulence, cavitation collapse (the rapid increase in velocity with a corresponding decrease in pressure generates high shear stress as well as gas bubbles to implode when the pressure downstream of the gap recovers) and strong impact and impingement [27, 30]. It is effective even for the homogenization of highly concentrated (up to 40% of lipid content) dispersions [31].

HPH can be used in two different production techniques: at elevated temperature, hot HPH, or below room temperature, cold HPH.

For the hot HPH technique, the lipid is melted at approximately 5°C to 10°C above its melting point, and the drug is dissolved or finely dispersed. Afterwards, this molten lipid phase is dispersed in a hot surfactant solution by a high-shear mixing device (Ultraturrax). The obtained coarse pre-emulsion is then homogenized using a high pressure homogenizer also above the lipid melting point, generally at a pressure ranging

from 100 to 1500 bar and submitted to one to three homogenization cycles (APV Gaulin LAB 40) or operated continuously for a certain period of time (Emulsiflex C3, Avestin). A hot nanoemulsion is obtained, which after cooling leads to recrystallization of the lipid and formation of lipid nanoparticles [20, 23]. This technique can be successfully applied to lipophilic drugs, while for hydrophilic compounds the cold homogenization is a preferred technique [18].

2.2 Characterization

An appropriate characterization of the solid lipid nanodispersions is required to control the product quality. However, it represents a challenge due to the small size of these colloidal carriers and the complexity of the system. Important key parameters, which have direct impact on the release kinetics and stability need to be considered. These include mean particle size, zeta potential, entrapment efficiency and drug loading, degree of lipid crystallinity and lipid modification [19].

2.2.1 Size

Several methods are available to characterize particle size, but none of them are fully satisfactory. Therefore, a combination of at least two methods, one of which based on microscopy, is highly recommended.

Dynamic light scattering

Dynamic light scattering (DLS, also known as photon correlation spectroscopy or quasi-elastic light scattering, QELS) is a technique for measuring the size of particles typically in the submicron region, ranging from 0.3 nm to 10 µm in the case of Zetasizer Nano ZS (Malvern) [32] and 0.6 nm to 7 µm for Delsa Nano C (Beckman Coulter) [33, 34], both of them available in the Pharmaceutics department DLS measures the fluctuation of the intensity of the scattered light of a laser beam caused by particle Brownian motion and relates this to the size of the particles. The larger the particle, the slower the Brownian motion will be. Thus, larger particles will diffuse more slowly than the smaller ones. The velocity of the particle Brownian motion is defined by a property known as the translational diffusion coefficient (usually given by the symbol, D). The size of a particle is then calculated from the translational diffusion coefficient by using the Stokes-Einstein equation,

$$d(H) = \frac{K_B T}{3\pi\eta D}$$ (2.1)

where $d(H)$ corresponds to the hydrodynamic diameter, K_B is Boltzmann's constant, T the absolute temperature, η the viscosity and D stands for the translational diffusion coefficient.

It should be noted that the diameter that is obtained by this technique corresponds to the diameter of a sphere that possesses the same translational diffusion coefficient as the particle, thus being denoted as hydrodynamic diameter [35-38].

Size is obtained from the correlation function, which describes the decay of the intensity of scattered light as a function of time, and contains the diffusion coefficient information required to be entered into the Stokes-Einstein equation. The diffusion coefficient is obtained by fitting the correlation function with a suitable algorithm, such as cumulants analysis, which determines a mean size and polydispersity index (PI). The PI is a dimensionless measure of the broadness of the size distribution, ranging from 0 to 1[35]. A PI value lower than 0.1 might be associated with a high homogeneity in the particle population (monodisperse), whereas high PI values suggest a broad size distribution (polydisperse) or even several populations (plurimodal).The latter situations suggest potential problems with the stability of the formulation, and the probability of aggregation of the particles has to be considered [39, 40].

Static light scattering

In a way similar to DLS, in static light scattering (SLS, or laser diffractometry, LD) the particles in a sample are illuminated by a light source such as a laser, with the particles scattering the light in all directions. But, instead of measuring the time dependent fluctuations in the scattering intensity, SLS is based on the dependence of the diffraction angle on the particle radius. The angle of the light scattered by a particle is inversely proportional to the size of that particle, so that smaller particles cause more intense scattering at high angles than do larger ones.

A clear advantage of LD is the coverage of a broad size range from the nanometer to the lower millimeter range, allowing to detect the presence of microparticles or particle agglomerates. Despite the simultaneous use of DLS and LD is highly recommended, it should be stressed that both methods are based on the detection of light scattering effects to "indirectly" calculate particle sizes. As such, difficulties may arise from nonspherical lipid particle shapes [41] or the presence of several populations of different size. Some of these limitations could be overcome by using additional techniques, such as high-resolution microscopy [42].

2.2.2 Morphology

Three types of high-resolution microscopy, scanning electron microscopy (SEM), transmission electron microscopy (TEM) and atomic force microscopy (AFM) are available for imaging of lipid nanoparticles.

Scanning electron microscopy

SEM is a microscopy technique that can yield information about the topography (surface features), morphology (shape and size of the particles) and even composition (elements and the relative amounts of them), allowing for an instrumental resolution on the order of 1-5 nm [39].

In SEM, a beam of highly energy (ranging from 0.1 to 30 keV and an acceleration voltage between 2 and 50kV) is focused in vacuum into a fine probe that is rastered over the surface of the specimen.

The electron beam passes through scan coils and objective lens that deflect horizontally and vertically so that the beam scans the surface of the sample. As the electrons penetrate the surface, a number of interactions occur that can result in different types of signals produced, including secondary electrons, backscattered electrons, characteristic x-rays, and other photons of various energies. Detectors of each type of electrons are placed in the microscope in proper positions to collect them. The imaging signals of greatest interest are the secondary and backscattered electrons because these vary primarily as a result of differences in surface topography [43].

Some constraints of the technique is that for the observation, the sample must be dried and coated with a thin layer of gold or platinum, when it is not conductive [19].

Transmission electron microscopy

Transmission electron microscopy (TEM) is a technique where an electron beam interacts and passes through a thin specimen (typically of the order of 5-100 nm for 100 keV electrons). The electrons are emitted in the electron gun and focused by a condenser-lens system onto the sample surface. The electrons that are elastically scattered consist the transmitted beams which are imaged by a lens system onto a fluorescent screen [44].

The operation of TEM requires an ultra-high vacuum and a high voltage (an acceleration voltage of routine instruments ranges from 100 to 200kV), allowing a resolution of 0.15-0.3 nm for conventional microscopes [44]. Additionally, it is a

technique that requires several steps of sample preparation, also involving high cost [39, 45].

Atomic force microscopy

AFM is a microscopy technique relatively not invasive that provides the three-dimensional topography as well as physical properties of a surface, by measuring forces between a sharpened probing tip, supported on a flexible cantilever, and that surface at very short distance (0.2-10 nm probe-sample separation) [46, 47]. It allows a spatial resolution of up to 0.01 nm for imaging [48].

Three modes can be used in atomic force microscopy depending mainly on the sensitivity of the tip to the respective forces used for imaging, i.e., contact mode (repulsive Van der Waals interactions), non-contact mode (attractive Van der Waals interactions) and intermittent or tapping mode. In contact mode, the tip touches the sample surface, which is good for rough samples. However, it may promote particle surface alterations (soft samples deformation or removal of particles from the area under investigation). In these cases, tapping mode or non-contact could be use, whereby the probe maintains a constant oscillation amplitude or does not contact the sample surface, respectively, although the latter mode is also associated with lower resolution [46, 47].

Apart the ability to magnify in the X, Y and Z axes, AFM allows imaging under hydrated conditions without pre-treatment of the samples as no vaccum is needed during operation and the samples does not need to be conductive [46, 49, 50].

2.2.3 Zeta potential

Zeta potential is a physical property which is exhibited by any particle in suspension, being related to its surface charge. It is a helpful parameter in predicting colloidal systems long-term stability [51]. Specifically, when a particle is in a medium, the liquid layer surrounding it exists as two parts: an inner region where the ions are strongly bound, the Stern layer, and an outer region where they are less firmly associated, the diffuse layer. Within the latter, there is a notional boundary inside wherein the ions and particles form a stable entity, so that, when a particle moves, ions within the boundary move it. Those ions beyond the boundary stay with the bulk dispersant. Zeta potential is considered the potential at this boundary, that is, at the slipping plane (Figure 2.4) [51].
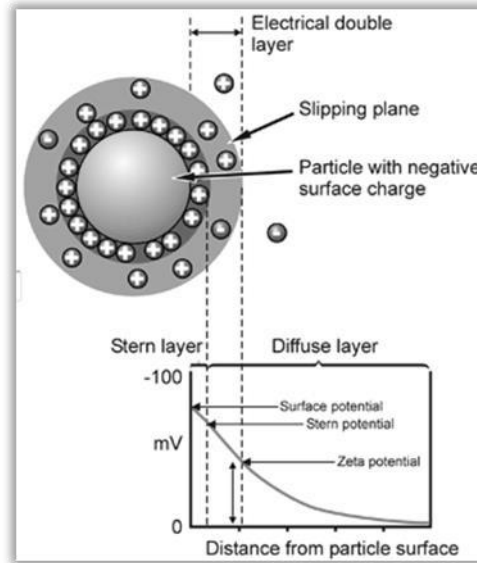
Figure 2.4 Schematic representation of the zeta potential. Adapted from reference [51].

The magnitude of the zeta potential gives an indication of the potential stability of the colloidal system, which is determined by the sum of attractive forces (Van der Waals) and repulsive forces (electrostatic) which particles experience as they approach one another. If the zeta potential is high, the particles are stable due to high electrostatic repulsion between particles. Conversely, a low zeta potential value (approaching zero) increases the probability of particles colliding, therefore, forming particle aggregates. Thus, zeta potential is used as an index of the dispersion stability of particles. A zeta value higher than |30| mV is generally taken to consider a suspension as stable [40, 51].

Electrophoretic light scattering

Electrophoretic light scattering (ELS) is a technique used to measure the electrophoretic mobility of particles in dispersion, based on the fundamental physical principle of electrophoresis.

The zeta potential, *z*, is related to the electrophoretic mobility, U_E, by the Henry equation

$$U_E = \frac{2\,\varepsilon\,z\,f(ka)}{3\,\eta} \tag{2.2}$$

where ε is the dielectric constant, η the viscosity, and *f(κa)* Henry's function. In many aqueous solutions containing an electrolyte, zeta potential can be calculated from the Smoluchowski equation, for which a value of 1.5 for $f(ka)$ is considered [51, 52].

2.2.4 Entrapment efficiency and drug loading

Drug entrapment efficiency and loading capacity are important parameters to evaluate the suitability of a carrier system. The former expresses the percentage of drug which is entrapped inside the lipid nanoparticles, being most frequently determined indirectly, that is, by quantifying the non-incorporated drug in the external aqueous phase after separation from the nanoparticles. It can be calculated by

$$\% \, EE = \frac{W_{total \, drug} - W_{free \, drug}}{W_{total \, drug}} \times 100 \qquad (2.3)$$

where $W_{total \, drug}$ stands for the total drug amount determined in the dispersion, $W_{free \, drug}$ is the amount of free drug detected in the external aqueous phase after separation of the nanoparticles, and W_{lipid} is the weight of the lipid phase.

The separation of the nanoparticles can be carried out by ultrafiltration-centrifugation, using centrifugal filter units with a specific molecular weight cut-off. According to this technique, nanoparticles are retained in the membrane, while the external aqueous phase is collected in the outer chamber after a certain optimized time of centrifugation. Note that the presence of drug crystals should be inspected by adequate techniques, such as polarized light microscopy, otherwise it will be retained together with nanoparticles, thus conducting to an increased mislead entrapment efficiency. In the latter situation, a suitable solvent should be added to the lipid nanoparticles dispersion.

The amount of free drug in the aqueous phase, after isolation of the system, can be quantified by an adequate method, such as high performance liquid chromatography (HPLC).

On the other hand, the drug loading capacity is calculated in percent of the lipid mass [20] by

$$\% \, DL = \frac{W_{total \, drug} - W_{free \, drug}}{W_{lipid}} \times 100 \qquad (2.4)$$

where W_{lipid} stands for lipid weight.

For lipophilic drugs, the entrapment efficiencies are typically between 90% and 98%, while for hydrophilic compounds, the loading capacity and the entrapment efficiency are obviously lower [20]. Several factors affect the loading capacity of drug in the lipid, especially the solubility of drug in melted lipid, the chemical and physical structure of solid lipid matrix and polymorphic state of lipid material. A high solubility of the drug in the lipid melt is a prerequisite, in order to assure a sufficient drug loading [42].

2.2.5 High performance liquid chromatography

High performance liquid chromatography has been established as the premier technique for the analysis and purification of a wide range of molecules. The enormous success of this technique can be attributed to several features such as the high reproducibility, ease of selectivity manipulation and high recoveries. Furthermore, in a single step process it can separate a mixture into its individual components and simultaneously provide a quantitative estimate of each constituent. Among the respective features, the most significant is the excellent resolution that can be achieved under a wide range of conditions for very closely related molecules as well as structurally distinct molecules, which arise from several interactive modes of chromatography.

The separation of a mixture of molecules in interactive modes of chromatography arises from the differential adsorption of each solute according to their respective affinity for the immobilized stationary phase. Thus, molecules with higher affinity to the stationary phase will be retained to a greater extent than other molecules with low affinity for the stationary phase. The degree and nature of the binding affinity is highly dependent on the structure of the solute and the immobilized ligands as well as the type of interaction established between the molecule and stationary phase. For instance, in case of affinity chromatography, binding involves a mixture of hydrophobic, electrostatic, and polar forces whereas in the case of ion-exchange chromatography is through electrostatic interactions. In the case of reverse –phase chromatography, separations are based primarily on hydrophobic interactions being the polarities of mobile (polar) and stationary phases (hydrophobic) reversed and mobile phases employed are mostly water-based solutions. Thus, the key factor that supports the development and employment of a successful separation protocol is the ability to manipulate the retention of the target molecule that it can be resolved from other non-target components [53].

2.2.6 Crystallinity and lipid modification

Special attention must be paid to the characterization of the crystallization behavior and the polymorphic lipid transitions occurring throughout the storage time, since these parameters are strongly related to drug incorporation and release rates [19]. These parameters can be inspected by differential scanning calorimetry (DSC) and attenuated total reflectance infrared spectroscopy (ATR-FTIR).

Differential scanning calorimetry

Differential scanning calorimetry (DSC) is a thermal analysis technique which allows determining, among others, the temperature and enthalpy associated with transitions involving heat transfer, as a function of time and temperature.

In a basic DSC experiment, energy is supplied simultaneously to the sample and to the reference cell, and temperatures of both are raised simultaneously over time. The difference in the input energy required to match the temperature of the sample to that of the reference will be the amount of excess heat absorbed or released by the sample material, depending whether the thermal event is endothermic or exothermic, respectively. This explains the introduction of the concept of heat excess, since more energy is required to bring the sample to the same temperature as the reference [54].

There are two types of DSC instruments, according to the mechanism of operation: power compensation or heat flux. In a power compensation DSC, the sample and reference pans are placed in separate furnaces heated by separate heaters. The sample and reference are maintained at the same temperature, and the respective difference in power, when a thermal event occurs, is measured and plotted as a function of temperature or time, according to

$$P = \frac{dQ}{dt} = I^2 R \qquad \textbf{(2.5)}$$

where $\frac{dQ}{dt}$ is the heating rate, the I current applied to the heater, and R the resistance of the heater [55].

In turn, heat flux DSC uses a single furnace which supplies heat to both the sample and reference, measuring the differential temperature and the consequent heat flow is determined by the thermal equivalent of Ohm's law

$$q = \frac{\Delta T}{R} \qquad \textbf{(2.6)}$$

where q is the sample heat flow, ΔT the temperature difference between sample and reference, and R the thermal resistance of the cell [54, 56].

DSC can be used to investigate the status of the lipid matrix in nanoparticles, providing information about the respective crystallization behavior, the occurrence of polymorphic transitions, the melting temperature and associated enthalpy [57].

It should be noted that nearly all lipid excipients exist under various polymorphic forms. In particular for glycerides, the main crystalline structures are hexagonal (α), orthorhombic (β′) and triclinic (β).These structures differ by their thermal properties (transition and melting temperature), depending also on the thermal history of the lipid [58]. In addition, the lipid packing density and the thermodynamic stability increase, while

drug incorporation rates decrease, in the following order: supercooled melt, α modification, β′ modification, β modification [19].

Thus, the lipid crystallization after nanoparticles preparation and throughout storage is an important point to monitor, since several polymorphic forms will condition different capacities of drug incorporation and particle shapes [19].

Additionally, DSC can be used to investigate the physical state of drug inside lipid nanoparticles matrix, allowing to infer about its localization by the presence or absence of melting peak transition.

Attenuated total reflectance infrared spectroscopy

Infrared spectroscopy is a technique that allows obtaining structural information by studying the vibration modes of specific molecular groups as a result of the interaction between infrared (IR) light and matter. Attenuated total reflectance (ATR) is a fast and non-destructive sampling technique for obtaining the IR spectrum of a material surface [59].

In ATR, the sample, usually not requiring preparation, is placed in a special crystal of a material with a high refraction index (e.g., ZnSe). The IR beam from the spectrometer is directed onto the crystal, wherein successively reflections occur and, subsequently, directed to the detector [60].

The use of ATR in spectroscopy is based on the fact that although complete internal reflection occurs at the sample–crystal interface, radiation only penetrates a few microns into the sample, which is designated as the evanescent wave. As such, there must be a good contact between the sample and the crystal surface. The interaction between the sample and the evanescent wave results in the absorption of radiation, allowing to obtain the corresponding spectrum [60].

ATR-FTIR allows obtaining information about the arrangement of lipid molecules in SLN and NLC, so as to complement information arising from DSC. It may also elucidate on how the components interact within such a complex matrix, e.g., whether the oil component penetrates into the solid lipid in NLC and how oil alters the conformation of the solid lipid hydrocarbon chains. [60, 61].

Additionally, FTIR-ATR permits studying the structure of the stratum corneum at the molecular level and, in particular, elucidate the mechanism of action of various penetration enhancers on the SC barrier function [62].

2.3 Optimization

Optimization strategies are procedures which attempt to find the optimal settings or conditions, e.g., for a certain formulation, product, process, or an analytical method, considering a number of factors or independent variables. Factors are parameters than can be set at given levels, such as components concentration, homogenization time, etc., and that affect the responses or dependent variable, which correspond to the outcome of a method or procedure. In turn, the factors are studied at different level ranges, constituting the experimental domain within which the overall best conditions are tried to find.

Complex systems usually require a multivariate approach, in which several factors are varied simultaneously. In this context, an experimental design, that is, an experimental set-up to simultaneously evaluate several factors at given numbers of levels in a predefined number of experiments, should be performed [63].

2.3.1 Factorial design

Factorial design is a system of experimental design intended to elucidate the effects of many factors simultaneously, to assess their relative importance, and to determine whether the factors interact [64].

When optimizing a formulation or process, there are a number of different methods for tackling the problem and the resulting data may also be analyzed in a number of different ways. In what concerns experimental designs, a rough classification into screening designs, response surface designs and mixture designs can be carried out. Screening designs, e.g., full factorial, fractional factorial, and Plackett–Burman designs, allow screening a relatively large number of factors in a relatively small number of experiments. They are used to identify the most influencing factors influencing the system, being applied in the context of optimizing processes. Most often, the factors are evaluated at two levels in these designs. In turn, response surface designs are applied to find the optimal factor settings, while mixture designs are used to optimize, for instance, the excipients composition in formulations [63, 65].

When the number of factors f is small, two-level full factorial designs might be applied for screening purposes. Focus will be given to these particular factorial designs, since they were often used for experimental planning throughout this work.

Two-level full factorial designs include all possible combinations between the f factors and their L = 2 levels, leading to a number of experiments, $N = L^f = 2^f$, to be performed.

These designs allow the simultaneous investigation of qualitative and quantitative factors [63, 65].

As example, the simplest design, which corresponds to two factors, X_1 and X_2, studied at two levels, 2^2, will be considered. First of all, the variables coding, that is, the process that brings the values of all factors into the same range, should be performed. For a two-level experiment, the lower is designated -1 and the upper level -1, thus yielding 4 different combinations (Figure 2.5).
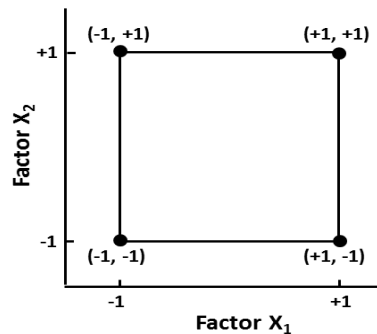
Figure 2.5 A two-factor, two-level experimental design, using coded values of the factors.

The values for the interaction term are obtained by multiplying together the values for the individual factors, e.g., for the experiment (-1, -1), the value of the interaction is -1 x (-1) = +1. A design matrix is thus constructed. These designs allow the estimation of all main (i.e., corresponding to each factor) and interaction effects [63, 65].

Main effects represent the average result of changing one factor from -1 to +1, and the interaction terms affect the result when two or more factors are simultaneously changed. If none of the factors produced an effect, then the responses would be scattered randomly around their mean value, given by the independent term [64].

For the evaluation of the mean effects and interactions resulting from a factorially designed experiment, a multiple linear regression analysis can be applied. The coded factors are now represented by x_1 and x_2, and the response by y. Therefore, an equation which takes into account all the main effects and interactions is

$$y = \beta_0 + \beta_1 x_1 + \beta_2 x_2 + \beta_{12} x_1 x_2 \qquad (2.7)$$

where y is the response, β_0 the intercept, and β_1 and β_2 the main regression coefficients, usually calculated using least squares regression,

$$b = (X^T X)^{-1} X^T y \qquad (2.8)$$

wherein X^T is the transposed matrix of X [63], the latter built according to equation (2.7), with unit values in the first column, the level values imposed in the experiments for

the factors in the next two, and the respective product in the fourth column, now related with the interaction. This matrix is built according to a corresponding procedure for other models.

The estimated coefficients are statistically assessed, to determine their significance, often by applying the t-test statistics. A t value for the factors is calculated and compared with a (tabulated) critical t value, tcritical, for a certain significance level (usually α = 0.05). All effects with a t value larger than or equal to tcritical are regarded as significant [66].

Additionally, an ANOVA approach is frequently used to assess the model [64].

2.4 Hydrogel-based formulation

Lipid nanoparticles dispersions can be incorporated into semisolid preparations such as hydrogels, in order to provide the appropriate consistency for administration [67, 68]. Generally, hydrophilic semi-solid gels present several advantages, such as low toxicity, unique physical properties, availability, biocompatibility and adhesiveness [40]. These can be prepared by using natural (e.g., chitosan, dextran) semi-synthetic (e.g., cellulose derivatives) or synthetic polymers (e.g., carbopols) [68].

The influence of the formulation components upon consistency should be critically monitored, since they will impact upon the drug release profile and, consequently, the therapeutic outcome.

In this context, rheology measurements and texture analysis are valuable tools for semi-solid product quality control.

2.4.1 Rheology

Rheology is formally defined as the study of deformation and flow behavior of various materials [69]. Thus, rheological techniques assess the molecular interactions, but may also to describe the dynamic properties, in particular the viscosity.

Multiphase systems, such as lipid nanoparticles dispersions may be considered viscoelastic systems, i.e. they exhibit a combination of viscous and elastic properties, being solid at short time deformation and liquids at long times of deformation [40].

To understand viscoelasticity, it is helpful to consider first the cases of perfect elasticity or viscosity, referring to relationships of Hooke law for solids and Newton-Stokes law for liquids, respectively. For an elastic solid, Hooke's law states that the applied shear stress (σ) is proportional to the produced shear strain (γ)

$$\sigma = G \, \gamma \tag{2.9}$$

where shear stress (σ) is the shear force per unit area and the strain (γ) the deformation. The proportionality constant (G) is called the Young modulus and is an intrinsic property of an elastic solid.

On the other hand, Newton-Stokes law of viscosity for liquids states that the shear stress (σ), that is, the force per unit area required to produce the motion is proportional to the velocity gradient or shear rate ($\dot{\gamma}$)

$$\sigma = \eta \, \dot{\gamma} \tag{2.10}$$

The proportionality constant (η) is defined as the viscosity of the material.

Thus, the rheological measurements convey the information of how "fluid-like" or how "solid-like" a material is as a function of shear rate or frequency of deformation. Two different methods are available to determine viscoelastic properties: rotational and oscillatory tests.

In rotational tests, the material is forced to flow by applying a controlled stress, and the resulting deformation is measured along the time (shear rate) or as a function of temperature. The rotational speed depends on the viscosity of the sample, which is calculated in these tests by dividing the stress by the shear rate. It is usually termed as shear viscosity [70].

In oscillatory tests, information about the structure and elasticity of the samples is obtained. These tests are supposedly not destructive, since the material does not move. Instead, a constant sinusoidal varying stress (at one or more frequencies) is applied to the sample and the equally varying strain is measured. The deformation of the sample depends on both frequency and stress applied, as such, and will increase with decreasing frequency, when measuring at a constant stress, and it will increase with stress, when frequency is kept constant. The complex viscosity, storage and loss complex moduli are the main parameters extracted, which can be measured as a function of frequency, time or temperature [70, 71].

Complex viscosity, η^*, is a mathematical representation of the viscosity in oscillatory tests and can be expressed as

$$\eta^* = \frac{\sqrt{G'^2 \, G''^2}}{\omega} \tag{2.11}$$

where G' is the storage modulus, a measure of the energy stored and recovered per cycle of sinusoidal deformation, G'' is the loss modulus, a measure of the energy dissipated or lost per cycle, and ω the angular frequency of deformation [70, 72].

Since oscillatory measurements are conducted with the aim at studying the structure of a material, the deformation has to be kept small. Additionally, the measurements must be performed in the linear viscoelastic regime, otherwise, the results of the frequency

sweep experiments will depend not only on the frequency but also on the applied stress or deformation. As such, a linearity test, the oscillation stress sweep, is carried out to obtain the values of shear stress for which the viscoelastic functions are independent from the magnitude of the applied stress [73]. Since such regions are usually observed at very low stresses, no important changes in the structure of the material will occur [71].

.

2.4.2 Texture analysis

The use of texture profile analysis (TPA) is relevant for the mechanical characterization of a pharmaceutical semisolid formulation, in order to determine interactions between formulation components, so as to complement the rheological information.

TPA is a technique that resorts to a texturometer, whereby a solid cylindrical probe executes two passes into the product with a predefined pause, allowing to obtain a typical force-time curve from which the textural properties of the product may be calculated. These include [74, 75] (Figure 2.6):

- hardness, given by the maximum peak force during the first compression cycle;

- compressibility, i.e., the work required to deform the sample during the first compression of the probe and calculated from area under the force–time curve 1 (AUC1);

- adhesiveness, the work required to overcome the attractive forces between the surface of the sample and the surface of the probe and is indicated as the negative force area for the first compression cycle and calculated from AUC2;

- cohesiveness, the ratio of the area under the force–time curve produced on the second compression cycle to that on the first compression cycle, where both compressions are separated by a defined recovery period;

- elasticity, the ratio of the time required to achieve maximum structural deformation on the second compression cycle to that on the first compression cycle.
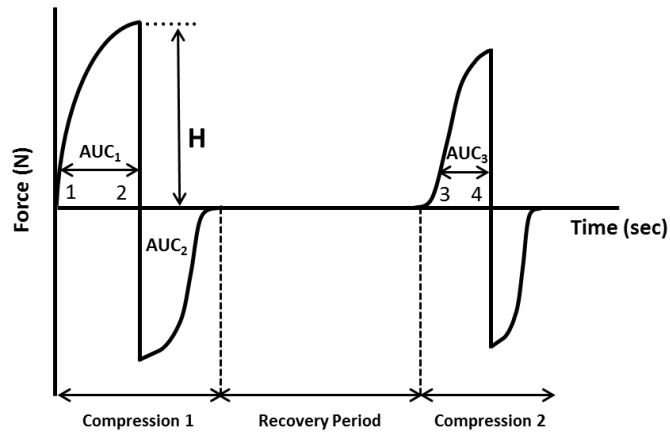
Figure 2.6 Graphical output from Texture Profile Analysis. Key: H=hardness; AUC_1= compressibility; AUC_2=adhesiveness. In addition, AUC_3 / AUC_1 corresponds to the cohesiveness and the elasticity is given by time diff 3:4/time diff 1:2. [74]

In the development of pharmaceutical semisolid preparations for transdermal application, several desirable product characteristics may be defined. These include optimal mechanical properties (such as spreadability), bioadhesion (prolonged contact time at administration site) and an acceptable viscosity [76].

2.5 Percutaneous absorption

In vitro permeation studies constitute a key assay in the assessment of product therapeutic performance. *In vitro* investigations are advantageous, since the experimental conditions can be controlled precisely, such that the only variables are the skin and the test formulation. Most common methods designed for evaluation of percutaneous absorption use diffusion cells, such as static (i.e. no flow) vertical Franz cells, which is a simple, reliable, and reproducible system of measuring drug release from dosage form and skin permeation.

2.5.1 Franz diffusion cells

Static Franz diffusion cells consist of two chambers, a donor and a receptor chamber, separated by an artificial or biological membrane and held together by a clamp (Figure 2.7). Formulations are applied in the donor compartment, while the receptor compartment contains a receptor fluid kept at a temperature regulated by thermostatically controlled water circulating through a jacket surrounding the chamber, in order to maintain the skin surface at 32°C. Homogenous temperature distribution in the

receptor solution is maintained by a magnetic stirring bar. Drug absorption is measured by periodically sampling the receptor fluid through a lateral arm.
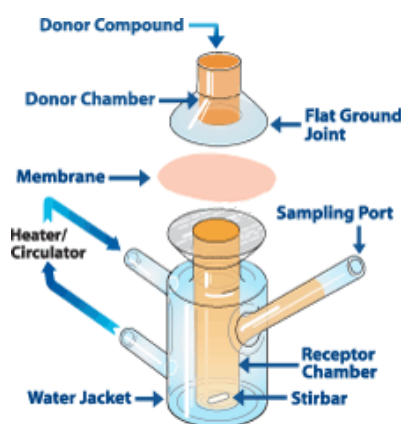
Figure 2.7 Schematic representation of a static vertical Franz diffusion cell.

The conditions under which skin absorption *in vitro* tests are performed are suitably documented in specific guidelines [77-79]. The test system includes a wide range of parameters, including species, membrane type, receptor fluid, integrity testing, test vehicle, dose applied, time points and experimental duration.

The choice of skin depends on the purpose of the test and the availability of skin samples. Although excised human skin is regarded as the "gold standard" for *in vitro* penetration experiments, animal skin, such as that of pig or rat, has been widely used as a substitute for human skin. In particular, pig skin could be used because of its similarity to human skin in terms of its morphology and permeability characteristics, making it a practical alternative [78].

Different methods can be used to prepare skin for *in vitro* experimentation, and usually three types of membranes can be employed in the Franz diffusion cell: full-thickness skin (incorporating the SC, viable epidermis, and dermis), dermatomed skin (in which the lower dermis has been removed), and epidermal membranes, comprising the viable epidermis and the SC, extracted by heat separation [80]. To prepare heat-separated epidermal membranes, full-thickness skin is immersed in water at 60ºC for 60 seconds. Following removal from the water, the epidermis is gently detached using a pair of blunt curved forceps [81].

The choice of membrane is mainly dependent on the nature of the permeant. Although *in vivo* the presence of blood flow will remove a considerable amount of the permeant reaching the dermis, *in vitro*, in the absence of blood flow, the relatively aqueous nature of the dermis, will represent an "artificial" barrier, thus reducing the

penetration of lipophilic compounds. Hence, the use of dermatomed or epidermal membranes is more appropriate for particularly lipophilic permeants [80].

Once obtained, the skin can be stored at -20 °C, providing the samples are not overly hydrated [82]. However, the membrane barrier integrity should be evaluated after storage. Although simple visual examination of specimens could give a qualitative indication of skin integrity, methods for a quantitative evaluation of its state should be employed, such as the measurement of skin conductance, transepidermal water loss, or the flux of a marker compound such as tritiated water. The skin samples found to be outside the "normal" range of values for such measurements must be discarded [80].

In what concerns the receptor medium, it must have adequate solubility for the compound under study, so that sink conditions can be ensured throughout the length of the study (the receptor media should not exceed 10% of the saturation solubility) [79]. This will allow the rate of absorption to proceed as it would normally under in vivo conditions, assuming a continuous removal by the circulatory system. In the case of water-soluble compounds, isotonic saline or buffered isotonic saline (pH 7.4) are considered the rational choice for the maintenance of a physiological environment. For lipophilic compounds, serum albumin or appropriate solubilisers can be added in amounts which do not interfere with membrane integrity [77, 83].

The exposure time should reflect in-use conditions. Permeation experiments are normally conducted for 24 or 48 h, although for long-term transdermal delivery systems, it could be prolonged up to 72 h or longer. In relation to the frequency of sampling, it will depend on the rate/extent of percutaneous absorption. It should be chosen adequately to allow estimating the steady-state and lag-time, that is, the time needed to attain steady-state. [80]

Regarding the test material, a suitable application procedure should be followed. There are two basic approaches to applying substances to the skin: finite and infinite methods. Finite dose techniques are designed to reproduce in-use conditions, involving the application of a dose that may show marked depletion during an experiment. Depletion occurs when the proportion of permeant entering the membrane is large, relative to the amount applied. With finite dosing, the permeation profile may exhibit the characteristic plateauing effect that accompanies donor depletion (Figure 2.8) [81].

On the other hand, infinite-dose techniques involve application of sufficient permeant to make negligible any changes (caused by diffusion or evaporation) in donor concentration, during the experimental period. This is desirable when the experimental objectives include calculation of diffusional parameters or for investigation of mechanisms of penetration enhancement [81].
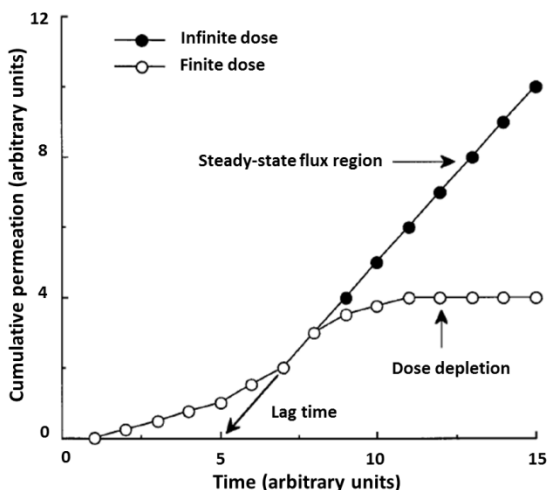
Figure 2.8 Typical permeation profiles obtained from experiments conducted under infinite and finite dose regimes. Note that under infinite dose, permeation usually reaches a steady-state flux region, whereas under finite dosing the permeation profile exhibits a plateau region instead, as a result of donor depletion. Adapted from [81].

In the case of infinite-dose studies, the objective will be to obtain constants that can define the kinetics of permeation, such as the permeability coefficient, K_p, and the lag time, t_{lag}. According to the profile depicted in Figure 2.7, after an initial lag period, the cumulative amount of drug in the receptor fluid will increase linearly with time, that is, the flux across the skin will reach a steady state. The value of t_{lag} can be determined from extrapolation of the linear portion of the plot to the x-axis [84], while K_p can be extracted indirectly from the slope, J_{ss}, of the terminal portion of the plot of cumulative amount penetrated *versus* time, through the following equation

$$J_{ss} = K_p \times C_0 \tag{2.12}$$

where C_0 is the drug concentration in the donor compartment. This Equation is readily obtained from Equation (1.1).

2.6 Molecular dynamics simulation

Molecular dynamics (MD) simulations provide, in this work, a route to studying the dynamics of lipid bilayers at the atomistic or near atomistic resolution, with the aim of understanding and predicting the respective macroscopic properties. These can be divided in (i) static equilibrium properties, such as the radial distribution function in a liquid, and (ii) dynamic or non-equilibrium properties, such as the diffusion process in a membrane [85].

MD essentially calculates forces acting on the particles of a single input system, by solving classical Newton's equations of motion,

$$m_i \frac{\partial^2 r_i}{\partial t^2} = F_i, i = 1 \dots N' \qquad\qquad \textbf{(2.13)}$$

with N interacting atoms, to update their positions (r) and velocities. These forces are calculated on the basis of a force field, which provides the functional form and the parameters needed for the calculation of the different potential energy terms.

MD simulations may, therefore, be used to provide insight into the interplay between penetration chemical enhancers and a model lipid membrane, such as dipalmitoylphosphatidylcholine (DPPC), at a level not attainable by experiment [86].

MD trajectories of bilayer systems are generally discussed in terms of standard analyses, such as area per lipid (AL), deuterium order parameter (Scd), probability density profile, radial distribution function (rdf) and mean square displacement (msd).

Information on the area per lipid and deuterium order parameter are frequently used as a starting point to validate the used model. The AL gives an idea of the lateral separation between the lipid heads, while Scd allow to characterize the degree of order along the lipid acyl chains. In this case, the order parameter for each CH2 is proportional to the respective conformational freedom. Additionally, probability density profiles for different key-atom groups return a very complete description of the bilayer structure, elucidating on the vertical positioning of characteristic atom groups relative to the inter-leaflet region. Radial distribution function is a more general analysis that describes the probability of finding a pair of atoms at a distance r apart, relative to the probability expected for a completely random distribution at the same density. Interacting systems are characterized by peaks and valleys describing regions of high and low density, respectively. Among several other applications, this parameter was convenient to assess the ability of water to penetrate bilayer surface. Lastly, mean square displacement is also used to calculate the lateral diffusion of lipid components, as well as the diffusion behavior of other molecules inserted in the bilayer [87].

Once achieved equilibration conditions for the system, many of these parameters are expected to be stable with time, which means that average values can be extracted and used as a rationale for the molecular dynamics. Relevant information on the structuring or disordering effect promoted by each solute can thus be obtained combining information from the different analyses [87].

2.7 Stability

Assessing the physical stability of aqueous lipid nanodispersions involves, among other aspects, the monitoring of the presence of particle aggregation, that may lead to creaming and sedimentation phenomena, as a function of temperature and storage time.

Additionally, lipid modifications might also change the structure of the system, influencing the load and/or release capability, the interfacial properties, and the *in vivo* performance. Thus, the consequences on size control and nanoparticle growth are important for preparing dispersions, and particular attention has to be focused on their evolution. The predictability in administration will also depend on the homogeneity of the product. If precipitation occurs during storage, the quantity of drug delivered for each administration is unknown [57].

Analytical centrifugation

Analytical centrifugation is a technique used to monitor dispersion modifications, that combine the centrifuge force with a NIR detector. Light is passed through the sample cells under centrifugation and the distribution of local transmission is recorded at preset time intervals over the entire sample length. By measuring the intensity of the transmitted NIR light, data are displayed as function of the radial position and as distance from the centre of rotation. The shape and progression of the transmission profiles contain the information on the kinetics of the separation process, as well as evaluation of particle–particle interactions [88].

The separation behavior of the individual samples can be compared and analysed in detail by tracing the variation in transmission at any position within the sample [89].

This technique is helpful in screening formulations, since by submitting samples to stress conditions, it can help predict the respective phase behavior.

Additionally, particle size, zeta potential, and entrapment efficiency measurements should also be monitored as a function of time and storage temperature, so as to complement stability information.

2.8 Cytotoxicity

Skin irritation refers to a reversible inflammatory reaction produced by the arachidonic acid cascade and cytokines in the viable keratinocytes and fibroblasts of the skin, following the application of a test chemical [90, 91]. The assessment of skin irritation has typically involved the use of laboratory animals, particularly rabbits via the

Draize test method [92]. However, due to increasing concern over animal experimentation, validated *in vitro* or *ex vivo* alternative test methods are now being developed, thus avoiding the pain and suffering of animals [93].

Cell culture has been applied as an *in vitro* technique for the assessment of skin irritancy [94]. Skin cultures are useful, because they allow the design of safer, more efficient and cost effective human skin irritation tests. However, despite the advantages of *in vitro* models, it should be noted that cell culture lacks some of the properties of intact skin, such as the selective barrier role or the interaction between different cell types. In any case, and although the irritation potential may be overestimated, these tests may function as a helpful prescreening tool [90, 95, 96].

In spite of the fact that lipid systems, as the ones probed in this work, are usually characterized by a low toxicity, due to their composition based on physiological lipids, especially when compared to other nanoparticulate systems (e.g., polymeric particles), assessment of the potential of skin irritation arising from the surfactants/stabilizers used or drugs incorporated should be performed [25].

In the present work, skin irritation of the optimized formulation was assessed using two cell lines: a spontaneously immortalized human keratinocyte cell line, HaCaT, and human adult dermal fibroblasts cells, Df, aiming at describing the effect upon human epidermis and dermis.

2.9 Pharmacokinetics

After *in vitro* studies, *in vivo* skin permeation data constitute a step further in terms of transdermal system development. A typical pharmacokinetic (PK) profile obtained with a transdermal system (single dose) includes three phases: the time to reach the steady-state plasma concentration (period of onset), the steady-state plateau, and a declining phase post system removal. The plasma concentration *vs.* time profiles allow to extract PK parameters, such as AUC_{0-t} (area under the time concentration curve from time 0 to time t, referring to systemic exposure to drug), $AUC_{0-\phi}$ (area under the time concentration curve from time 0 to infinity), C_{max} (maximal plasma drug concentration), t_{max} (time to maximal plasma drug concentration), and C_{ss} (plasma concentration at steady state) [97]. C_{max} and AUC are useful to characterize the rate and extent of drug delivery (Figure 2.9).
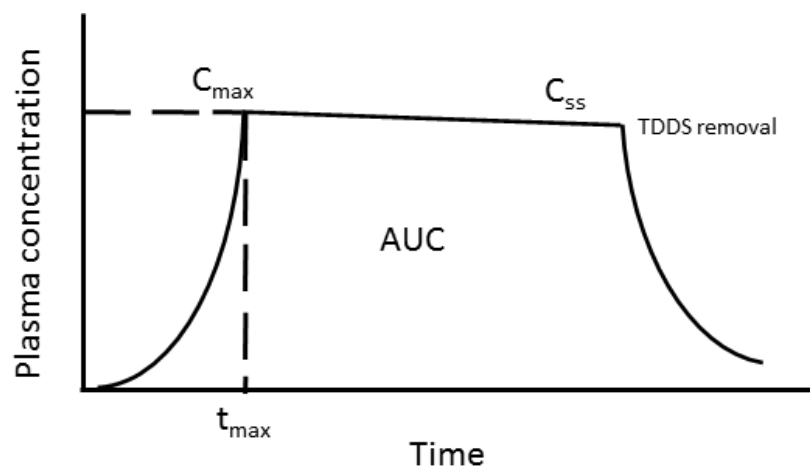
Figure 2.9 Idealized PK profile. Adapted from [98].

Since the TDDS is overloaded with drug in order to maintain a steady-state drug flux over the application time (the Fickian diffusion being the driving force), a large part of the drug TDDS content remains in the TDDS at removal. Therefore, absolute bioavailability is not quite relevant to characterize the TDDS performance. However, it can give an insight of the percentage of the drug that is effectively delivered. The steady-state concentration, C_{ss}, however, is the most relevant PK parameters, because it can give access to the permeation rate provided by the TDDS (and, therefore, allows a comparison with *in vitro* studies). Indeed, since C_{ss} is reached when the steady-state skin absorption rate, *Ra*, equals the steady-state elimination rate, *Re*, the steady-state flux through skin, J_{ss} , can be calculated using the following equation:

$$J_{ss} \times A = C_{ss} \times Cl \tag{2.14}$$

where A is the area of TDDS in contact with the skin, C_{ss} the steady-state plasma concentration (which should correspond to the blood level target for therapeutic efficiency) and Cl the systemic clearance, since Ra = J_{ss} $\times A$ and Re = C_{ss} $\times Cl$, and Ra = Re.

The conditions of application of this equation are that either PK of the drug is linear, or, if such a linearity is unknown, *Cl* has been determined from concentration ranges close to the C_{ss} concentration obtained with the TDDS.

For the *in vivo* experiments, the rat is a commonly used species [78]. Thus, a comprehensive PK study of *in vitro*/*in vivo* relations for animal skin was carried out using rat tissue for the assessment of the feasibility of the developed TDDS (Chapter 4).

References

1. Schwarz, C., W. Mehnert, J.S. Lucks, and R.H. Müller, Solid lipid nanoparticles (SLN) for controlled drug delivery. I. Production, characterization and sterilization. Journal of Controlled Release, 1994. 30(1): p. 83-96.

2. Souto, E.B., S.A. Wissing, C.M. Barbosa, and R.H. Müller, Development of a controlled release formulation based on SLN and NLC for topical clotrimazole delivery. International Journal of Pharmaceutics, 2004. 278(1): p. 71-77.

3. zur Mühlen, A., C. Schwarz, and W. Mehnert, Solid lipid nanoparticles (SLN) for controlled drug delivery – Drug release and release mechanism. European Journal of Pharmaceutics and Biopharmaceutics, 1998. 45(2): p. 149-155.

4. Ugazio, E., R. Cavalli, and M.R. Gasco, Incorporation of cyclosporin A in solid lipid nanoparticles (SLN). International Journal of Pharmaceutics, 2002. 241(2): p. 341-344.

5. Serpe, L., R. Canaparo, M. Daperno, R. Sostegni, G. Martinasso, E. Muntoni, L. Ippolito, N. Vivenza, A. Pera, M. Eandi, M.R. Gasco, and G.P. Zara, Solid lipid nanoparticles as anti-inflammatory drug delivery system in a human inflammatory bowel disease whole-blood model. European Journal of Pharmaceutical Sciences, 2010. 39(5): p. 428-436.

6. Sjöström, B. and B. Bergenståhl, Preparation of submicron drug particles in lecithin-stabilized o/w emulsions I. Model studies of the precipitation of cholesteryl acetate. International Journal of Pharmaceutics, 1992. 88(1–3): p. 53-62.

7. Siekmann, B. and K. Westesen, Investigations on solid lipid nanoparticles prepared by precipitation in o/w emulsions. European Journal of Pharmaceutics and Biopharmaceutics, 1996. 42(2): p. 104-109.

8. Hu, F.Q., H. Yuan, H.H. Zhang, and M. Fang, Preparation of solid lipid nanoparticles with clobetasol propionate by a novel solvent diffusion method in aqueous system and physicochemical characterization. International Journal of Pharmaceutics, 2002. 239(1–2): p. 121-128.

9. Trotta, M., F. Debernardi, and O. Caputo, Preparation of solid lipid nanoparticles by a solvent emulsification–diffusion technique. International Journal of Pharmaceutics, 2003. 257(1–2): p. 153-160.

10. Urban-Morlan, Z., A. Ganem-Rondero, L. Maria Melgoza-Contreras, J. Juan Escobar-Chavez, M. Guadalupe Nava-Arzaluz, and D. Quintanar-Guerrero, Preparation and characterization of solid lipid nanoparticles containing cyclosporine by the emulsification-diffusion method. International Journal of Nanomedicine, 2010. 5: p. 611-620.

11. Gallarate, M., M. Trotta, L. Battaglia, and D. Chirio, Preparation of solid lipid nanoparticles from W/O/W emulsions: Preliminary studies on insulin encapsulation. Journal of Microencapsulation, 2009. 26(5): p. 394-402.

12. Cortesi, R., E. Esposjto, G. Luca, and C. Nastruzzi, Production of lipospheres as carriers for bioactive compounds. Biomaterials, 2002. 23(11): p. 2283-94.

13. Carbone, C., B. Tomasello, B. Ruozi, M. Renis, and G. Puglisi, Preparation and optimization of PIT solid lipid nanoparticles via statistical factorial design. European Journal of Medicinal Chemistry, 2012. 49(0): p. 110-117.

14. Montenegro, L., M.G. Sarpietro, S. Ottimo, G. Puglisi, and F. Castelli, Differential scanning calorimetry studies on sunscreen loaded solid lipid nanoparticles prepared by the phase inversion temperature method. International Journal of Pharmaceutics, 2011. 415(1–2): p. 301-306.

15. Heurtault, B., P. Saulnier, B. Pech, J.-E. Proust, and J.-P. Benoit, A Novel Phase Inversion-Based Process for the Preparation of Lipid Nanocarriers. Pharmaceutical Research, 2002. 19(6): p. 875-880.

16. Kristl, J., B. Volk, M. Gašperlin, M. Šentjurc, and P. Jurkovič, Effect of colloidal carriers on ascorbyl palmitate stability. European Journal of Pharmaceutical Sciences, 2003. 19(4): p. 181-189.

17. Mei, Z., H. Chen, T. Weng, Y. Yang, and X. Yang, Solid lipid nanoparticle and microemulsion for topical delivery of triptolide. European Journal of Pharmaceutics and Biopharmaceutics, 2003. 56(2): p. 189-196.

18. Parhi, R. and P. Suresh, Preparation and characterization of solid lipid nanoparticles-a review. Curr Drug Discov Technol, 2012. 9(1): p. 2-16.

19. Mäder, K. and W. Mehnert, eds. 1 - Solid Lipid Nanoparticles—Concepts, Procedures, and Physicochemical Aspects, Lipospheres in drug targets and delivery: approaches, methods, and applications. ed. C. Nastruzzi2004, CRC Press. 1 - 22.

20. Thassu, D., Nanoparticulate drug delivery systems. Drugs and the pharmaceutical sciences, 1662007, New York [u.a.]: Informa Healthcare. Chapter 14: 213-233.

21. Vitorino, C., F.A. Carvalho, A.J. Almeida, J.J. Sousa, and A.A. Pais, The size of solid lipid nanoparticles: an interpretation from experimental design. Colloids Surf B Biointerfaces, 2011. 84(1): p. 117-30.

22. Silverson: Homogenizing. Available from: http://www.silverson.com/us/process/homogenizing.html, accessed on 27/04/2013.

23. Uner, M., Preparation, characterization and physico-chemical properties of solid lipid nanoparticles (SLN) and nanostructured lipid carriers (NLC): their benefits as colloidal drug carrier systems. Pharmazie, 2006. 61(5): p. 375-86.

24. Hallberg, D., I. Holm, A.L. Obel, O. Schuberth, and A. Wretlind, Fat emulsion for complete intravenous nutrition. Postgrad Med, 1967. 42(5): p. A149-52.

25. Müller, R.H., R. Shegokar, and C.M. Keck, 20 Years of Lipid Nanoparticles (SLN and NLC): Present State of Development and Industrial Applications. Curr Drug Discov Technol, 2011.

26. Mehnert, W. and K. Mäder, Solid lipid nanoparticles Production, characterization and applications. Adv Drug Deliv Rev, 2012.

27. Clarke, A., T. Prescott, A. Khan, and A.G. Olabi, Causes of breakage and disruption in a homogeniser. Applied Energy, 2010. 87(12): p. 3680-3690.

28. Emulsiflex High Pressure Homogenizers. Available from: http://img02.b2b.hc360.com/pic-2/handbook-pic-8/2-8-756328.pdf, accessed on 28/04/2013.

29. Vitorino, C., J. Almeida, L.M. Gonçalves, A.J. Almeida, J.J. Sousa, and A.A.C.C. Pais, Co-encapsulating nanostructured lipid carriers for transdermal application: From experimental design to the molecular detail. Journal of Controlled Release, 2013. 167(3): p. 301-314.

30. Muller, R.H. and C.M. Keck, Challenges and solutions for the delivery of biotech drugs - a review of drug nanocrystal technology and lipid nanoparticles. Journal of Biotechnology, 2004. 113(1-3): p. 151-170.

31. Lippacher, A., R.H. Müller, and K. Mäder, Investigation on the viscoelastic properties of lipid based colloidal drug carriers. International Journal of Pharmaceutics, 2000. 196(2): p. 227-230.

32. Zetasizer Nano ZS Available from: http://www.malvern.com/labeng/technology/dynamic_light_scattering/dynamic_light_scattering.htm, accessed on 28/04/2013.

33. ISO13321, Methods for Determination of Particle Size Distribution Part 8: Photon Correlation Spectroscopy, International Organisation for Standardisaton (ISO). 1996.

34. Delsa™Nano C. Available from: https://www.beckmancoulter.com/wsrportal/wsr/industrial/products/zeta-potential-and-submicron-particle-size-analyzer/delsanano-c/index.htm, accessed on 28/04/2013.

35. Malvern - Dynamic Light Scattering: An Introduction in 30 Minutes. Available from: http://chemikalie.upol.cz/skripta/msk/MRK656.pdf, accessed on 28/04/2013.

36. Xu, R., Progress in nanoparticles characterization: Sizing and zeta potential measurement. Particuology, 2008. 6(2): p. 112-115.

37. Malvern - Dynamic light scattering: Common terms defined. Available from: http://www.biophysics.bioc.cam.ac.uk/wp-content/uploads/2011/02/DLS_Terms_defined_Malvern.pdf, accessed on 28/04/2013.

38. Brar, S.K. and M. Verma, Measurement of nanoparticles by light-scattering techniques. TrAC Trends in Analytical Chemistry, 2011. 30(1): p. 4-17.

39. Gaumet, M., A. Vargas, R. Gurny, and F. Delie, Nanoparticles for drug delivery: The need for precision in reporting particle size parameters. European Journal of Pharmaceutics and Biopharmaceutics, 2008. 69(1): p. 1-9.

40. Doktorovova, S. and E.B. Souto, Nanostructured lipid carrier-based hydrogel formulations for drug delivery: A comprehensive review. Expert Opinion on Drug Delivery, 2009. 6(2): p. 165-176.

41. Jores, K., W. Mehnert, M. Drechsler, H. Bunjes, C. Johann, and K. Mäder, Investigations on the structure of solid lipid nanoparticles (SLN) and oil-loaded solid lipid nanoparticles by photon correlation spectroscopy, field-flow fractionation and transmission electron microscopy. Journal of Controlled Release, 2004. 95(2): p. 217-227.

42. Müller, R.H., K. Mäder, and S. Gohla, Solid lipid nanoparticles (SLN) for controlled drug delivery - a review of the state of the art. European Journal of Pharmaceutics and Biopharmaceutics, 2000. 50(1): p. 161-177.

43. Goldstein, J., Scanning electron microscopy and x-ray microanalysis2003: Springer London, Limited.

44. Reimer, L. and H. Kohl, Transmission Electron Microscopy: Physics of Image Formation2008: Springer.

45. Duclairoir, C. and E. Nakache, Polymer Nanoparticle Characterization in Aqueous Suspensions. International Journal of Polymer Analysis and Characterization, 2002. 7(4): p. 284-313.

46. Mühlen, A.z., E.z. Mühlen, H. Niehus, and W. Mehnert, Atomic Force Microscopy Studies of Solid Lipid Nanoparticles. Pharmaceutical Research, 1996. 13(9): p. 1411-1416.

47. Wilson, R. and H. Bullen. Basic Theory: Atomic Force Microscopy (AFM). Available from: /http://asdlib.org/onlineArticles/ecourseware/Bullen/SPMModule_BasicTheoryAFM.pdf, accessed on 29/04/2013.

48. Ruozi, B., G. Tosi, F. Forni, M. Fresta, and M.A. Vandelli, Atomic force microscopy and photon correlation spectroscopy: Two techniques for rapid characterization of liposomes. European Journal of Pharmaceutical Sciences, 2005. 25(1): p. 81-89.

49. Dubes, A., H. Parrot-Lopez, W. Abdelwahed, G. Degobert, H. Fessi, P. Shahgaldian, and A.W. Coleman, Scanning electron microscopy and atomic force microscopy imaging of solid lipid nanoparticles derived from amphiphilic cyclodextrins. European Journal of Pharmaceutics and Biopharmaceutics, 2003. 55(3): p. 279-282.

50. West, P.E., Introduction to Atomic Force Microscopy: Theory, Practice, Applications2006: P. West.

51. Malvern - Zeta Potential: An Introduction in 30 Minutes. Available from: http://www.nbtc.cornell.edu/facilities/downloads/Zeta%20potential%20-%20An%20introduction%20in%2030%20minutes.pdf, accessed on 30/04/2013.

52. Beckman Coulter, Delsa™Nano C - Zeta Potential: Determination by Electrophoretic Light Scattering. Available from: https://www.beckmancoulter.com/wsrportal/wsr/industrial/products/zeta-potential-and-submicron-particle-size-analyzer/delsanano-c/index.htm, accessed on 30/04/2013.

53. Dong, M.W., Modern HPLC for Practicing Scientists2006: Wiley.

54. Gill, P., T.T. Moghadam, and B. Ranjbar, Differential scanning calorimetry techniques: applications in biology and nanoscience. J Biomol Tech, 2010. 21(4): p. 167-93.

55. Höhne, G., W.F. Hemminger, and H.J. Flammersheim, Differential Scanning Calorimetry2003: Springer.

56. Brown, M.E., Handbook of Thermal Analysis and Calorimetry: Principles and Practice1998: Elsevier Science.

57. Heurtault, B., P. Saulnier, B. Pech, J.-E. Proust, and J.-P. Benoit, Physico-chemical stability of colloidal lipid particles. Biomaterials, 2003. 24(23): p. 4283-4300.

58. Jannin, V., J. Musakhanian, and D. Marchaud, Approaches for the development of solid and semi-solid lipid-based formulations. Advanced Drug Delivery Reviews, 2008. 60(6): p. 734-746.

59. Smith, B.C., Fundamentals of Fourier Transform Infrared Spectroscopy, Second Edition2011: Taylor & Francis.

60. Wartewig, S. and R.H.H. Neubert, Pharmaceutical applications of Mid-IR and Raman spectroscopy. Advanced Drug Delivery Reviews, 2005. 57(8): p. 1144-1170.

61. Lin, X., X. Li, L. Zheng, L. Yu, Q. Zhang, and W. Liu, Preparation and characterization of monocaprate nanostructured lipid carriers. Colloids and Surfaces A: Physicochemical and Engineering Aspects, 2007. 311(1-3): p. 106-111.

62. Hadgraft, J. and M.E. Lane, Skin Permeation: Spectroscopic Methods, in Transdermal and Topical Drug Delivery2011, John Wiley & Sons, Inc. p. 155-166.

63. Dejaegher, B. and Y. Vander Heyden, Experimental designs and their recent advances in set-up, data interpretation, and analytical applications. Journal of Pharmaceutical and Biomedical Analysis, 2011. 56(2): p. 141-158.

64. Factorial Design of Experiments, in Pharmaceutical Experimental Design and Interpretation, 2nd Edition2006, Informa Healthcare. p. 83-133.

65. Tauler, R. and S.D. Brown, Comprehensive Chemometrics: Chemical and Biochemical Data Analysis. Vol. Chapter 7. 2009: Elsevier Science.

66. Dejaegher, B. and Y. Vander Heyden, The use of experimental design in separation science. Acta Chromatographica, 2009. 21(2): p. 161-201.

67. Souto, E.B., S.A. Wissing, C.M. Barbosa, and R.H. Müller, Evaluation of the physical stability of SLN and NLC before and after incorporation into hydrogel formulations. European Journal of Pharmaceutics and Biopharmaceutics, 2004. 58(1): p. 83-90.

68. Bhaskar, K., J. Anbu, V. Ravichandiran, V. Venkateswarlu, and Y.M. Rao, Lipid nanoparticles for transdermal delivery of flurbiprofen: formulation, in vitro, ex vivo and in vivo studies. Lipids Health Dis, 2009. 8(6): p. 8-6.

69. Macosko, C.W., Rheology - Principles, Measurements and Applications, 1994, John Wiley & Sons.

70. Mezger, T.G., The Rheology Handbook: For Users of Rotational and Oscillatory Rheometers2006: Vincentz Network.

71. Antunes, F.E., Mixed Solutions of Polymers and Surfactants: Relation between Rheology and Nanostructure, in Department of Chemistry2006, University of Coimbra.

72. Holmberg, K., B. Jönsson, B. Kronberg, and B. Lindman, An Introduction to the Rheology of Polymer and Surfactant Solutions, in Surfactants and Polymers in Aqueous Solution2003, John Wiley & Sons, Ltd. p. 317-335.

73. Silva, S.M.C., F.V. Pinto, F.E. Antunes, M.G. Miguel, J.J.S. Sousa, and A.A.C.C. Pais, Aggregation and gelation in hydroxypropylmethyl cellulose aqueous solutions. Journal of Colloid and Interface Science, 2008. 327(2): p. 333-340.

74. Jones, D.S., A.D. Woolfson, and A.F. Brown, Textural Analysis and Flow Rheometry of Novel, Bioadhesive Antimicrobial Oral Gels. Pharmaceutical Research, 1997. 14(4): p. 450-457.

75. Jones, D.S., A.D. Woolfson, and J. Djokic, Texture profile analysis of bioadhesive polymeric semisolids: Mechanical characterization and investigation of interactions between formulation components. Journal of Applied Polymer Science, 1996. 61(12): p. 2229-2234.

76. Hurler, J., A. Engesland, B. Poorahmary Kermany, and N. Škalko-Basnet, Improved texture analysis for hydrogel characterization: Gel cohesiveness, adhesiveness, and hardness. Journal of Applied Polymer Science, 2012. 125(1): p. 180-188.

77. OECD, Test No. 428: Skin Absorption: In Vitro Method: OECD Publishing.

78. Co-operation, O.f.E., D.J.M.o.t.C. Committee, P. the Working Party on Chemicals, and Biotechnology, Guidance Document for the Conduct of Skin Absorption Studies2004: OECD, Environment Directorate.

79. <725> Topical and Transdermal Drug Products—Product Performance Tests. Available from: http://www.usp.org/sites/default/files/usp_pdf/EN/USPNF/transdermalGenChapter725.pdf, accessed on 03/05/2013.

80. Heather, A.E.B., Adam C. Watkinson, Topical and Transdermal Drug Delivery - Principles and Practice. Wiley, 2012. 5th Chapter: In vitro Skin Permeation Methodology: p. 85-108.

81. Kenneth, W., W. Adam, and B. Keith, Methods for Studying Percutaneous Absorption, in Dermatological and Transdermal Formulations2002, Informa Healthcare.

82. OECD, GUIDANCE NOTES ON DERMAL ABSORPTION. DRAFT 22 OCTOBER 2010.

83. Finnin, B., K.A. Walters, and T.J. Franz, In Vitro Skin Permeation Methodology, in Transdermal and Topical Drug Delivery2011, John Wiley & Sons, Inc. p. 85-108.

84. Li, S.K., W. Suh, H.H. Parikh, A.-H. Ghanem, S.C. Mehta, K.D. Peck, and W.I. Higuchi, Lag time data for characterizing the pore pathway of intact and chemically pretreated human epidermal membrane. International Journal of Pharmaceutics, 1998. 170(1): p. 93-108.

85. GROMACS User Manual version 4.6. Available from: http://www.gromacs.org/@api/deki/files/189/=manual-4.6.pdf, accessed on 04/05/2013.

86. Gurtovenko, A.A. and J. Anwar, Modulating the Structure and Properties of Cell Membranes: The Molecular Mechanism of Action of Dimethyl Sulfoxide. The Journal of Physical Chemistry B, 2007. 111(35): p. 10453-10460.

87. Vattulainen, I., M. Karttunen, and H.y.H.I.o. Physics, Modeling of Biologically Motivated Soft Matter Systems2004: Helsinki Institute of Physics, University of Helsinki.

88. Chiu, H.-T., C.-Y. Chang, T.-Y. Chiang, M.-T. Kuo, and Y.-H. Wang, Using analytical centrifugation to characterize the dispersibility and particle size distributions of organic/inorganic composite coatings. Journal of Polymer Research, 2011. 18(6): p. 1587-1596.

89. Sobisch, T. and D. Lerche, Thickener performance traced by multisample analytical centrifugation. Colloids and Surfaces A: Physicochemical and Engineering Aspects, 2008. 331(1–2): p. 114-118.

90. Sanchez, L., M. Mitjans, M.R. Infante, and M.P. Vinardell, Assessment of the Potential Skin Irritation of Lysine-Derivative Anionic Surfactants Using Mouse Fibroblasts and Human

Keratinocytes as An Alternative to Animal Testing. Pharmaceutical Research, 2004. 21(9): p. 1637-1641.

91. Moreno, J.J., Arachidonic acid release and prostaglandin E2 synthesis as irritant index of surfactants in 3T6 fibroblast cultures. Toxicology, 2000. 143(3): p. 275-282.

92. Draize, J.H., G. Woodard, and H.O. Calvery, Methods for the study of irritation and toxicity of substances applied topically to the skin and mucous membranes. J.Pharmacol.Exp.Ther., 1944. 8: p. 377-390.

93. Test No. 439: In Vitro Skin Irritation: Reconstructed Human Epidermis Test Method. OECD Guidelines for the Testing of Chemicals, 2010. 1(4): p. 1-18.

94. van de Sandt, J., P. Roguet, C. Cohen, D. Esdaile, M. Ponec, E. Corsini, C. Barker, N. Fusenig, M. Liebsch, D. Benford, A.D. de Fraissinette, and M. Fartasch, The use of human keratinocytes and human skin models for predicting skin irritation - The report and recommendations of ECVAM Workshop 38. Atla-Alternatives to Laboratory Animals, 1999. 27(5): p. 723-743.

95. Eun, H.C. and D.H. Suh, Comprehensive outlook of in vitro tests for assessing skin irritancy as alternatives to Draize tests. Journal of Dermatological Science, 2000. 24(2): p. 77-91.

96. Lawrence, J.N., Application of in vitro human skin models to dermal irritancy: a brief overview and future prospects. Toxicology in Vitro, 1997. 11(3): p. 305-312.

97. Farahmand, S. and H.I. Maibach, Transdermal drug pharmacokinetics in man: Interindividual variability and partial prediction. International Journal of Pharmaceutics, 2009. 367(1–2): p. 1-15.

98. Miller, K.J., Transdermal Product Formulation Development, in Transdermal and Topical Drug Delivery2011, John Wiley & Sons, Inc. p. 287-308.

Chapter 3

Optimization of solid lipid nanoparticles by solvent emulsification-evaporation

3.1 Introduction

Solid lipid nanoparticles are systems of remarkable technological relevance from a pharmaceutical perspective. The production of SLN can be carried out using different methods, including high shear homogenization, ultrasound, high pressure homogenization, or via microemulsion and solvent emulsification-evaporation techniques, as discussed in Chapter 2. Some of these can be combined in order to obtain stable particles, with suitable properties, such as particle size and size distribution [1, 2]. Since skin hydration and the occlusion effect depend on the small size of lipid nanoparticles, these characteristics are crucial in SLN production, and result from both the preparation method and, to a larger extent, the particle composition [3].

In the work presented in this chapter [4], SLN production was studied using a modified solvent emulsification-evaporation method, in which high shear homogenization and ultrasound were also employed. The aim was to systematically assess how different parameters, such as lipid type and concentration, amount of solvent, emulsifier type and concentration, influence the size of solid lipid nanoparticles. This has been addressed using a factorial analysis, which allows not only to extract the maximum amount of information from the collected data, resorting to a limited number of experiments, but also to establish the influence of multiple factors on the formulation properties. The direct effect of each factor was studied, and the respective interaction with other factors was also assessed in detail. Designs in different factor domains were additionally carried out, in order to describe the system behavior under different compositions. A detailed physicochemical characterization of the systems and a rationale for the observations are

also provided. It should be noted that the usefulness of experimental design in the formulation of lipid nanoparticles (see e.g., ref. [5]) is being increasingly acknowledged.

SLN loaded with simvastatin, as a model of a poorly water-soluble drug, were firstly prepared. Its influence on particle size, zeta potential and entrapment efficiency in the previously optimized formulation was also assessed.

3.2 Materials and methods

3.2.1 Materials

Glyceryl tripalmitate (tripalmitin, T8127, melting point 66ºC) was purchased from Sigma, Compritol® 888 ATO (glyceryl behenate, melting point: 71–74 ∘C), and Precirol® ATO 5 (glyceryl palmitostearate, melting point: 53–56 ∘C) were kindly provided by Gattefossé (Saint-Priest, France). Polyvinyl alcohol 87-89% hydrolyzed (PVA, typical MW 13.000-23.000) and polysorbate 80 (Tween® 80) were purchased from Sigma-Aldrich. Simvastatin was kindly provided by Labesfal - Laboratórios Almiro, S.A. (Santiago de Besteiros, Portugal). All other chemicals were of analytical grade or equivalent. Water was purified (Millipore®) and filtered through a 0.22 µm nylon filter before use.

3.2.2 Preparation of SLN

The SLN were prepared using a modification of the widely used emulsification-solvent evaporation method described elsewhere [2]. Briefly, the lipid was dissolved in dichloromethane (DCM) and then added dropwise to 30 mL of emulsifier solution in a high shear homogenizer (L5M-A, Silverson, UK) at 12 300 rpm for 7 min. In the final, optimized, method of preparation, the inner lipid phase was added dropwise to the external phase under ultra-sonication (40W, 5 min; Branson, Sonifier 250). The pre-dispersion obtained was then high-shear homogenized (12 300 rpm, 7 min). The dispersion obtained in both cases was then magnetically stirred at 200 rpm for 4 h, in order to allow the solvent evaporation. In the drug loaded SLN, the lipid and simvastatin were dissolved in DCM, and subjected to the conditions described above.

3.2.3 Dynamic light scattering

Particle size was determined by dynamic light scattering, which yields the mean particle size (Z-average), and the polydispersity index, which measures the width of the size distribution. DLS was performed with Zetasizer Nano S (Malvern Instruments,

Malvern, UK) at a detection angle of 173º, at 25ºC. Samples were suitably diluted in ultrapurified water. Each value was measured in triplicate. The results are shown as mean ± standard deviation.

3.2.4 Zeta potential

ZP was determined using a Zetasizer 2000 (Malvern Instruments, Malvern, UK) at 25ºC. For the measurements, samples were diluted appropriately with ultrapurified water (pH≈5.5).

3.2.5 Factorial design

An experimental design with a two-level, three-variable, 2^k full factorial planning was performed for the optimization of the particles composition. The experimental design and the polynomial models were solved resorting to the GNU Octave software [6], with specific programs developed by the authors. The mathematical model

$$D = \beta_0 + \beta_1 x_1 + \beta_2 x_2 + \beta_3 x_3 + \beta_{12} x_1 x_2 + \beta_{23} x_2 x_3 + \beta_{13} x_1 x_3 \qquad \textbf{(3.1)}$$

was applied in two different situations, to describe the principal effects and interactions among the identified variables. Coded (-1, +1) levels were used for each independent variable, x_1, x_2, and x_3, in which the -1 level corresponds to the lower value of each variable and +1 to the upper one. The choice of these limits was based on acceptable domains for each variable, considering a therapeutic application, and the optimization procedure was carried out within these domains. In Equation (**3.1**), β_0 is the arithmetic mean response, β_1–β_3 are the coefficients of the respective independent variables and β_{12}, β_{23} and β_{13} their respective interaction terms, and D, the mean particle size, is the dependent variable or response. ANOVA and Student's t-test were applied to test the fitted models. Statistical analysis was considered significant if the p values were less than 0.05.

3.2.6 Laser diffractometry

Laser diffractometry (LD) was additionally performed in order to detect the presence of microparticles, using a laser diffraction particle size analyzer (Beckman Coulter® LS 13 320, Miami, Florida) with polarization intensity differential scattering (PIDS). The real refractive index and the imaginary refractive index were set to 1.54 and 0.1, respectively. The LD data were expressed using volume distributions, and given as diameter values corresponding to percentiles of 10%, 50%, and 90%. The span value is a statistical

parameter useful to characterize the particle size distribution, and was calculated using [7]

$$Span = \frac{d90\% - d10\%}{d50\%}$$ (**3.2**)

A high value of span indicates a wide size distribution and a high polydispersity.

3.2.7 Determination of residual PVA

The amount of residual PVA associated with the SLN surface was determined using a colorimetric method based on the formation of a colored complex between adjacent hydroxyl groups of PVA and an iodine molecule [8]. For this determination, only a few formulations were selected. Briefly, a 250 µL volume of the nanosuspensions was ultrafiltered-centrifuged for 30 minutes through Amicon® Ultra-4 centrifugal filter units (100KDa MWCO, Millipore, Ireland) and 50 µL of the particles collected in the inner chamber were treated with 2 mL of 0.5 M NaOH for 15 min at 60 ºC. Each sample was neutralized with 900 µL of 1 N HCl and the volume was adjusted to 5 mL with distilled water. To each sample, 3 mL of a 0.65 M solution of boric acid, and 0.5 mL of a solution of I_2/KI (0.05 M/ 0.15 M) were added. The final volume was adjusted to 10 mL with distilled water. Finally, the absorbance was measured at 690 nm after 15 min incubation at room temperature. A standard curve for PVA was prepared under identical conditions.

3.2.8 Differential scanning calorimetry

The crystal structure was inferred from the thermal behavior of the tripalmitin SLN using DSC equipment (Pyris 1 DSC, Perkin-Elmer, Massachusetts, USA). Lyophilized SLN (1.5-2.5 mg) were placed in aluminium pans and hermetically sealed. Empty pans were used as reference. The individual components of SLN were also analysed as raw materials. Each sample was heated from 10ºC to 80ºC, at 10ºC/min, and then cooled down to 10ºC at the same rate. A physical mixture of the components was also analysed as a control.

3.2.9 Attenuated total reflectance infrared spectroscopy

In order to obtain information about the structure of the particles, ATR infrared spectra of the particles were recorded using an FT-IR/FT-NIR spectrometer (Spectrum 400, Perkin-Elmer, Massachusetts, USA) with an ATR accessory fitted with a Zn-Se crystal plate. Lyophilized samples were placed in the ATR device without previous

treatment, and measured using 4 scans for each spectrum, with a resolution of 1 cm^{-1} and a scan speed of 0.5. Spectra were collected between 4000 and 650 cm^{-1}.

3.2.10 Atomic force microscopy

A NanoWizard II equipment *(JPK Instruments, Germany)* mounted on the top of an Axiovert 200 inverted microscope (Carl Zeiss, Germany) was used for imaging and atomic force spectroscopy experiments. The AFM head is equipped with a 15 µm z-range linearized piezoelectric scanner and an infrared laser. The SLN optimized formulation was diluted in ultrapurified water (1:100) and deposited on a poly-L-lysine treated glass slide. After approximately 20 min, the preparation was washed with ultrapurified water and air-dried.

SLN imaging was performed in air by tapping mode. Oxidized sharpened silicon tips with a tip radius of 6 nm, resonant frequency of about 60 kHz and a spring constant of 3 N/m were used for imaging. Imaging parameters were adjusted to minimize the force applied on the scanning of the nanoparticles topography. This low force is particularly useful to study soft or easily deformable samples. Imaging data were analyzed with the JPK image processing v.3 (JPK Instruments, Germany).

3.2.11 Scanning electronic microscopy

The SEM analysis was also performed in order to investigate the morphological characteristics of the particles. Prior to analysis, the sample was diluted with ultrapurified water, placed on a double-side carbon tape mounted onto an alumium stud, and dried in a desiccator. The sample was then sputter coated with gold in order to make it conducting. SEM images were recorded on a Jeol, JSM 5310, (Tokyo, Japan) scanning electron microscope, with an acceleration voltage of 25kV.

3.2.12 Fluorescence microscopy

The Nile red (NR) staining assay was used to confirm the SLN particle size. A stock solution of NR 0.5 mg/mL in acetone was previously prepared. Subsequently, a working solution was obtained by adding 0.05 mL of stock solution to 50 mL of a 75:25 glycerol-water mixture. A drop of the working solution was added to the particles. The SLN were observed using an Olympus BX51 M microscope, equipped with a UplanFL N 100×/1.30 oil-immersion objective lens (∞/0.17/FN26.5) and a filter set type MNIBA3 (470-495 nm excitation and 505 nm dichromatic mirror). Images were scanned to a computer through a video camera (Olympus digital camera DP70) and analyzed with an image processor

(Olympus DP Controller 2.1.1.176, Olympus DP Manager 2.1.1.158). All observations were carried out at 25 ⁰C.

3.2.13 Stability studies

The optimized SLN formulation (see below) was studied for stability at 4⁰C and 25⁰C. PCS particle size and zeta potential values were monitored for a period of 6 months. The stability of the formulation was also assessed using the LUMiFuge (L.U.M.GmbH, Germany) stability analyzer, which measures the intensity of transmitted near infrared (NIR) light over the full length of the sample, as a function of time. All data are stored and displayed in real time as a function of radial position, thus enabling analysis at the micron level, signaling changes in the dispersion characteristics. The separation behavior of individual samples can be compared and measured in detail by detecting changes in light transmission at any part of the sample, or by following the movement of any phase boundary [9]. The formulation stability was analyzed after 126 minutes of centrifugation, at an acceleration of 2600 x g and 20⁰C.

3.2.14 Entrapment efficiency and drug loading

The simvastatin entrapment efficiency was determined indirectly by measuring the concentration of the free drug in the aqueous phase of the nanoparticle dispersion. The ultrafiltration-centrifugation method was carried out through centrifugal filters (Amicon® Ultra-4, Millipore, Germany) with a 100 kDa molecular weight cut-off. Briefly, 1 mL of SLN loaded with simvastatin plus 1 mL of methanol were placed into the upper chamber of the centrifuge filter, which was centrifuged at 4,000 x g for 90 min at 4⁰C. Methanol was added in order to dissolve crystals possibly present in the external phase of the SLN dispersion. The amount of free drug in the aqueous dispersion phase, collected in the outer chamber of the centrifugal filter after separation, was determined by high performance liquid chromatography (HPLC) as described below. The entrapment efficiency (EE) and drug loading (DL) of SV nanoparticles were calculated according to Equations (2.3) and (2.4), wherein $W_{total\ drug}$' refers to the amount of SV initially used for the assay.

3.2.15 HPLC determination of simvastatin

The HPLC analysis was carried out by a Shimadzu LC-2010CHT apparatus equipped with a quaternary pump, an autosampler unit, and a L2450 UV/Visible dual wavelength detector. A RP18 (4.6mm×125mm) Lichrospher® 100 analytical column

(Merck KGaA, Germany) was used for the analysis. The mobile phase consisted of a 90:10 (v/v) mixture of methanol/water pumped and a constant flow rate of 0.8 mL/min was used for 5 min. The detection was carried out at 238 nm. An injection volume of 10 µL was used for all standards and samples. For these conditions, simvastatin is eluted at a retention time of 3.1 min.

3.3 Results and discussion

Before the experimental design was constructed, preliminary formulation studies included the selection of the appropriate lipid phase and emulsifier type, and are described in what follows.

3.2.16 Preliminary factor screening

The effect in particle size of three different lipids was studied using Precirol®, tripalmitin and Compritol® (Table 3.1). Tripalmitin was chosen due to the smaller particle size and narrow size distribution of the resulting SLN.

Table 3.1 Mean particle size (Z-average) of formulations containing Precirol®, Compritol®, and tripalmitin. Values are indicated for 5 mL DCM/250 mg lipid (ratio 1:50) and 1 mL DCM/100 mg lipid (ratio 1:100) preparations. A concentration of 1.25% (w/V) of the emulsifier was used.

Formulation	Z-av. (nm)	PI	Formulation	Z-av. (nm)	PI	Formulation	Z-av. (nm)	PI
Precirol® 1:100 Tween®80	754.1	0.746	Compritol® 1:100 Tween®80	1402.0	0.325	Tripalmitin 1:100 Tween®80	1642.0	0.878
Precirol® 1:100 PVA	1253.0	0.523	Compritol® 1:100 PVA	838.0	0.516	Tripalmitin 1:100 PVA	602.7	0.595
Precirol® 5:250 Tween®80	403.5	0.820	Compritol® 5:250 Tween®80	1321.0	0.635	Tripalmitin 5:250 Tween®80	542.5	1.000
Precirol® 5:250 PVA	908.9	0.483	Compritol® 5:250 PVA	728.8	0.402	Tripalmitin 5:250 PVA	253.0	0.314

The choice of the emulsifier is of utmost importance in the optimization of any nanoparticles formulation. This component contributes not only to control the particle size and stability of the dispersions, but also to control the crystallization behaviour, including polymorphs [2, 10]. The effect upon particle size of two different emulsifiers, polysorbate 80 (Tween® 80) and polyvinyl alcohol (PVA) was studied, indicating that PVA generally leads to smaller particles with narrower particle size distributions (Figure 3.1), which has prompted experiments to be carried out within a broader emulsifier concentration range.
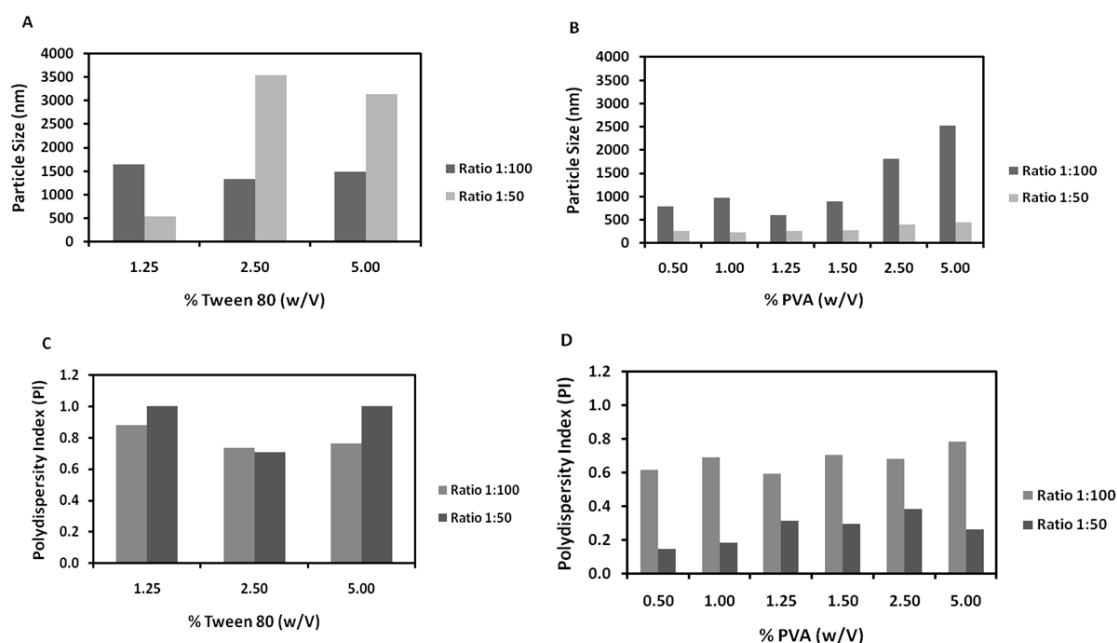
Figure 3.1 Mean size of particles and polydispersity indexes (PI) in formulations containing Tween® 80 (A and C) and PVA (B and D), as a function of emulsifier concentration. Values are indicated for 5 ml DCM/250 mg lipid (ratio 1:50) and 1 ml DCM/100 mg lipid (ratio 1:100) preparations.

3.2.17 Factorial design

The preliminary results clearly indicated that this system is highly influenced by the lipid type, emulsifier type and concentration. It should be noted that these are widely recognized as major factors influencing the size of SLN [1]. In this design, the lipid and emulsifier types were imposed (tripalmitin and PVA), as a consequence of the preliminary results, constituting the lipid concentration the first design variable. The solvent:lipid ratio represented the second variable, and the emulsifier concentration the third one.

The choice of variables is a task of paramount importance, because it conditions both results and interpretation. The choice must be based on the particular characteristics of the system. The current option was to use one composition variable, the lipid concentration, that establishes a relationship between the inner phase and the system as a whole and, implicitly, between the inner and external phases. The emulsifier concentration also uses the whole system as reference, and the respective choice was based on the fact that the emulsifier is an interface component, which can be found in both the inner and external phases. Finally, the influence of the solvent was assessed through the solvent:lipid ratio, as selected variable. As such, it allowed the characterization of the inner phase, and focused, implicitly, on the respective properties (the amount of lipid dissolved per volume of organic solvent influences, for example, the viscosity, at least in the initial stages of the particle formation).

Table 3.2 describes the composition of SLN, prepared according to a double 2^3 factorial planning. It includes a low, a medium and a high level of the lipid phase concentration, that are combined in a low/medium (L1 to M6) and a medium/high (M1 to L4) designs. Combining the information of the two designs, a general approach can be extracted from the first one, in which a wider particle size range is presented, while in the second one a fine tuning of the optimization can be performed. For the factorial designs, M2 and M5 formulations were not included. These additional experiments were carried out in order to complete the formulation optimization process (see below).

Table 3.2 SLN composition for the different levels considered in the two 2^3 factorial designs. Key: L, lower level; M, middle level; H, higher level of lipid phase concentration. Composition: $Weight_{lipid}:Volume_{DCM}:Concentration_{(\%w/V)PVA}$; Ratio: $Volume_{DCM}:Weight_{lipid}$; PI: Polydispersity Index. Results include standard deviation (n=3).

Formulation	Composition ($W_{lipid}{}^a:V_{DCM}:C_{PVA}$)	Ratio $W_{DCM}:V_{lipid}$	Particle Size (nm)	PI	Zeta Potential (mV)
L1	100:1:0.5	1:100	789±80	0.618	-17.9±0.5
L2	100:1:1.5	1:100	892±64	0.707	-16.1±0.4
L3	100:2:0.5	1:50	287±34	0.330	-17.5±0.6
L4	100:2:1.5	1:50	334±13	0.367	-16.0±0.5
M1	250:2.5:0.5	1:100	261.±5	0.240	-26.2±0.2
M2	250:2.5:1	1:100	300±14	0.385	-35.3±0.6
M3	250:2.5:1.5	1:100	437.±7	0.506	-26.0±0.6
M4	250:5:0.5	1:50	264.±4	0.145	-28.67±0.06
M5	250:5:1	1:50	226.±3	0.187	-36.2±0.4
M6	250:5:1.5	1:50	275.±3	0.295	-24.6±0.9
H1	500:5:0.5	1:100	300.±3	0.175	-19.33±0.06
H2	500:5:1.5	1:100	296.4±0.8	0.307	-16.0±0.3
H3	500:10:0.5	1:50	380.9±1.3	0.268	-18.3±0.4
H4	500:10:1.5	1:50	269.±3	0.226	-15.4±0.6

[a]Note that, in this table, the total weight of the lipid is used for simplicity. The formal values for lipid concentration (w/V) are, respectively, 0.33%, 0.83%, and 1.67% for the L, M and H levels (see also Table III).

The lipid concentration, solvent:lipid ratio and emulsifier concentration are denoted respectively as x_1, x_2 and x_3 in Equation (3.1), and the combined terms describe the respective interaction. Table 3.3 defines the coded values.

Table 3.3 Coding of factorial design variables.

Factorial design	Coded level	Lipid Weight/Solvent:Lipid Ratio/Emulsifier Concentration
L/M	-1	100/1:100/0.5%
	+1	250/1:50/1.5%
M/H	-1	250/1:100/0.5%
	+1	500/1:50/1.5%

In order to evaluate the influence of each variable, and the respective combination in the response term, the polynomial coefficients of Equation (3.1) were determined. The higher the magnitude of each coefficient, the higher is the respective main effect on the system. A positive coefficient sign indicates that an increase in the parameter level leads to an increase in particle size. Taking into account the interaction coefficients, the response must be analysed in terms of how the variation of one factor modulates the effect of another factor. To illustrate this point, consider the coefficient for variable 1, affected by the interaction with variable 2 (and neglecting other possible interaction terms),

$$(\beta_1 + \beta_{12}x_2)x_1$$

If we take $\beta_{12}>0$ and $x_2<0$, three situations are possible, depending on the value of β_1:

i)   for $\beta_1<0$, the interaction reinforces the negative effect of x_1;

ii)   for $\beta_1>0$, and $\beta_1 > |\beta_{12}x_2|$, the influence of x_1 decreases;

iii)   for $\beta_1>0$, and $\beta_1 < |\beta_{12}x_2|$, the effect of x_1 is reversed in signal.

A similar reasoning can be presented for $x_2>0$, or in case $\beta_{12}<0$. When the number of interaction terms increases, the analysis becomes more complicated but proceeds along the same lines.

Table 3.4 gathers the values of the coefficients obtained for the low/medium and medium/high designs, as well as the corresponding levels of confidence, while Figure 3.2 displays the response surfaces as a function of the major factors for the two designs under consideration. To test whether the terms were statistically significant in the regression model, t-tests were performed using a 95% (α=0.05) level of significance. The Student's t-test analysis shows that the parameters are highly significant, with the single exception of the β_{13} interaction coefficient for the medium/high design. Additionally, ANOVA results are gathered in Table 3.5, as a further characterization of the fittings.

Table 3.4 Parameters of the response surfaces for size obtained from a 2^3 factorial planning in the indicated formulations and Student's t-test analysis.

Formulations	β_0	β_1	β_2	β_3	β_{12}	β_{23}	β_{13}
L1 to M6	442.2	-133.0	-152.4	42.3	112.6	-27.7	4.6
Significance level	100.0	46.6	100.0	100.0	100.0	100.0	100.0
t	53.2	-16.0	-18.3	5.1	13.6	-3.3	0.6
M1 to H4	310.4	1.2	-13.3	8.9	26.5	-34.2	-37.9
Significance level	100.0	100.0	100.0	100.0	100.0	99.6	41.2
t	164.2	0.6	-7.0	4.7	14.0	-18.1	-20.1
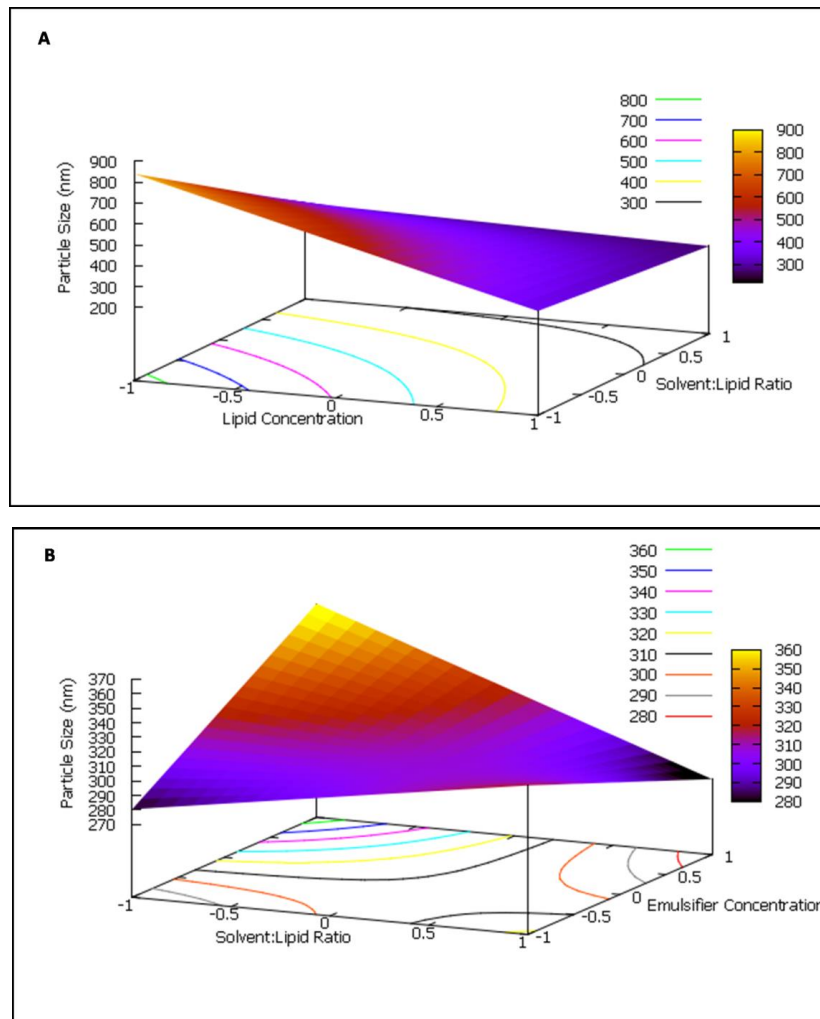
Figure 3.2 Particle size response surfaces for the two more significant factors at each fitted mathematical model. a) Low/medium design; b) medium/high design. The value of the third, least significant, factor was set to zero.

Two Fisher's tests were used to assess the validity of the models fitting. According to the F1= MS_{REG}/MS_{PE} test, a ratio much larger than 1 indicates a good correlation between the experimental and predicted responses and that the model is adequate to describe the response variations. In turn, for F2 = MS_{LOF}/MS_{PE} test, the validity of the regression model is indicated by a ratio close to 1.

ANOVA analysis (Table 3.5) of the model fitting procedure for the low/medium design suggests that the estimated responses are well described by the model, as evidenced by both F1 and F2 tests. In contrast, for the medium/high design, there are statistically significant deviations from the mathematical model, as evidenced by the F2 test. However, according to the F1 test, the model itself is still highly significant and explains the major part of the deviations of the responses from their mean value [11].

Table 3.5 ANOVA parameters for the characterization of the fitting in Equation (**3.1**).

L1 to M6	Degrees of freedom (DOF)	Sum of squares (SS)	Mean square (MS)	F	Significance *p* value
Total	23	1.38×10^6			
Regression (REG)	6	1.35×10^6	2.25×10^5	151.89^a	3.43×10^{-13}
Residual	17	2.82×10^4	1656.20		
Lack of fit (LOF)	1	4488.10	4488.10	3.03^b	0.10
Pure error (PE)	16	2.37×10^4	1479.20		

M1 to H4	Degrees of freedom (DOF)	Sum of squares (SS)	Mean square (MS)	F	Significance *p* value
Total	23	8.71×10^4			
Regression (REG)	6	8.56×10^4	1.43×10^4	989.79^a	1.22×10^{-19}
Residual	17	1457.60	85.74		
Lack of fit (LOF)	1	1226.90	1226.90	85.11^b	8.33×10^{-8}
Pure error (PE)	16	230.66	14.42		

^{a}F1 = MS_{REG}/MS_{PE}; ^{b}F2 = MS_{LOF}/MS_{PE}

The low/medium design results were analyzed as follows, focusing specifically in the model description and in the assessment of the importance of factors.

It is seen that the main parameter influencing mean particle size was the lipid:solvent (dichloromethane) ratio, followed by the lipid concentration and, to a lesser extent, the emulsifier concentration. It is also seen that, in this model, the isolated effect of each parameter is stronger than the corresponding interactions.

In fact, the mean particle size depends on the lipid concentration in the organic phase, since a higher lipid content results in a more viscous dispersed phase, and thus decreases the efficiency of homogenization [2]. Naturally, a higher lipid content in each initial DCM droplet will also promote larger particles after solvent evaporation, as represented in Figure 3.3.

Solvent:lipid ratio

(a) Low solvent:lipid ratio

(b) High solvent:lipid ratio
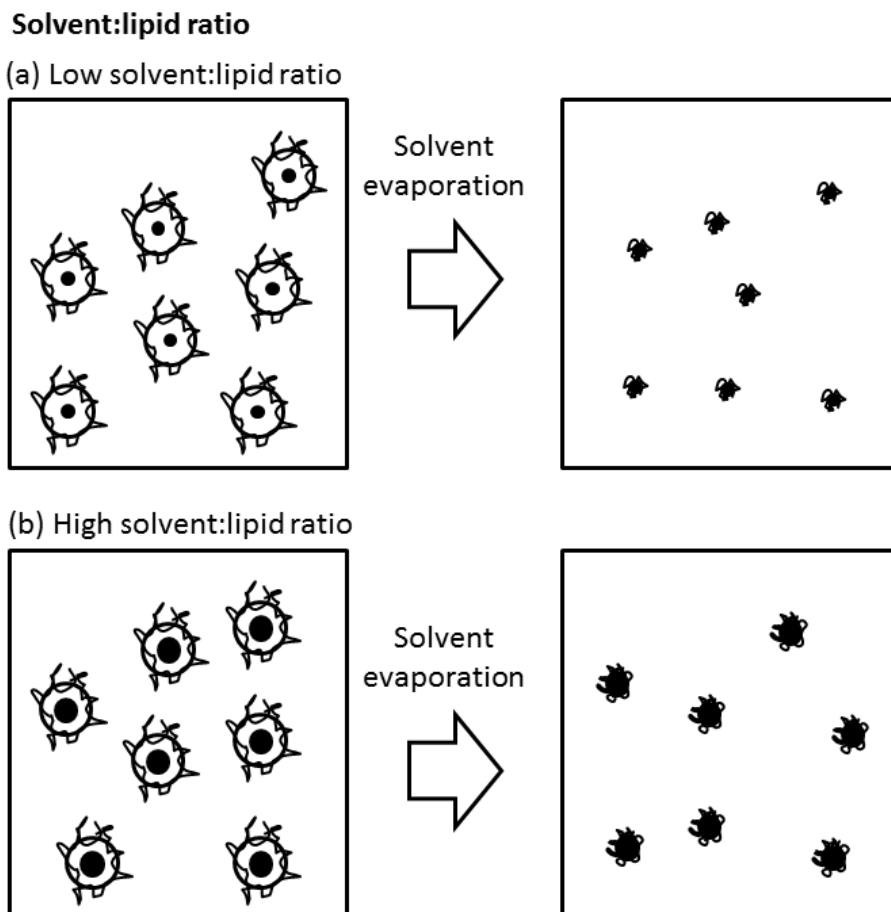
Figure 3.3 Influence of the solvent:lipid ratio upon particle size. The size of the droplets pertaining to the internal phase is, in the initial stages, governed mainly by the solvent. After evaporation, a lower lipid content in each droplet results in smaller particles. Viscosity effects also contribute to this result.

These effects were evident in the L formulations, when the ratio 1:100 was switched to 1:50, as clearly indicated in Figure 3.2(A) by the marked negative slope and the color change of the surface response plot. The effect was also present, but less marked, for higher lipid concentrations. A closer inspection of Table 3.1 suggests that this was a general trend, present irrespectively of lipid- and surfactant-types.

Comparing the matching L and M formulations, the decrease in particle size originated by an increase in lipid content becomes evident (remember the negative signal in β_1). Note that, for these matching formulations, the lipid:solvent ratio remained

constant. Various studies have reported that increasing the lipid content results in larger particles and broader particle size distributions [1, 12, 13]. However, this increase in the amount of lipid is usually associated to an increase of its relative amount with respect to external phase, which makes it difficult to discriminate among factors. Other authors have observed an increase in lipid concentration associated to a concentration-dependent increase in particle size, but only when the lipid concentration exceeds a critical value [5, 14]. Below this value, an increase in lipid concentration has only a minor impact upon particle size. A similar observation was contained in the present results, in the case of moving between the L and M formulations with a 1:50 solvent:lipid ratio. It is seen that the slope is negligible, when compared to the opposite side of the response surface.

A closer inspection of Figure 3.2(A) reveals a further trend. The highest size obtained corresponded to a formulation with a low amount of inner phase. If this amount is increased, either by augmenting the lipid content, the organic solvent content or both, the size markedly diminished. This may be ascribed to a deficient dispersion if the size of inner phase is too small. Another aspect is related to the solvent diffusion rate, and thus the rate of evaporation. A higher solvent content maintains the inner phase less viscous for a longer time, and therefore originates smaller particles. Similar findings have been obtained in previous works, although remaining largely unexplained [15, 16]. The above considerations allowed concluding that the characteristics of the pre-emulsion affect, to a larger degree, the properties of the nanoparticles ultimately obtained.

Focusing now in the emulsifier effect at the L/M design, this was the factor with the lowest importance for particle size, as indicated by the relatively small coefficient. Its contribution became clear in the increase of particle size when comparing the L and M formulations with 0.5% and 1.5% of PVA, while keeping constant the other parameter. A possible explanation is that an excess of emulsifier in solution for the L formulation leads to supersaturation of the emulsifier at the interface, induced by a diffusion process [3], resulting in an increase of particle size, as will be detailed below.

The second factorial planning was applied to the medium/high design (M1 to H4 formulations) and yielded the parameter values presented in the second half of Table 3.3. A representation of the response surface is given in Figure 3.2(B).

In this design, the effect of the different parameters in particle size was much lower than in the previous one. The solvent:lipid ratio was again the dominant factor, followed by the emulsifier and lipid concentrations. Also, the interaction between the parameters had a higher influence than the isolated factors.

Particle size tends to increase mainly for a lower solvent:lipid ratio combined with a higher emulsifier concentration and, less markedly, when a higher solvent:lipid ratio and

lower emulsifier concentration are associated. The opposite conditions tend to decrease particle size. This behavior was applicable irrespectively of the lipid concentration, i.e. both for the M and H formulations, although for different reasons. In the case of the H formulations, and similarly to what was explained above, increasing the inner phase for a low amount of emulsifier may render this amount insufficient and results in an increase of particle size. On the other hand, an increase in the emulsifier concentration from 0.5 to 1.5% tends to reduce the size markedly for higher solvent:lipid ratios, although the effect is less important for the lower ratios. This behavior could be attributed simply to the need of a larger amount of surfactant when a higher amount of inner phase is present [17]. Regarding the M level, the changes induced by the different compositions were less relevant, with the exception of the M3 formulation. In this case, the presence of a higher number of emulsifier molecules tends to increase particle size, probably due to a higher degree of deposition on its surface and because of bridging effects promoting aggregation.

As stated above, the emulsifier concentration was, in relative terms, the less significant parameter in the L/M design. However, it should be stressed that the respective effect was, in absolute value, more important in the M/H design. Overall, three distinct regions can be identified: one in which the system is above the optimal surface coverage, one in which it is close to this optimal value, and another in which it is below that level [17]. The L formulations are in the first region, and a direct correlation was observed between particle size and emulsifier concentration. The same occurs for the M formulations with a lower amount of solvent. The M4-M6 formulations display an almost constant size, which means they are close to the optimal surface coverage. Finally, the H formulations are below this optimal value, and particle size decreases with emulsifier concentration. Figure 3.4 summarizes, pictorially, the above considerations.
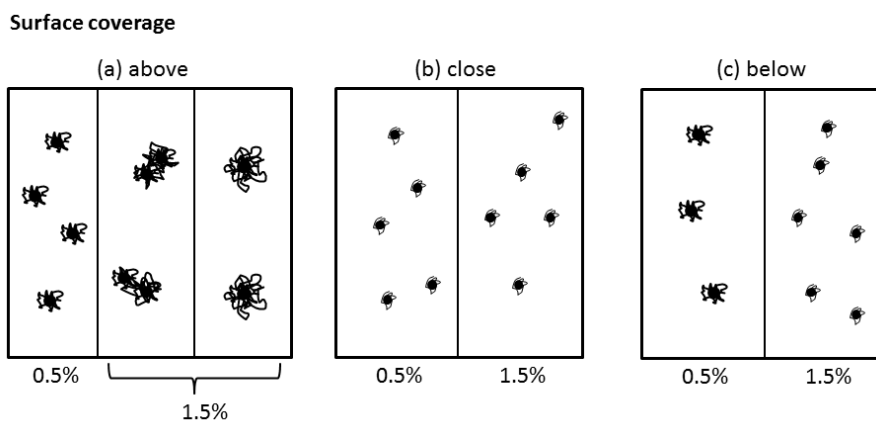
Figure 3.4 Schematic representation of the influence of the emulsifier amount for situations in which the systems are above (L), close (M) and below (H) optimal surface coverage. (a) A large excess of emulsifier, relative to the lipid content, incorporates in the

particles, making them larger. This leads to bridging and, eventually, coalescence, resulting in further growth. (b) For situations in the vicinity of the optimal surface coverage, an increase in the amount of emulsifier produces a negligible effect. (c) For high lipid concentrations, an increase in the emulsifier amount leads to an increase in the surface area and, thus, to a reduction in size. The latter is the behavior commonly reported in the literature.

Table 3.2 reveals that, according to the zeta potential measurements, the most stable formulations were in the M level. Both L and H formulations were located above -20 mV. If this result is combined with the overall output of the experimental design, taking into account both the L/M and M/H designs, there is a clear indication that a close to optimal formulation is found for compositions in the M level. Note that the intention was not to extrapolate beyond the domain of the experiments: it was selected (see above) so as to establish acceptable amounts in terms of the subsidiary substances, namely emulsifier and organic solvent. The choices in the amount of lipid were, in contrast, more arbitrary.

In terms of selecting an 'optimal formulation', the M level was further detailed with the introduction of formulations M2 and M5. The latter corresponds both to the smaller size and the more negative value for the zeta potential. It is located in intermediate value of the lipid amount, emulsifier concentration and DCM amount (albeit not solvent:lipid ratio, for which it is an extreme value). In what follows, this is considered as the optimal formulation, but others are also subjected to study for comparison purposes.

3.2.18 Optimization of the preparation method

It is known that the effect of ultrasound waves in a liquid macroscopic dispersion is generating cavitation bubbles, which tend to implode, and thus provide sufficient local energy to generate nanometric-scaled droplets [3]. Thus, once selected the optimal composition according to the factorial design results, a sonication step was introduced in the method of preparation, so as to further reduce particle size. A final mean particle size of 209.±3 nm, with a very small PI value of 0.094, and a zeta potential value of -32.±3 mV were obtained. This formulation is denoted, in what follows, as M5/S.

3.2.19 Physicochemical characterization

Additional size measurements

Laser diffractometry (LD) was used in order to discard the presence of large aggregates in the optimized formulation. This technique was also applied to other selected formulations (Table 3.6).

Table 3.6 Particle size determined by laser diffractometry.

Formulation	d10% (µm)	d50% (µm)	d90% (µm)	Span Value
L1	0.405	4.113	18.31	4.353
M5	0.113	0.325	0.979	2.665
H1	0.236	0.396	1.039	2.028
M5/S	0.112	0.255	0.458	1.357

LD and PCS yield different results, with the former identifying larger aggregates in the L1 formulation, as a consequence of the wider size range allowed by the technique (0.040-2000 µm). However, the results are in good agreement for the optimized formulations, M5 and M5/S. Note that in LD, an analysis by % volume was carried out, which renders a higher contribution for larger particles. The exclusive presence of nanoparticles is warranted by the d90% value, which is lower than 458 nm for the M5/S formulation. Note, additionally, that the sonicated formulation presents the lowest span value, which indicates a narrower size distribution, again in agreement with the PCS findings and determined PI. The effect of the sonication step was also evident on the volume distribution profile (Figure 3.5), in which a small population with diameters larger than 1 µm, present in the M5 formulation, was no longer visible after sonication.
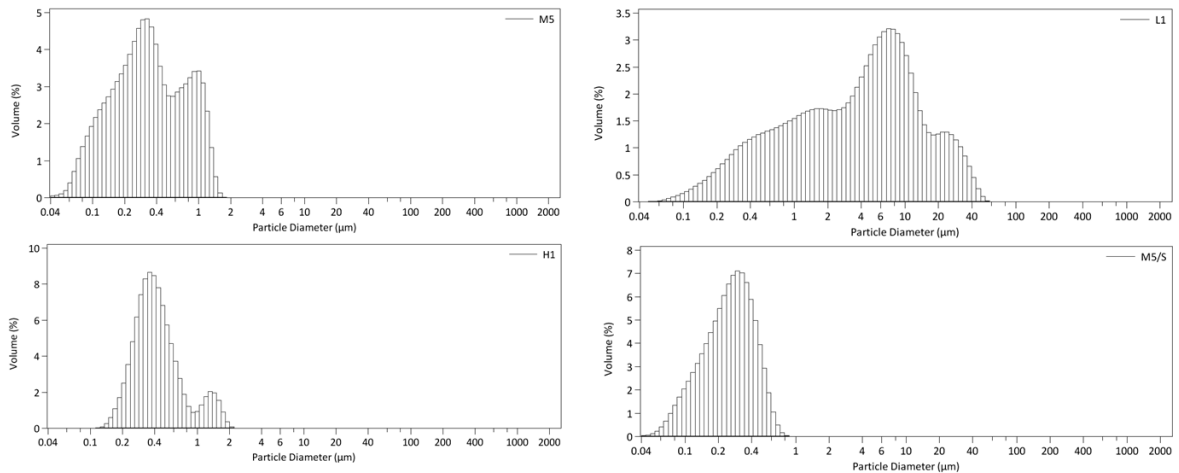
Figure 3.5 Particle size distribution profiles of L1, M5, H1 and sonicated formulations.

Determination of residual PVA

The results for the determination of residual PVA, i.e. the amount of PVA which remained associated to the particles, are presented in Table 3.7. For this determination, only one formulation of each level of the factorial design and the sonicated formulation were selected. The results support the particles surface supersaturation phenomena suggested for the L formulations (high amount of PVA in the external phase). The amount of PVA in the particles obviously increased with the lipid concentration. M5 and M5/S formulations correspond to the intermediate state, being the residual PVA values for the M5/S formulation slightly higher than for M5, probably because of the wider available surface area, as a consequence of the larger number of particles formed.

Table 3.7 Percentage of PVA that remains associated to particles.

Formulation	% Residual PVA
L1	47.8±1.1
M5	61.8±3.1
H1	70.0±4.2
M5/S	68.0±0.3

Differential scanning calorimetry

The crystal structure of the lipid matrix, here inferred by the thermal behaviour, is considered to influence the shape of SLN, as mentioned in previous studies [17]. DSC thermograms of tripalmitin SLN usually exhibit two polymorphic transitions, α to β' and β' to β, represented in the heating cycle as two exothermic peaks at 47 and 52ºC and three endothermic peaks at 43-44 ºC, 55 ºC and 62-64 ºC (Figure 3.6) [18]. The latter peaks correspond to the melting of each form. In the thermograms, the transition β' to β was often absent, since its formation and conversion to β is likely to be too fast to be detected by the instrument. These transitions are related with a shape change from spherical lipid crystals to needle or platelet-like particles, thereby increasing the hydrodynamic radius of SLN [17, 19].
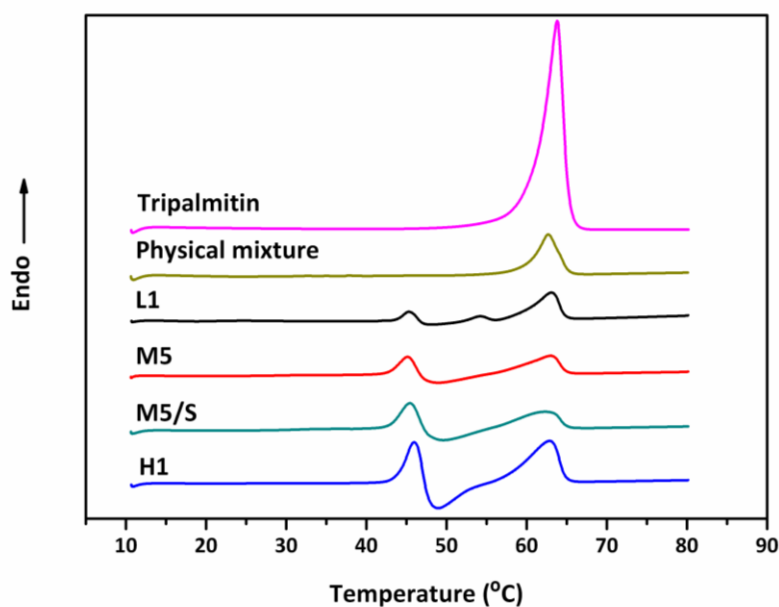
Figure 3.6 SLN and tripalmitin thermograms.

The heating step was performed to investigate the effect of the emulsifier packing and concentration in the crystal structure and, consequently, in the size of the particles. As such, enthalpies for each transition and the molar fractions (x_β) of the polymorphic forms were calculated (Table 3.8). The molar fractions were obtained using the molar enthalpies from reference [20].

Table 3.8 Molar faction (x) associated to the β polymorphic form. For completeness, all formulations are included.

Formulation	x_β	Formulation	x_β
L1	86.5	M5	65.2
L2	57.2	M6	46.9
L3	75.9	H1	59.1
L4	61.4	H2	54.9
M1	66.0	H3	68.5
M2	47.4	H4	38.0
M3	49.2	M5/S	39.0
M4	51.6		

According to the results, in most cases, the β form was dominant, although there were a few exceptions. Also, there was a general tendency for a decrease in the amount of β form as the emulsifier concentration increased from 0.5% to 1.5%. This behavior is supported by some findings of Bunjes *et al* [21]. According to these authors, PVA seems to act by causing an immobilization of the triglyceride molecules in the interfacial region, avoiding its structural reorientation to β form. This effect was clearly exacerbated when the amount of emulsifier was increased. In some cases, however, for which the intermediate 1% concentration was also assessed, the behavior was slightly more complex. The highest content of the β form was found for formulations with lower amounts of lipid (L1 and L3). Sonication promoted a clear increase in the content of the α form. The relationship between particle size and polymorphic forms was not trivial. Although in a significant number of cases, particle size tends to increase with the amount of α form, it is possible that this only reflects a common emulsifier action on both size and polymorphism [21]. This suggests a correlation between the lipid crystal matrix and the emulsifier packing which could explain the increase in mean particle size in the cases above mentioned.

Attenuated total reflectance infrared spectroscopy

The intermolecular interaction in the SLN systems was also assessed resorting to ATR-FTIR. The FTIR spectrum of pure PVA displays a broad peak around 3325 cm^{-1}, corresponding to the stretching of the hydroxyl groups and peaks at 2923 cm^{-1} and 2850 cm^{-1} due to C-H stretching. In what concerns the spectrum of pure tripalmitin, the peaks for the C-H stretching are visible at 2851 cm^{-1} and 2919 cm^{-1}, that corresponding the

stretching of C=O is found at 1735 cm^{-1}, while the stretching of C-O appears at 1473 cm^{-1} (**Figure 3.7**).
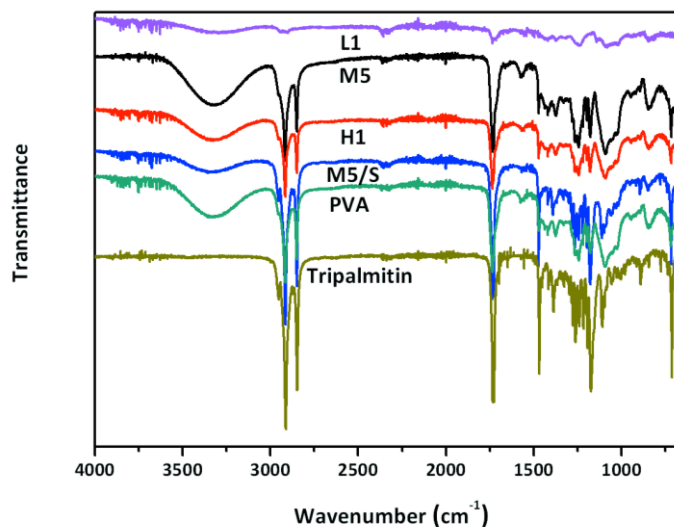
Figure 3.7 FTIR spectra of PVA, tripalmitin and some SLN formulations.

In the SLN spectra, a broad peak was detected around 3425 cm^{1}, corresponding to the stretching of the hydroxyl groups of PVA. Most of the remaining profile can be directly related to features arising from tripalmitin (Figure 3.7).

Overall, these results are extremely coherent, and are also consistent with the previously discussed DSC data. For a full characterization, results for all formulations are presented. Pure tripalmitin is essentially found in the more stable β crystalline form. Note that the features present in the spectra and related to both the C=O and C-H stretching have been used to discriminate between α, β' and β forms [20]. Focus is firstly directed to the former (see Figure 3.8). In these FTIR spectra, this region is characterized by two well separated peaks (at ca. 1728 and 1737 cm^{-1}), while a small shoulder is visible connected to that at 1734 cm^{-1}. Variations in the amount of PVA seem to strongly influence the spectra in this region. While in formulations containing lower amounts of PVA, this region was very similar to that found for pure tripalmitin, when the amount of PVA was increased, especially for the lower lipid contents, the two separated peaks evolved into a convoluted structure that, in some cases, can better be described as a single, broad peak. It should be noted that this evolution clearly followed the one previously extracted from the DSC results. As such, a lower presence of the β form gave rise to less discrete peaks, probably as a result from the coexistence of the different forms, originating slightly different frequencies. This observation can be extended to formulations subjected to sonication. For these, DSC indicated a lower β content and FTIR showed convoluted C=O peaks.
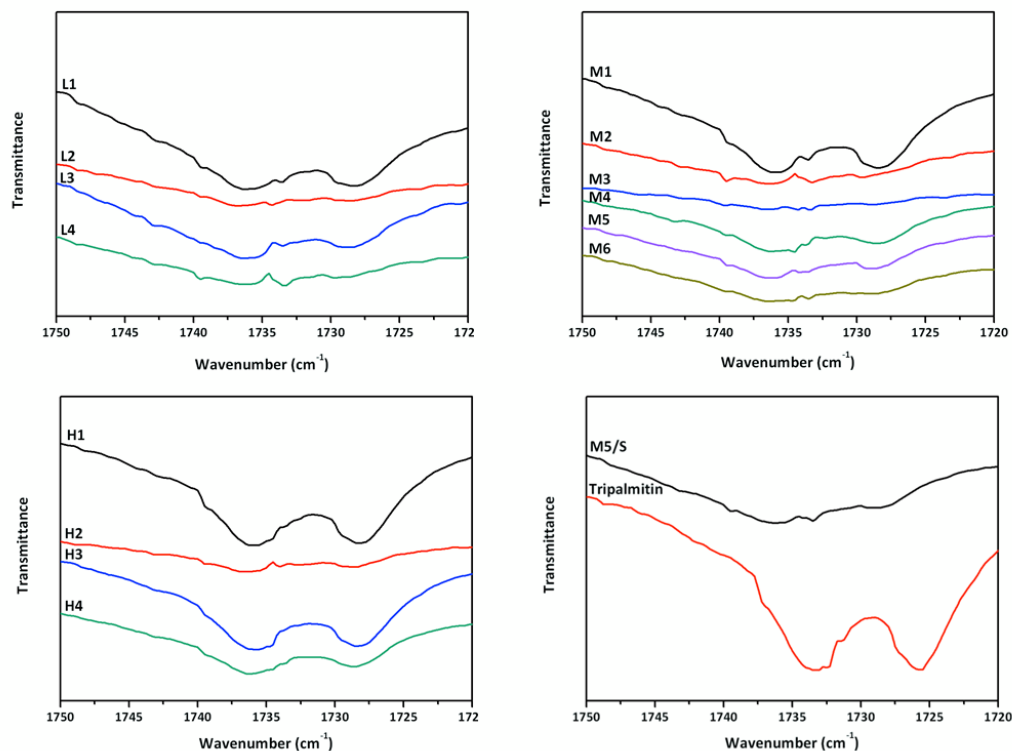
Figure 3.8 C=O stretching observed for all formulations.

Atomic force microscopy

Figure 3.9 shows the AFM images and the cross-section profiles from the height and error images of the optimized SLN. Particle sizes obtained using AFM images were similar to those established from the PCS analysis. A thorough inspection of 3D image and the cross-section profiles, in which the diameter of the particles corresponds to the width of the peak at the base of the graphic and the height to the particles surface, indicates that particles present an irregular and rough surface. Note that a slight increase in particle size may result from the deposition of the particles upon the glass slide. Also, the poly-L-lysine slide surface, conversely for instance to mica, is detectable in the height profiles (see the initial and terminal zones of the height curve).
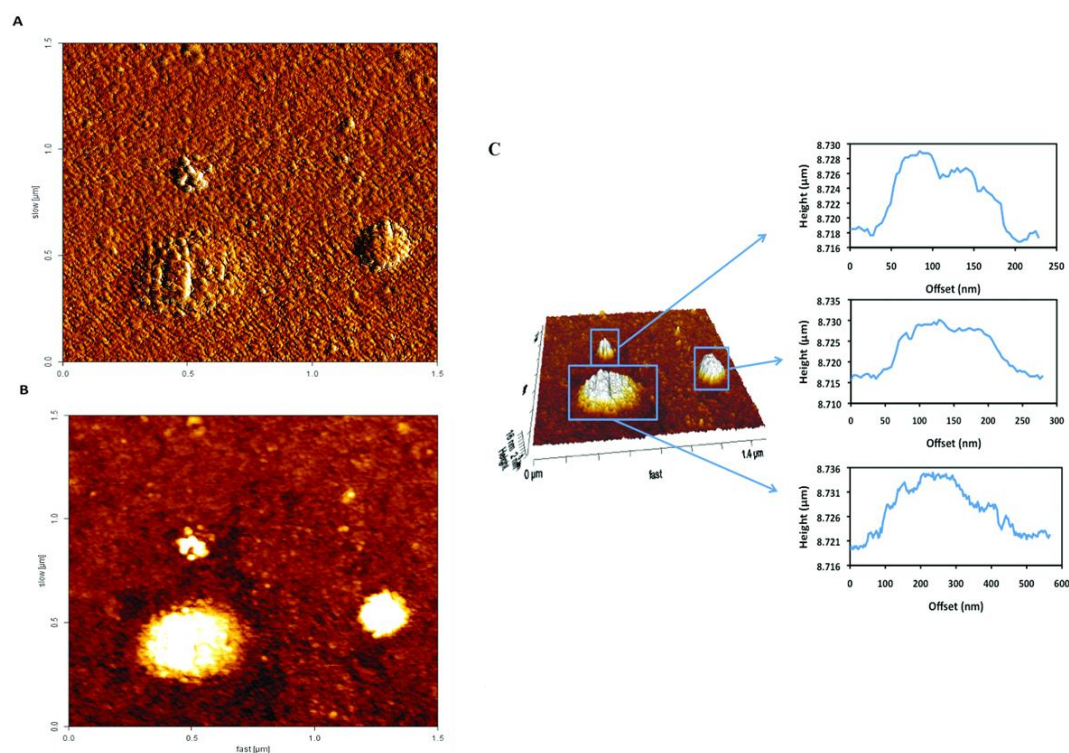
Figure 3.9 AFM images: (a) error trace, (b) height trace and (c) 3D and respective cross-section height profiles from the optimized formulation (M5/S).

Scanning electronic microscopy

SEM analysis (see Figure 3.10) was also performed to complete the information about particle size and morphology. The SEM image shows a relatively homogenous system which is consistent with the polydispersity index observed. The presence of the emulsifier, covering the particles surface, is evident, stressing the importance of this parameter in the lipid packing and in the shape modeling.
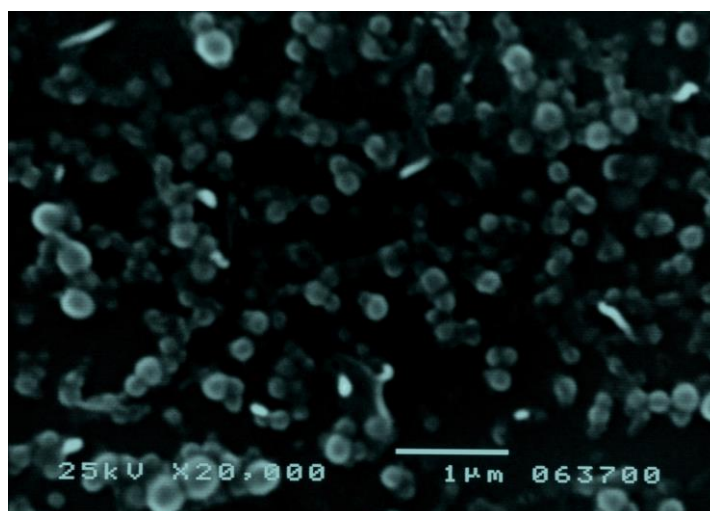
Figure 3.10 SEM images from the optimized formulation (M5/S).

Fluorescence microscopy

Fluorescence images allowed also inspecting SLN directly in the suspension medium. The images confirm previous observations. As seen in Figure 3.11 (A-D), a reduction in particle size was evident from the L and H formulations to the M ones. This illustrates the influence of the different compositions on the system. In the L1 formulation, larger particles were formed as a consequence of the low amount of inner phase. For the H1 formulation, the number of particles tended to increase due to a higher lipid concentration, although with a slightly larger particle size. Conversely, a well-structured and homogeneous system can be observed in the M5 and M5/S formulations, for which a balance for the amount of three different components was found. This not only contributed to reduce the particle size, but also to increase the respective stability. Note that for formulation M5/S there is additional difficulty in the observation of the particles, probably due to their smaller size. Larger aggregates are visible in some of the formulations (panels A-B). This, again, corroborates the findings from PCS and LD.
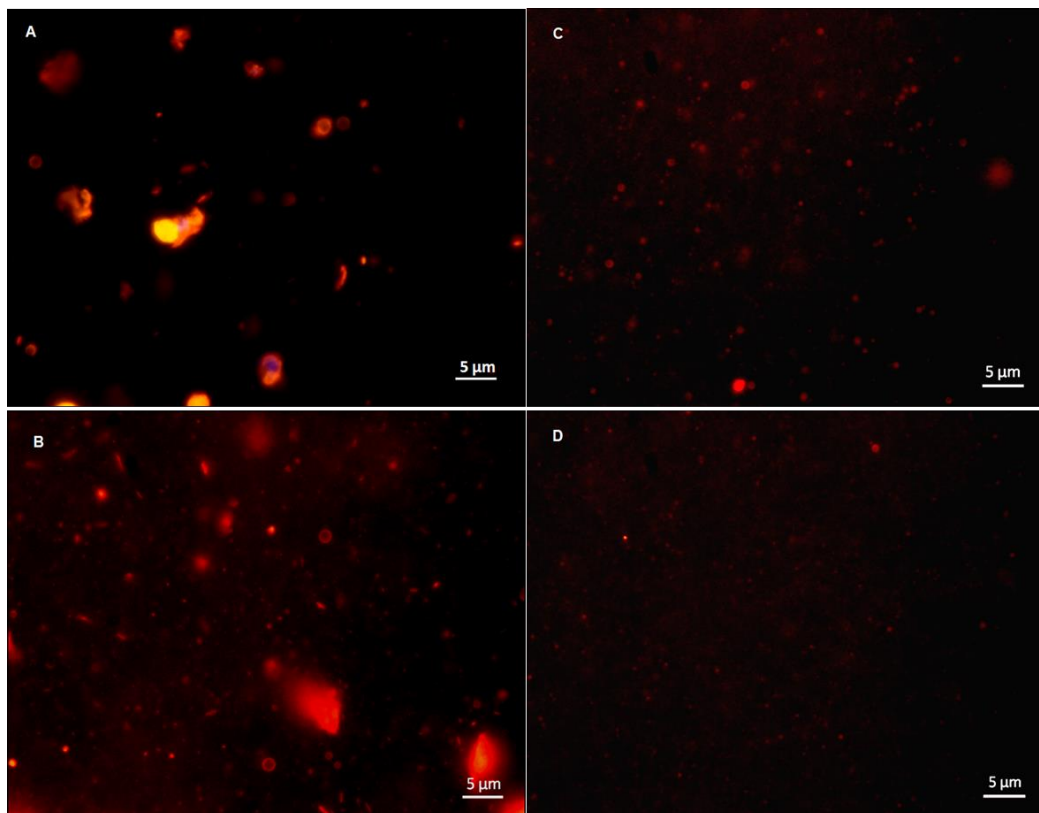
Figure 3.11 Fluorescence microscopy images depicting differences among SLN formulations. A: L1 formulation; B: H1 formulation; C: M5 formulation; D: M5/S formulation.

Stability studies

The physicochemical stability of the optimized formulation (M5/S) was evaluated at 4 ºC and 25ºC for 6 months via PCS particle size and zeta potential (Table 3.9).

Results reveal that the SLN size was not affected by storage temperature within the range tested and did not significantly change after 6 months. The stability of the particles, indicated by the zeta potential, remained essentially unaltered, once stored at low temperature (4ºC).

Table 3.9 PCS particle size and zeta potential of the optimized formulation for 6 months.

Storage Conditions	Particle Size (nm)	PI	Zeta Potential
After preparation	209.3±2.7	0.094	-31.6±3.3
6 months			
25ºC	217.1±4.9	0.114	-20.1±0.1
4 ºC	218.1±6.5	0.110	-31.5±0.9

The M5/S formulation stability was also assessed through LUMiFuge stability analyzer, which combines the centrifuge force with near infrared transmission measurements. This technique allows the separation process to be measured rapidly and thus gives a fast and accurate means of evaluating nanoemulsion dispersion stability.[9]

The graphic representation of the transmission as a function of the local position reveals the corresponding transmission profile. By Figure 3.12, it can be concluded that the M5/S formulation is relatively stable, due to the low transmission profiles, even after submitted at a high centrifuge force for 126 min. The evolution of the transmission profiles during the centrifugation allows detecting local alterations of particles concentration, which are reflected as changes in light transmission. Zones of well mixed dispersions scatter and absorb the light, so transmission is low. In contrast, any separation process (clarification) allows more light to pass and transmission rises.
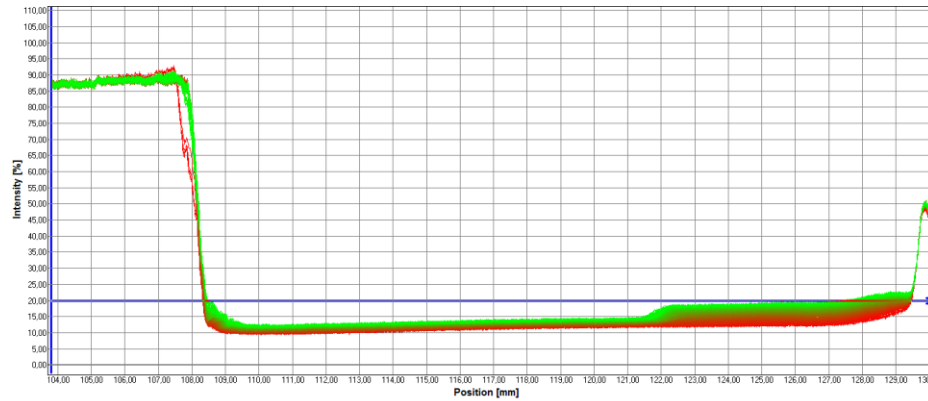
Figure 3.12 Progression of transmission profiles of the M5/S formulation. The corresponding sequence of profiles is shown from red for the first profiles to green for the last ones.

Drug-loaded SLN

Simvastatin was encapsulated as a model drug, in order to assess its influence upon particle properties, such as particle size, zeta potential and entrapment efficiency.

According to the results, increasing the amount of drug in the particles lead to an increase in the mean particle size and in the polydispersity, and a decrease of the absolute value of the zeta potential (Figure 3.13(A-B)). In contrast, the entrapment efficiency remained almost constant (Figure 3.13(C)). Note also the existence of two distinct regions, respectively 5-10 and 12.5-17.5 mg. The increase either in particle size or polydispersity associated with the decrease of the zeta potential observed in the frontier of these two regions suggests matrix saturation with the accumulation of the drug at the particle surface. This also impacted on the zeta potential, which became less negative and indicates some instability.
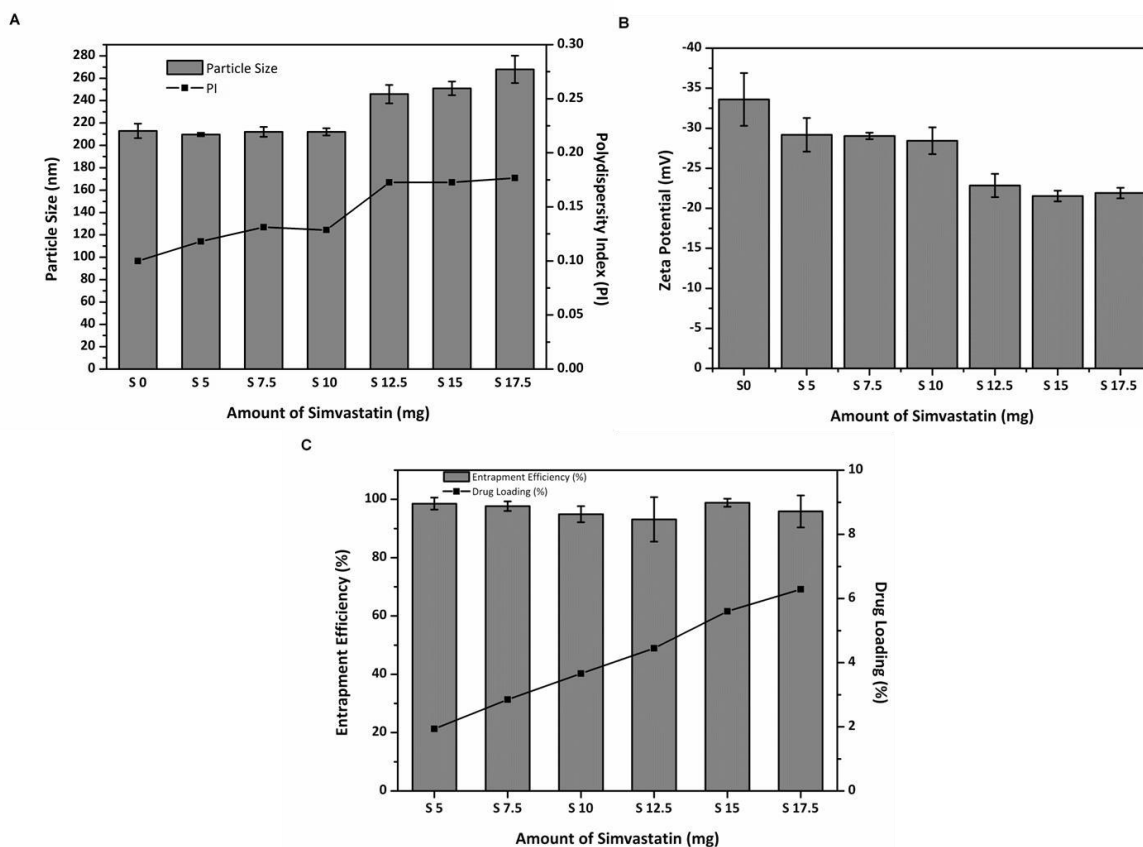
Figure 3.13 Characterization of solid lipid nanoparticles loaded with increasing amounts of simvastatin (S), ranging from 5 mg to 17.5 mg. Key: A – Particle size and polydispersity index. B – Zeta potential. C – Entrapment efficiency and drug loading. (n=3; mean ± SD)

3.3 Conclusion

Factorial design enabled to successfully formulate solid lipid nanoparticles with an optimized nanometric particle size, and good stability. A clear assessment of the importance of factors was provided by this analysis. Solvent:lipid ratio represented the main factor influencing particle size, and did not seem to depend on lipid or surfactant molecule. The amount of emulsifier had a non-trivial impact upon size, depending on whether systems were located below, above or close to the optimal surface coverage and, finally, the amount of lipid had a limited influence upon particle size. The mathematical analysis clearly showed that the influence of the composition parameters is crucial for determining the particle size of the SLN prepared by the emulsification-solvent evaporation method developed, and also facilitated the interpretation of the underlying physicochemical phenomena. The results were supported by the complementary analyses by DSC and FTIR, which provided some insight in the molecular structure and arrangements, compatible with rationales extracted from the experimental design, while

microscopy techniques allowed direct visualization of particle size and morphology, corroborating size measurements by PCS and LD.

The SLN have also proved being an effective lipophilic drug carrier. In the present experimental conditions, simvastatin loading only promoted minor changes upon SLN properties.

Finally, the design planning methodology has clearly shown its usefulness in this optimization process, and this research constituted a solid framework for the understanding of SLN formation.

References

1. Mehnert, W. and K. Mäder, Solid lipid nanoparticles: Production, characterization and applications. Advanced Drug Delivery Reviews, 2001. 47(2-3): p. 165-196.

2. Mäder, K., W. Mehnert, and Solid Lipid Nanoparticles — Concepts, Procedures, and Physicochemical Aspects

Liposheres in drug targets and delivery: approaches, methods, and applications, 2005. Chapter 1: p. 1-22.

3. Anton, N., J.-P. Benoit, and P. Saulnier, Design and production of nanoparticles formulated from nano-emulsion templates--A review. Journal of Controlled Release, 2008. 128(3): p. 185-199.

4. Vitorino, C., F.A. Carvalho, A.J. Almeida, J.J. Sousa, and A.A. Pais, The size of solid lipid nanoparticles: an interpretation from experimental design. Colloids Surf B Biointerfaces, 2011. 84(1): p. 117-30.

5. Zhang, J., Y. Fan, and E. Smith, Experimental design for the optimization of lipid nanoparticles. Journal of Pharmaceutical Sciences, 2009. 98(5): p. 1813-1819.

6. Eaton, J.W., GNU Octave software, version 3.2.3. 2009.

7. Teeranachaideekul, V., E.B. Souto, V.B. Junyaprasert, and R.H. Müller, Cetyl palmitate-based NLC for topical delivery of Coenzyme Q10 - Development, physicochemical characterization and in vitro release studies. European Journal of Pharmaceutics and Biopharmaceutics, 2007. 67(1): p. 141-148.

8. Sahoo, S.K., J. Panyam, S. Prabha, and V. Labhasetwar, Residual polyvinyl alcohol associated with poly (,-lactide-co-glycolide) nanoparticles affects their physical properties and cellular uptake. Journal of Controlled Release, 2002. 82(1): p. 105-114.

9. Lerche, D., Dispersion Stability and Particle Characterization by Sedimentation Kinetics in a Centrifugal Field. Journal of Dispersion Science and Technology, 2002. 23(5): p. 699 - 709.

10. Bunjes, H., M.H.J. Koch, and K. Westesen, Influence of emulsifiers on the crystallization of solid lipid nanoparticles. Journal of Pharmaceutical Sciences, 2003. 92(7): p. 1509-1520.

11. Lewis, G.A., D. Mathieu, and R. Phan-Tan-Luu, eds. Pharmaceutical Experimental Design (Drugs and the Pharmaceutical Sciences). Vol. 92. 1999, Marcel Dekker, Inc.: New York. 498.

12. Subedi, R.K., K.W. Kang, and H.-K. Choi, Preparation and characterization of solid lipid nanoparticles loaded with doxorubicin. European Journal of Pharmaceutical Sciences, 2009. 37(3-4): p. 508-513.

13. Trotta, M., F. Debernardi, and O. Caputo, Preparation of solid lipid nanoparticles by a solvent emulsification-diffusion technique. International Journal of Pharmaceutics, 2003. 257(1-2): p. 153-160.

14. Schubert, M.A. and C.C. Müller-Goymann, Solvent injection as a new approach for manufacturing lipid nanoparticles - evaluation of the method and process parameters. European Journal of Pharmaceutics and Biopharmaceutics, 2003. 55(1): p. 125-131.

15. Shah, M. and K. Pathak, Development and Statistical Optimization of Solid Lipid Nanoparticles of Simvastatin by Using 23 Full-Factorial Design. AAPS PharmSciTech, 2010.

16. Suranan, A. and et al., Chemical and structural investigation of lipid nanoparticles: drug–lipid interaction and molecular distribution. Nanotechnology, 2010. 21(12): p. 125102.

17. Helgason, T., T.S. Awad, K. Kristbergsson, D.J. McClements, and J. Weiss, Effect of surfactant surface coverage on formation of solid lipid nanoparticles (SLN). Journal of Colloid and Interface Science, 2009. 334(1): p. 75-81.

18. Helgason, T., T. Awad, K. Kristbergsson, D. McClements, and J. Weiss, Influence of Polymorphic Transformations on Gelation of Tripalmitin Solid Lipid Nanoparticle Suspensions. Journal of the American Oil Chemists' Society, 2008. 85(6): p. 501-511.

19. Bunjes, H., K. Westesen, and M.H.J. Koch, Crystallization tendency and polymorphic transitions in triglyceride nanoparticles. International Journal of Pharmaceutics, 1996. 129(1-2): p. 159-173.

20. Bresson, S., M. El Marssi, and B. Khelifa, Conformational influences of the polymorphic forms on the CO and C-H stretching modes of five saturated monoacid triglycerides studied by Raman spectroscopy at various temperatures. Vibrational Spectroscopy, 2006. 40(2): p. 263-269.

21. Rosenblatt, K.M. and H. Bunjes, Poly(vinyl alcohol) as emulsifier stabilizes solid triglyceride drug carrier nanoparticles in the alpha-modification. Mol Pharm, 2009. 6(1): p. 105-20.

Chapter 4

Optimization of co-encapsulating nanostructured lipid carriers by high pressure homogenization:
in vitro, *in silico* **and cellular viability approaches**

4.1 Introduction

In this chapter, a dual objective is pursued: assessing the NLC as a vehicle for olanzapine and simvastatin co-encapsulation, and proposing a strategy for transdermal administration, combining these carriers with common penetration enhancers.

The combination of chemical enhancers with nanocarriers is an innovative approach in the design of a transdermal formulation [16]. For that, the effect of classical terpenes, such as menthol, cineole, and limonene, in ethanol as co-solvent, was studied. The terpene screening was supported on experimental testing based on permeation studies, and rationalized by molecular dynamics simulation, as a computational approach.

The design and optimization of a new transdermal delivery system based on NLC, prepared by the hot high pressure homogenization technique, for concomitant administration of OL and SV is thus presented. The final system was obtained by the incorporation of the NLC into a hydrogel containing terpene in ethanol, as vehicle. The overall process was addressed using a two-step factorial planning, firstly applied to NLC preparation, wherein an analysis of particle size, and also zeta potential and entrapment efficiency was conducted, and then to the final formulation, mainly focusing on the permeation rate as biological performance outcome. This experimental design tool allowed the simultaneous study of the influence of each independent variable upon the system and the respective interaction, using a limited number of experiments [17]. Finally, the NLC dispersion was assessed in what concerns cytotoxicity.

4.2 Materials and methods

4.2.1 Materials

Simvastatin was kindly provided by Labesfal - Laboratórios Almiro, S.A. (Santiago de Besteiros, Portugal). Olanzapine was purchased from Zhejiang Myjoy (Hangzhou, China). Glyceryl tripalmitate (tripalmitin, T8127), phosphate buffer saline pH 7.4, polysorbate 80 (Tween[®] 80), 1,8-cineole (99%) and (1R, 2S, 5S)-(-)-Menthol (99%) were purchased from Sigma. Miglyol[®] 812 (a mixture of triglycerides of caprylic and capric acid) was acquired from Axo (Wavre, Belgium). Labrafac PG (propylene glycol dicaprylocaprate) was a kind offer from Gattefossé (Gennevilliers, France). Oleic acid and limonene (>98%) were acquired from Fluka. Carbopol[®] Ultrez 10 NF was kindly provided by Lubrizol (Quimidroga, Barcelona, Spain). All other reagents and solvents were from analytical or high performance liquid chromatography (HPLC) grade.

4.2.2 Drug-in-lipid solubility studies

In a first stage, the solubility of SV and OL was determined in the solid lipid, tripalmitin, and in Mygliol[®], Labrafac[®] PG and oleic acid as liquid lipids. For the solubility study in tripalmitin, 2 g of the solid lipid were previously melted at 10 ºC above the respective melting point in a controlled temperature water bath. Small amounts (ca. 2 mg) of SV and OL were then successively added until the saturation of the lipid was achieved [18]. For the liquid lipids, an excess of drug was dispersed in screw-capped tubes containing the liquid compounds (5 mL each) and magnetically stirred for 48 h at 25 ºC. The samples were then centrifuged for 10 min at 11 740 x g in a Minispin[®] (Eppendorf Ibérica S.L., Madrid, Spain), and 0.5 mL of the clear supernatant was suitably diluted with methanol and analysed by HPLC. Each determination was carried out in triplicate.

4.2.3 Preparation of aqueous NLC dispersions and hydrogels

The NLC were prepared by the hot high pressure homogenization technique described elsewhere [19]. Briefly, a pre-emulsion was obtained by the dispersion of the melted lipid phase, containing the solid and liquid lipids, tripalmitin and oleic acid, respectively, corresponding to a total amount of 750 mg, in 30 mL of a hot emulsifier solution (Tween[®] 80) at 80 ºC. This dispersion was prepared using an Ultra-Turrax X1020 (Ystral GmbH D-7801, Dottingen, Germany) at 25000 rpm for 2 min. It was further subjected to a hot high-pressure homogenization (HPH) procedure through an

Emulsiflex®-C3 (Avestin, Inc., Ottawa, Canada) at 1000 bar for a specific time (see below). The lipid dispersion thus obtained was cooled at 4 ⁰C to form the NLC. In the drug loaded formulation, which will be referred as Combo-NLC, the addition of both drugs (80 mg of each), SV and OL, was carried out in the initial lipid melted phase. These quantities were chosen based on maximization of the amount within a suitable entrapment efficiency, as established from preliminary tests.

In order to obtain viscosity values adequate for transdermal application, a hydrogel was prepared. For that, 0.5% (w/V) of Carbopol® Ultrez 10 and the selected permeation enhancers, terpene (see section 4.2.14.) in 30% (V/V) of ethanol, were added to the NLC dispersion, and left to hydrate under gentle magnetic agitation for 1 h. The Carbopol dispersion was subsequently neutralized using triethanolamine, so as to promote gelation.

4.2.4 Particle size analysis

Particle size was determined by dynamic light scattering, yielding the mean particle size and the PI. DLS was performed in a Delsa Nano C Submicron (Beckman Coulter, Krefeld, Germany) apparatus at a detection angle of 160⁰ and a temperature of 25 ⁰C. Samples were suitably diluted with ultrapurified water. Each value was measured in triplicate. Results are presented as mean ± standard deviation, extracted from the Cumulants algorithm [20, 21].

4.2.5 Zeta potential

Zeta potential determinations were carried out by electrophoretic light scattering in a Delsa Nano C Submicron (Beckman Coulter, Krefeld, Germany) apparatus at 25 ⁰C. The ZP was calculated using the Helmholtz–Smoluchowsky equation. For the measurements, samples were diluted appropriately with ultrapurified water (pH≈5.5).

4.2.6 Entrapment efficiency and drug loading

The entrapment efficiency of SV and OL in the NLC was determined indirectly by measuring the concentration of free drug in the aqueous phase of the nanoparticle dispersion, as described elsewhere [17]. Simultaneously, the total drug amount present in the system was also calculated. For that, a specific volume of the dispersion was suitably diluted with mobile phase (ammonium acetate (0.02 M in water), methanol, and acetonitrile mixture, 30:35:35 (V/V/V)) and heated at 60 ⁰C for 15 min. This dispersion was further centrifuged and the supernatant filtered by a 0.22 μm membrane. This

additional determination was performed in order to take into account the drug losses during the experimental procedures. All drug determinations were carried out by HPLC, as described below. The EE and DL were calculated using the Equations (2.3) and (2.4).

4.2.7 Factorial design

Two experimental designs with a two-level, three- and two-variable 2^k full factorial plannings were performed, respectively, for the optimization of the nanoparticles preparation and final formulation. The experimental designs and the polynomial models were solved using the GNU Octave software [23], with specific programs developed by the authors, that included ANOVA and Student's t-test applied to the fitted models. The mathematical models applied for the first and second cases were $R = \beta_0 + \beta_1 x_1 + \beta_2 x_2 + \beta_3 x_3 + \beta_{12} x_1 x_2 + \beta_{23} x_2 x_3 + \beta_{13} x_1 x_3$ (NLC) and $R = \beta_0 + \beta_1 x_1 + \beta_2 x_2 + \beta_{12} x_1 x_2$ (final formulation), respectively. Coded (−1, +1) levels were considered for each independent variable, x_1, x_2, and x_3, the latter in the case of the three-variable model, as described in sections 4.3.2 and 4.3.6, respectively, in which the −1 level corresponds to the lower value of each variable and +1 to the upper one. β_0 is the arithmetic mean of the response, β_1–β_3 are the coefficients of the respective independent variables and β_{12}, β_{23} and β_{13} the interaction terms, and similarly for the second equation. As responses or dependent variables (R), particle size and permeation rate indicated by the flux at steady state (J_{ss}) were selected, respectively, for the first and second factorials.

4.2.8 Transmission electron microscopy

The shape and surface morphology of the Combo–NLC were observed by transmission electron microscopy. The sample was prepared by placing a drop of the dispersion onto Parafilm®, upon which a copper grid was applied for 2 min. Subsequently, it was dried with paper filter and treated with 7% (w/V) uranium acetate in 50% (V/V) of ethanol for 1 min followed by lead citrate. The grids were then observed in a transmission electron microscope JEOL 1010 (Tokyo, Japan) at 80 KV, coupled to a Morada Olympus SIS numerical camera.

4.2.9 Atomic force microscopy

The surface properties of Combo-NLC were also examined by atomic force microscopy in a FlexAFM (Nanosurf, Basel, Switzerland). A drop of the Combo-NLC dispersion previously diluted (1:10) was deposited on a glass slide and left to dry. The experiments were carried out in air, operating in contact mode (constant force). Oxidized

sharpened silicon tips and a spring constant of 0.2 N/m were used for imaging. Imaging data were analyzed with the Easyscan 2 software.

4.2.10 Confocal laser scanning microscopy (CLSM)

In order to investigate the structure of NLC before and after hydrogel incorporation, 0.05% (with regard to the lipid matrix) Nile red-labeled Combo-NLC were prepared and inspected by CLSM. For that, a drop of glycerol was applied upon samples and examined using a confocal FV-1000 station installed on an inverted microscope IX-81 (Olympus, Tokyo, Japan). Images were obtained with an Olympus UplanSapo x60 w, 1.2 NA, objective lens (800 x 800 pixels, 0.088 µm/pixel). Samples were excited with 543 nm line of a HeNe laser. The emitted fluorescence was detected through spectral detection channel 555-655 nm.

4.2.11 *In vitro* release studies

In vitro release studies were performed using static Franz diffusion cells (PermeGear, Inc., PA, USA) with a diffusion area of 0.636 cm^2 and a receptor compartment of 5 mL. A dialysis cellulose membrane (MWCO~12000, avg. flat width 33 mm, D9652, Sigma-Aldrich), as artificial membrane, was placed between both compartments and a receptor solution composed of PBS (pH = 7.4) with 30% (V/V) of ethanol to warrant sink conditions was used. This receptor phase was stirred at 600 rpm and maintained at 37 ± 0.5 ºC by a thermostatic water pump, which circulated water through each chamber jacket. By maintaining the receptor solutions at 37 ºC, a temperature of 32 ºC at the surface was assured, thus mimicking human skin conditions. 400 µL of the formulations were applied in the donor compartments, and occluded with Parafilm® to prevent evaporation. The experiments were carried out over a period of 48 h and at predetermined time points, 300 µL aliquots of the receptor compartment was collected and replaced with fresh medium. All drugs were determined using the HPLC method described below.

4.2.12 *In vitro* permeation studies: skin preparation and integrity tests

In vitro permeation studies were performed in static Franz diffusion cells, in the same conditions of the *in vitro* release studies, but using newborn pig epidermis as skin model, clamped between the donor and receptor compartments, with the stratum corneum side facing up. The newborn pig (3 weeks, ~6 kg) was provided by a local slaughterhouse. The subcutaneous fat was sectioned off, and the epidermis separated from the

underlying dermis using the heat separation technique [24-26]. The use of heat-separated epidermal membranes is more appropriate for permeants that are poorly water soluble [27]. Briefly, the skin was immersed into hot water at 60 ◦C, for 1 min, and subsequently, the epidermal layer was gently separated from the dermis. The epidermis sheets were cut into 2.5x2.5 cm^2 pieces, wrapped with aluminum foil and stored at −20 ◦C until used. The storage time for the skin samples was less than 3 months. Prior to the experiments, the frozen skin pieces were thawed, and hydrated by placing in PBS (pH=7.4) overnight in a refrigerator (at about 4 °C). The barrier function of the skin was monitored by measuring the transepidermal water loss (TEWL). Only those skin samples that were found below 15 g/m^2.h, the usual range of TEWL values for such measurements, were used for the experiments.
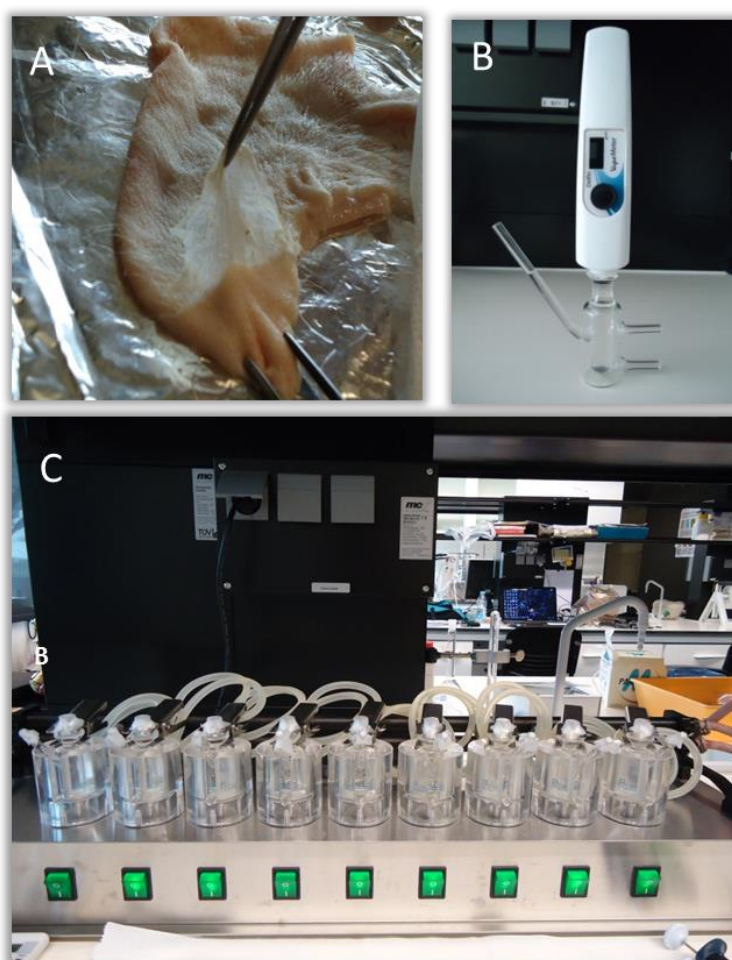
Figure 4.1 *In vitro* permeation studies: preparation of newborn pig epidermis (A), measurement of TEWL as skin integrity test (B), and Franz diffusion cells system (C).

4.2.13 Calculations

The cumulative amount of olanzapine and simvastatin diffused per unit area of the excised skin (Q_n) [28]

$$Q_n = \frac{C_n \times V_0 + \sum_{i=1}^{n-1} C_i \times V_i}{A} \tag{4.1}$$

expressed in µg/cm^2, was plotted as a function of time (t, h). In equation (4.1), C_n corresponds to the drug concentration of the receptor medium at each sampling time, C_i is the drug concentration of the ith sample, A the effective diffusion area, V_0 and V_i stand for the volumes of the receptor compartment and the sample, respectively. The total quantities of the drugs obtained after 24 h (*Q24*) and 48 h (*Q48*) were used for comparison among formulations. The slope of the linear region on the representation of the amount of drug permeated by unit area versus time was used to calculate the flux at steady state [29]. According to Fick's first law of diffusion, the flux (J_{ss}, µg/cm^2/h) can be expressed by Equations (1.1) and (2.12). The permeability coefficient, K_p, and the lag time of permeation, t_{lag}, a parameter related to the time required to achieve the steady-state flux of a drug through the skin, were also taken into consideration. It was determined from the extrapolation of the linear portion of the plot to the x-axis [30].

In the case of the release studies, only the cumulative percentage of drug was taken into consideration and represented, following an approach similar to that described above for the permeation assays.

4.2.14 Screening of terpenes

Terpenes are naturally occurring compounds derived from essential oils, which contain repeated isoprene (C_5H_8) units. Menthol (monoterpene alcohol, log *P* 3.23 [31]) limonene (monoterpene hydrocarbon, log *P* 4.58) and cineole (monoterpene ether, log *P* 2.82) [32] were the terpenes considered for the screening studies. They have been considered as very effective penetration enhancers, generally regarded as safe (GRAS) materials in transdermal delivery. [33, 34]

Permeation enhancement

The terpenes (menthol, limonene and cineole) were tested at two different concentrations, 2 and 5% (w/V). They were dissolved in ethanol and added to NLC dispersions in a final proportion of 30:70 (V/V). All formulations were uniform upon visual inspection. The effect of ethanol without terpene was also investigated, in order to assess its own influence on the interaction with SC. The permeation studies were conducted according to the procedure described in section 4.2.12.

Simulation details

System The effect of a number of terpene molecules of different hydrophobicity on a fully hydrated dipalmitoylphosphatidylcholine (DPPC) bilayer was studied by molecular dynamics (MD) simulation. DPPC is a relatively common lipid often chosen to monitor membrane structure and dynamics when exposed to external agents [35-37]. Consequently, comparison with relevant results from the literature is largely facilitated. This simple and well-characterized model has been used specifically in studies similar to that described in this work, so as to assess effects over the permeation and membrane behavior [38-42]. DPPC and SPC water were described using the original definitions of the GROMOS 53a6 force field [43]. This force field and variants have been extensively used for modeling membrane properties along with a variety of organic molecules [35, 44-46]. Supported on this force field, topology for each solute (menthol, cineole and limonene) was generated by the ATB [47] platform. A DPPC bilayer, consisting of 128 phospholipid molecules equally distributed by two leaflets and 3655 SPC water molecules, was used as made available by Kukol [37]. It should be noted that, for simplicity, a single solute molar fraction of ca. 5% was consider in this study. Such approach is suitable for studying the interaction of each solute with the surrounding lipids, as well as assessing the preferential positioning and respective action on the bilayer. The system was solved resorting to the GROMACS package, version 4.5.4 [48], that is one of the most frequent choices for problems akin to that addressed here [49].

Parameters and data analysis

All MD simulations were carried out in the NPT ensemble and under periodic boundary conditions. A standard time step of 2 fs was used for both the equilibration and production runs. Non-bonded interactions were computed on the basis of a neighbor list, updated every 10 steps. Long-range electrostatics was computed using the particle mesh Ewald (PME) method, as recommended for charged polymer simulations. For Lennard-Jones energies, a cut-off of 1.4 nm was applied. Temperature and pressure were coupled to the Berendsen external baths maintained at 325 K and 1 bar, with coupling constants of 0.1 and 0.5 ps, respectively. To obtain a starting configuration, each system was firstly subjected to an energy minimization step. The systems were then left to evolve up to 100 ns, using the LINCS algorithm [50] to keep bonds containing H atoms under positional restraint conditions. The first 40 ns were considered sufficient to attain equilibrated systems, while the last 60 ns of production runs were subsequently subjected to standard analysis, such as atom-atom (group-group) distance distributions

and radial distribution functions (rdf). MD trajectories were visualized, and configuration images extracted using the VMD 1.8.6 software [51].

4.2.15 HPLC determination of simvastatin and olanzapine

The quantification of the two drugs was performed using a validated HPLC method [52] (see Chapter 5) by a Shimadzu LC-2010 CHT apparatus equipped with a quaternary pump, an autosampler unit, and a L2450 UV/visible dual wavelength detector. For the determination of olanzapine, simvastatin and its main metabolite, simvastatin acid, a Luna Phenyl-Hexyl (5 µm; 150 mm × 3 mm) Phenomenex (USA) analytical column was used. The mobile phase consisted of a 30:35:35 (V/V/V) mixture of aqueous ammonium acetate solution 0.02 M: methanol:acetonitrile at a constant flow rate of 0.8 mL/min. A run time of 7 min was established for separation of the compounds. The detection was carried out at 230 nm. An injection volume of 10 µL was used for all standards and samples. For these conditions, simvastatin acid, olanzapine and simvastatin were eluted at 1.7, 2.0 and 5.5 min, respectively. Note that the former corresponds to the active form of the pro-drug simvastatin, and is a result of the metabolic conversion of the latter. The hydroxy acid form should be considered, since the receptor compartment medium is composed by PBS pH 7.4 plus 30% (V/V) of ethanol, a pH that favors the conversion of simvastatin into simvastatin acid [53, 54]. The partial validation of the method in this medium is described in Appendix 1.

4.2.16 Cytotoxicity studies

Cell culture conditions

Human adult dermal fibroblasts cells Df (ZenBio, Inc.,USA), and a spontaneously immortalized human keratinocyte cell line, HaCaT, (CLS, Germany) were grown in RPMI-1640® (Gibco, UK) medium supplemented with 10% (w/V) fetal bovine serum (FCS, Life Technologies, Inc., UK), penicillin (100 IU/ml), and streptomycin (100 µg/ml) in a humidified 95% O_2/5% CO_2 environment at 37 ºC. For the subculture, cells growing as monolayer were detached from the tissue flasks by treatment with 0.05% (w/V) trypsin/EDTA (Invitrogen, UK). The viability and cell count were monitored routinely using Trypan blue dye exclusion method [55].

Cytotoxicity assays

To determine *in vitro* drug effects on cell viability, cells (cultured in 96-well microplates) were incubated with drugs, vehicle (DMSO), NLC containing drugs and

empty NLC for 72 h and the cell viability was determined by the reduction of MTT (3-(4,5-dimethylthiazol-2-yl)-2,5-diphenyltetrazolium bromide) into a blue formazan salt that is quantitatively measured after extraction from cells [56]. Briefly, the day before experiment, human adult dermal fibroblasts cells Df (ZenBio, Inc., USA), and a spontaneously immortalized human keratinocyte cell line, HaCaT, (CLS, Germany) were seeded in 96 well tissue culture plates at a cell density of $2,5 \times 10^4$ cells/well, in RPMI 1640 culture medium supplemented with 10% fetal serum bovine, 100 units of penicillin G (sodium salt) and 100 μg/mL of streptomycin sulfate and 2 mM L-glutamine. On the next day, cells were incubated with drugs, vehicle (DMSO), NLC containing drugs and empty NLC for 72 h. After time of incubation, cell media containing DMSO (for control cells) or tested compound solution (for test cells) was removed and replaced with fresh medium containing MTT dye to a final concentration of 0.5 mg/mL. After 3 h of incubation the media was removed and the intracellular formazan crystals were solubilized and extracted with DMSO. After 15 min at room temperature the absorbance was measured at 570 nm in Microplate Reader (Infinite M200, Tecan, Austria) [56, 57]. Within an experiment, each condition was assayed in triplicate and every experiment was performed at least three times, with a total of nine replicates. The percentage of viable cells was established relatively to cells treated with vehicle, for drug in solution, and culture medium for drugs into NLC. Inhibitory concentrations (IC_{50}) were calculated by applying non-linear regression procedure to the concentration-response data using GraphPad PRISM software (GraphPad Software, Inc., USA).

Cell uptake studies

For evaluation of cell uptake, Nile red-labeled Combo-NLC and hydrogel containing Nile red-labeled Combo-NLC plus permeation enhancers, were added to HaCaT cells (CLS, Germany) grown on glass 4 wells Chamber slides (Lab-Tek II, Nunc, USA). Cells were exposed for 1 hour to formulations. After the incubation period, cells were washed with 10 mM phosphate buffer saline (PBS) containing 10 mM glycine, fixed with 4% (w/V) solution of paraformaldehyde for 15 min in dark, followed by three times washing with 10 mM PBS. Glass Chamber slides containing cells were treated with fluorescent mounting medium (ProLong Antifade, Invitrogen, UK) including DAPI for nucleus labeling. The cells were observed and microphotographed in a Zeiss Axioskop 4.0 fluorescence microscope (Zeiss, Germany). The uptake of Nile red-labeled Combo-NLC and hydrogel by HaCaT cells was quantified by flow cytometry in an EasyCyte 5HT equipment (Guava, Millipore, Germany).

4.2.17 Stability studies

The optimized NLC formulation was studied for stability at 4ºC and 25ºC. Particle size, zeta potential values and entrapment efficiency were monitored for a period of 6 months.

4.2.18 Statistical analysis

The significance of differences was evaluated using Student's t-test at the probability level of 0.05. This analysis was performed using Microsoft Excel® (Microsoft Corp., Redmond, WA).

4.3   Results and discussion

An optimization process supported on two experimental designs applied to the NLC preparation and final formulation, based on the hot high pressure homogenization technique and permeation studies, respectively, will be described. Before the experimental designs were constructed, preliminary screening solubility studies were performed for the selection of the appropriate lipid, described in what follows.

4.3.1   Screening of the lipid phase composition

The choice of tripalmitin as solid lipid was based on previous studies [17]. The solubility of simvastatin in tripalmitin (34.5±4.1 mg/g) was considerably higher than that of olanzapine, which is below 12 mg/g. Solubility of the drug in the melted lipid is known to be an important precondition to obtain sufficient EE [58]. Since the focus of this study was the co-encapsulation of both drugs, to maximize olanzapine solubility, liquid lipids were included. Thus, the choice was Miglyol® 812, as medium chain (C_8-C_{10}) triglycerides, Labrafac® PG (propylene glycol dicaprylocaprate) as polyalcohol esters of fatty acids, and oleic acid as long chain fatty acid. The solubility of the drugs in the different lipids is presented in Table 4.1.

Table 4.1 Solubility of the drugs in the different liquid lipids. Data are expressed as mean ± standard deviation (SD), n=3.

Liquid lipid	Simvastatin solubility (mg/mL)	Olanzapine solubility (mg/mL)
Mygliol®	10.±1	7.8±0.3
Labrafac® PG	14.7±0.3	9.7±0.5
Oleic Acid	17.1±0.2	177.±5

According to the results, oleic acid was selected as liquid lipid to include in the formulation, because it allowed maximal solubility for both drugs. In addition, oleic acid is also a well-established skin permeation enhancer [59]. Its penetration enhancing effects are attributed to an intercalation into the structured lipids of the SC and disturbance of the lipid packing order [60].

4.3.2 Optimization of the NLC preparation

The optimal conditions for the preparation of NLC were selected using a two-level, three-variable, 2^k full factorial planning. For that, the most critical independent variables were identified. These included the liquid:solid lipid ratio, the emulsifier concentration and the HPH time (see Table 4.2). This choice is thus based on two composition variables, one which influences the inner phase behavior, the liquid:solid lipid ratio, and another one related to the external phase, with impact on the interface stabilization, the emulsifier concentration. The third variable considered, the HPH time, is a production condition with impact on the whole system. As dependent variables, the present work focused on particle size, but zeta potential and entrapment efficiency were also analyzed. The 2^k factorial design yielded 8 different experiments, for which the response are summarized in Table 4.2.

Table 4.2 NLC composition according to the two-level, three-variable, 2^3, factorial design. Key: F: Formulation; PI: Polydispersity Index; EE SV: Entrapment Efficiency for simvastatin; EE OL: Entrapment Efficiency for olanzapine. Results are expressed as mean ± SD (n = 6). The coded values (-1) and (+1) correspond, respectively, to 150 and 300 for the HPH time (sec), 25:75 and 50:50 for the liquid:solid lipid ratio (w/w), and 1.5 and 3.0 for the emulsifier concentration % (w/V). Index for coefficients in model follow the same order: β_1, β_2 and β_3 corresponds to HPH time, liquid:solid lipid ratio, and emulsifier concentration, respectively. The interaction terms follow the same notation.

	Independent Variables			Dependent Variables				
F	**HPH time (sec)**	**Liquid:solid lipid ratio %(w/w)**	**Emulsifier concentration %(w/V)**	**Particle Size (nm)**	**PI**	**Zeta Potential (mV)**	**EE SV (%)**	**EE OL (%)**
1	150	25:75	3.0	191.±2	0.249	-29.±1	96.±2	93.±2
2	150	25:75	1.5	180±18	0.257	-26.±1	99.6±0.1	96.6±0.2
3	150	50:50	3.0	149±18	0.271	-36.±2	99.72±0.05	97.0±0.5
4	150	50:50	1.5	209±14	0.283	-29.2±0.7	99.6±0.1	97.65±0.04
5	300	25:75	3.0	206±20	0.161	-34.±0.8	98.6±0.6	95.3±0.9
6	300	25:75	1.5	224±62	0.123	-30.8±0.6	99.1±0.5	96.23±0.04
7	300	50:50	3.0	140±12	0.270	-31.±2	99.7±0.1	97.14±0.06
8	300	50:50	1.5	156.±7	0.249	-30.7±0.8	99.65±0.05	97.9±0.2

In order to evaluate the influence of each variable, and the respective combination in the particle size as response term, the polynomial coefficients for the first design (NLC) were determined and are displayed in Table 4.3. The higher the magnitude of each coefficient, the higher is the respective main effect upon the system. A negative coefficient sign indicates that an increase in the parameter level leads to a reduction in particle size [17].

Table 4.3 Parameters of the response surfaces for size obtained from a 2^3 factorial planning in the indicated formulations and results of Student's t-test analysis.

Response term	β_0	β_1	β_2	β_3	β_{12}	β_{23}	β_{13}
Particle size	181.78	-0.46	-18.49	-10.37	-15.10	-8.35	1.79
Significance level	100.00	9.29	100.00	98.81	99.96	95.97	34.83
t value	46.13	-0.12	-4.69	-2.63	-3.83	-2.12	0.45

To test whether the terms were statistically significant in the regression model, t-tests were performed using a 95% (α=0.05) level of significance. The Student's t-test analysis showed that the parameters are highly significant, with the exception of the β_1 and β_{13} coefficients. Additionally, ANOVA parameters were calculated and gathered in Table 4.4, as a further characterization of the fittings. ANOVA analysis of the model fitting suggests that the model is highly significant.

Table 4.4 ANOVA parameters for the characterization of the fitting from the 2^3 design of section 2.7.

F1-F8	Degrees of freedom (DOF)	Sum of squares (SS)	Mean square (MS)	F	Significance *p* value
Total	47	6.6579 x 10^4			
Regression (REG)	6	3.6024 x 10^4	6004.0	9.0640[a]	0
Residual	41	3.0555 x 10^4	745.24		
Lack of fit (LOF)	1	4059.0	4059.0	6.1277[b]	0.017640
Pure error (PE)	40	2.6496 x 10^4	662.40		

[a] F1 = MS_{REG}/MS_{PE}

[b] F2 = MS_{LOF}/MS_{PE}

Regarding the estimated coefficients (Table 4.3), it is seen that the main parameter influencing mean particle size is the liquid:solid lipid ratio, followed by the emulsifier concentration and, to a lesser extent, the HPH time. This suggests that the composition of the system has a dominant effect on particle size, when compared to the production conditions. In fact, the lipid phase is described on the basis of the combination of lipids in different physical states at room or body temperature. If the proportion of liquid lipid is increased in relation to the solid lipid, a reduction in size is observed. This can be attributed to a lower viscosity of the dispersed phase [61]. Also, it is described that the mean particle size is increased with higher melting point lipids [62]. Focusing now in the emulsifier concentration, a reduction in particle size is observed when the concentration is doubled. An increase in the emulsifier amount leads to an increase in the surface area and, thus, to a reduction in size [17, 63].

The HPH time is the parameter with less direct influence on size. However, its effect is marked in the interaction terms, particularly when combined with lipid ratio. An increase in the time of homogenization stresses the lipid ratio effect, mainly for a higher proportion of the liquid lipid. Shear stress and cavitation forces applied for a longer time,

with a higher proportion of liquid lipid phase, will cause the disruption of the particles to nano size, and thus promote the increase in homogenization efficiency [2]. On the other hand, the HPH time reveals a small interaction with the emulsifier concentration, corresponding to the less significant interaction term. All these observations emphasize the need of a balance between composition and production variables to obtain particles with optimal size.

Finally, a significant interaction between inner and interface/external composition variables is also detected. Both the isolated effects and the interaction promote a reduction in the mean particle size, if the lipid ratio and emulsifier concentration are increased.

It should be noted that the PI values for the studied formulations were lower than 0.3, which is considered an optimal value for the dispersion and homogeneity of these nanoparticles [64].

Regarding the zeta potential and entrapment efficiency as response terms, small amplitude differences were found, indicating a minor influence of the preparation conditions on the surface and loading properties.

Based on the results from the factorial design, formulations F3 and F7 display the lowest particle sizes. These formulations only differ on HPH time. F3 was selected because of the lower HPH time, allowing reducing production time and cost, with only a marginal particle size increase relative to F7. Note also that the F3 formulation is the more stable, as indicated by the lowest negative value obtained for zeta potential. It also assures an entrapment efficiency closer to 100% for both drugs, associated to a drug loading of $10.637 \pm 0.005\%$ for simvastatin and $10.34 \pm 0.05\%$ for olanzapine, which validates their application for co-encapsulation. An additional fine tuning of the optimization process was not deemed necessary.

Note also that the diameter of the particles observed in the TEM and AFM images (Figure 4.1) corroborates the DLS measurements. AFM images of Combo-NLC also indicate an irregular and rough surface.
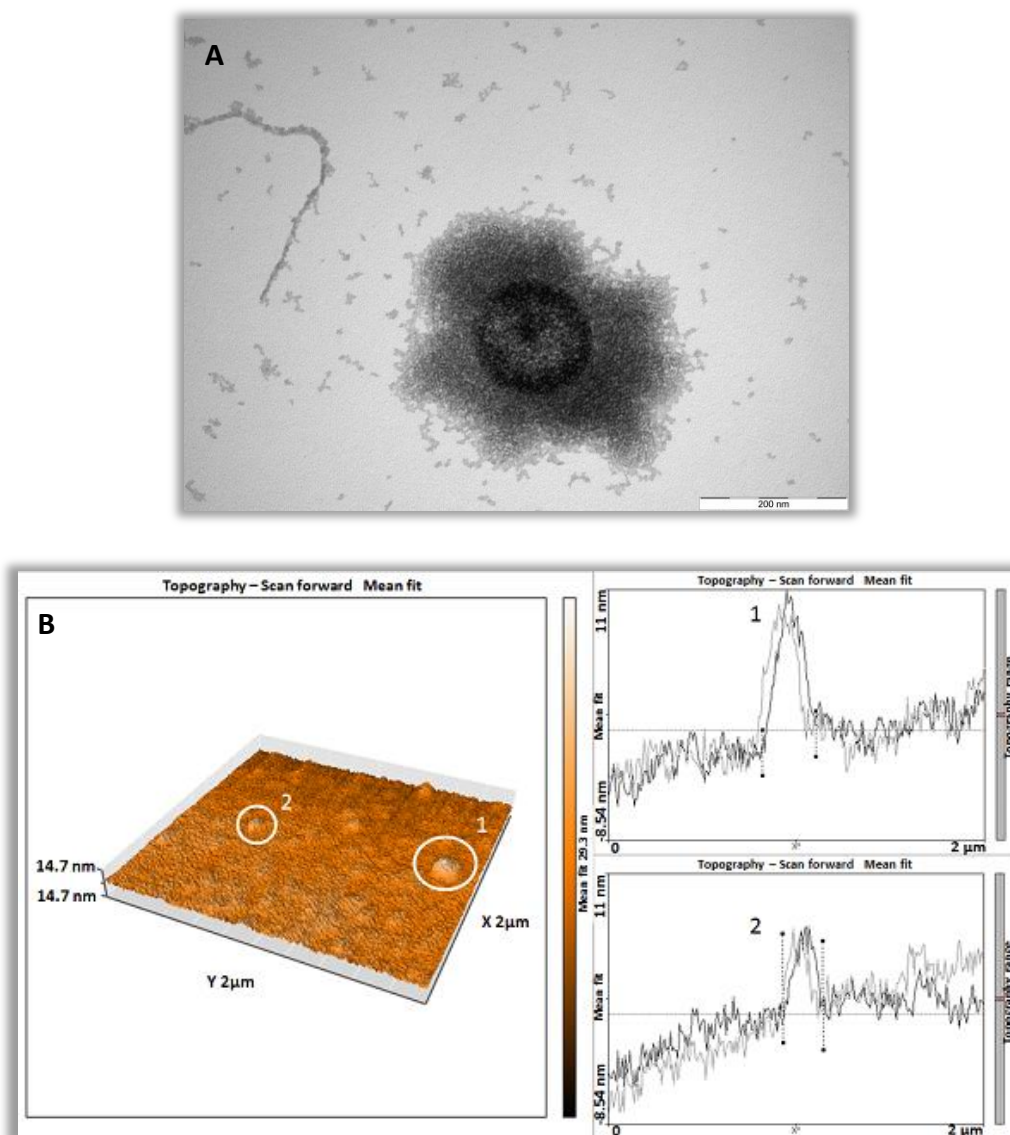
Figure 4.2 (A) TEM image of a particle present in the Combo-NLC formulation (scale bar 200 nm). (B) AFM images of the Combo-NLC: 3D (left) and respective cross-section height profiles (right) from the optimized formulation.

4.3.3 Optimization of the NLC formulation

Since the focus of the present work was the transdermal co-administration of OL and SV, *in vitro* permeation studies were firstly performed using the formulation previously selected. According to the calculated parameters for the Combo-NLC (Table 4.5), it is seen that the degree of permeation is small. This behavior can be attributed to the hydrophobic nature of the drugs, and thus a low partition between lipid (which corresponds only to 2.5% (w/V)) and external aqueous phase. This trend is more marked for simvastatin, the more hydrophobic drug. Thus, the composition of the vehicle may markedly influence the degree of penetration of the drug [65].

Table 4.5 Permeation parameters of the Combo-NLC formulation across newborn pig skin. Data are expressed as mean±standard error of the mean (SEM). (n=3)

Permeation parameters	OL	SV
J_{ss} (µg/cm^2/h)	0.24±0.05	0.116±0.007
Kp (cm/h)	$1.1 \times 10^{-4} \pm 0.2 \times 10^{-4}$	$0.48 \times 10^{-4} \pm 0.03 \times 10^{-4}$
Q24 (µg/cm^2)	3.5±0.7	1.0±0.1
Q48 (µg/cm^2)	9.±3	5.9±0.3
% Drug permeated (48h)	0.7±0.1	0.38±0.02
Lag time (h)	9.5±0.8	15.±2

A simple strategy to overcome this solubility related limitation consisted on the use of ethanol, after a screening procedure involving also transcutol, propylene glycol and glycofurol (data not shown). For that, 30% (V/V) of the former alcohol was included in the formulation. This inclusion promoted an increase in the flux at the steady state of ca. 7.9 for OL and 6.4 for SV (Table 4.6). Ethanol is known to be a skin penetration enhancer and therefore alters the barrier properties of the skin, which is partly responsible for the high flux values obtained [66].

4.3.4 Effect of chemical penetration enhancers

To further enhance permeation, 2% (w/V) of menthol, cineole and limonene in the above NLC ethanolic dispersion were firstly studied. The co-incorporation of terpenes and ethanol promotes in general a higher flux when compared to the application of ethanol alone. The tertiary combination of NLC+ethanol+limonene yields the higher flux enhancement ratio, followed by cineole and, lastly, menthol (see Table 4.6). The cooperative effect of ethanol and limonene has already been reported to be an effective binary enhancer system [34].

When this concentration was increased to 5% (w/V), permeation in the presence of limonene significantly augments, yielding a flux enhancement ratio of ca. 64 and 60 respectively for OL and SV, when the NLC formulation is considered as reference. Conversely, for menthol and cineole, an increase in the concentration leads to a decrease in the permeation rate (Table 4.6). This behavior has already been observed for menthol, having been attributed to the limited solubility of hydrophobic terpenes in 40% (V/V) of ethanol solution used in the experiments [67]. The same trend has been reported for other terpenes, although no clear explanation has been provided [68, 69].

Table 4.6 Olanzapine (OL) and simvastatin (SV) fluxes at steady state (J_{ss}) along with the different chemical (ethanol and terpenes) enhancers used in combination with Combo-NLC. Key: Et: ethanol; M: menthol; C: cineole; L: limonene. The ethanol concentration is expressed in % (V/V), and that of terpenes is in % (w/V). [a] p<0.05 vs NLC as reference, [b] p<0.05 *vs*. NLC+30% ethanol as reference; n=3, for all the cases, with the exception of formulations signaled with asterisk, for which n=6. Data are expressed as mean±SEM.

Formulations	J_{ss} OL (µg/cm^2/h)	ER J_{ss} OL	J_{ss} SV (µg/cm^2/h)	ER J_{ss} SV
NLC	0.24±0.05	1.0	0.116±0.007	1.00
NLC+30%Et*	1.9±0.4[a]	7.9	0.74±0.08[a]	6.4
NLC+30%Et+2%M	1.9±0.8	8.0	0.8±0.4	7
NLC+30%Et+5%M	1.4±0.2[a]	6.0	0.4±0.1[a]	4
NLC+30%Et+2%C	4.3±0.9[a,b]	18	2.1±0.2[a,b]	18
NLC+30%Et+5%C	2.8±0.1[a]	12	1.00±0.07[a,b]	8.60
NLC+30%Et+2%L	9.±1[a,b]	37	3.3±0.6[a,b]	28
NLC+30%Et+5%L[*]	15.±2[a.b]	64	7.0±0.8[a,b]	60

All these observations are corroborated by the percentage of drug permeated after 48 h, which are summarized in Figure 4.3.
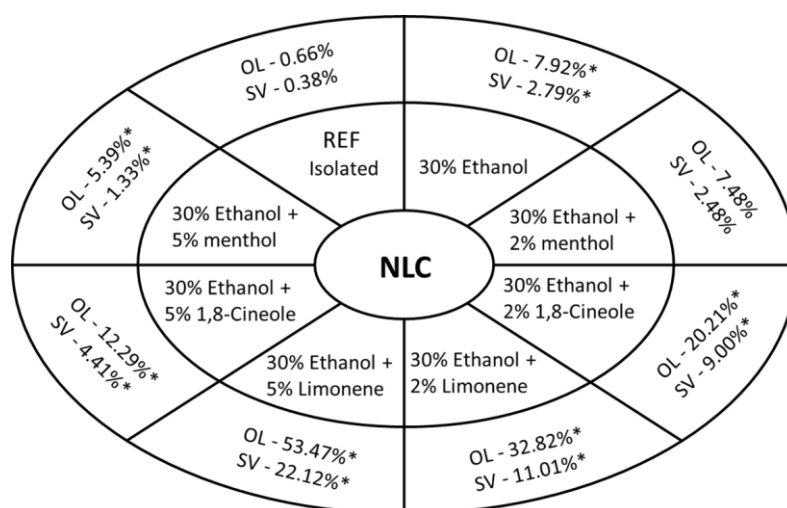
Figure 4.3 Different chemical (ethanol and terpenes) enhancers used in combination with Combo-NLC along with % olanzapine (OL) and simvastatin (SV) permeated after 48h. Key: * p<0.05 vs NLC isolated as reference (REF).

4.3.5 Molecular dynamics simulations

To rationalize the previous results and elucidate the mechanism of action of each terpene assayed, a molecular dynamics simulation study was performed.

Figure 4.4 depicts the density profiles for some relevant groups and molecules across the bilayer. From these profiles, it is clear that the limonene and cineole molecules are mostly embedded in the hydrophobic region, while menthol molecules are preferentially positioned close to the interface. Limonene is likely to be found at the interleaflet region, easily switching between the two leaflets as suggested by the mean square displacement (MSD) profile (panel (a) of Figure 4.5). Cineole molecules are found in an upper position, but yet well embedded in the hydrophobic region. Menthol is, among the three terpenes under study, the one that appears to interact more strongly with the lipid polar heads, with evidence of establishing hydrogen-bonding, and displaying a reduced probability of crossing the center of the bilayer. Accordingly, diffusion of these menthol molecules is relatively slow compared with that of the two other. Representative snapshots, Figure 4.6, illustrate the described preferential position of each solute.

Note that the above observations (i) are compatible with the fact that one of the terpenes contains hydrogen bonding donor groups (menthol), one other a hydrogen-bonding acceptor group (cineole), and a last one that does not form hydrogen bonds (limonene). Note also that although (ii) terpenes can in principle, weaken the hydrogen-bonding interactions at the membrane–water interface, the present results suggest that the effects of terpenes on the membranes do not necessarily depend on direct competition for H-bonds with the polar headgroups. Finally, (iii) these results suggest that the effects of terpenes do not relate to specific characteristics of SC membranes and that the basic characteristics for terpenes to affect membranes are their ability to penetrate the bilayer. These points have already been addressed in previous work [70], and a rationale is now provided from the simulation results.

Extending the MSD analysis to the DPPC molecules, panel b) of Figure 4.5 clearly shows that the incorporation of ca. 5% of limonene is responsible for a significant increase in the DPPC lateral diffusion, when compared with the small increase prompted by cineole. In turn, a slight decrease in the lateral diffusion of the DPPC molecules is found in the presence of menthol.

No significant differences were found in terms of the hydration of the carbonyl-ester atoms of DPPC tails (Figure 4.7A), this corresponding to the upper part of the hydrophobic region. However, a close up of the first hydration shell reveals that limonene is responsible for an increase in the water content, closely followed by cineole. In contrast, a decrease in the amount of water is observed for the incorporation of menthol.

Such behavior is compatible with an increase of the order promoted by the presence of menthol.

A more detailed analysis on the order of the membrane is presented from the estimated deuterium order parameter (Figure 4.7B). This shows that both the cineole and menthol molecules induce an increased organization along the alkyl chains. For the limonene molecules, an opposite effect is found close to the bilayer center. Although the differences are small, the order found for the DPPC/terpene systems is in good agreement with the experimental results, pertaining to permeation. Based on the membrane perturbation results retrieved by MD, and for the concentration regime considered, menthol is identified as the least and limonene as the most effective permeation enhancer of the study. Nevertheless, the effectiveness of menthol has been suggested for enhancing the permeation of hydrophilic drugs [33]. This can be explained by the ability of menthol to drag water into the bilayer, also visible in the simulation, as illustrated in the snapshot (Figure 4.8). This indicates that the lipophilicity of the permeant, as well as the enhancer molecule play an important role in determining the penetration promoting mechanism [34].
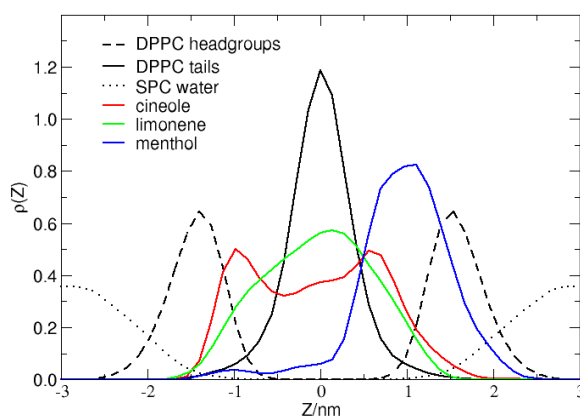
Figure 4.4 Probability density profiles for the terminal methyl groups of the DPPC tails (black solid line) and respective headgroups (black dashed line), SPC water (black dotted line), and for the center of mass of the inserted molecules (solid colored lines) relative to the Z-axis. Note that the Z-coordinate represents the normal to the bilayer plane and each distribution is normalized to unity.
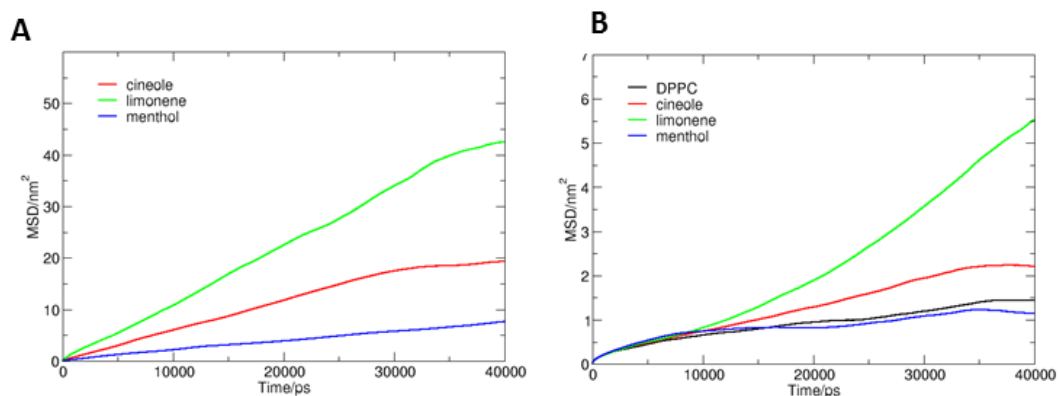
Figure 4.5 Mean square displacement (MSD) of (A) DPPC and (B) molecules under study.

| Cineole | Limonene | Menthol |
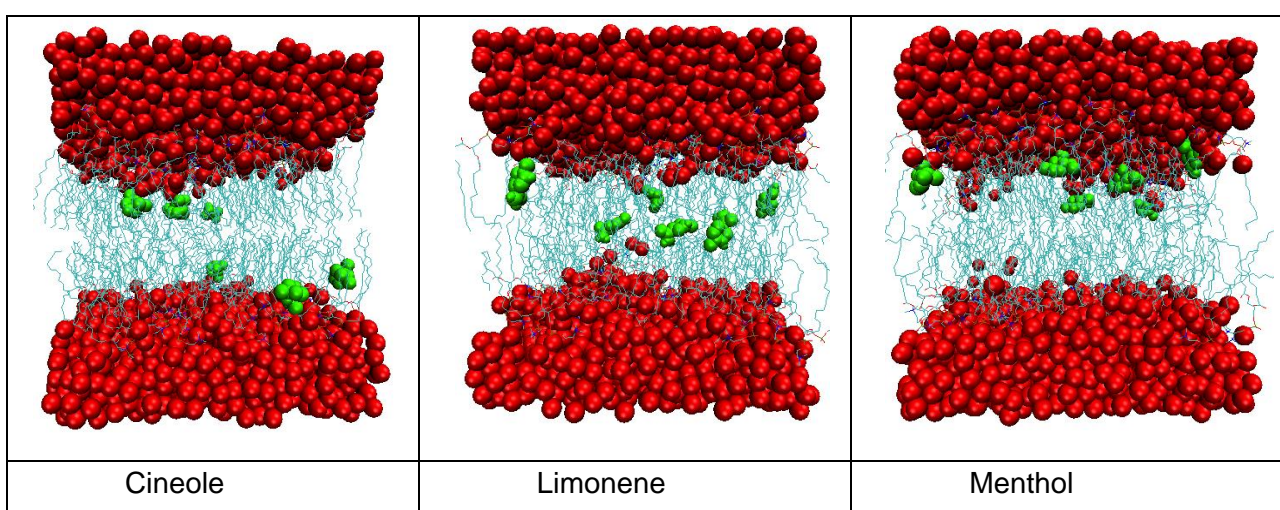
Figure 4.6 Snapshots illustrating typical positioning of the residues embedded in the bilayer. Key: water, terpenes and DPPC are represented in red, green and blue, respectively.
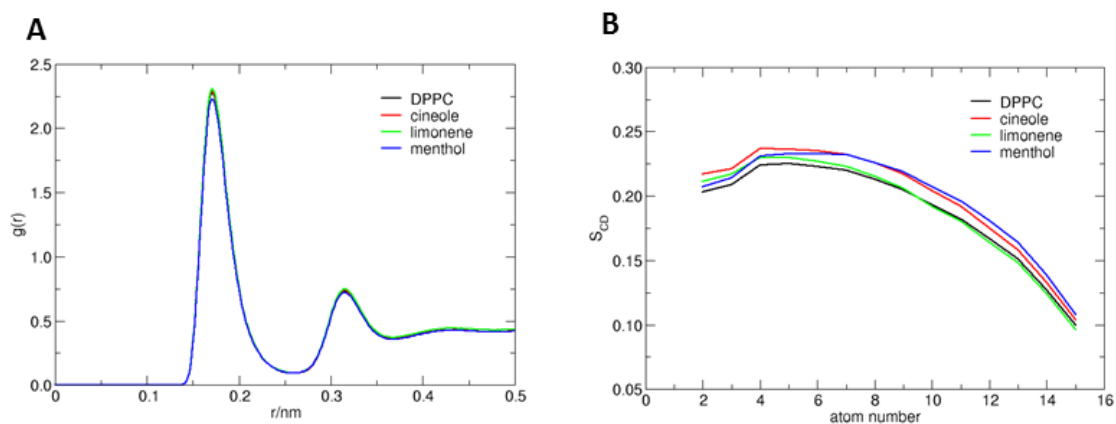
Figure 4.7 Results from MD analysis: (A) radial distribution function (RDF) of water hydrogens around the carbonyl-ester atoms for the sn_1 and sn_2 chains of DPPC. (B)

deuterium order parameter, SCD, estimated along the bilayer depth for DPPC chains (and averaged over the sn_1 and sn_2 chains) in the presence of the indicated solutes.
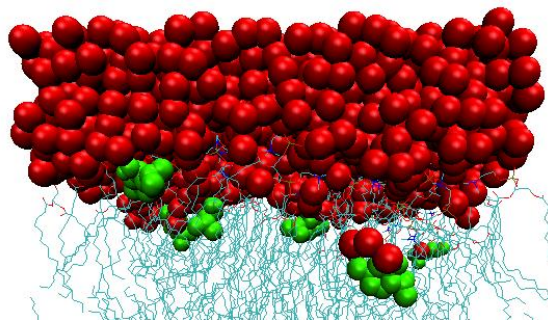
Figure 4.8 Snapshot illustrating menthol dragging water molecules into the DPPC bilayer.

4.3.6 The combined effect of NLC and a chemical enhancer

Factorial design

Based on the above findings, limonene was the terpene included in the final formulation. The next step was to quantify the permeation enhancement coming from each of the main skin penetration strategies employed, nanocarriers and chemical enhancers, represented by NLC and limonene plus ethanol as co-solvent, respectively. Their isolated and combined effects were assessed using a second factorial planning, two-level, two-variable, 2^2. As independent variables, the absence (-1 level) or presence (+1 level) of limonene (5% (w/V)) and NLC were considered. For that, four different sets of experiments were carried out, in which 30% (V/V) of ethanol was included. In the experiments without nanoparticles, saturated solutions of both drugs were prepared. As dependent or response variables, olanzapine and simvastatin fluxes at steady state, permeability coefficient, Q24 and Q48h were analysed (Table 4.7).

Table 4.7 Formulations and respective permeation parameters for olanzapine according to the 2^2 factorial design. Key: Et: Ethanol; L: Limonene; J_{ss} = Flux at steady-state; Kp = Permeability coefficient; Q24 and Q48 = Cumulative amount of olanzapine permeated after 24h and 48h, respectively; ER = Enhancement ratio. Again, the ethanol concentration is expressed in % (V/V), and that of terpenes in % (w/V). For the calculation of ER, experiment 1 was considered as reference. Data are expressed as mean±SEM. (n=6)

	Exp. #	Formulation	J_{ss} ($\mu g/cm^2/h$)	ER (J_{ss})	Kp (cm/h) ($\times 10^{-3}$)	ER (Kp)	Q24 ($\mu g/cm^2$)	Q48 ($\mu g/cm^2$)	Lag time (h)	Time* (h)
OL	1	Saturated solution (30%Et)	0.32±0.05	1.0	2.1±0.3	1.0	9.±2	15.±3	-	6.±1
	2	NLC + 30%Et	1.9±0.4	5.9	1.2±0.2	0.57	29.±7	79±18	9.±4	3.9±0.8
	3	Saturated solution (30%Et +5%L)	0.49±0.04	1.5	1.9±0.2	0.91	10.6±0.8	20.±2	-	3.5±0.8
	4	NLC + 30%Et + 5%L	15. ±2	48	10.±1	4.6	261±51	534±33	7.±5	1.3±0.3
SV	1	Saturated solution (30%Et)	0.34±0.05	1.0	1.6±0.2	1.0	8.±2	15.±3	-	7.±2
	2	NLC + 30%Et	0.74±0.08	2.2	0.42±0.05	0.26	13.±3	31.±5	10.±4	7.±2
	3	Saturated solution (30%Et + 5%L)	0.22±0.05	0.64	1.±1	0.5	7.±1	12.±2	-	7.2±0.3
	4	NLC + 30%Et + 5%L	7.0±0.8	21	3.9±0.5	2.4	82±19	249±36	14.±4	2.9±0.7

* Estimate of time after which drug is detected in the receptor compartment.

Considering the flux at steady-state as response, the polynomial coefficients for the second design (final formulation) were calculated (see Table 4.8).

Table 4.8 Parameters of the response surfaces for flux at steady-state obtained from a 2^2 factorial planning in the indicated formulations and Student's t-test analysis.

Response Term	β_0	β_1	β_2	β_{12}
OL J_{ss} ($\mu g/cm^2/h$)	4.498	3.395	4.093	3.307
Significance level	100.0	100.0	100.0	100.0
t value	9.059	6.836	8.242	6.660
SV J_{ss} ($\mu g/cm^2/h$)	2.077	1.537	1.797	1.598
Significance level	100.0	100.0	100.0	100.0
t value	9.665	7.150	8.361	7.437

The coefficients obtained from the factorial design stress the higher importance of the presence of NLC in the formulation, relative to that of limonene, for the permeation enhancement, within the working ranges under consideration. This suggests that NLC acts as a drug reservoir, thus assuring a high driving force upon the drug, suitable for transdermal delivery, in comparison to the corresponding saturated solutions. Moreover, the interaction terms point to a synergistic effect between both permeation enhancement strategies (Table 4.8). The increase in the flux corresponds to an increase in the product of the diffusion coefficient (D) by the partition coefficient (K) and the concentration in the vehicle (C_0). The NLC, acting as a reservoir system, promote an increase in C_0. However, it is difficult to estimate the real value of the drug concentration throughout the experiment. Assuming that the drug is fully available, which clearly corresponds to an overestimation, it is still possible to check if there is an increase in the D x K value. If that is the case, there is no doubt that there are two contributions for the enhancement of the flux: one provided by the NLC reservoir and the other by the disruption promoted by the permeation enhancers, that probably increase both drug diffusion and partitioning. This is what is observed when limonene is added to the system, yielding a flux enhancement ratio of 48 and 21, respectively for olanzapine and simvastatin, relative to the reference saturated system. Also, this system promotes a significantly lower enhancement ratio in what concerns Kp, 4.6 and 2.4, in the same order (Table 4.7). The latter values are undoubtedly underestimated because of the use of a majorant for C_0, i.e., the reservoir effect has been withdrawn after division by an excessive gradient.

Note that adding limonene to the water/ethanol saturated solution promotes only a marginal increase in the flux of olanzapine, and a slight decrease in that of simvastatin. This suggests that the hydroalcoholic solution does not favor the incorporation of the enhancer into the skin. It is possible that limonene is not homogeneously distributed in the solution, affecting particularly the partitioning of the most hydrophobic drug, with affinity for limonene rich domains that do not efficiently contact with the skin.

On the other hand, the NLC/ethanol system is a better medium to transport and incorporate limonene into the skin. It promotes a homogeneous distribution of the enhancer in the formulation, as a result of the affinity of the hydrophobic limonene to the lipid nanoparticle. Additionally, the increased contact with the skin surface determined by the small size of the particles enforces the effect of limonene, significantly increasing permeation of both drugs.

Simvastatin vs. olanzapine

Focusing now on the differential behavior of the co-encapsulated drugs, the slower permeation observed with simvastatin can be attributed to a difference in the solubility of the drugs in the lipids used as internal phase. Since simvastatin has a higher solubility in the solid lipid, due to its solid matrix nature, the release is further sustained. In the case of olanzapine, due to its higher solubility in the liquid component, the release tends to be less controlled, thus showing a positive influence in the respective penetration degree.

Another topic that should be remarked is related to the parameters *Q24* and *Q48*. According to the current oral dosing regimen, a daily dose of 5 to 10 mg for olanzapine and 20 to 40 mg for simvastatin is required for a therapeutic effect. Since oral bioavailability is approximately 60% for OL and 5% for SV, the estimated transdermal dose should be approximately 3-6 mg and 1-2 mg per day, respectively. Thus, the target transdermal flux, according to *in vitro* permeation evaluations should be 3.1-6.2 $\mu g/cm^2/h$ for OL and 1.04-2.08 $\mu g/cm^2/h$ for SV, considering a 40 cm^2 patch. This yields an amount permeated per day of 75-150 $\mu g/cm^2$ and 25-83 $\mu g/cm^2$, respectively for OL and SV. In addition, the amount permeated after 48 h (Q48) was approximately twice the amount permeated after 24 h (Q24), which suggests a constant delivery over time, even for a long-term administration. The flux can also be established from $J_{ss} = C_{ss}$ x Cl/A, now taking into consideration literature values for the therapeutic blood level (C_{ss}, 0.0093 $\mu g/mL$ [71] and 0.0003 $\mu g/mL$ [72] for OL and SV, respectively) and clearance (Cl/F, 26100 mL/h [73] and 3749160 mL/h [72] for OL and SV, respectively, where F corresponds to the bioavailability) of typical administered oral doses of OL and SV for a specific area of skin application (A, 40 cm^2). This yields an estimated flow rate of 3.64 $\mu g/cm^2/h$ for OL and 1.42 $\mu g/cm^2/h$ for SV, which is in good agreement with the previous calculations. The *in vitro* results obtained in the present work are above these target values and although a fine-tuning of the doses can be easily performed, it should be noted that the present results are very promising for most common therapeutic indications.

Along with the significant enhancement action, the lag time for OL is also shorter than that of SV, and no significant difference was found for OL when limonene was added to the NLC. Although the time reported to achieve steady state for simvastatin is increased with limonene inclusion, it should be noted that the flux is higher, and starts earlier (see Table 4.7). A similar observation is made for OL. In turn, saturated solutions do not allow the estimation of this parameter, due to the small flux. It should be noted that, due to the chronic nature of these particular diseases, the relatively long lag times, are not considered an issue if the therapeutic response is ensured.

Permeation, EE and release

Complementary studies for the assessment of the effect of ethanol and limonene in the EE and release behavior were also performed. Ethanol decreases both the entrapment efficiency for SV and OL, relative to the NLC dispersion, as demonstrated in the supplementary information (see Table 4.9). Interestingly, the further addition of limonene increases this EE, although values are still below those found for the aqueous dispersion. This could be ascribed to the hydrophobic nature of limonene, characterized by a high partition coefficient. The NLC dispersion, in turn, displays the lowest release rate (Figure 4.9), both for SV and OL. When ethanol is added, the release rate markedly increases. Upon the addition of limonene, the release decreases for OL, although the values are still clearly above those corresponding to the dispersion. In the case of SV, the release profiles for NLC+Et and NLC+Et+L are very similar. It should be noted that this behavior cannot be directly related with that found for permeation. In fact, there is only a relatively small increase in the total drug released after 48 h when the NLC dispersion is successively added with ethanol and limonene. However, a drastic increase in the permeation rate, respectively, 8 and 10 times higher for OL and SV, by the addition of limonene, is observed. As such, while ethanol favors both the permeation and release, the further addition of limonene increases permeation, but has a deleterious effect on release. Note that this reinforces the findings from the experimental design, above in this section, indicating a synergistic effect between NLC and permeation enhancers. Note also that these results point to a direct permeation enhancement effect of limonene, rather than a simple effect upon the release rate.

Table 4.9 OL and SV entrapment efficiency for the NLC dispersion and after the addition of the permeation enhancers. Results are expressed as mean±SD, n=3.

Formulation	EE (%) SV	EE (%) OL
NLC	99.74±0.08	96.4±0.3
NLC + 30%Et	86.±2	84.±2
NLC + 30%Et + 5%L	97.3±0.2	90.7±0.3
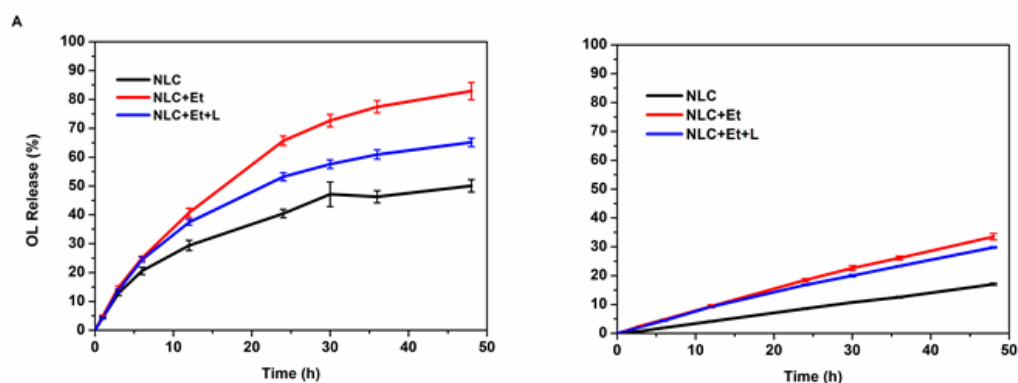
Figure 4.9 Release profiles of NLC before and after the addition of ethanol and limonene. (A) olanzapine, (B) simvastatin. Results are expressed as mean±SEM (n=3)

4.3.7 Effect of hydrogel

From the factorial design based on permeation, the optimal formulation was selected to be incorporated into a Carbopol® Ultrez 10 hydrogel. Comparing the permeation profiles obtained from Combo-NLC+Et+L dispersions and hydrogels (Figure 4.10), a decrease in the flux (15±2 to 7.5±0.3 $\mu g/cm^2/h$ for OL and 7.0±0.8 to 3.6±0.3 $\mu g/cm^2/h$ for SV) and permeability coefficient ($10\times10^{-3}\pm1\times10^{-3}$ to $4.8\times10^{-3}\pm0.2\times10^{-3}$ for OL and $3.9\times10^{-3}\pm0.5\times10^{-3}$ cm/h to $2.1\times10^{-3}\pm0.2\times10^{-3}$ for SV) roughly by half was observed for both drugs. This behaviour might be due to the release retarding effect of the polymeric matrix and the increasing viscosity promoted by the gelling agent. Similar effects have already been observed [74]. However, the values obtained still remain above the target flux described above, which corroborate the feasibility of transdermal delivery.
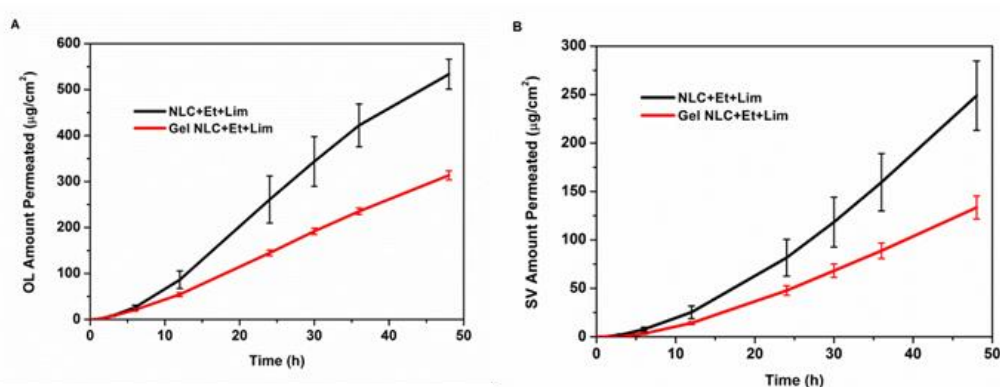
Figure 4.10 Permeation profiles obtained for the previously optimized dispersion and respective hydrogel: (A) olanzapine, (B) simvastatin. (mean±SEM; n=6)

In order to elucidate the structure of the hydrogel, Nile red-labeled Combo-NLC were prepared and analyzed by CLSM, before and after incorporation into hydrogel (Figure 4.11).
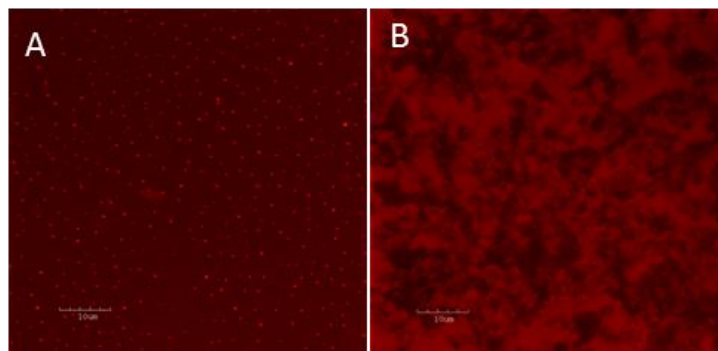
Figure 4.11 Fluorescence images of the Nile red-labeled Combo-NLC dispersion (A) and after incorporation into hydrogel (B).

The fluorescence image of NLC corroborates the DLS results, illustrating a homogeneous dispersion. After incorporation into the hydrogel, nanoparticles were entrapped in the entanglements of the gelling polymer forming grain domains, although preserving a relatively uniform distribution.

4.3.8 Cytotoxicity and cell uptake studies

To investigate the potential cytotoxicity of the NLC dispersions, the cell viability was evaluated using Df and HaCaT cell lines in a MTT assay. Firstly, the effect of the pure compounds, OL and SV, was assessed, and subsequently, that of the NLC dispersions, including unloaded NLC, SV-NLC, OL-NLC and Combo-NLC formulations. Hydrogel formulations, with and without permeation enhancers and Combo-NLC were also analyzed for completeness.

SV and OL presented different behaviors in terms of cell toxicity, depending on the cells tested. OL is not cytotoxic in both Df and HaCaT cells on the range of concentrations tested, 7-216 µM (Table 4.10). SV is only cytotoxic for HaCaT cells in the range tested (5-161 µM), presenting an IC_{50} of 12.±1 µM (Table 4.10). This value is not significantly altered in the presence of OL (IC_{50} 13.±1 µM, see Table 4.10). The NLC encapsulating 10 µM of SV (Figure 4.12), either alone or co-encapsulated with OL at the same concentrations, present a cytotoxicity similar to that of the free drug, which is compatible with release throughout the assay.

Table 4.10 IC_{50} calculated for the drug solutions considered in the cytotoxicity studies using Df and HaCaT cell lines.

IC_{50} (µM)	Cell lines	
Drug solution	**Df**	**HaCaT**
OL	>216	>216
SV	>161	12.±1
OL+SV	>161	13.±1
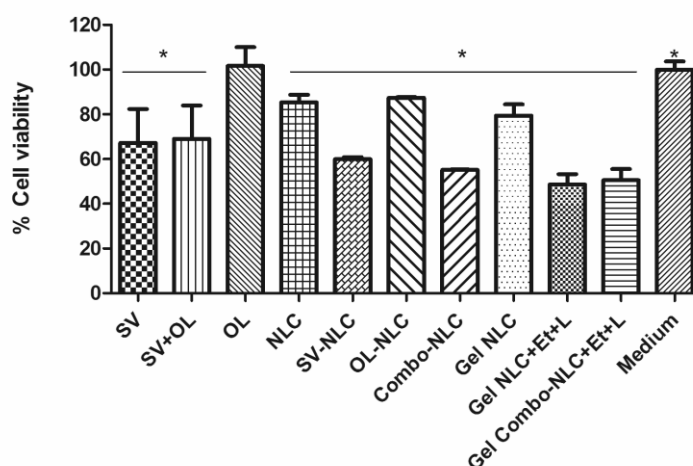
Figure 4.12 Viability of HaCaT cells after 72 h of incubation with SV in the concentration of 10 µM, either in the free form or incorporated into the NLC. Results pertaining to the hydrogel permeation enhancers are also presented. For these formulations, a concentration of 7 µM of SV was considered as a result of the incorporation of enhancers. Data are expressed as mean±SD. (n=9) * p < 0.05 vs medium.

The incorporation of NLC into the hydrogel did not increase the cytotoxicity, in contrast to what happens when ethanol and limonene were added to the formulation, in which some increase is observed. However, the respective amounts are generally reported as safe and used in different applications [75, 76]. Finally, the NLC hydrogel formulation containing both drugs and permeation enhancers did not result in additional cytotoxicity. Note that, according to the relevant OECD guideline [77], an irritant substance is predicted if the mean relative tissue viability is found below 50% of the mean viability of the negative controls for a 15-60 min exposition time. In the present assay, cells were exposed to test samples for 72 h with the cell viability above 50%, both for the NLC dispersion and gel. Thus, the formulations can be considered non-irritant.

The uptake by HaCaT cells of Nile red labeled Combo-NLC, both in dispersion and incorporated into the hydrogel containing the enhancers, was performed in order to assess the degree of NLC internalization (Figure 4.13). After 1h of incubation, the NLC aqueous dispersion led to a mean fluorescent intensity four times higher than that of the hydrogel (496 *vs.* 131, respectively). These results corroborate a good affinity and biocompatibility between the nanoparticles formulations and skin model cells. This conclusion holds even when internalization takes place, which is especially relevant in the case of contact with damaged skin. [78]
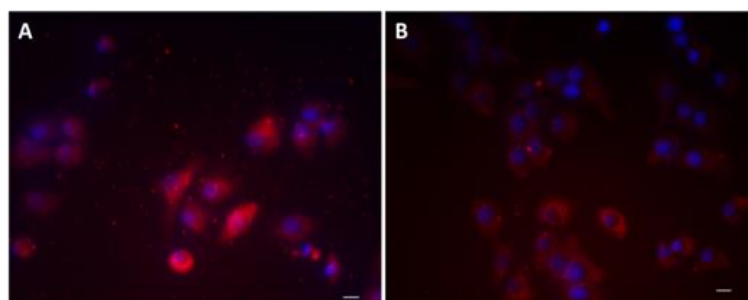
Figure 4.13 Fluorescent microphotographies (40x) in Zeiss Microscope Axioskope 40 (AxioCam HRc) of the nanoparticles Nile red labeled uptake by HaCaT keratinocyte cell line: (A) Combo-NLC; (B) Hydrogel Combo-NLC+Et+L (scale bar 20 µm).

4.3.9 Stability studies

The results pertaining to the physicochemical stability of the optimized formulation (Figure 4.14) reveal that the NLC size is not affected by storage temperature, within the range tested, and is not significantly altered after 6 months. The stability of the particles, indicated by the zeta potential, remains essentially unaltered, once stored at low temperature (4ºC). Regarding the entrapment efficiency, it remains higher than 95% for both drugs, although there is evidence of OL degradation when stored at 25ºC.
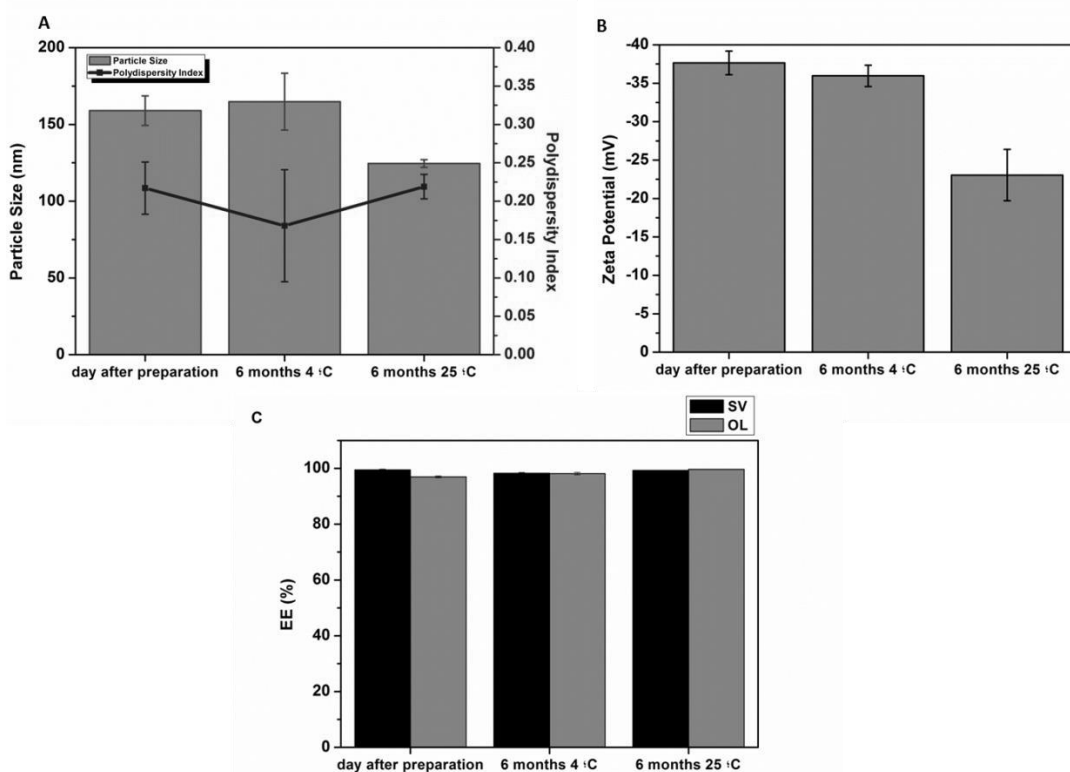
Figure 4.14 (A) Particle size, (B) zeta potential and (C) entrapment efficiency of the optimized formulation for six months.

4.4 Conclusions

Factorial design has proved to be a useful tool, both for rationalization of the system behavior and optimization of the formulation composition. NLC formulations were able to efficiently co-entrap olanzapine and simvastatin, and provide a reservoir system for long-term administration. Molecular dynamics simulation provided direct insight on the mechanism of drug enhancement associated to some terpenes considered in the screening phase, and corroborated the experimental results. The combination of NLC plus ethanol and limonene yielded the best permeation rate, with a marked synergistic effect. In addition, the developed formulations can be considered non-irritant. Biocompatibility, the ability to sustainably deliver a broad range of APIs and the versatility to modulate formulation design turn these lipid nanoparticles into a delivery system very appropriate for a concomitant transdermal administration of olanzapine and simvastatin.

References

1. Kenneth, W. and R. Michael, The Structure and Function of Skin, in Dermatological and Transdermal Formulations2002, Informa Healthcare.

2. Muller, R.H. and C.M. Keck, Challenges and solutions for the delivery of biotech drugs - a review of drug nanocrystal technology and lipid nanoparticles. Journal of Biotechnology, 2004. 113(1-3): p. 151-170.

3. Jenning, V., M. Schäfer-Korting, and S. Gohla, Vitamin A-loaded solid lipid nanoparticles for topical use: drug release properties. Journal of Controlled Release, 2000. 66(2–3): p. 115-126.

4. Müller, R.H., R.D. Petersen, A. Hommoss, and J. Pardeike, Nanostructured lipid carriers (NLC) in cosmetic dermal products. Advanced Drug Delivery Reviews, 2007. 59(6): p. 522-530.

5. Sanna, V., G. Caria, and A. Mariani, Effect of lipid nanoparticles containing fatty alcohols having different chain length on the ex vivo skin permeability of Econazole nitrate. Powder Technology, 2010. 201(1): p. 32-36.

6. Puglia, C. and F. Bonina, Lipid nanoparticles as novel delivery systems for cosmetics and dermal pharmaceuticals. Expert Opinion on Drug Delivery, 2012. 9(4): p. 429-441.

7. Kantrowitz, J.T. and L. Citrome, Olanzapine: review of safety 2008. Expert Opinion on Drug Safety, 2008. 7(6): p. 761-769.

8. Lieberman, J.A., T.S. Stroup, J.P. McEvoy, M.S. Swartz, R.A. Rosenheck, D.O. Perkins, R.S.E. Keefe, S.M. Davis, C.E. Davis, B.D. Lebowitz, J. Severe, and J.K. Hsiao, Effectiveness of Antipsychotic Drugs in Patients with Chronic Schizophrenia. New England Journal of Medicine, 2005. 353(12): p. 1209-1223.

9. McEvoy, J.P., J.M. Meyer, D.C. Goff, H.A. Nasrallah, S.M. Davis, L. Sullivan, H.Y. Meltzer, J. Hsiao, T. Scott Stroup, and J.A. Lieberman, Prevalence of the metabolic syndrome in patients with schizophrenia: Baseline results from the Clinical Antipsychotic Trials of Intervention Effectiveness (CATIE) schizophrenia trial and comparison with national estimates from NHANES III. Schizophrenia Research, 2005. 80(1): p. 19-32.

10. Capasso, R.M., T.W. Lineberry, J.M. Bostwick, P.A. Decker, and J. St. Sauver, Mortality in schizophrenia and schizoaffective disorder: An Olmsted County, Minnesota cohort: 1950–2005. Schizophrenia Research, 2008. 98(1): p. 287-294.

11. Saha, S., D. Chant, and J. McGrath, A systematic review of mortality in schizophrenia: Is the differential mortality gap worsening over time? Archives of General Psychiatry, 2007. 64(10): p. 1123-1131.

12. Ballantyne, C.M., A.G. Olsson, T.J. Cook, M.F. Mercuri, T.R. Pedersen, J. Kjekshus, and f.t.S.S.S.S. Group, Influence of Low High-Density Lipoprotein Cholesterol and Elevated Triglyceride on Coronary Heart Disease Events and Response to Simvastatin Therapy in 4S. Circulation, 2001. 104(25): p. 3046-3051.

13. Heart Protection Study Collaborative, G., Effects on 11-year mortality and morbidity of lowering LDL cholesterol with simvastatin for about 5 years in 20?536 high-risk individuals: a randomised controlled trial. The Lancet, 2011. 378(9808): p. 2013-2020.

14. Mauri, M.C., L.S. Volonteri, A. Colasanti, A. Fiorentini, I.F. De Gaspari, and S.R. Bareggi, Clinical Pharmacokinetics of Atypical Antipsychotics: A Critical Review of the Relationship Between Plasma Concentrations and Clinical Response. Clinical Pharmacokinetics, 2007. 46(5): p. 359-388.

15. Schachter, M., Chemical, pharmacokinetic and pharmacodynamic properties of statins: an update. Fundamental & Clinical Pharmacology, 2005. 19(1): p. 117-125.

16. Alexander, A., S. Dwivedi, Ajazuddin, T.K. Giri, S. Saraf, S. Saraf, and D.K. Tripathi, Approaches for breaking the barriers of drug permeation through transdermal drug delivery. Journal of Controlled Release, 2012. 164(1): p. 26-40.

17. Vitorino, C., F.A. Carvalho, A.J. Almeida, J.J. Sousa, and A.A.C.C. Pais, The size of solid lipid nanoparticles: An interpretation from experimental design. Colloids and Surfaces B: Biointerfaces, 2011. 84(1): p. 117-130.

18. Joshi, M. and V. Patravale, Formulation and Evaluation of Nanostructured Lipid Carrier (NLC)–based Gel of Valdecoxib. Drug Development and Industrial Pharmacy, 2006. 32(8): p. 911 - 918.

19. Pardeike, J., A. Hommoss, and R.H. Müller, Lipid nanoparticles (SLN, NLC) in cosmetic and pharmaceutical dermal products. International Journal of Pharmaceutics, 2009. 366(1-2): p. 170-184.

20. ISO13321, Methods for Determination of Particle Size Distribution Part 8: Photon Correlation Spectroscopy, International Organisation for Standardisaton (ISO). 1996.

21. ISO22412, Particle Size Analysis – Dynamic Light Scattering, International Organisation for Standardisation (ISO). 2008.

22. Doktorovova, S. and E.B. Souto, Nanostructured lipid carrier-based hydrogel formulations for drug delivery: A comprehensive review. Expert Opinion on Drug Delivery, 2009. 6(2): p. 165-176.

23. Eaton, J.W., GNU Octave software, version 3.2.3. 2009.

24. Kenneth, W., W. Adam, and B. Keith, Methods for Studying Percutaneous Absorption, in Dermatological and Transdermal Formulations2002, Informa Healthcare.

25. Junyaprasert, V.B., V. Teeranachaideekul, E.B. Souto, P. Boonme, and R.H. Müller, Q10-loaded NLC versus nanoemulsions: Stability, rheology and in vitro skin permeation. International Journal of Pharmaceutics, 2009. 377(1–2): p. 207-214.

26. Kassis, V. and J. Søndergaard, Heat-separation of normal human skin for epidermal and dermal prostaglandin analysis. Archives of Dermatological Research, 1982. 273(3): p. 301-306.

27. Finnin, B., K.A. Walters, and T.J. Franz, In vitro Skin Permeation Methodology, in Transdermal and Topical Drug Delivery2011, John Wiley & Sons, Inc. p. 85-108.

28. Lv, Q., A. Yu, Y. Xi, H. Li, Z. Song, J. Cui, F. Cao, and G. Zhai, Development and evaluation of penciclovir-loaded solid lipid nanoparticles for topical delivery. International Journal of Pharmaceutics, 2009. 372(1-2): p. 191-198.

29. Mandawgade, S.D. and V.B. Patravale, Development of SLNs from natural lipids: Application to topical delivery of tretinoin. International Journal of Pharmaceutics, 2008. 363(1–2): p. 132-138.

30. Li, S.K., W. Suh, H.H. Parikh, A.-H. Ghanem, S.C. Mehta, K.D. Peck, and W.I. Higuchi, Lag time data for characterizing the pore pathway of intact and chemically pretreated human epidermal membrane. International Journal of Pharmaceutics, 1998. 170(1): p. 93-108.

31. Kang, L., C.W. Yap, P.F.C. Lim, Y.Z. Chen, P.C. Ho, Y.W. Chan, G.P. Wong, and S.Y. Chan, Formulation development of transdermal dosage forms: Quantitative structure-activity relationship model for predicting activities of terpenes that enhance drug penetration through human skin. Journal of Controlled Release, 2007. 120(3): p. 211-219.

32. El-Kattan, A.F., C.S. Asbill, and B.B. Michniak, The effect of terpene enhancer lipophilicity on the percutaneous permeation of hydrocortisone formulated in HPMC gel systems. International Journal of Pharmaceutics, 2000. 198(2): p. 179-189.

33. Aqil, M., A. Ahad, Y. Sultana, and A. Ali, Status of terpenes as skin penetration enhancers. Drug Discovery Today, 2007. 12(23–24): p. 1061-1067.

34. Sapra, B., S. Jain, and A. Tiwary, Percutaneous Permeation Enhancement by Terpenes: Mechanistic View. The AAPS Journal, 2008. 10(1): p. 120-132.

35. Bennett, W.F.D., J.L. MacCallum, and D.P. Tieleman, Thermodynamic Analysis of the Effect of Cholesterol on Dipalmitoylphosphatidylcholine Lipid Membranes. Journal of the American Chemical Society, 2009. 131(5): p. 1972-1978.

36. Almeida, J.A.S., E.F. Marques, A.S. Jurado, and A.A.C.C. Pais, The effect of cationic gemini surfactants upon lipid membranes. An experimental and molecular dynamics simulation study. Physical Chemistry Chemical Physics, 2010. 12(43): p. 14462-14476.

37. Kukol, A., Lipid Models for United-Atom Molecular Dynamics Simulations of Proteins. Journal of Chemical Theory and Computation, 2009. 5(3): p. 615-626.

38. Kyrikou, I., S.K. Hadjikakou, D. Kovala-Demertzi, K. Viras, and T. Mavromoustakos, Effects of non-steroid anti-inflammatory drugs in membrane bilayers. Chemistry and Physics of Lipids, 2004. 132(2): p. 157-169.

39. Gurtovenko, A.A. and J. Anwar, Modulating the Structure and Properties of Cell Membranes: The Molecular Mechanism of Action of Dimethyl Sulfoxide. The Journal of Physical Chemistry B, 2007. 111(35): p. 10453-10460.

40. Notman, R., M. Noro, B. O'Malley, and J. Anwar, Molecular Basis for Dimethylsulfoxide (DMSO) Action on Lipid Membranes. Journal of the American Chemical Society, 2006. 128(43): p. 13982-13983.

41. Cerezo, J., J. Zúñiga, A. Bastida, A. Requena, and J.P. Cerón-Carrasco, Atomistic Molecular Dynamics Simulations of the Interactions of Oleic and 2-Hydroxyoleic Acids with Phosphatidylcholine Bilayers. The Journal of Physical Chemistry B, 2011. 115(40): p. 11727-11738.

42. Almeida, J.A.S., H. Faneca, R.A. Carvalho, E.F. Marques, and A.A.C.C. Pais, Dicationic Alkylammonium Bromide Gemini Surfactants. Membrane Perturbation and Skin Irritation. PLoS ONE, 2011. 6(11): p. e26965.

43. Schuler, L.D., X. Daura, and W.F. Van Gunsteren, An improved GROMOS96 force field for aliphatic hydrocarbons in the condensed phase. Journal of Computational Chemistry, 2001. 22(11): p. 1205-1218.

44. Piggot, T.J., Á. Piñeiro, and S. Khalid, Molecular Dynamics Simulations of Phosphatidylcholine Membranes: A Comparative Force Field Study. Journal of Chemical Theory and Computation, 2012. 8(11): p. 4593-4609.

45. Poger, D. and A.E. Mark, On the Validation of Molecular Dynamics Simulations of Saturated and cis-Monounsaturated Phosphatidylcholine Lipid Bilayers: A Comparison with Experiment. Journal of Chemical Theory and Computation, 2009. 6(1): p. 325-336.

46. Schuttelkopf, A.W. and D.M.F. van Aalten, PRODRG: a tool for high-throughput crystallography of protein-ligand complexes. Acta Crystallographica Section D, 2004. 60(8): p. 1355-1363.

47. Malde, A.K., L. Zuo, M. Breeze, M. Stroet, D. Poger, P.C. Nair, C. Oostenbrink, and A.E. Mark, An Automated Force Field Topology Builder (ATB) and Repository: Version 1.0. Journal of Chemical Theory and Computation, 2011. 7(12): p. 4026-4037.

48. Hess, B., C. Kutzner, D. van der Spoel, and E. Lindahl, GROMACS 4: Algorithms for Highly Efficient, Load-Balanced, and Scalable Molecular Simulation. Journal of Chemical Theory and Computation, 2008. 4(3): p. 435-447.

49. van der Spoel, D., P.J. van Maaren, and C. Caleman, GROMACS molecule & liquid database. Bioinformatics, 2012. 28(5): p. 752-753.

50. Hess, B., H. Bekker, H.J.C. Berendsen, and J. Fraaije, LINCS: A linear constraint solver for molecular simulations. Journal of Computational Chemistry, 1997. 18(12): p. 1463-1472.

51. Humphrey, W., A. Dalke, and K. Schulten, VMD: Visual molecular dynamics. Journal of Molecular Graphics, 1996. 14(1): p. 33-38.

52. Vitorino, C., J.J. Sousa, and A.A.C.C. Canelas, Manuscript in preparation.

53. Piecha, M., M. Sarakha, P. Trebše, and D. Kočar, Stability studies of cholesterol lowering statin drugs in aqueous samples using HPLC and LC–MS. Environmental Chemistry Letters, 2010. 8(2): p. 185-191.

54. Jemal, M., Z. Ouyang, and M.L. Powell, Direct-injection LC–MS–MS method for high-throughput simultaneous quantitation of simvastatin and simvastatin acid in human plasma. Journal of Pharmaceutical and Biomedical Analysis, 2000. 23(2–3): p. 323-340.

55. Strober, W., Trypan Blue Exclusion Test of Cell Viability, in Current Protocols in Immunology2001, John Wiley & Sons, Inc.

56. Cadete, A., L. Figueiredo, R. Lopes, C.C.R. Calado, A.J. Almeida, and L.M.D. Gonçalves, Development and characterization of a new plasmid delivery system based on chitosan–sodium deoxycholate nanoparticles. European Journal of Pharmaceutical Sciences, 2012. 45(4): p. 451-458.

57. Lopes, R., C.V. Eleutério, L.M.D. Gonçalves, M.E.M. Cruz, and A.J. Almeida, Lipid nanoparticles containing oryzalin for the treatment of leishmaniasis. European Journal of Pharmaceutical Sciences, 2012. 45(4): p. 442-450.

58. Subedi, R.K., K.W. Kang, and H.-K. Choi, Preparation and characterization of solid lipid nanoparticles loaded with doxorubicin. European Journal of Pharmaceutical Sciences, 2009. 37(3-4): p. 508-513.

59. Williams, A.C. and B.W. Barry, Penetration enhancers. Advanced Drug Delivery Reviews, 2004. 56(5): p. 603-618.

60. Trommer, H. and R.H.H. Neubert, Overcoming the Stratum Corneum: The Modulation of Skin Penetration. Skin Pharmacology and Physiology, 2006. 19(2): p. 106-121.

61. Mehnert, W. and K. Mäder, Solid lipid nanoparticles: Production, characterization and applications. Advanced Drug Delivery Reviews, 2001. 47(2-3): p. 165-196.

62. Mäder, K. and W. Mehnert, eds. 1 - Solid Lipid Nanoparticles—Concepts, Procedures, and Physicochemical Aspects. Lipospheres in drug targets and delivery: approaches, methods, and applications, ed. C. Nastruzzi2004, CRC Press. 1 - 22.

63. Helgason, T., T.S. Awad, K. Kristbergsson, D.J. McClements, and J. Weiss, Effect of surfactant surface coverage on formation of solid lipid nanoparticles (SLN). Journal of Colloid and Interface Science, 2009. 334(1): p. 75-81.

64. Iqbal, M.A., S. Md, J.K. Sahni, S. Baboota, S. Dang, and J. Ali, Nanostructured lipid carriers system: Recent advances in drug delivery. Journal of Drug Targeting, 2012. 20(10): p. 813-830.

65. Walker, R.B. and E.W. Smith, The role of percutaneous penetration enhancers. Advanced Drug Delivery Reviews, 1996. 18(3): p. 295-301.

66. Narishetty, S.T.K. and R. Panchagnula, Transdermal delivery system for zidovudine: in vitro, ex vivo and in vivo evaluation. Biopharmaceutics & Drug Disposition, 2004. 25(1): p. 9-20.

67. Kunta, J.R., V.R. Goskonda, H.O. Brotherton, M.A. Khan, and I.K. Reddy, Effect of menthol and related terpenes on the percutaneous absorption of propranolol across excised hairless mouse skin. Journal of Pharmaceutical Sciences, 1997. 86(12): p. 1369-1373.

68. Kararli, T.T., C.F. Kirchhoff, and S.C. Penzotti Jr, Enhancement of transdermal transport of azidothymidine (AZT) with novel terpene and terpene-like enhancers: In vivo-in vitro correlations. Journal of Controlled Release, 1995. 34(1): p. 43-51.

69. Nokhodchi, A., K. Sharabiani, M.R. Rashidi, and T. Ghafourian, The effect of terpene concentrations on the skin penetration of diclofenac sodium. International Journal of Pharmaceutics, 2007. 335(1–2): p. 97-105.

70. dos Anjos, J.L.V. and A. Alonso, Terpenes increase the partitioning and molecular dynamics of an amphipathic spin label in stratum corneum membranes. International Journal of Pharmaceutics, 2008. 350(1–2): p. 103-112.

71. Perry, P.J., T. Sanger, and C. Beasley, Olanzapine Plasma Concentrations and Clinical Response in Acutely Ill Schizophrenic Patients. Journal of Clinical Psychopharmacology, 1997. 17(6): p. 472-477.

72. Tubic-Grozdanis, M., J. Hilfinger, G. Amidon, J. Kim, P. Kijek, P. Staubach, and P. Langguth, Pharmacokinetics of the CYP 3A Substrate Simvastatin following Administration of Delayed Versus Immediate Release Oral Dosage Forms. Pharmaceutical Research, 2008. 25(7): p. 1591-1600.

73. Callaghan, J.T., R.F. Bergstrom, L.R. Ptak, and C.M. Beasley, Olanzapine: Pharmacokinetic and Pharmacodynamic Profile. Clinical Pharmacokinetics, 1999. 37(3): p. 177-193.

74. Bhaskar, K., C.K. Mohan, M. Lingam, S.J. Mohan, V. Venkateswarlu, Y.M. Rao, J. Anbu, and V. Ravichandran, Development of SLN and NLC Enriched Hydrogels for Transdermal Delivery of Nitrendipine: In vitro and In Vivo Characteristics. Drug Development and Industrial Pharmacy, 2009. 35(1): p. 98-113.

75. Prasad, R., V. Koul, S. Anand, and R.K. Khar, Effect of DC/mDC iontophoresis and terpenes on transdermal permeation of methotrexate: In vitro study. International Journal of Pharmaceutics, 2007. 333(1–2): p. 70-78.

76. Zhao, K. and J. Singh, In vitro percutaneous absorption enhancement of propranolol hydrochloride through porcine epidermis by terpenes/ethanol. Journal of Controlled Release, 1999. 62(3): p. 359-366.

77. Test No. 439: In vitro Skin Irritation: Reconstructed Human Epidermis Test Method. OECD Guidelines for the Testing of Chemicals, 2010. 1(4): p. 1-18.

78. Küchler, S., M.R. Radowski, T. Blaschke, M. Dathe, J. Plendl, R. Haag, M. Schäfer-Korting, and K.D. Kramer, Nanoparticles for skin penetration enhancement – A comparison of a dendritic core-multishell-nanotransporter and solid lipid nanoparticles. European Journal of Pharmaceutics and Biopharmaceutics, 2009. 71(2): p. 243-250.

Chapter 5

Development and validation of a rapid reversed-phase HPLC method for the simultaneous analysis of olanzapine and simvastatin in nanostructured lipid carriers

5.1 Introduction

The characterization of the Combo-NLC formulation described in the previous chapter requires a suitable and validated method for a critical assessment of pharmaceutical parameters such as drug content. Literature review reveals that HPLC methods have been reported for the quantitation of simvastatin [1] and olanzapine [2] separately, in combination with other drugs [3-5] and a few bioanalytical methods are also reported [6-9]. However, up to now, there have been no published reports about the simultaneous quantitation of simvastatin and olanzapine by HPLC in a pharmaceutical formulation.

In the present chapter, the development and validation of a simple and time-saving RP-HPLC method with UV detection for simultaneous determination of OL, SV and SVA is described. The latter was also considered for analysis, since it is known that the lactone form of statins would be easily converted to their corresponding hydroxy acids in water and plasma, and the conversion would be enhanced in alkaline conditions [50].

The validated method was applied to quantify both the content of SV/SVA and OL incorporated in the NLC after preparation.

5.2 Materials and methods

5.2.1 Materials

Simvastatin (99.4%) was kindly provided by Labesfal - Laboratórios Almiro, S.A. (Santiago de Besteiros, Portugal). Olanzapine (98.9%) was purchased from Zhejiang MYJOY Import & Export Co.,Ltd (Hangzhou, China). Glyceryl tripalmitate (tripalmitin, T8127) and polysorbate 80 (Tween® 80) were purchased from Sigma. Oleic acid was acquired from Fluka. Carbopol® Ultrez 10 NF was a gift from Lubrizol (Quimidroga, Barcelona, Spain). All other reagents and solvents were from analytical or HPLC grade.

5.2.2 Instrumentation and chromatographic conditions

The HPLC analysis of OL, SV and the active form SVA was carried out in a Shimadzu LC-2010C HT apparatus (Shimadzu Co., Kyoto, Japan) equipped with a quaternary pump, a vacuum degasser, an autosampler, an oven and a variable UV/visible dual wavelength detector. The column used for the analysis was a Luna Phenyl-Hexyl, Phenomenex® (Torrance, USA), with 5 µm particle size, 3 mm internal diameter and 150 mm length, supported with a SecurityGuard™ cartridge Phenomenex® (Torrance, USA), with 3 mm internal diameter, in an oven at a temperature of 35ºC. The results were acquired and processed using Shimadzu LC-solution version 1.12 software. Chromatographic analysis was conducted in isocratic mode. The mobile phase consisted of a mixture of ammonium acetate aqueous solution 0.02 M:methanol:acetonitrile, 30:35:35 (V/V/V), at a constant flow rate of 0.8 mL/min. A run time of 7 min was established for separation of the three compounds. The detection was carried out at 230 nm. An injection volume of 10 µL was used for all standards and samples.

5.2.3 Preparation of stock solutions, calibration standards and quality controls

Three methanolic stock solutions at 1 mg/mL of OL, SV and SVA were prepared. The OL and SV stock solutions were prepared by accurately weighing approximately 10 mg of OL and SV in 10 mL of methanol. Regarding SVA, since it is reported that lactones are unstable at alkaline pH [10], it was obtained by alkaline hydrolysis of SV, according to references [11, 12]. Briefly, a SV methanolic solution of 2 mg/mL was firstly prepared. One volume of this solution was added to one volume of 0.04 M NaOH, heated at 60ºC for 45 min and kept overnight at room temperature. The mixture was subsequently

neutralized with 1M HCl, yielding a SVA solution with a concentration of ca. 1 mg/mL. The complete hydrolysis of SV was confirmed by the absence of the SV peak in HPLC. These results were also supported by LC-MS/MS, which presented a transition ion m/z at 459.5/343.3 in the positive-ion mode, comparable to what is reported in the literature [13]. Two working standard solutions containing OL, SV and SVA at concentrations of 100 and 10 µg/mL were prepared by further dilution of each stock solution with mobile phase. Eight standard solutions (0.5, 1, 5, 10, 25, 50, 75 and 100 µg/mL) were obtained by appropriate dilution of the working standard solutions with mobile phase. As quality control (QC), six replicates of 0.5, 1.5, 50 and 100 µg/mL standards containing the three compounds were considered. For determination of the limit of detection (LD) and limit of quantitation (LQ) of the method, six standard solutions, namely, 0.1, 0.25, 0.5, 0.75, 1 and 1.25 µg/mL were obtained from the 10 µg/mL working solution. All stock solutions were stored at -20 ºC and working solutions were freshly prepared each day.

5.2.4 Method validation

The HPLC method was validated according to the US Food and Drug Administration (FDA) regulations [14], including also some complementary aspects taken from the International Conference on Harmonization (ICH) guidelines [15]. The parameters considered for the validation included selectivity and specificity, linearity, accuracy, precision, recovery, limits of detection and quantitation, system suitability and stability.

System suitability

The system suitability parameters were determined by injecting six times the standard solution containing OL, SV and SVA at a concentration of 75 µg/mL. The acceptance limit was RSD ≤2% of the peak area and the retention time of the three compounds [16]. Other chromatographic parameters, such as capacity factor (k'), resolution (R) tailing factor (T) and theoretical plate number (N) were also analyzed [17]. The capacity factor is a measure of where the peak of interest is located with respect to the void volume, i.e., corresponds to the elution time of the non-retained components. R is a measure of the degree of separation of two peaks. The tailing factor is a measure of the peak symmetry, and the theoretical plate number is a measure of the column efficiency, that is, how many peaks can be located per unit run-time of the chromatogram [18].

Limits of detection and quantification

The limits of detection and quantitation were determined based on a specific calibration curve obtained from six standard solutions (0.1, 0.25, 0.5, 0.75, 1 and 1.25 µg/mL) containing the three analytes at concentrations in the proximity of these limits values. LD and LQ were calculated according to LD = 3.3 σ/S and LQ = 10 σ/S, where σ is the standard deviation of the response and S is the slope of the calibration curve [15].

Linearity

Calibration curves were constructed with eight standard solutions, containing the three compounds simultaneously, ranging from 0.5 to 100 µg/mL. Linearity was determined through the calculation of a regression line by the method of least squares, representing the peak area as a function of the standard concentration. Data collected was analyzed using the Analysis ToolPak of Microsoft Excel$^{®}$ (Microsoft Corp., Redmond, WA) with linear regression by the least squares method. The analysis of the response factors, that is, the peak area divided by the concentration of each standard was also considered.

Accuracy and precision

Precision indicates the closeness of agreement, i.e., the degree of scatter between a series of measurements obtained from multiple sampling of the same homogeneous sample and it was determined by repeatability (intra-day) and intermediate precision (inter-day) for three consecutive days. Four standard solutions (quality controls), 0.5, 1.5, 50 and 100 µg/mL, respectively, were prepared six times each and analyzed according to the proposed method (intra-day precision) and three consecutive days (inter-day precision). The relative standard deviation (RSD) determined at each concentration level should not exceed 15%, except for the lower limit of quantitation, where it should not exceed 20% [14].

The accuracy of the method expresses the closeness of agreement between the conventional true value and the value found. It was determined by measuring six replicates of the four quality controls and by calculating the percentage of bias for each compound according to the equation: % accuracy = observed concentration/nominal concentration) x 100. The mean value should be within 15% of the actual value, except at the LQ, where it should not deviate by more than 20% [3, 14].

Specificity

The specificity of a method may be defined as the ability to accurately measure the analyte in the presence of all potential sample components [17]. In this method, the response of OL, SV and SVA, the major metabolite of SV degradation was compared with the response of a solution containing only the analytes, and used as measure of its specificity. This comparison has been made both with the nanoparticles components and the respective supernatant, the latter containing excess of lipids and surfactants.

Stability

The stability of OL, SV and SVA quality controls was assessed after a short-term storage at room temperature (~25 ºC) for 12 h, after a long-term storage for 30 days at -20 °C, in order to simulate sample handling and after 24 h of storage in the autosampler for the autosampler stability. The effect of three freeze–thaw cycles on the stability of the analytes was also investigated. QC samples were stored at -20 °C for 24 h, thawed unassisted at room temperature and, when completely thawed, the samples were refrozen for 24 h under the same conditions until completion of the three cycles [14].

Recovery

The recovery of OL, SV and SVA from the nanoparticles supernatant was determined by comparing the respective concentrations with those of standard solutions in mobile phase at three concentration levels 1, 50 and 100 µg/mL by repeated analysis (n = 6).

5.2.5 Method applicability

Preparation of Combo-NLC dispersion

The NLC were prepared by a hot high pressure homogenization technique, optimized as described in **Chapter 4** [13].

Determination of entrapment efficiency and drug loading

The entrapment efficiency of SV and OL in the NLC was determined indirectly by calculating the total amount of drug and subtracting that of the free drug in the aqueous phase of the nanoparticle dispersion. The separation of the two phases was carried out

by ultrafiltration, using Amicon® Ultra-4 centrifugal filter units (Merck Millipore, Darmstadt, Germany) with a 100 kDa molecular weight cut-off. The amount of free drug present in the aqueous phase was collected in the outer chamber of the centrifugal unit after separation, suitably diluted with mobile phase, filtered by a 0.22 µm membrane and determined by HPLC. For the estimation of the total drug, a specific volume of NLC suspension was accurately taken, diluted with mobile phase and heated at 60 °C for 15 min. The dispersion was further centrifuged for 10 min at 11,740×g in a Minispin® (Eppendorf Ibérica S.L., Madrid, Spain), and the supernatant filtered by a 0.22 µm membrane and analysed by HPLC. The entrapment efficiency (EE) and drug loading (DL) were calculated using the Equations (2.3) and (2.4), respectively, as described in Chapter 2.

As stated above, since statins exist, in general, in the lactone and hydroxy acid form, the respective conversion was taken into consideration, and both forms were quantified. Thus, SV entrapment efficiency is a result of the sum of SV (after stoichiometric conversion into SVA) and SVA contributions.

5.3   Results and discussion

5.3.1   Method development and optimization

A high performance liquid chromatography method for the estimation of olanzapine, simvastatin and simvastatin acid in a nanoparticulate dosage form has been developed according to the principles of Good Laboratory Practices. Optimization trials were carried out using a Lichrospher C18, by testing different proportions of ammonium acetate aqueous solution (0.02M):methanol:acetonitrile. Since OL and SV are poorly water soluble and more soluble in organic solvents, a higher percentage of methanol and acetonitrile was considered to diminish the retention time. By changing the column to Phenyl-hexyl, the retention times became even shorter and the peaks sharper. The optimized mobile phase was 30:35:35 (V/V/V) of ammonium acetate aqueous solution 0.02M:methanol:acetonitrile at a flow rate of 0.8 mL/min. For these conditions, simvastatin acid, olanzapine and simvastatin eluted at 1.7, 2.0 and 5.5 min, respectively. The method was validated over the range 0.5-100 µg/mL.

5.3.2 Method validation

System suitability

The RSD of peak area and retention time for OL, SV and SVA (Table 5.1, Figure 5.1) were lower than 2%, which indicates that the system is appropriate to simultaneously analyze the three compounds. The assessment of the column efficiency by the number of theoretical plates (N), the tailing factor (T), resolution (R_s) and capacity factor (k') show that the peaks were symmetric and generally well resolved. Although a $R_s \geq 2$ is reported, if the peaks are not significantly different in heights and possess nearly Gaussian shapes, the British Pharmacopoeia recommends $R_s \geq 1.5$ [16] for their complete separation at the baseline level.

Table 5.1 System suitability test parameters.

Chromatographic Parameters	OL (75µg/mL)		SV (75µg/mL)		SVA (75µg/mL)		Acceptance criteria
	Retention time (min)	Peak area	Retention time (min)	Peak area	Retention time (min)	Peak area	
Mean (n=6)	2.035	4877.466	5.662	2903.323	1.671	2834.957	-
S.D.	0.008	23.228	0.033	18.022	0.012	33.826	-
%RSD	0.41	2.04	0.59	0.62	0.71	1.19	≤2.0%[a]
Theoretical plates (N)	1661		4951		1340		>1000[a]
Capacity factor (k')	1.07		4.86		0.73		> 2.0[b]
Tailing factor (T)	1.71		1.18		1.67		≤ 2.0[b]
Resolution (R_s)	1.76		1.98		1.86		> 2.0[b]

[a] (Épshtein 2004), [b] (FDA 1994)
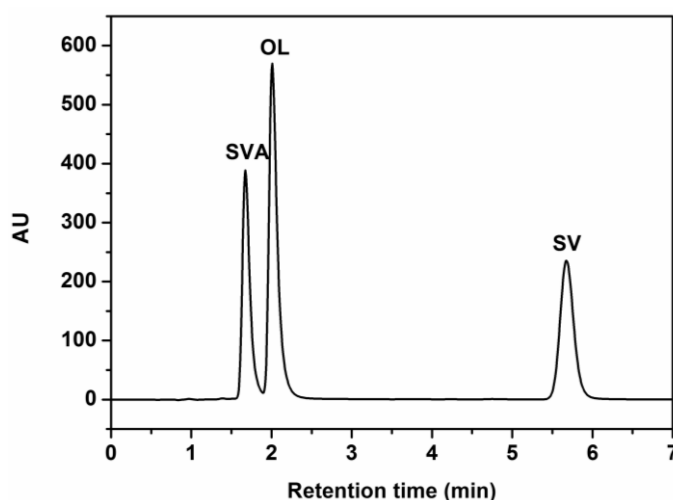
Figure 5.1 Chromatogram of the standard 75µg/mL solution of OL, SVA, and SV considered for the assessment of the system suitability.

Limits of detection and quantitation

The estimated LD for OL, SV and SVA were 0.07, 0.12 and 0.09 µg/mL, respectively. The LQ found for OL, SV and SVA were 0.22, 0.36 and 0.27 µg/mL, respectively.

Linearity

Linearity was evaluated over the concentration range 0.5-100 µg/mL for the OL, SV and SVA (Figure 5.2A, C, and E), estimating the regression equation and the determination coefficient (R^2) obtained from the least squares method (Table 5.2). The coefficients of determination for the calibration curves of the three compounds were higher than 0.999, which is generally considered as evidence of an acceptable fit of the data to the regression line [15, 17], and indicating a good linearity over the concentration range proposed. Moreover, from the analysis of the response factors (Figure 5.2B, D, and F) a slope close to zero was obtained (-0.0389, -0.0054 and -0.0377 , for OL, SV and SVA, respectively) and a relative residual standard deviation of 3.29%, 3.37% and 4.31%, thus confirming the method as linear [19, 20].
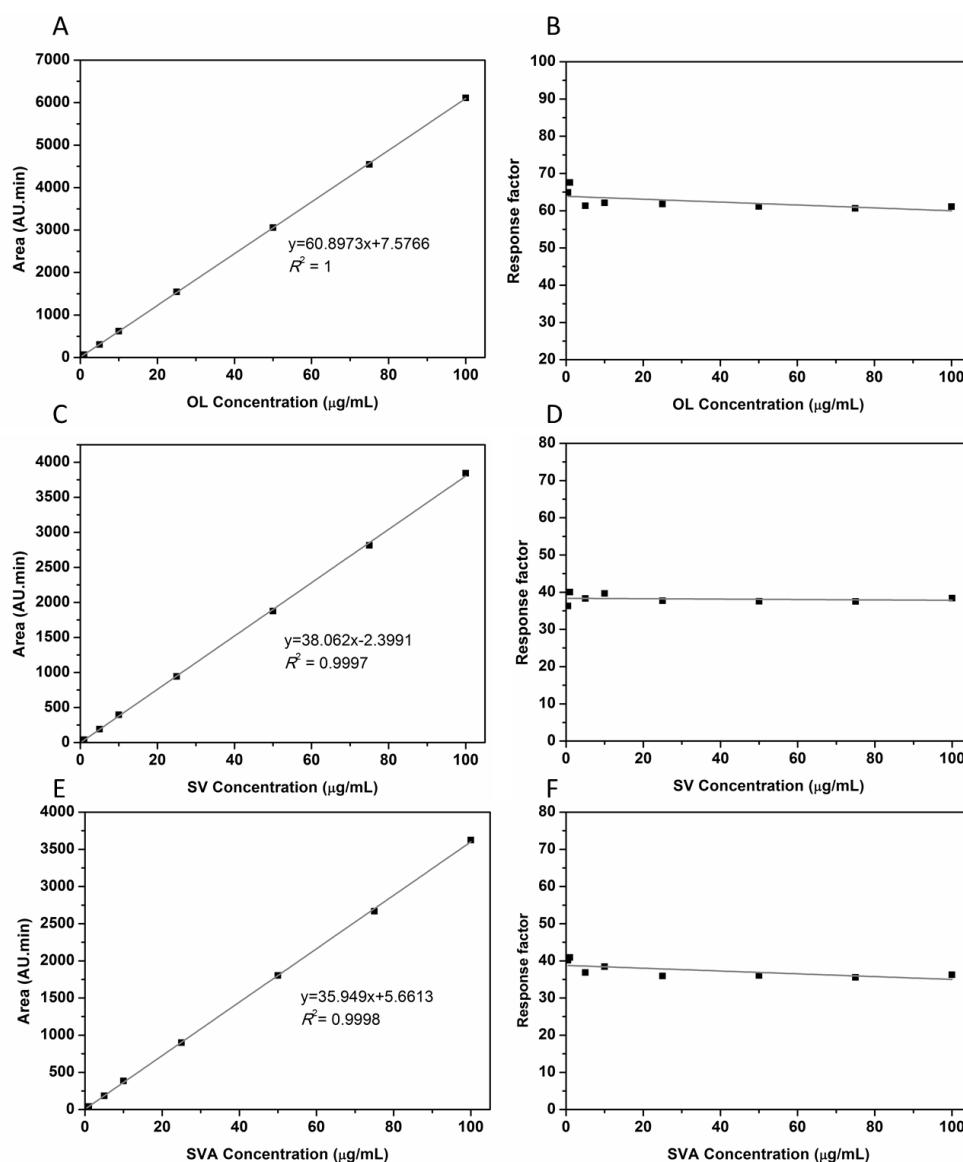
Figure 5.2 Linearity studies for the developed HPLC method: calibration curves obtained with OL (A), SV (C) and SVA (E) standard solutions, and response factor *versus* OL (B), SV (D) and SVA (F) standard solutions concentrations, respectively.

Table 5.2 Results obtained from the regression analysis by the least squares method for OL, SV and SVA.

Analyte	Mean R^2 ± S.D.	Mean slope ± S.D. (n=6)	Mean intercept[a] ± S.D. (n=6)
OL	0.9996 ± 0.0003	57.8358 ± 4.1183	3.8553 ± 3.8012
SV	0.9998 ± 0.0002	37.1250 ± 2.1538	-0.3705 ± 5.1047
SVA	0.9994 ± 0.0007	35.8302 ± 1.0523	3.0684 ± 2.1422

[a] Intercept is expressed in µg/mL.

Accuracy and precision

Accuracy and precision for the quality controls in the intra-day and inter-day run are shown in Table 5.3. All the data fulfill the acceptance criteria. The intra- and inter-day RSD values did not exceed 9.014%. The intra- and inter-day bias values were found in the interval -2.11 to 3.08%, -1.429 to 7.575%, and -4.15 to 1.91%, for OL, SV and SVA, respectively. These data indicate that the developed method is accurate, reliable and reproducible, since neither RSD nor bias exceeded 15%, which is in agreement with acceptance recommendations [14].

Table 5.3 Intra-day and inter-day precision and accuracy results for OL, SV and SVA. (n=6)

Nominal concentration (μg/mL)	Intraday (n=6)			Interday (n=18)		
	Measured Concentration (μg/mL) Mean±SD	Precision % RSD	Accuracy % Bias	Measured Concentration (μg/mL) Mean±SD	Precision % RSD	Accuracy % Bias
OL (0.5)	0.489±0.029	5.852	-2.109	0.506±0.034	6.812	1.122
OL (1.5)	1.501±0.068	4.560	0.086	1.546±0.123	7.948	3.076
OL (50)	49.347±0.222	0.449	-1.307	49.386±0.362	0.733	-1.229
OL (100)	99.764±1.467	1.470	-0.236	100.367±1.673	1.667	0.367
SV (0.5)	0.523±0.019	3.662	4.541	0.506±0.043	8.494	1.291
SV (1.5)	1.600±0.117	7.325	6.692	1.581±0.105	6.627	5.414
SV (50)	49.286±0.158	0.321	-1.429	49.408±0.840	1.701	-1.185
SV (100)	107.575±0.815	0.757	7.575	103.798±3.200	3.083	3.798
SVA (0.5)	0.506±0.023	4.453	1.144	0.492±0.044	9.014	-1.682
SVA (1.5)	1.529±0.070	4.577	1.905	1.487±0.083	5.572	-0.879
SVA (50)	49.609±0.361	0.728	-0.781	49.035±0.614	1.251	-1.929
SVA (100)	99.888±0.891	0.892	-0.112	95.852±3.082	3.215	-4.148

Specificity

The specificity of the method was analyzed both in the presence of components and the supernatant of the nanoparticles, containing excess of lipids and surfactants (see chromatograms, Figure 5.3A and B, respectively). As shown, neither the nanoparticles content or supernatant exhibit peaks interfering with those of the analytes, thus indicating that the method is specific.
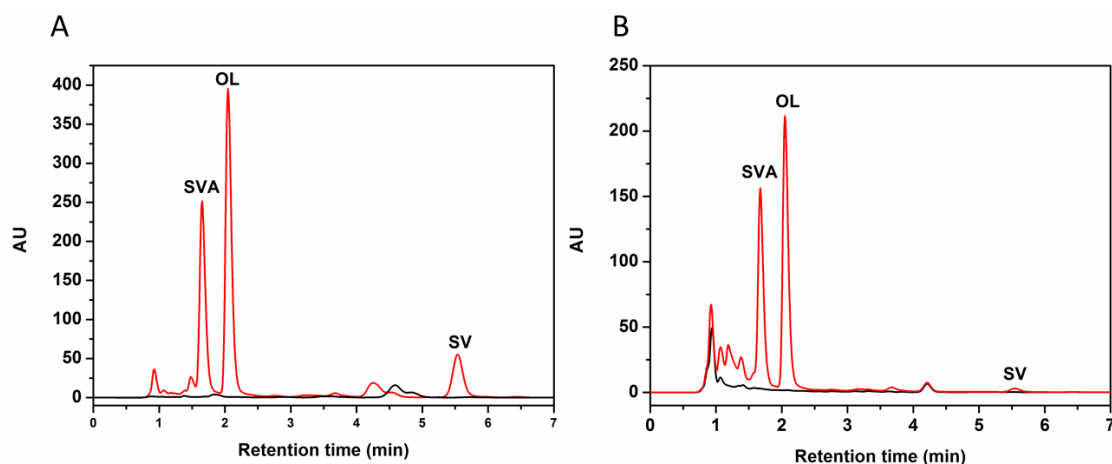
Figure 5.3 (A) Chromatograms of nanoparticles components (black) and total Combo-NLC (red). (B) Chromatograms of nanoparticles (black) and Combo-NLC (red) supernatants.

Stability

The stability data for OL, SV and SVA under conditions likely to be found during the analytical process and sample storage included short-term, long-term, autosampler and freeze-thaw stability analysis and are gathered in Table 5.4. According to the results, it can be inferred that the analytes are stable under the studied conditions, since the % mean concentration found was within the acceptance limit (90-110%) [3].

Table 5.4 Short-term, long-term, autosampler and freeze-thaw stability (values in percentage of nominal concentration) of OL, SV and SVA quality controls (n=6).

Stability conditions	Nominal concentration (μg/mL)											
	Olanzapine				Simvastatin				Simvastatin acid			
	0.5	1.5	50	100	0.5	1.5	50	100	0.5	1.5	50	100
Short-term stability												
% Mean[a]	104.116	104.213	102.465	99.679	104.428	105.359	107.721	111.992	101.118	102.456	105.823	105.297
SD	0.052	0.137	2.334	3.437	0.042	0.174	2.436	2.969	0.049	0.080	2.723	1.895
%RSD	9.978	8.735	4.556	3.448	7.949	10.994	4.522	2.651	9.771	5.192	5.145	1.800
Long-term stability												
% Mean[a]	96.223	94.415	97.806	102.736	96.164	99.121	99.457	105.218	98.539	99.421	98.393	98.342
SD	0.045	0.023	2.169	7.990	0.032	0.074	1.922	8.448	0.045	0.028	1.854	6.802
%RSD	9.453	1.613	4.434	7.777	6.733	4.968	3.865	8.029	9.041	1.892	3.769	6.916
Autosampler stability												
% Mean[a]	98.166	102.545	102.573	105.030	109.442	98.841	98.124	103.848	105.916	102.676	98.311	94.646
SD	0.047	0.017	0.601	1.796	0.052	0.111	0.688	1.714	0.056	0.063	1.139	1.096
%RSD	9.670	1.082	1.171	1.710	9.500	7.461	1.402	1.651	10.552	4.120	2.317	1.158
Freeze-thaw stability												
% Mean[a]	98.114	104.703	95.745	96.416	108.116	104.359	95.304	103.647	97.930	102.172	95.608	95.659
SD	0.042	0.064	0.455	7.988	0.050	0.032	0.718	2.577	0.028	0.040	0.485	1.060
%RSD	8.500	4.052	0.950	8.285	9.323	2.072	1.508	2.487	5.643	2.587	1.014	1.108

[a] Expressed as percentage of nominal concentration

Recovery

The % recovery of OL, SV and SVA from the NLC supernatant was comprised between 93.32 and 102.55, 94.02 and 97.60, and 91.71 and 97.95, respectively (Table 5.5). This indicates that the developed method is adequate to simultaneously quantify the three compounds.

Table 5.5 Percentage of recovery of OL, SV and SVA from nanoparticles supernatant (n=6).

% Recovery	Nominal concentration (µg/mL)								
	Olanzapine			Simvastatin			Simvastatin acid		
	1	50	100	1	50	100	1	50	100
	102.7	92.1	92.5	97.3	94. 9	92.5	91.6	93.8	92.4

5.3.3 Method applicability

The method developed was used to determine the content of OL and SV in NLC with a mean particle size of 150 nm and a zeta potential of ca. -36 mV. To calculate the entrapment efficiency of Combo-NLC, nanoparticles were submitted to ultrafiltration-centrifugation and the free drug determined indirectly in the filtrate, as described in Section 5.2.4. A total percentage of 77.±2 for OL and 96.±4 for SV (corresponding to the joint contribution of SV and SVA) was obtained from the nanoparticles dispersion. This yielded an EE of 99.72±0.05% for SV and 97.0±0.5% for OL, which corresponded to a drug loading of 10.637±0.005% for SV and 10.34±0.05% for OL [13], thus making these carriers suitable for co-encapsulation of drugs with a different polarity.

5.4 Conclusion

A specific, linear, accurate, reliable and reproducible new method for the simultaneous quantitation of OL, SV and SVA, the active form of SV, was developed and fully validated over the range 0.5-100 µg/mL. The method was successfully applied to measure the drug content in Combo-NLC formulation after preparation. The optimized Combo-NLC dispersion with a mean particle size of ca. 150 nm and a zeta potential of -36 mV, renders an entrapment efficiency in excess of 97% for both drugs, which indicates that these nanoparticles are efficient carriers for co-encapsulation.

References

1. Abu-Nameh, E.S.M., R.A. Shawabkeh, and A. Ali, High-performance liquid chromatographic determination of simvastatin in medical drugs. Journal of Analytical Chemistry, 2006. 61(1): p. 63-66.

2. Raggi, M.A., G. Casamenti, R. Mandrioli, G. Izzo, and E. Kenndler, Quantitation of olanzapine in tablets by HPLC, CZE, derivative spectrometry and linear voltammetry. Journal of Pharmaceutical and Biomedical Analysis, 2000. 23(6): p. 973-981.

3. Ali, H. and S. Nazzal, Development and validation of a reversed-phase HPLC method for the simultaneous analysis of simvastatin and tocotrienols in combined dosage forms. Journal of Pharmaceutical and Biomedical Analysis, 2009. 49(4): p. 950-956.

4. Reddy, B., K. Reddy, J. Sreeramulu, and G. Kanumula, Simultaneous Determination of Olanzapine and Fluoxetine by HPLC. Chromatographia, 2007. 66(1): p. 111-114.

5. Zhang, G., A.V. Terry, Jr., and M.G. Bartlett, Simultaneous determination of five antipsychotic drugs in rat plasma by high performance liquid chromatography with ultraviolet detection. Journal of Chromatography B-Analytical Technologies in the Biomedical and Life Sciences, 2007. 856(1-2): p. 20-28.

6. Carlucci, G., P. Mazzeo, L. Biordi, and M. Bologna, Simultaneous determination of simvastatin and its hydroxy acid form in human plasma by high-performance liquid chromatography with UV detection. Journal of Pharmaceutical and Biomedical Analysis, 1992. 10(9): p. 693-697.

7. Kim, B.C., E. Ban, J.S. Park, Y.K. Song, and C.K. Kim, Determination of Simvastatin in Human Plasma by Column-Switching HPLC with UV Detection. Journal of Liquid Chromatography & Related Technologies, 2005. 27(19): p. 3089-3102.

8. Dusci, L.J., L. Peter Hackett, L.M. Fellows, and K.F. Ilett, Determination of olanzapine in plasma by high-performance liquid chromatography using ultraviolet absorbance detection. Journal of Chromatography B, 2002. 773(2): p. 191-197.

9. Boulton, D.W., J.S. Markowitz, and C.L. DeVane, A high-performance liquid chromatography assay with ultraviolet detection for olanzapine in human plasma and urine. Journal of Chromatography B, 2001. 759(2): p. 319-323.

10. Yang, D.-J. and L.S. Hwang, Study on the conversion of three natural statins from lactone forms to their corresponding hydroxy acid forms and their determination in Pu-Erh tea. Journal of Chromatography A, 2006. 1119(1–2): p. 277-284.

11. Suchocka, Z., J. Swatowska, J. Pachecka, and P. Suchocki, RP-HPLC determination of paraoxonase 3 activity in human blood serum. Journal of Pharmaceutical and Biomedical Analysis, 2006. 42(1): p. 113-119.

12. Madan, J., V. Thakkar, A.K. Dwivedi, and S. Singh, Ion pairing RP-HPLC analytical methods for simultaneous estimation of simvastatin and its (a)over-cap-hydroxy acid. Journal of Scientific & Industrial Research, 2007. 66(5): p. 371-376.

13. Vitorino, C., J. Almeida, L.M. Gonçalves, A.J. Almeida, J.J. Sousa, and A.A.C.C. Pais, Co-encapsulating nanostructured lipid carriers for transdermal application: From experimental design to the molecular detail. Journal of Controlled Release, 2013. 167(3): p. 301-314.

14. FDA, Guidance for Industry: Bioanalytical Method Validation.2001: US Department of Health and Human Services, Food and Drug Administration, Center for Drug Evaluation and Research and Center for Veterinary Medicine.

15. ICH, Guidance for industry: Q2B validation of analytical procedures, methodology, ed. E. Center for Drug, et al.1996, Rockville, MD: U.S. Dept. of Health and Human Services, Food and Drug Administration, Center for Drug Evaluation and Research: Center for Biologics Evaluation and Research.

16. Épshtein, N.A., Validation of HPLC Techniques for Pharmaceutical Analysis. Pharmaceutical Chemistry Journal, 2004. 38(4): p. 212-228.

17. Shabir, G.A., Validation of high-performance liquid chromatography methods for pharmaceutical analysis. Understanding the differences and similarities between validation requirements of the US Food and Drug Administration, the US Pharmacopeia and the International Conference on Harmonization. J Chromatogr A, 2003. 987(1-2): p. 57-66.

18. FDA, Center for Drug Evaluation Research, United States. Food Drug Administration, Reviewer Guidance: Validation of Chromatographic Methods1994: U.S. Department of Health and Human Services, Public Health Service, Food and Drug Administration.

19. das Neves, J., B. Sarmento, M.M. Amiji, and M.F. Bahia, Development and validation of a rapid reversed-phase HPLC method for the determination of the non-nucleoside reverse transcriptase inhibitor dapivirine from polymeric nanoparticles. Journal of Pharmaceutical and Biomedical Analysis, 2010. 52(2): p. 167-172.

20. LoBrutto, R. and T. Patel, Method Validation, in HPLC for Pharmaceutical Scientists2006, John Wiley & Sons, Inc. p. 455-502.

Chapter 6

Nanostructured lipid carriers characterization based on physicochemical, rheological and mechanical properties

6.1 Introduction

The incorporation of NLC into a hydrogel, the latter acting as a semi-solid vehicle to provide an appropriate formulation consistency for application upon the skin is a common approach in transdermal administration. Thus, in previous chapter, a hydrogel composed by NLC as drug reservoir combined with classical skin enhancers, ethanol and limonene, in proportions optimized in what pertains permeation rate, was developed.

Carbopol® Ultrez 10 NF was selected as the gelling agent for the preparation of the hydrogel. It is a carbomer (cross-linked high molecular weight polyacrylic acid) interpolymer, i.e., a carbomer homopolymer or copolymer that contains a block copolymer of polyethylene glycol and a long chain alkyl acid ester. The selection of this polymer was based on its self-dispersion grade which enables ease of handling and processing, specifically for hydroalcoholic gels. It allows for a larger versatility in formulating and processing because it quickly wets, yet hydrates slowly. In comparison with traditional carbomer polymers, Carbopol® Ultrez 10 NF provides dispersions in water that are much lower in viscosity prior to neutralization, which enables easier handling while mixing with other components. Moreover, compatibility with many excipients with different polarities, such as ethanol and limonene, constitutes an additional advantage. The aqueous dispersions of the carbomer are acidic (pH~3 for 0.5 % w/w aqueous dispersion). Consequently, when the pH of the solution is above the respective pKa (around 6, according to information from supplier), it leads to a sol-gel transition [1]. Since the polymer is neutralized, it is a highly efficient thickener [2]. Additionally, carbomer polymers are known to exhibit good bioadhesive, thermostable, and organoleptic properties which make the systems attractive both from a pharmaceutical point of view and with respect to the patient acceptance [3].

The physicochemical properties of these nanocarriers are governed, among other factors, by the interface/external medium, which condition parameters with a real impact on the *in vitro/in vivo* performance, such as the loading capacity, the release and permeation rates. The contribution of each component in what pertains permeation enhancement was the target of a previous chapter [4]. How the different co-solvents interact with the nanoparticle formulation and contribute to the system stability and product performance is of paramount importance in the perspective of pharmaceutical development, and is now analyzed. In the present chapter, an understanding of such interactions and a rational for such behavior is provided by the monitoring of the particle size and zeta potential, rheological and textural analysis and sedimentation profile as a function of temperature and formulation composition. Finally, a rationale for the permeation enhancement mechanisms associated to the current strategies is provided, based on the use of both NLC and chemical enhancers and relying on occlusivity and infrared studies of the SC/NLC/enhancers system.

6.2 Materials and methods

6.2.1 Materials

Glyceryl tripalmitate (tripalmitin, T8127) and polysorbate 80 (Tween® 80) were purchased from Sigma. Oleic acid and limonene were acquired from Fluka. Carbopol® Ultrez 10 NF was kindly provided by Lubrizol (Quimidroga, Barcelona, Spain). Simvastatin was a kind gift from Labesfal (Santiago de Besteiros, Portugal). Olanzapine was purchased from Zhejiang Myjoy (Hangzhou, China). All other reagents and solvents are of analytical grade.

6.2.2 Preparation of NLC by the hot high pressure homogenization technique

The NLC were prepared by the hot high pressure homogenization technique previously optimized [5]. Although the general method has been already described, it is mentioned again so as to introduce some particular aspects pertaining to the present chapter. Briefly, a pre-emulsion was obtained by the dispersion of the melted lipid phase, containing tripalmitin and oleic acid in a 50:50 ratio (2.5 % w/V in relation to external phase), in 30 mL of a hot surfactant solution (Tween® 80, 3 % w/V, 80 ºC) through an Ultra-Turrax (Ystral GmbH D-7801, Dottingen, Germany) at 25000 rpm for 2 min. This hot pre-emulsion was further subjected to hot high-pressure homogenization (HPH) using an Emulsiflex®-C3 (Avestin, Inc., Ottawa, Canada) at 1000 bar for 2 min 30 sec.

The lipid dispersion thus obtained was cooled at 4 ºC to form the NLC formulations. In the Combo-NLC formulation, the addition of 80 mg of both drugs, simvastatin and olanzapine, was carried out in the initial lipid melted phase. It should be noted that at the pH of this formulation (ca. 6), the oleic acid molecule is negatively charged, while that of tripalmitin is neutral. It should be also stressed that Tween® 80 was chosen as emulsifier to avoid interference of clouding effects within the working range temperatures.

6.2.3 Composition of the formulations and preparation of hydrogels

To assess the influence of each component present in the final formulation, different hydrogels were prepared according to the composition depicted in Table 6.1. For the preparation of the hydrogels, Carbopol® Ultrez 10 NF, ethanol and limonene were added to the NLC dispersions or to water in the case of reference hydrogels, and left to hydrate under gentle magnetic agitation for 1 h. The Carbopol® dispersions were subsequently neutralized (pH 7-8), using triethanolamine, to promote gelation.

All formulations was prepared as 70:30 (V/V) of NLC dispersion combined with ethanol, to which 5 % (w/V) of limonene and 0.5 % (w/V) of Carbopol® Ultrez 10 NF were added, yielding the percentages in weight depicted in the Table 6.1.

For comparison purposes, dispersions were also assessed. Therefore, formulations Combo-NLC – Combo-NLC+Et+L in Table 6.1 were considered in the analysis.

Table 6.1 Notation for the formulations, and respective composition (% w/w). The following key is used for the components: NLC=unloaded NLC; Combo-NLC=drug loaded NLC; Et=ethanol; L=limonene; Gel=Carbopol® Ultrez 10 NF.

Formulation	Carbopol® Ultrez 10 NF	Ethanol	Limonene	NLC	Combo NLC	Water q.s.
Combo-NLC	-	-	-	-	100	
Combo-NLC+Et	-	25.9	-	-	74.1	
Combo-NLC+L	-	-	4.8	-	95.2	
Combo-NLC+Et+L	-	24.6	5	-	70.4	
Gel	0.5	-	-	-	-	100
Gel+Et	0.5	24.5	-	-	-	100
Gel+Et+L	0.5	24.5	5	-	-	100
NLC+Et+L Gel	0.5	24.5	5	70	-	-
Combo-NLC+Et+L Gel	0.5	24.5	5	-	70	-

6.2.4 Particle size analysis

Particle size was determined by dynamic light scattering, using a Delsa Nano C Submicron (Beckman Coulter, Krefeld, Germany) at a detection angle of 160⁰ and a temperature range of 25 – 50 ⁰C, for increments of 5 ⁰C. The effect of the enhancers in the particle size was also assessed. Samples (Combo-NLC – Combo-NLC+Et+L and Combo-NLC+Et+L Gel) were suitably diluted with ultrapurified water. Each value was measured in triplicate. Results are presented as mean ± standard deviation.

6.2.5 Mercury porosimetry

Mercury porosimetry (MP) measures the intruded volume of mercury in relation to the mass of the sample at a specific pressure [6]. Thus, it allows to calculating the average pore sizes in the range of 5.5 nm and 360 µm and their distributions. Porosity is a useful parameter, since it can influence the rate the drug is released. Mercury intrusion measurements were made in lyophilized unloaded and loaded-NLC using a Micromeritics Autopore IV 9500 mercury porosimeter. Samples were frozen at -80⁰C and lyophilized in a freeze-dryer (Lyph-lock 6 apparatus, Labconco) for 48 h. Gas was evacuated from the samples until a vacuum of 50 mmHg, and the samples were then immersed in mercury. A low pressure test, with increments from 0.5 to 25 psi, and a high pressure test, with increments from 25 to 33000 psi were performed. Pore size distribution was estimated according to Washburn equation, which correlates the pressure applied with the pore diameter.

6.2.6 Rheological experiments

Rheological experiments were conducted in a Haake Mars III (Thermo Scientific, Dias de Sousa, Portugal) rheometer, equipped with a Peltier system as temperature control unit. For the tests, a C35 mm cone, with an angle of 1⁰ probe was used.

Rotational measurements were carried out at 25 ⁰C between 1 and 100 Pa of shear stress, in order to investigate the effect of each formulation component on the Newtonian viscosity. For the evaluation of the thermal behaviour a constant shear stress of 0.25 Pa for the NLC dispersions and 8 Pa for hydrogels was used in steady state and within a temperature range of 20 ⁰C - 50 ⁰C interval, with increments of 5 ⁰C.

Oscillatory measurements were also performed to study the structure of the materials at small deformations. The small amplitude dynamic tests provide information about the linear viscoelastic behaviour of materials [7, 8]. G' and G'' can be extracted from oscillatory tests. G' is the storage (elastic) modulus, which is a measure of the energy

stored and recovered per cycle of deformation and reflects the solid-like component of the viscoelastic behaviour of the material, while G'' is the loss (viscous) modulus, which is a measure of the energy lost per cycle and reflects the liquid-like component. In addition to the storage and loss moduli, an important consideration in oscillatory analysis is the loss tangent (tan δ), a dimensionless term that describes the ratio of the loss modulus (G'') to the storage modulus (G') and which may be usefully employed to convey information concerning the structure of the polymeric system in question. As the loss tangent approaches zero, the elastic structure of the system predominates, whereas, if the loss tangent exceeds unity, the system is considered to be primarily viscous [9]. The stress sweep tests were performed to find the resistance to deformation at a constant frequency of 1 Hz. The complex viscosity modulus η∗, a mathematical representation of the viscosity in oscillatory tests, was also obtained. The effect of temperature (25 ºC – 50 ºC, with increments of 5 ºC) was still assessed.

6.2.7 Texture profile analysis

A Texture Analyzer TA.XT Plus (Stable Micro Systems Ltd., Surrey, UK) was used to examine textural characteristics (hardness, elasticity, compressibility, adhesiveness and cohesiveness) of the hydrogels. TPA mode was carried out using an analytical probe (P/10, 10 mm Delrin) which was twice depressed into the sample at a defined rate (5 mm/s) to a desired depth (15 mm), allowing 15 sec of delay between consecutive compressions. The samples were placed into cylindrical tubes of the same dimension (at a fixed height). Six replicates were performed at 25 ºC in the temperature controlled Peltier Cabinet for each formulation. An analysis at 32 ºC, to simulate skin surface temperature, was also conducted (n=6) for the optimized formulation (Combo-NLC+Et+L Gel). Data collection and calculation were performed using the Texture Exponent 3.0.5.0 software package of the instrument.

6.2.8 Stability studies

Analytical centrifugation

Adding a new component can, to some extent, condition the stability of a formulation. This technique allows to retrieve stability information, even for colloidal systems, as the nanocarriers studied here. The multisample dispersion analyzer LUMiSizer (LUM GmbH, Berlin, Germany) was used to characterize the stability of the Combo-NLC, Combo-NLC+Et+L and Combo-NLC+Et+L Gel formulations. This technique uses an analytical centrifugation system that measures the intensity of transmitted near infrared (NIR) light

while the sample is being centrifuged. The data are displayed in function of the radial position, as distance from the centre of rotation (transmission profiles). The shape and progression of the transmission profiles contains the information on the kinetics of the separation process by detecting changes in light transmission at any part of the sample, or by following the movement of any phase boundary [10-12]. From the kinetics of transmission profiles, the demixing behaviour and/or the dispersion stability can be traced.

The stability of the three formulations indicated above was firstly analysed after 3 h 30 min of centrifugation, at an acceleration of 2300 x g and 15 ºC. Subsequently, the time of centrifugation was increased up to 12 h for the two more stable formulations. Finally, the effect of temperature was assessed only in the most stable formulation.

Zeta potential analysis

The effect of the addition of each component on the zeta potential value was also assessed by electrophoretic light scattering through a Delsa Nano C Submicron (Beckman Coulter, Krefeld, Germany) at 25 ºC. The ZP was calculated using the Helmholtz–Smoluchowsky equation. For the measurements, samples (Combo-NLC, Combo-NLC+Et+L and Combo-NLC+Et+L Gel) were diluted appropriately with ultrapurified water.

6.2.9 *In vitro* skin occlusivity test

In order to study the effect of Combo-NLC on skin occlusivity, an *in vitro* occlusion test was performed. [13, 14] According to this test, the evaporation of water through a membrane was measured and the occlusion factor, F, was calculated. For that, beakers (50 ml) were filled with 30 g of water, covered with filter paper (cellulose acetate filter, 90 mm, whatman nº6, cutoff size 3 µm), and sealed. 600 µL of NLC were spread homogenously with a spatula on the filter surface of 15.9 cm2 and stored at 32 ºC for 48 h to simulate skin surface temperature. The weight of water remaining in the beakers was monitored at 6, 24 and 48 h. Beakers in the same conditions, but covered with 600 µL of water was used as reference. [15] The tests were conducted in triplicate. The occlusion factor F of Combo-NLC was calculated according to the equation

$$F = (A - B/A) \times 100 \tag{6.1}$$

wherein A is the water loss without sample (reference) and B the water loss with NLC. An F value of 0 indicates no occlusive effect compared to the reference, while an F value of 100 corresponds to maximum occlusiveness.

6.2.10 Attenuated total reflectance – Fourier transform infrared spectroscopy

The effect of the Combo-NLC coupled with the selected ethanolic terpene upon the skin was also inspected. For that, epidermal samples were treated with this formulation for 48 h, washed and dried in a desiccator for 24 h [16]. The samples were then subjected to ATR–FTIR study using an FT-IR/FT-NIR spectrometer (Spectrum 400, Perkin-Elmer, Massachusetts, USA) with an ATR accessory fitted with a ZnSe crystal plate. The dried epidermal sheets were placed in the ATR device stratum corneum side down, and measured using 16 scans for each spectrum, with a resolution of 4 cm^{-1} and a scan speed of 1 cm/s. Spectra were collected in triplicate between 4000 and 650 cm^{-1}. The C–H stretching, C=O stretching, and amide peak absorbances were analyzed for each sample [17]. Epidermal samples without treatment were considered for control.

6.3   Results

6.3.1   Mercury porosimetry

Mercury porosimetry was first carried out, in order to investigate the porosity of the particles before and after drug incorporation. This is a parameter with particular interest, since it can affect the capillary action of the dissolved drug and consequently, influence the rate of release of drugs from nanoparticles. Thus, drug release is affected not only by particle size, but also by the respective porosity. Unloaded-NLC and Combo-NLC presented an average pore diameter of 9.4 nm and 9.8 nm, corresponding to a porosity of 6.040% and 7.085%, respectively. According to the results obtained, it can be inferred that the porosity after drug loading only slightly increased. This indicates that the composition remains generally unaltered, suggesting that the nanoparticles are quite stable.

6.3.2   Particle size

Size control and nanoparticle growth are important considerations when preparing NLC dispersions, and monitoring their evolution has to be taken when designing a formulation. The results obtained from particle size analysis as a function of temperature for NLC are shown in Figure 6.1a. The rise in the temperature up to 50ºC promoted an increase in the mean NLC particle size, although the polydispersity index (PI) remained between 0.10 and 0.15, the particles keeping their colloidal nature. This evidences the stability of the NLC when submitted to a heating procedure.

DLS results from the analysis of the formulations Combo-NLC – Combo-NLC+Et+L Gel revealed different effects of the enhancers addition on the particle size (Figure 6.1b). Ethanol generally tended to increase particle size, in contrast with limonene, which did not affect this parameter. The former effect seems to be associated to a swelling mechanism. The subsequent incorporation of the NLC into the hydrogel led to further increase in particle size. This may be ascribed to the existence of carbomer/NLC interactions, promoting bridging and particle aggregation. The nature of this interaction will be discussed below. Note, however, that the PI remained lower than 0.25, which reflects relatively low differences between particle sizes within the formulation, differences which could otherwise trigger potential problems in terms of stability of the system [18].
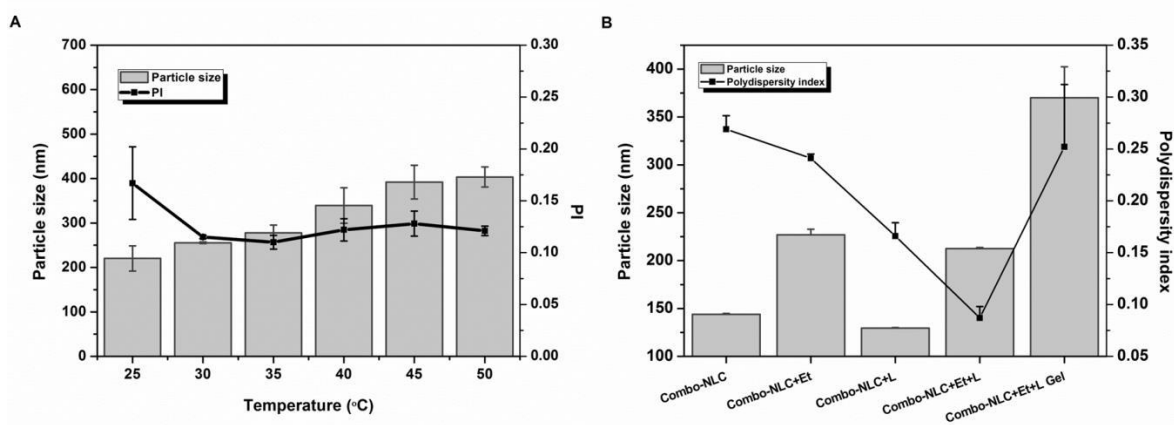
Figure 6.1 (A) Influence of temperature in the mean particle size of the Combo-NLC dispersion. (B) Particle size and polydispersity index for different formulations, including those with addition of permeation enhancers and gelling agent.

6.3.3 Rheological measurements

In order to understand the influence of the co-solvents in the steady-shear rheological behaviour of NLC as liquid dispersion, the measurement of the viscosity as a function of the stress applied and temperature was firstly carried out. According to Figure 6.2a, the addition of ethanol to the formulations promoted an increase in viscosity. This result seemed to be consistent with the increase in particle size observed above, supporting the swelling mechanism of the particles promoted by ethanol. The same behaviour was observed when a screening of temperatures was performed (Figure 6.2b).
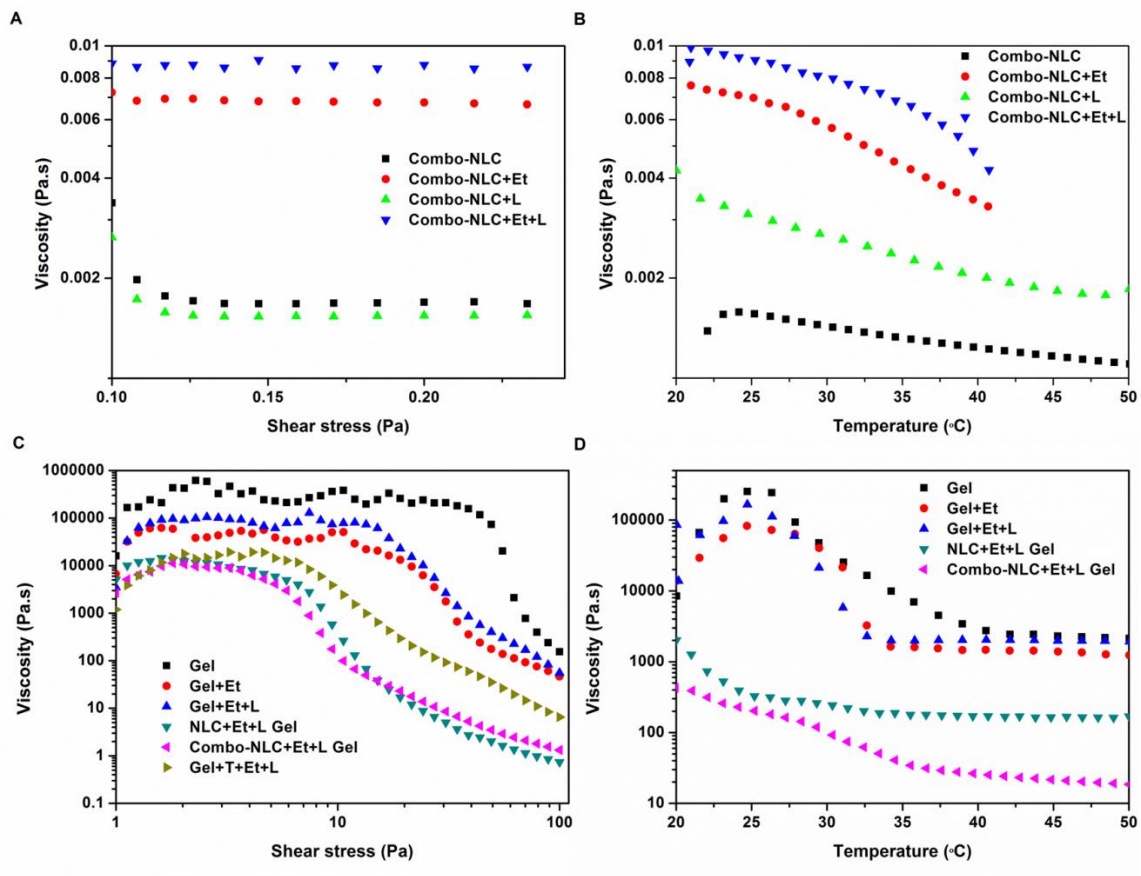
Figure 6.3 Dependence of shear viscosity on the shear stress, measured one week after the preparation of the dispersions (A) and hydrogels (C), at 25 ºC, and as a function of the temperature for a constant shear stress of 0.25 Pa (B) and 8 Pa (D), respectively. Note that an additional formulation containing 3% (V/V) of Tween® 80 (Cp/T/E/L) was introduced in (C), for comprehension of the system.

The influence of the NLC, ethanol and limonene in the rheological properties of a 0.5 % (w/V) Carbopol® Ultrez 10 NF hydrogel was subsequently investigated [19]. The inclusion of less hydrophilic co-solvents, such as ethanol and limonene led to a decrease in the viscosity (Figure 6.2c). It is known that the polymer conformation and thus the polymer entanglement and the gelation strongly depend on the compromise between polymer-polymer and polymer-solvent interactions [8, 20, 21]. Thus, a more apolar bulk will induce contraction of the polymer chains and reduction of the entanglements, giving rise to a less 'viscous' system. The yield stress, i.e., the onset of shear thinning behaviour was also lower for the hydrogels containing ethanol. The role of ethanol is therefore complex, and while it suggests inducing a swelling effect, and thus an increase in viscosity in polymer-free dispersions, it determines the opposite behaviour when the polymer is present, probably due to some dehydration [22].

The further inclusion of the NLC in the system disrupts or weakens even more the polymer network, as seen by a more marked decrease in the shear viscosity. This may be partially ascribed to the action of Tween[®] 80, as illustrated by the difference between the Gel+T+Et+L and Combo-NLC+Et+L Gel rheograms (Figure 6.2c). The surfactant-polymer binding occurring mainly through a hydrogen-bonding interaction seems to be the mechanism that leads to the polymer aggregation (Figure 6.3a). This behaviour has already been reported for similar systems [23].

Note, however, that the nanoparticles as a whole promoted a further decrease in viscosity (Figure 6.2c). Polymer/nanoparticle hydrophobic interactions as a result of the lipid nature of the latter, can be pointed out as the prevalent mechanism, combined to polymer/surfactant H-bonding at the particle surface [23]. Polymer-rich domains are thus created, perturbing the polymer network (see Figure 6.3b). This behavior contrasts to some reports [24-26] in which NLC are used as viscosity enhancers, probably due to the high concentrations employed and the increasing of the inter-particle adhesive forces.

Temperature effects are described in Figure 6.2d. An increase in the temperature generally resulted in a decrease in the viscosity, being this effect more evident for non-NLC hydrogels. The maximal viscosity present at ca. 25ºC for the formulations without NLC disappeared when the particles are present. It should be stressed, however, and from an application point of view, that the viscosity of the NLC hydrogels is adequate for use as a transdermal delivery system within the physiological temperature range.
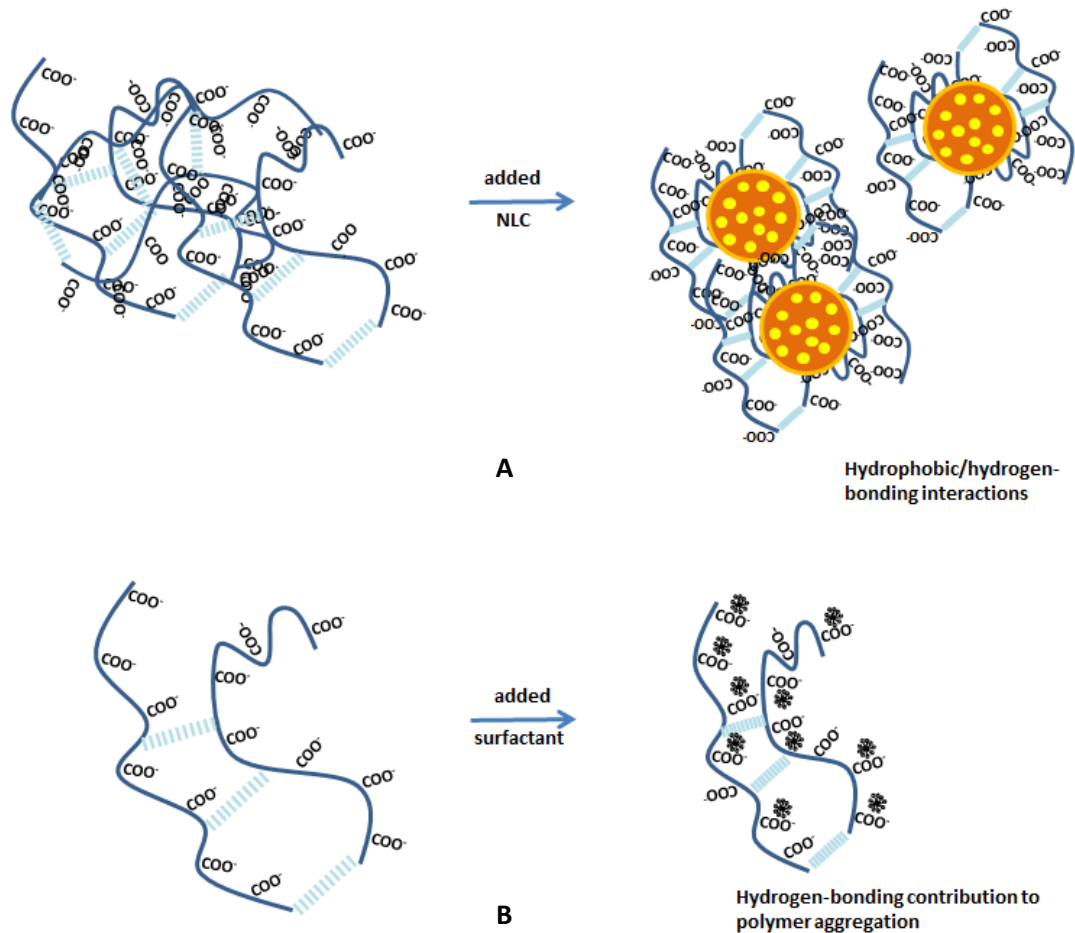
Figure 6.3 Schematic representation of the NLC (A) and surfactant (B) effects upon polymer gelling agent network. Note that the micelles and NLC structures are not drawn to scale. In (A), interaction between NLC and the carbomer produces both particle aggregation, visible as an increase in the mean particle size, and partial disruption of the polymer network, promoting a lower viscosity. In panel (B), a decrease in size is represented for each carbomer chain, resulting in less interchain entanglement and, again, lower viscosity.

Figure 6.4 describes the influence of shear rate on shear stress, from which the yield stress, ie. the stress applied in order to make system start to flow could be extracted. The yield values for NLC hydrogels were substantially lower, compared with the non-NLC hydrogels, which is clearly consistent with the trends reported above for viscosity. This again emphasizes the polymer compaction as a result of the interaction of the less hydrophilic components with the gelling agent. Also, the rheological analysis of hydrogels containing NLC shows a typical pseudoplastic behavior, which makes them convenient for transdermal purposes.
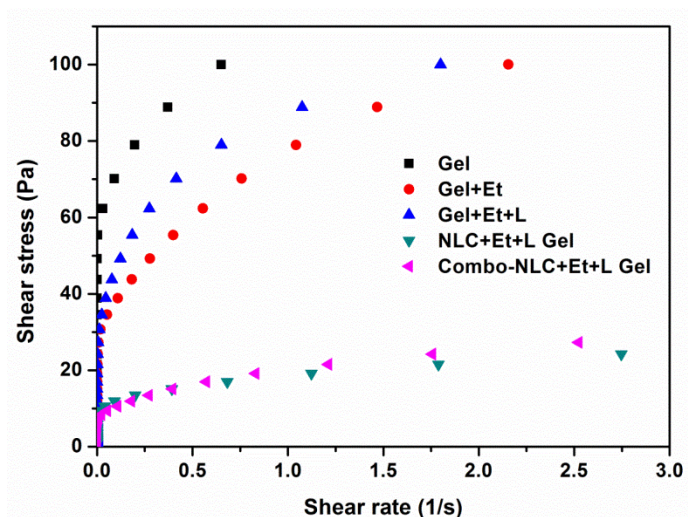
Figure 6.4 Dependence of shear stress on shear rate. The inflexion point of the curves corresponds to yield stress.

These trends were verified through oscillatory (dynamic) rheology experiments (see Figure 6.5), where the addition of ethanol and limonene, has again reduced the interactions between the polymer and the solvent (water), as shown by the decline in the storage modulus (G') curve. However, the system maintained the gel structure (solid character, G'>G'') due to the presence of the gelling agent, which assured elasticity enough for the tested stresses range (G'=G'' for higher shear stresses, see Figure 6.5), irrespective of the presence of the enhancers. In turn, the incorporation of NLC conducted to a sharper decrease in G', and a loss of the elasticity for the lower stresses applied was visible.
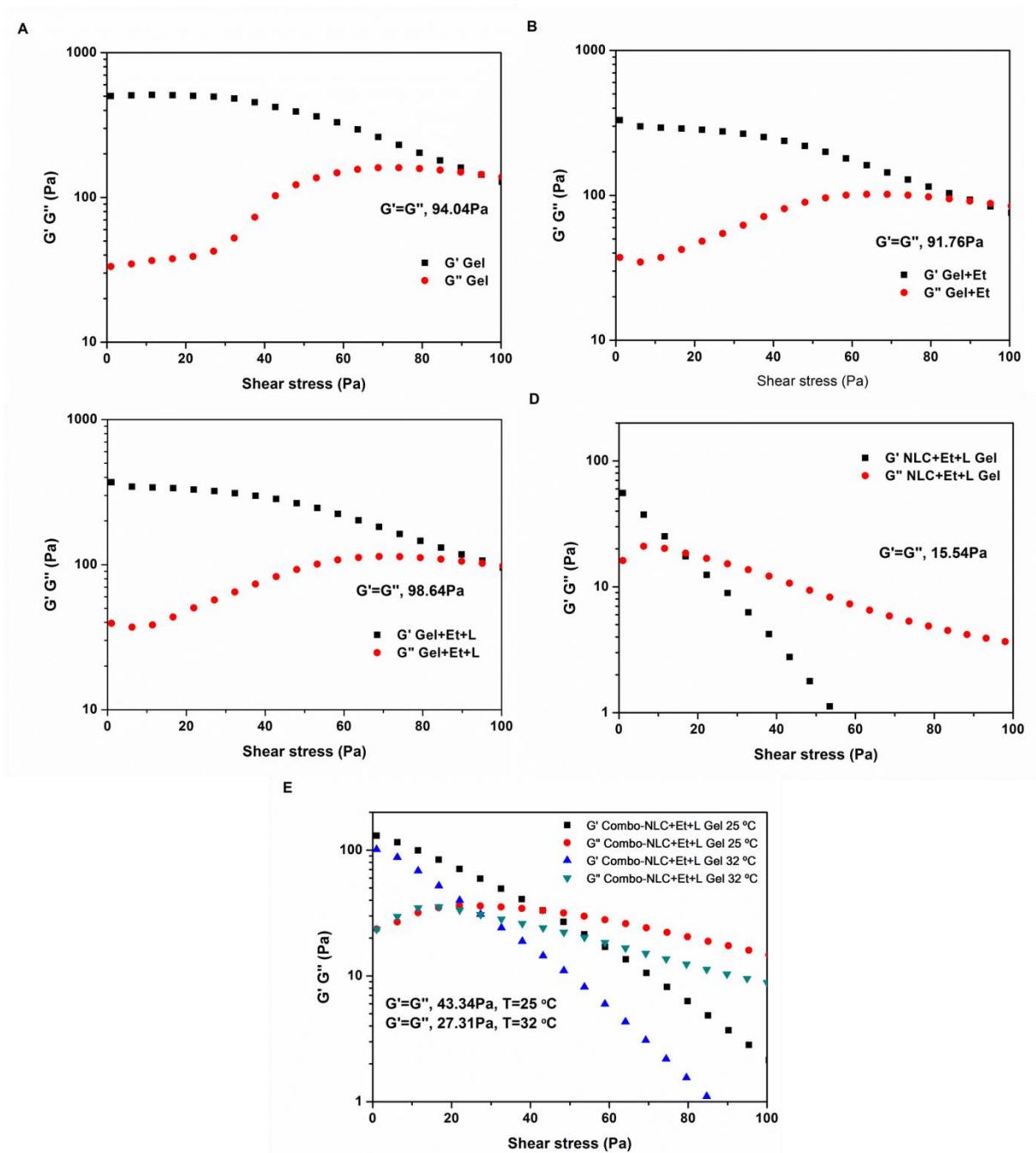
Figure 6.5 Dependence of storage (G') and loss (G'') moduli on shear stress, determined at 25⁰C. A) Gel; B) Gel+Et; C) Gel+Et+L; D) NLC+Et+L Gel; E) Combo-NLC+Et+L Gel. All the experiments were carried out at 25 ºC, with exception of the optimized formulation (Combo-NLC+Et+L Gel), for which the temperature of 32 ºC was also considered.

The dependence of loss tangent (Tan δ) on the applied stress, which is obtained by the G''/G' ratio, corroborated the considerations described above, showing that lower values of shear stresses are needed to attain loss tangent values higher than 1, in the

hydrogels containing NLC (Figure 6.6). This indicates that the viscous component of the system predominates upon the elastic, and the system lost its gel structure earlier.
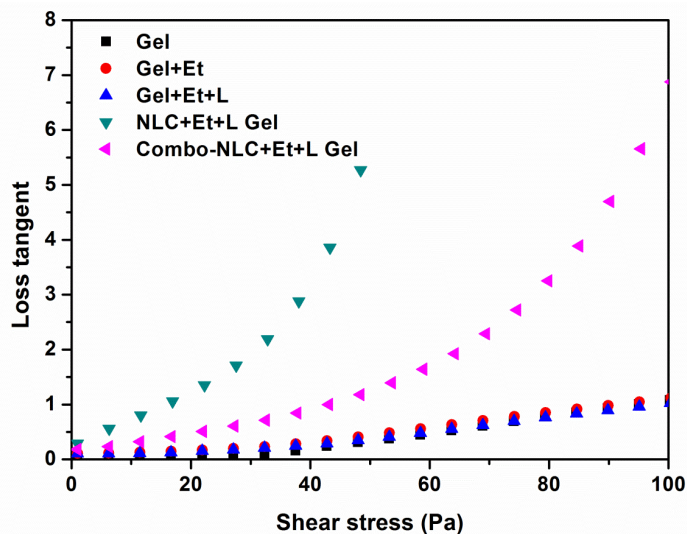
Figure 6.6 Dependence of loss tangent (Tan δ) on the applied stress.

The storage modulus was also sensitive to temperature (Figure 6.5e). The elasticity values, as well as the viscosity, dropped at 32ºC (reporting to the skin temperature), which may be associated to a better spreadability.

Aditionally, the presence of the drugs in the optimized system (Combo-NLC+Et+L Gel in comparison with NLC+Et+L Gel), increased the shear stress for which G'=G'' (Table 6.3).

Table 6.3 Shear stress for which storage modulus (G') equals loss modulus (G''), as a function of the temperature, for hydrogels containing NLC.

Temperature (ºC)	NLC+Et+L Gel Shear stress (Pa) G'=G''	Combo-NLC+Et+L Gel Shear stress (Pa) G'=G''
25	15.54	43.34
30	12.12	25.92
32	14.46	27.31
35	10.97	19.86
40	16.42	25.31
45	17.85	24.72
50	17.57	24.43

Analyzing now the effect of the temperature upon the optimized formulation with and without drugs (Figure 6.7), it can be inferred that for a fixed stress of 0.1 Pa, the system properties (complex viscosity, G', and G''), and thus its microstructure were generally not

affected by temperature. This indicates that hydrogels containing NLC keep their stability over the temperature range typical for a transdermal administration.
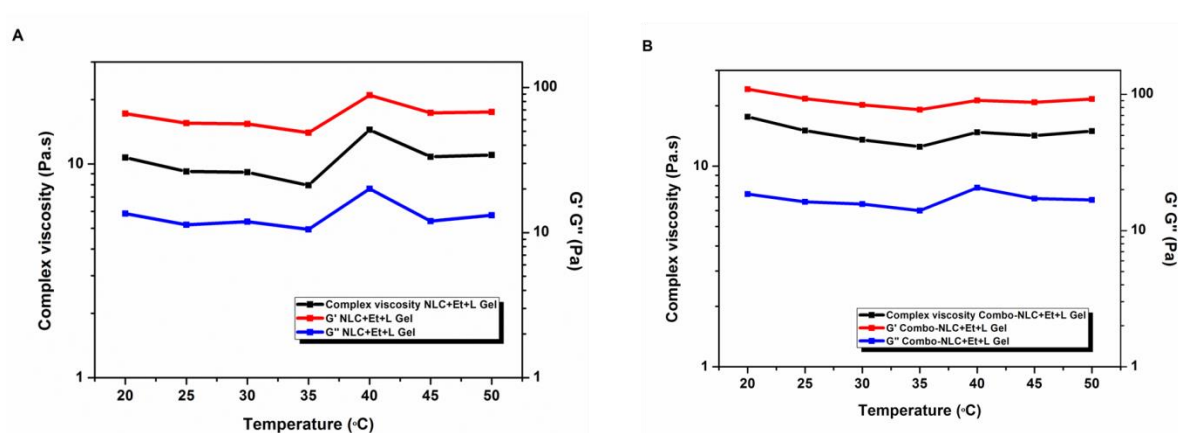
Figure 6.7 Complex viscosity of (A) NLC+Et+L Gel and (B) Combo-NLC+Et+L Gel formulations as a function of the temperature and its correlation with G' and G'', for a shear stress of 0.1 Pa.

6.3.4 Texture profile analysis

Carbomer physical properties strongly affected the rheological behaviour of the formulations, which may influence adhesion on the application area and thus compromise drug release rates. Focusing now on a characterization directed to a pharmaceutical application and product performance, so as to complement the more fundamental approach carried out so far, mechanical properties of formulations are presented. Texture profile analysis (TPA) is an adequate and straightforward method for the mechanical characterization of semisolid drug dosage forms, and to assess the influence of the different components on hydrogel properties. Through TPA mode, parameters such as compressibility, hardness, adhesiveness, elasticity and cohesiveness can be extracted from the compression graphs. The results are presented in Table 6.4.

Pertaining to gel hardness, which expresses the ease with which the gel is applicable on the skin, a slight decrease was observed when the enhancers, ethanol and limonene, were added. In turn, the subsequent addition of NLC caused an abrupt decline in this parameter. According to previous studies, the hardness values obtained in this work are acceptable for skin gel application [27-29]. This is due to a lower viscosity associated to a decrease in the degree of polymer entanglement, as extracted from the rheological results. The same trend was observed for compressibility and adhesiveness, which are correlated to the spreadability of the gel on the skin surface and bioadhesion,

respectively [29]. Again, the results reflect an easier application and a lower adhesion, although the latter is sufficient to keep the formulation in contact with the skin. This is compatible with an increase in the number of free carboxylic acid groups present on the polymer chains [30]. It should be stressed that the compressibility value must be low to extract the prepared gel from the container and to easily spread it on the skin [31]. For the elasticity value, which is defined as the rate at which the deformed sample returns to its original condition after the removal of the deforming force, a slight decrease after NLC incorporation was observed. It is described that lower quantitative values of elasticity obtained from TPA indicate a larger gel elasticity [30]. Thus, it can be inferred that the NLC contribute to an increase of hydrogel elasticity. Regarding cohesiveness, it provides information on the structural reformation following gel application, and usually, a high value is associated with a full structural recovery [29, 32]. The analysis of the present results indicated that the addition of enhancers and NLC to the reference hydrogel did not impact this parameter, and the values obtained are suitable for skin application.

When the temperature was increased from 25 ºC to 32 ºC, the usual temperature at the skin surface, only compressibility and hardness seemed to be affected, with a decrease associated to that of the viscosity. This decrease again reflects a better performance when applying the hydrogel to the skin.

Table 6.4 Mechanical properties of the Gel – Combo-NLC+Et+L Gel formulations extracted from the TPA mode. Results are indicated as a mean of six replicates ± standard deviation.

Formulations	Compressibility (g.sec)	Hardness (g)	Adhesiveness (g.sec)	Elasticity	Cohesiveness
Gel 25ºC	13.±2	16.0±0.5	-12.±3	0.52±0.04	0.92±0.04
Gel+Et 25ºC	10.±1	12.0±0.2	-11.±2	0.48±0.05	0.91±0.06
Gel+Et+L 25ºC	11.±2	11.8±0.7	-9.±3	0.59±0.07	0.94±0.09
NLC+Et+L Gel 25ºC	0.9±0.1	0.3±1.7	-3.0±0.9	0.25±0.02	0.9±0.2
Combo-NLC+Et+L Gel 25ºC	3.0±0.3	3.1±0.7	-3.±2	0.40±0.02	0.99±0.09
Combo-NLC+Et+L Gel 32ºC	1.8±0.3	0.2±0.2	-3.±1	0.30±0.02	0.9±0.1

6.3.5 Stability studies

Analytical centrifugation

The stability of Combo-NLC, Combo-NLC+Et+L and Combo-NLC+Et+L Gel formulations was assessed, in order to investigate the effect of the addition of each component on the sedimentation kinetics of the final formulation. A preliminary test was conducted for the three formulations at an acceleration of 2300 x *g* for 3 h 30 min. Figure 6.8a illustrates the set of transmission profiles obtained for Combo-NLC. The transmission profiles are representative of the variation of particle concentration inside the sample (low transmission means high concentration, and conversely) [11]. According to this test, in the Combo-NLC dispersion a separation occurred since the first centrifugation cycle (indicated by the high transmission of the red profiles) being more evident as time elapses, as shown by the narrower distance between consecutive green profiles. Such behavior is indicative of the sedimentation profile of a suspension. The sediment formed exhibits a low height, which is in good agreement with the DLS findings, and are compatible with both a low polydispersity index and a low particle size.

Figure 6.8b shows the kinetics of the evolution in the zones of clarification, displayed against the measuring time, and revealed the appearance of a creaming layer in the top of the cell. This indicates that the addition of the enhancers contributes to delay the separation process, and the character of the dispersion changes, becoming closer to an emulsion. Finally, the addition of the gelling agent, as depicted in Figure 6.8c clearly contributed to an increased stability, since there was no evidence of a separation process. For a better comparison between different systems, the dispersion stability can be quantitatively described by the instability index. This parameter is indicative of the overall demixing of each sample. Numbers close to 1 represent completely or almost completely demixed samples, numbers close to 0 indicate no or very slow demixing during the measurement. The analysis of this parameter (Figure 6.8d) also allows to order the formulations according to increasing stability as Combo-NLC<Combo-NLC+Et+L<Combo-NLC+Et+L Gel.

A second test with an extended time of centrifugation was performed, in order to further assess the two more stable formulations (Figure 6.9a, b and c). This test revealed that the gel kept its structure and integrity, even after 12 h of centrifugation at 2300 x *g*, since no high transmission zones were evident.

Finally, the temperature effect from 15 °C until 30 °C with increments of 5 °C on the optimized gel formulation (Combo-NLC+Et+L Gel) was assessed (Figure 6.10). Comparing the instability index curves, only at 30 °C, some separation was observed.

Note that an increase in the temperature has generally resulted in a decrease in the viscosity, as extracted from rheological and mechanical results (sections 3.2 and 3.3) above reported. The results allow to conclude that when stored between 15 to 25ºC, the gel maintains its structure.
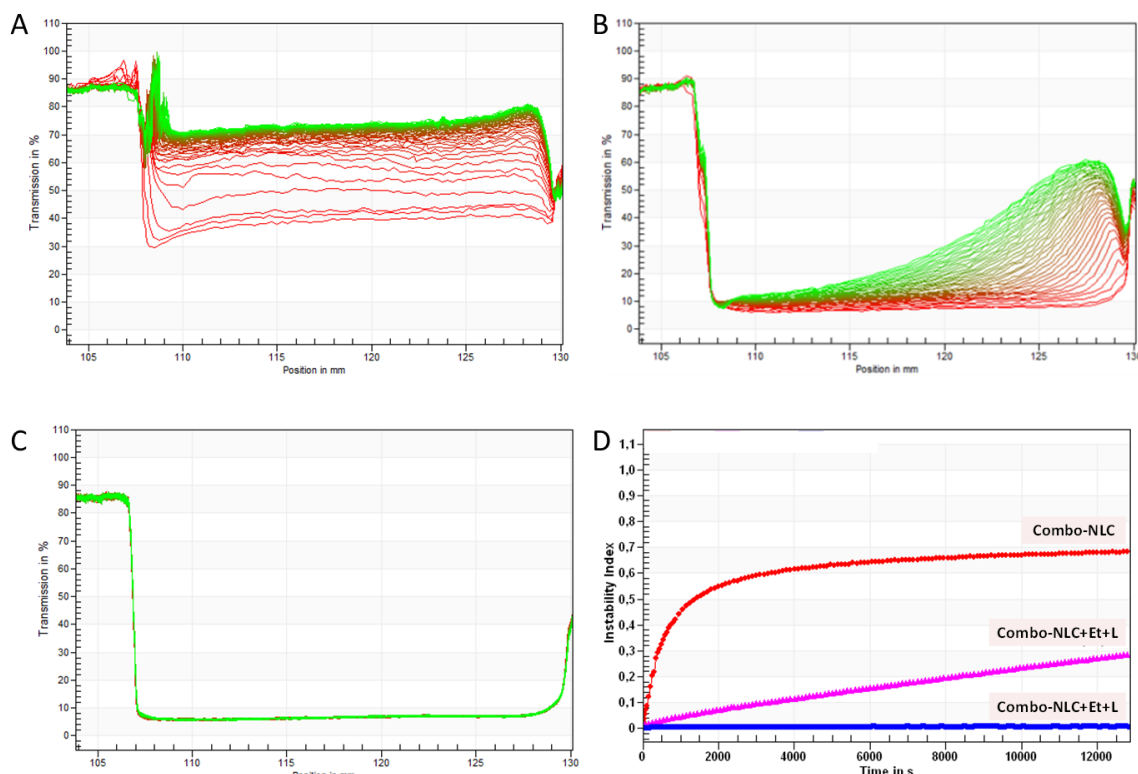
Figure 6.8 Evolution of transmission profiles of the a) Combo-NLC, b) Combo-NLC+Et+L, c) Combo-NLC+Et+L Gel formulations. The corresponding sequences of profiles are shown from red for the first profiles to green for the last ones. d) Instability indexes of Combo-NLC, Combo-NLC+Et+L, and Combo-NLC+Et+L Gel formulations, submitted to an acceleration of 2300 x g for 3 h 30 min.
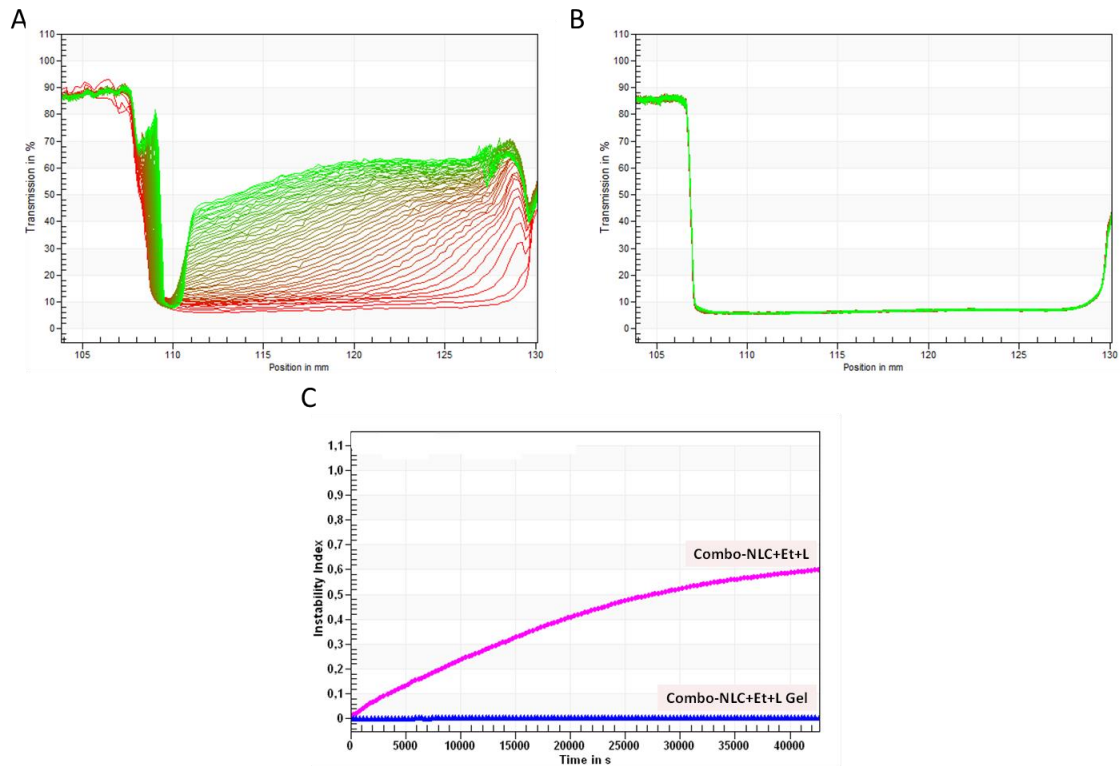
Figure 6.9 Progression transmission profiles of (A) Combo-NLC+Et+L, and (B) Combo-NLC+Et+L Gel formulations submitted to an acceleration of 2300 x *g* for 12 h. (C) Instability indexes of the formulations previously referred.
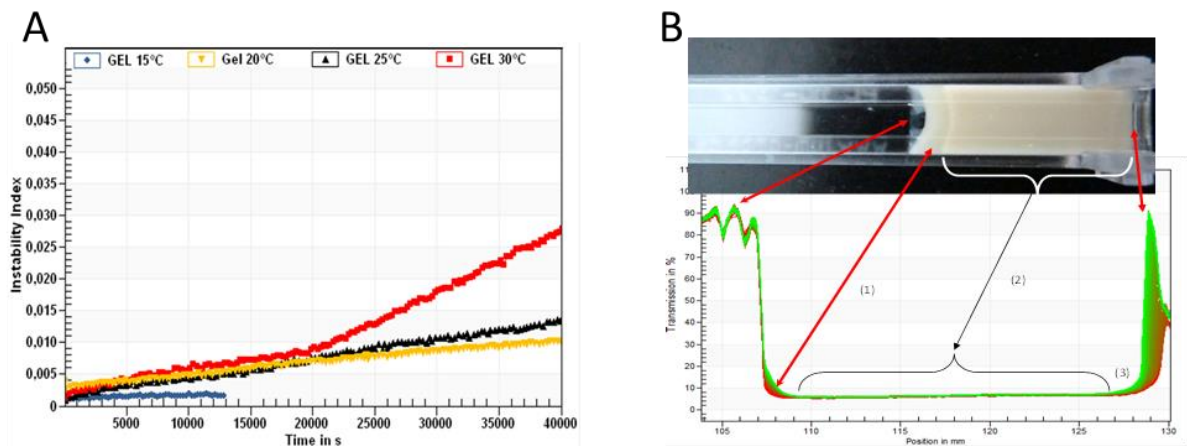
Figure 6.10 (A) Instability indexes of the gel formulation (Combo-NLC+Et+L Gel) submitted to an acceleration of 2300 x *g* for 12h at temperatures of 15ºC, 20ºC, 25ºC and 30ºC, respectively. (B) Progression transmission profiles of the gel formulation (Combo-NLC+Et+L Gel) submitted to an acceleration of 2300 x *g* for 12 h at 30 ºC. At the end of the test, three distinct layers are evident: (1) creaming layer (2) stable layer, and (3) sediment layer.

Zeta potential

The determination of zeta potential was performed to assess the influence of each enhancer and gelling agent in the system stability, so as to complement the previous transmission information (Table 6.5). NLC presented a negative zeta potential value, which might be attributed to the oleate molecules and polar groups of Tween® 80. The addition of ethanol and limonene tended to promote more negative zeta potential values, which stabilized the dispersion. The reason for this behavior may be explained by the slight increase in the pH when ethanol or limonene were added, which leads to an increase in the ionization of oleic acid. However, when Carbopol® Ultrez 10 NF hydrogel was added, zeta potential values became much more negative, as a result of the presence of carboxylate groups, leading to a more stable system. These results are in good agreement with LUMisizer analysis and rheological results. Note that the lowest zeta potential values are found for systems in which both carbopol and NLC are present, which is compatible with the model depicted in Figure 6.4(a). The drug loaded nanoparticles presented, in general, a slightly more negative or almost unchanged zeta potential relative to the unloaded nanoparticles (data not shown).

Table 6.5 Influence of enhancers and hydrogel into zeta potential value of NLC.

Formulations	Zeta Potential (mV)	pH
Combo-NLC	-29.2±0.6	6.2
Combo-NLC+Et	-35.±2	6.5
Combo-NLC+L	-38.±1	6.6
Combo-NLC+Et+L	-39.3±0.7	7.0
Combo-NLC+Et+L Gel	-68.±1	7.3
Gel+Et+L	-47.2±0.8	7.7

6.3.6 Interaction with the skin

As previously reported, it is generally accepted that the NLC act by promoting occlusion, as a consequence of a thin film formation with the stratum corneum (SC) [33, 34]. On the other hand, the ethanolic solution of limonene promotes an alteration of the barrier properties of the SC [35]. To support these mechanisms, an *in vitro* occlusion test and ATR-FTIR measurements were performed.

ATR-FTIR spectra of control (untreated skin) and newborn pig epidermis treated with Combo-NLC+Et+L Gel formulation after 48 h are shown in **Figure 6.11**. The spectra show a broad absorbance at 2100-3500 cm^{-1} due to O–H stretching vibrations, major

absorptions bands at 2920 and 2852 cm^{-1}, due to asymmetric and symmetric C–H stretching, respectively, a strong band at 1642 cm^{-1} due to C=O stretching vibrations of amide I band, and one at 1535 cm^{-1} due to N-H bending vibrations of amide II. The ATR-FTIR spectrum of the treated epidermis depicts a clearly lower intensity in the O−H band, which is probably the result of an interaction with ethanol coupled with the NLC occlusion effect, suggesting a certain degree of lipid extraction, see panel (a). In the region of the C–H stretching, a decrease in the intensity of the bands may be ascribed to the interaction of the limonene with the ceramide tails. In panel (b), changes in the amide I and II region are also evident, which points to some interaction with the protein domain (see Section 4.3.5).
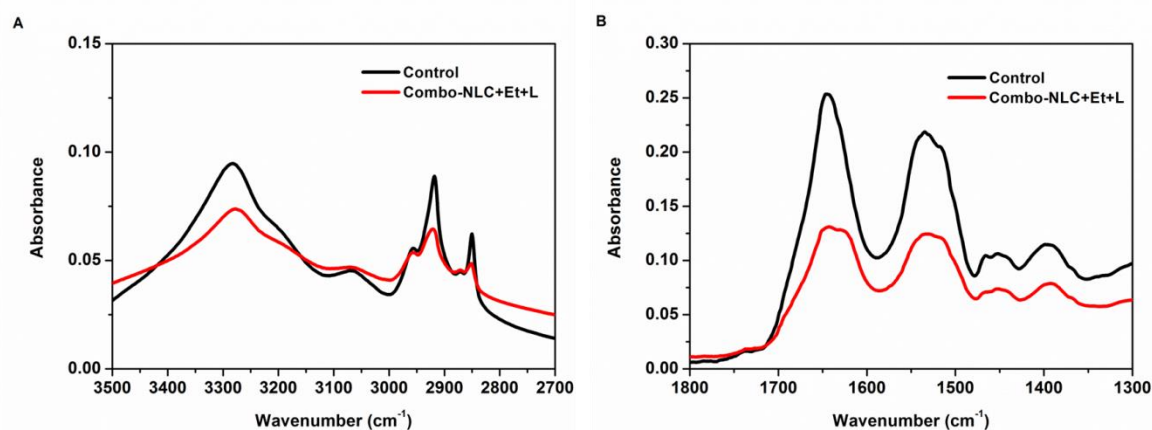
Figure 6.11 ATR-FTIR spectra of untreated skin and skin treated with the Combo-NLC dispersion, containing ethanol and limonene in the (A) regions of O–H and C–H stretching and in the (B) regions of amide I and II.

In Figure 6.12 the results pertaining to the occlusion factor are depicted. Some occlusive effect from the nanoparticles is noticeable, especially in the first 6 hours. For longer periods, this effect becomes less pronounced, but remains essentially constant after 24 h.
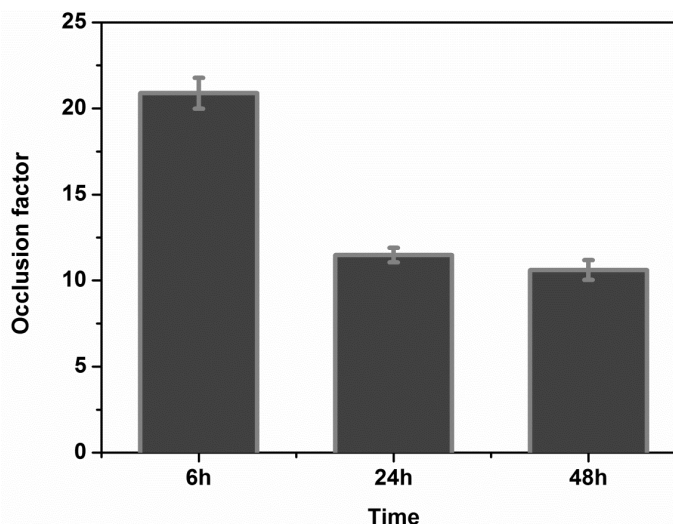
Figure 6.12 Occlusion factor of Combo-NLC at different times after application.

6.4   Conclusions

A full characterization in terms of particle size, rheological and mechanical properties, and physicochemical stability is provided for a NLC formulation intended for transdermal administration. NLC particle size does not significantly vary with the composition of the formulation. The rheological characterization indicated that ethanol, limonene, and NLC led to a subsequent decrease in polymer entanglement that resulted in a loss of hydrogel viscosity. Changes in the polarity of the medium and dehydration effects concur for these observations. Mechanical properties elucidated by the texture profile analysis confirmed the rheological findings and indicated that the optimized formulation was suitable for skin application. The inclusion of enhancers and the incorporation of NLC into a hydrogel network promoted an increase in the physicochemical stability of the overall system. From a pharmaceutical and technological point of view, the results obtained allowed insight into important features that can modulate and impart formulation performance, particularly in the release and permeation behavior. This was confirmed by the interaction with the SC promoted by the final formulation.

References

1. Thrimawithana, T.R., INVITED REVIEW - Environment-sensitive polymers for ophthalmic drug delivery. Journal of drug delivery science and technology, 2012. 22(2): p. 114.

2. Szabó, B., K. Süvegh, and R. Zelkó, Effect of storage on microstructural changes of Carbopol polymers tracked by the combination of positron annihilation lifetime spectroscopy and FT-IR spectroscopy. International Journal of Pharmaceutics, 2011. 416(1): p. 160-163.

3. Hurler, J., A. Engesland, B. Poorahmary Kermany, and N. Škalko-Basnet, Improved texture analysis for hydrogel characterization: Gel cohesiveness, adhesiveness, and hardness. Journal of Applied Polymer Science, 2012. 125(1): p. 180-188.

4. Vitorino, C., J. Almeida, L.M. Gonçalves, A.J. Almeida, J.J. Sousa, and A.A.C.C. Pais, Co-encapsulating nanostructured lipid carriers for transdermal application: From experimental design to the molecular detail. Journal of Controlled Release, 2013. 167(3): p. 301-314.

5. Vitorino, C., J. Almeida, L.M. Gonçalves, A.J. Almeida, J.J. Sousa, and A.A.C.C. Pais, Co-encapsulating nanostructured lipid carriers for transdermal application: From experimental design to the molecular detail. Accepted in Journal of Controlled Release.

6. Gane, P.A.C., C.J. Ridgway, E. Lehtinen, R. Valiullin, I. Furó, J. Schoelkopf, H. Paulapuro, and J. Daicic, Comparison of NMR Cryoporometry, Mercury Intrusion Porosimetry, and DSC Thermoporosimetry in Characterizing Pore Size Distributions of Compressed Finely Ground Calcium Carbonate Structures. Industrial & Engineering Chemistry Research, 2004. 43(24): p. 7920-7927.

7. Silva, S.M.C., F.V. Pinto, F.E. Antunes, M.G. Miguel, J.J.S. Sousa, and A.A.C.C. Pais, Aggregation and gelation in hydroxypropylmethyl cellulose aqueous solutions. Journal of Colloid and Interface Science, 2008. 327(2): p. 333-340.

8. Ferry, J.D., VISCOELASTIC PROPERTIES OF POLYMER SOLUTIONS. Journal of Research of the National Bureau of Standards, 1948. 41(1): p. 53-62.

9. Jones, D.S., A.F. Brown, and A.D. Woolfson, Rheological characterization of bioadhesive, antimicrobial, semisolids designed for the treatment of periodontal diseases: Transient and dynamic viscoelastic and continuous shear analysis. Journal of Pharmaceutical Sciences, 2001. 90(12): p. 1978-1990.

10. Lerche, D., Dispersion Stability and Particle Characterization by Sedimentation Kinetics in a Centrifugal Field. Journal of Dispersion Science and Technology, 2002. 23(5): p. 699 - 709.

11. Sobisch, T. and D. Lerche, Thickener performance traced by multisample analytical centrifugation. Colloids and Surfaces A: Physicochemical and Engineering Aspects, 2008. 331(1–2): p. 114-118.

12. Detloff, T., T. Sobisch, and D. Lerche, Particle size distribution by space or time dependent extinction profiles obtained by analytical centrifugation (concentrated systems). Powder Technology, 2007. 174(1–2): p. 50-55.

13. Vringer, T.d., Topical preparation containing a suspension of solid

lipid particles. European Patent, 1992. No. 91200664.

14. Wissing, S., A. Lippacher, and R. Müller, Investigations on the occlusive properties of solid lipid nanoparticles (SLN). Journal of cosmetic science, 2001. 52(5): p. 313-324.

15. Teeranachaideekul, V., P. Boonme, E.B. Souto, R.H. Müller, and V.B. Junyaprasert, Influence of oil content on physicochemical properties and skin distribution of Nile red-loaded NLC. Journal of Controlled Release, 2008. 128(2): p. 134-141.

16. Jain, A.K., N.S. Thomas, and R. Panchagnula, Transdermal drug delivery of imipramine hydrochloride.: I. Effect of terpenes. Journal of Controlled Release, 2002. 79(1–3): p. 93-101.

17. Prasad, R., S. Anand, R.K. Khar, A.K. Dinda, and V. Koul, Studies on in vitro and in vivo transdermal flux enhancement of methotrexate by a combinational approach in comparison to oral delivery. Drug Development and Industrial Pharmacy, 2009. 35(11): p. 1281-1292.

18. Doktorovova, S. and E.B. Souto, Nanostructured lipid carrier-based hydrogel formulations for drug delivery: A comprehensive review. Expert Opinion on Drug Delivery, 2009. 6(2): p. 165-176.

19. Islam, M., N. Rodríguez-Hornedo, S. Ciotti, and C. Ackermann, Rheological Characterization of Topical Carbomer Gels Neutralized to Different pH. Pharmaceutical Research, 2004. 21(7): p. 1192-1199.

20. Fresno, M.J.C., A.D. Ramírez, and M.M. Jiménez, Systematic study of the flow behaviour and mechanical properties of Carbopol® Ultrez™ 10 hydroalcoholic gels. European Journal of Pharmaceutics and Biopharmaceutics, 2002. 54(3): p. 329-335.

21. Holmberg, K., B. Jönsson, B. Kronberg, and B. Lindman, Polymers in Solution, in Surfactants and Polymers in Aqueous Solution 2003, John Wiley & Sons, Ltd. p. 193-214.

22. Contreras, M.D. and R. Sánchez, Application of a factorial design to the study of specific parameters of a Carbopol ETD 2020 gel. Part I. Viscoelastic parameters. International Journal of Pharmaceutics, 2002. 234(1-2): p. 139-147.

23. Barreiro-Iglesias, R., C. Alvarez-Lorenzo, and A. Concheiro, Poly(acrylic acid) microgels (carbopol® 934)/surfactant interactions in aqueous media: Part I: Nonionic surfactants. International Journal of Pharmaceutics, 2003. 258(1–2): p. 165-177.

24. Souto, E.B., S.A. Wissing, C.M. Barbosa, and R.H. Müller, Evaluation of the physical stability of SLN and NLC before and after incorporation into hydrogel formulations. European Journal of Pharmaceutics and Biopharmaceutics, 2004. 58(1): p. 83-90.

25. Silva, A.C., D. Santos, D.C. Ferreira, and E.B. Souto, Minoxidil-loaded nanostructured lipid carriers (NLC): characterization and rheological behaviour of topical formulations. Pharmazie, 2009. 64(3): p. 177-82.

26. Souto, E.B., Almeida, A.J., Müller, R.H., SLN and NLC as viscoelastic enhancers for topical drug delivery. Proc. XIV International Workshop on Bioencapsulation & COST 865 meeting (Lausanne, Switzerland) 2006. O6-5.

27. Bruschi, M.L., D.S. Jones, H. Panzeri, M.P.D. Gremião, O. de Freitas, and E.H.G. Lara, Semisolid systems containing propolis for the treatment of periodontal disease: In Vitro release kinetics, syringeability, rheological, textural, and mucoadhesive properties. Journal of Pharmaceutical Sciences, 2007. 96(8): p. 2074-2089.

28. Jones, D.S., A.D. Woolfson, and A.F. Brown, Textural Analysis and Flow Rheometry of Novel, Bioadhesive Antimicrobial Oral Gels. Pharmaceutical Research, 1997. 14(4): p. 450-457.

29. Şenyiğit, T., I. Tekmen, Ü. Sönmez, P. Santi, and Ö. Özer, Deoxycholate hydrogels of betamethasone-17-valerate intended for topical use: In vitro and in vivo evaluation. International Journal of Pharmaceutics, 2011. 403(1–2): p. 123-129.

30. Jones, D.S., A.D. Woolfson, and J. Djokic, Texture profile analysis of bioadhesive polymeric semisolids: Mechanical characterization and investigation of interactions between formulation components. Journal of Applied Polymer Science, 1996. 61(12): p. 2229-2234.

31. Yaprak Karavana, S., P. Güneri, and G. Ertan, Benzydamine hydrochloride buccal bioadhesive gels designed for oral ulcers: Preparation, rheological, textural, mucoadhesive and release properties. Pharmaceutical Development and Technology, 2009. 14(6): p. 623-631.

32. Jones, D.S., A.D. Woolfson, A.F. Brown, and M.J. O'Neill, Mucoadhesive, syringeable drug delivery systems for controlled application of metronidazole to the periodontal pocket: In vitro release kinetics, syringeability, mechanical and mucoadhesive properties. Journal of Controlled Release, 1997. 49(1): p. 71-79.

33. Pardeike, J., A. Hommoss, and R.H. Müller, Lipid nanoparticles (SLN, NLC) in cosmetic and pharmaceutical dermal products. International Journal of Pharmaceutics, 2009. 366(1-2): p. 170-184.

34. Pardeike, J., K. Schwabe, and R.H. Müller, Influence of nanostructured lipid carriers (NLC) on the physical properties of the Cutanova Nanorepair Q10 cream and the in vivo skin hydration effect. International Journal of Pharmaceutics, 2010. 396(1–2): p. 166-173.

35. Williams, A.C. and B.W. Barry, Penetration enhancers. Advanced Drug Delivery Reviews, 2004. 56(5): p. 603-618.

Chapter 7

Passive and active strategies for transdermal delivery using co-encapsulating nanostructured lipid carriers:
in vitro vs. in vivo **studies**

7.1 Introduction

The work described in this chapter is the corollary of the different stages for the development of a final formulation, that is to be assayed in a pharmacokinetic study for the assessment of transdermal performance.

Numerous passive and active methods or the combination of both have been used to enhance the drug skin permeation [1]. Within passive methods, the combined use of lipid nanoparticles and chemical enhancers has emerged as a promising strategy to improve drug permeation [2]. The active microneedle-mediated delivery of nanoparticles into the skin has been regarded as an appealing method to potentiate drug transport through the skin [3, 4].

This chapter is designed in three distinct, but complementary parts. Firstly, the development of an appropriate NLC formulation, based on two different methods of production, solvent emulsification-evaporation and high pressure homogenization, for the coencapsulation of olanzapine and simvastatin is presented. Secondly, *in vitro* release studies with kinetic analysis and *in vitro* permeation are established. *In vitro* drug release fitted with different mathematical models elucidates the mechanisms involved in drug release, important to understand the *in vivo* performance of the dosage form. *In vitro* skin experiments range not only the assessment of the NLC and NLC combined with chemical enhancers formulations, but also the influence of NLC while aqueous dispersion or as semi-solid formulation using a hydrogel as transdermal vehicle. Thirdly, *in vivo* pharmacokinetic studies in rats are conducted in order to examine the ability of the aqueous NLC dispersion and hydrogel, both including chemical enhancers, as TDDS

to provide a steady-state plasma concentration of the drugs as well to correlate the *in vitro* and *in vivo* permeability data. Additionally, the potential of the combination of skin perforation with the application of the colloidal drug carrier system is evaluated. As an alternative route of administration, the pharmacokinetic profile of NLC subcutaneous injection is finally investigated.

7.2 Materials and methods

7.2.1 Chemicals

Simvastatin was kindly provided by Labesfal (Santiago de Besteiros, Portugal). Olanzapine was purchased from Zhejiang Myjoy (Hangzhou, China). Simvastatin hydroxy acid ammonium salt and olanzapine-D3 were purchased from @rtmolecule (Poitiers, France). Glyceryl tripalmitate (tripalmitin, T8127), phosphate buffer saline pH 7.4, polyvinyl alcohol 87–89% hydrolyzed (PVA, typical MW13.000-23.000), polysorbate 80 (Tween®80) and polyethylene glycol 400 (PEG 400) were purchased from Sigma. Oleic acid and limonene were acquired from Fluka. Carbopol® Ultrez 10 NF was kindly provided by Lubrizol (Quimidroga, Barcelona, Spain). The microneedle devices Dermaroller® MC905 and MC 915 (equipped with 192 stainless steel microneedles of 500 μm, or 1500 μm length, respectively) were bought from Distrimed S.a.r.l. (Luxembourg). All chemicals used were of analytical grade, and solvents were of high-performance liquid chromatography (HPLC) grade.

7.2.2 Preparation of NLC by solvent emulsification/evaporation method

The production of NLC by solvent emulsification-evaporation (SE/E) was based on a previously optimized method for the preparation of solid lipid nanoparticles [5]. Briefly, the solid and liquid lipids, tripalmitin and oleic acid, respectively, corresponding to a total amount of 250 mg, and 15 mg of both simvastatin and olanzapine (for detailed formulae and variations, see the Results and Discussion Section) were dissolved in 5 mL of dichloromethane and then added dropwise to 30 ml of 1% (w/V) PVA solution, under ultrasonication (40 W, 5 min; Branson, Sonifier 250). The obtained pre-dispersion was submitted to high shear homogenization (L5M-A, Silverson, UK), at 13,000 rpm for 7 min. The dispersion was, finally, stirred at 200 rpm for 4 hours, in order to allow the solvent evaporation. The combined drug formulation will be referred as Combo-NLC SE/E.

7.2.3 Preparation of NLC by high pressure homogenization method

The NLC were alternatively prepared by the hot high pressure homogenization (HPH) technique previously optimized [2], in which 750 mg of the lipid phase (tripalmitin:oleic acid, 50:50 weight ratio) melted at 80°C was pre-emulsified in 30 mL of a 3 % (w/V) polysorbate 80 solution at 80 ºC for 2 min, using an Ultra-Turrax X1020 (Ystral GmbH, Dottingen, Germany) set to 25000 rpm. The pre-emulsion was further subjected to hot HPH at 1000 bar for 2.5 min using an Emulsiflex®-C3 (Avestin Inc., Ottawa, Canada). The dispersion thus obtained was cooled at 4ºC to form the NLC.

For drug encapsulation, 80 mg of OL and/or SV were added to the melted lipid phase, to produce NLC loaded with SV (SV-NLC HPH) or OL (OL-NLC HPH) or with both drugs (Combo-NLC HPH).

7.2.4 Formulations for in vivo PK studies

For the *in vivo* skin permeation studies, the optimized Combo-NLC formulation (see the Results and discussion section) was mixed with the permeation enhancers ethanol and limonene (as 70.4:24.6:5 wt%, respectively). This formulation was referred to as Combo-NLC+Et+L. An alternative gel formulation, referred to as Combo-NLC+Et+L Gel was prepared by adding 0.5% (w/w) carbomer (Carbopol® Ultrez 10 NF) and the gel-inducer triethanolamine (final pH: 7.0-7.5) to the Combo-NLC+Et+L.

In order to estimate basic pharmacokinetic (PK) parameters, drug solution for intravenous injections was prepared by dissolving simvastatin and olanzapine in PEG 400 (2 mg/mL, for each drug).

7.2.5 Particle size analysis

The average particle diameter and polydispersity index (PI) were determined by dynamic light scattering at 25ºC, using a Delsa Nano C Submicron (Beckman Coulter, Krefeld, Germany) set at a 160º detection angle (backscattering). Samples were analysed three times and results were presented as mean ± standard deviation (SD), extracted from the Cumulants algorithm [6, 7].

7.2.6 Zeta potential

Zeta potential (ZP) determinations were carried out in ultrapurified water (pH≈5.5) at 25 ºC by electrophoretic light scattering, using a Delsa Nano C Submicron (Beckman

Coulter, Krefeld, Germany). ZP was calculated using the Helmholtz–Smoluchowsky equation.

7.2.7 Entrapment efficiency and drug loading

The entrapment efficiency of simvastatin and olanzapine in the NLC was determined indirectly, using Equations (2.3) and (2.4) in the case of NLC prepared by HPH and Equations (3.3) and (3.4) in the case of NLC prepared by SE/E.

7.2.8 Thermal analysis

Differential scanning calorimetry (DSC) analysis performed using a DSC-60 differential scanning calorimeter (Shimadzu, Japan) was carried out to characterize the degree of crystallinity of the NLC and the drug lipid interactions. Pure compounds and lyophilized nanoparticles (2-3 mg) were placed in aluminum pans hermetically sealed. Empty pans were used as reference. Each sample was submitted to a heating cycle from 25 to 210 °C, at the rate of 10 °C/min, with a nitrogen purge of 30 ml/min. The onset temperature (Ton), melting point (Tpeak), and enthalpy (ΔH) were evaluated using the TA Software (Shimadzu, Japan).

7.2.9 Attenuated total reflectance infrared

In order to characterize the conformational changes of lipid molecules in the matrices and to analyse the influence of drug loaded in NLC, ATR infrared spectra of the particles were recorded using a FT-IR/FT-NIR spectrometer (Spectrum 400, Perkin-Elmer, Massachusetts, USA) with an ATR accessory fitted with a ZnSe crystal plate. Lyophilized samples were placed in the ATR device without previous treatment, and measured using 16 scans for each spectrum, with a resolution of 4 cm^{-1} and a scan speed of 1 cm/s. Spectra were collected between 4000 and 650 cm^{-1}.

7.2.10 *In vitro* release studies

In vitro release studies were performed using static Franz diffusion cells (PermeGear, Inc., PA, USA) as previously described in Section 4.2.11.

The release pattern of SV and OL from the different nanoparticle formulations was also fitted to several mathematical models (see Results, Section 7.3.2).

7.2.11 *In vitro* permeation studies

In vitro skin permeation studies were performed through static Franz diffusion cells, using human and newborn pig epidermis as skin models in the same conditions as in *in vitro* release studies. The skin was obtained according to the procedure described previously in Section 4.2.12 [2].

The cumulative amount of OL and SV penetrated as a function of time was calculated according to Equation (4.1). Note that SV cumulative amount is a result of the sum of SV (after stoichiometric conversion into SVA) and SVA contributions, since pH 7.4 favors the conversion of pro-drug SV into the respective active metabolite SVA [9]. The steady-state flux (J_{ss}) was obtained from the slope of the linear region of the curve, representing the amount of drug permeated per unit area versus time [10]. Based on the flux (J_{ss}), the permeability coefficient (Kp) was estimated according to Equation (2.12)

7.2.12 *In vivo* studies

Animals

Work with animals was conducted in compliance with EC Directive 2010/63/EU under agreement N° 86 051. Male Sprague-Dawley (SD) rats (n=36) from Janvier Laboratories (Le Genest-St-Isle, France), weighing between 270 and 330 g, were acclimatized in wire cages in a 12-h light-dark cycle with free access to food (A03, Safe; Villemoisson-sur-Orge, France) and water for a minimum of 5 days before starting experiments.

Implantation of femoral vein and artery catheters

One day before pharmacokinetic (PK) experiments, the rats were anesthetized with isoflurane (Forene®, Abbot; Rungis, France) inhalation, by placing them into a hermetic enclosure, supplied with a 3.9 % air-isoflurane mixture at a flow rate of 500 ml/min (Anesthesia Unity, Univentor 400; Phymep, Paris, France). When animals were asleep, a mask was placed onto the muzzle, and the concentration of isoflurane was decreased to 1.5 - 2% during the surgery. The animals were then placed in the dorsal position with the tail toward the experimenter. Polyethylene catheters constituted with the connection of a small-diameter catheter (inner diameter of 0.26 mm and outer diameter of 0.61 mm; Phymep, Paris, France) with a larger catheter (inner diameter of 0.58 mm and outer diameter of 0.96 mm; Harvard, Les Ulis, France) were implanted in the left femoral artery for blood sampling.

Rats for IV PK studies were equipped with a second catheter in the left femoral vein for IV administration of drug solution. After surgery, rats were maintained under a heating lamp until the first signs of movement. They were then placed in individual cages with free access to food and water. Food was withdrawn 12 h before the PK experiments [11].

Plasma pharmacokinetic studies

Rats were divided in 6 groups (n = 6) for transdermal (4 groups), subcutaneous (1 group) or intravenous (1 group) administrations.

Transdermal administration: For transdermal administrations, four treatments were studied, based on a two-level, two-variable, 2^k full factorial planning: (1) Transdermal Combo-NLC+Et+L formulation, (2) Transdermal Combo-NLC+Et+L formulation plus skin microneedle device pre-treatment, (3) Transdermal Combo-NLC+Et+L Gel formulation, and (4) Transdermal Combo-NLC+Et+L Gel formulation plus skin microneedle pre-treatment. These groups were established taking the use of gel (x_1) and skin microneedle pre-treatment (x_2) as independent variables and pharmacokinetic parameters, such as, C_{max}, t_{max}, AUC_{0-48h}, C_{ss} and J_{ss} as responses (R) or dependent variables. The mathematical model

$$R = \beta_0 + \beta_1 x_1 + \beta_2 x_2 + \beta_{12} x_1 x_2 \qquad (7.1)$$

was applied for interpretation of the direct influence and interaction between variables, where β_0 corresponds to the arithmetic mean of the response, β_1 and β_2 are the coefficients of the respective independent variables, and β_{12} the interaction term. Two coded values (-1) and (+1) were considered, corresponding, respectively, to the absence and presence of the independent variables.

The rats were anesthetized by isoflurane inhalation as described in above and the upper back region was carefully shaved with an electric hair clipper. The integrity of the shaved skin was checked by measuring the transepidermal water loss using a vapometer (Delfin Technology, Kuopio, Finland). TEWL values lower than 10 g/cm^2/h were considered as normal skin values [12]. A rubber ring (22 mm inner diameter and 3.5 mm thickness) delimiting a diffusion area of 3.8 cm^2 was then attached to the shaved skin with surgical glue (Vetbond®, 3M Co., St. Paul, MN, USA), in order to form a reservoir for the formulation applications. Subsequently, 800 µL of the transdermal formulations (corresponding to 1.45 mg of OL and SV) were applied, and the reservoir was tightly closed with Tegaderm film (3M Co., St. Paul, MN, USA), in order to prevent both formulation leakage and solvent evaporation. In the groups pretreated with

microneedles, the device was rolled in four different directions, ten times for each over the rat skin surface before sticking the rubber ring.
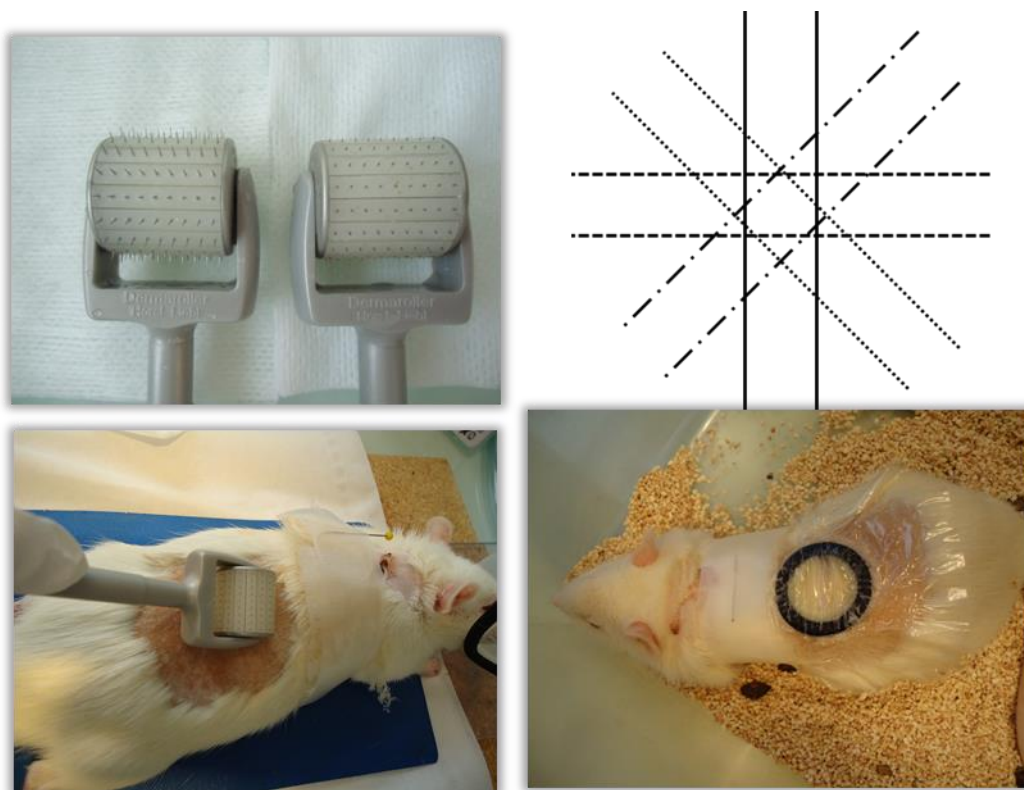
Figure 7.1 Demaroller® pretreatment and formulation application to rats.

Blood samples were collected from the femoral artery catheter at predetermined time points over 48 h after formulation application. Plasma was separated by centrifugation (3 000 rpm, 10 min) and frozen at -80°C until analysis.

Subcutaneous administration: Subcutaneous administration of Combo-NLC (5 mg of each drug per kg of body weight) was performed in the back region of the animals. Arterial blood samples were collected over 48 h postdosing via the left femoral artery catheter and handled as described above.

Intravenous administration: The OL and SV solution for intravenous (IV) administration (1 mg drug per kg of body weight) was infused over 30 min via the left femoral vein, using a syringe pump (CMA 100 microdialysis pump; Phymep, Paris, France). Arterial blood samples were collected over 5 h, via the left femoral artery catheter and were handled as described above.

Transepidermal water loss measurements

The rats were anesthesized with intraperitoneal injections of 60 mg/kg of pentobarbital. Subsequently, the back regions of the rats were shaved as described in 7.2.12.3 and were divided in 3 areas. Two areas were treated with microneedle devices bearing 500 or 1500 µm-length microneedles, and the third one was used as control. TEWL measurements were performed before and 1 min, and every 15 min over 180 min, after skin treatment.

LC-MS/MS analysis of SV, SVA and OL

A validated liquid chromatography–tandem mass spectrometry (LC/MS/MS) method (see Appendix 2) was used to determine the concentration of simvastatin, simvastatin acid and olanzapine in the plasma samples, using mevastatin (MEV) and the deuterated olanzapine (OL-D3) as internal standards (IS), respectively.

Reversed-phase chromatography was performed on a Jupiter C18 column (5.0 µm, 50 mm x 2.1 m; Phenomenex, Le Pecq Cedex, France). The mobile phase at a 0.2 mL/min flow rate was an ammonium formate (2 mM in water) and acetonitrile mixture, 25:75 (V/V). Injection volumes were of 20 µL for OL and 10 µL for SV and SVA quantitation. The LC-MS/MS system consisted of an Agilent 1100 separation module equipped with a binary pump, an autosampler thermostated at 4°C, and an API 3000, Sciex tandem mass spectrometer with an electrospray ionization (ESI) interface. The ESI source was operated in the positive-ion mode. Ions were analyzed by multiple-reaction monitoring (MRM), with transition ions m/z 313.2/256.1 for olanzapine, 441.2/325.3 for simvastatin, 459.5/343.3 for simvastatin acid, 316.2/256.1 for olanzapine-D3 and 413.2/311.2 for mevastatin. Calibration curves for OL, SV, and SVA concentrations ranged from 0.25 to 100 ng/mL. For calibration standards, controls, and samples, a two-step liquid-liquid extraction from plasma was carried out in order to extract sequentially analytes, i.e. first SV and SVA at pH 4.5, which is a pH shown to minimize conversion of SV into SVA [13], and second OL at pH 10. Briefly, 200 µL of Titrisol buffer, pH 4, and 50 µL of OL-D3 solution (20 pg/µL in water) were added to 100 µL plasma sample. After vortexing, 2 mL of diethyl ether were added. The mixture was vortexed for 1 min and then centrifuged at 3000 rpm for 10 min. The diethyl ether supernatant (containing mostly SV and SVA molecules) was then transferred to a glass tube and evaporated to dryness under a gentle stream of N_2 gas at 45 °C. Dry residues were re-dissolved in 70 µL of mobile phase and 50 µL of MEV solution (200 pg/µL in Titrisol buffer at pH 4). For OL extraction, 30 µL of NaOH 1.0 M were added to the aqueous phase (final pH: 10). After vortexing, 2 mL diethyl ether were added and the mixture was vortexed for 1 min and centrifuged at 3000 rpm for 10 min. The supernatant was transferred to a

glass tube and evaporated as described above. Dry residues were finally re-dissolved with 120 µL of mobile phase and transferred to the LC-MS/MS vials.

The between-day variabilities for OL, SV, and SVA were characterized at the three levels of concentrations (n=6), with a precision and accuracy of less than 15%.

All data were processed using Analyst Version 4.1.2 software.

Pharmacokinetic analysis

The clearance was determined through IV administration data, analyzed using a non-compartmental model, through the WinNonLin software (version 5.3, Pharsight Corporation, Mountain View, California, USA) and taking into consideration the half-life elimination time ($t_{1/2}$). The half-life of elimination from plasma was determined by linear regression of the terminal portion of the log (plasma concentration) versus time curves. The same procedure was applied to subcutaneous administration data.

In the case of transdermal delivery, pharmacokinetic parameters, such as the maximal plasma drug concentration (C_{max}) and the time to reach maximal plasma concentration (t_{max}), were inspected directly from each individual plasma concentration–time profiles. The steady-state concentration of each drug was calculated by the average of the four last time points of concentration *vs.* time profile, in order to calculate the transdermal flux from the dispersion/hydrogel formulation at steady-state (J_{ss}) using equation 2.14 [14] $J_{ss} \times A = C_{ss} \times Cl$, where A is the area of the applied formulation (3.80 cm^2), C_{ss} is the steady-state plasma concentration (ng/mL) obtained from transdermal plasma profiles and Cl the total body clearance determined from the intravenous pharmacokinetic study. Data are expressed as the mean ± S.D. In the case of the calculation of the transdermal flux of SV, since it is rapidly converted into SVA post absorption, resulting in low SV concentration (see results), J_{ss} was calculated using C_{ss} of SVA added to C_{ss} of SV previously converted into the corresponding stoichiometric SVA quantity. The same applies for the plasma concentration–time profiles.

7.2.13 Confocal laser scanning microscopy

In order to investigate the NLC skin distribution, 0.05% (w/w of lipids) Nile red-labeled Combo-NLC were formulated with ethanol, limonene with or without carbomer (NR-Combo-NLC+Et+L and NR-Combo-NLC+Et+L Gel, respectively) as in 7.2.4 and were applied for 1 h 30 and 48 h on the back region of the rats, according to the procedure described in 7.2.12. For NR-Combo-NLC+Et+L Gel, the effect of Dermaroller® (D) was also assessed. After application, rats were sacrificed and the rubber rings removed. The

site of application of the formulation was wiped with wet gauze and an 8 mm full thickness biopsy taken. A piece of tissue (ca. 0.3 x 0.3 cm) of each biopsy was then cut out, embedded in optimal cutting temperature (OCT) compound and frozen at -20ºC. Ten transversal sections from the dermis to stratum corneum with a thickness of 50 µm were obtained using a cryostat (Leica (CM3050S, Wetslar, Germany) and stored at 4 ºC until confocal laser scanning microscopy (CLSM) imaging. A drop of glycerol was applied upon the slide containing the skin sections, which were then examined using a confocal FV-1000 station installed on an inverted IX-81 (Olympus, Tokyo, Japan) microscope. Images were obtained with an Olympus UplanSapo x20, 0.75 NA, objective lens (800 x 800 pixels, 0.53 µm/pixel), with an exciting 543 nm laser wavelength and a 555-655 nm detection channel. Light images were obtained simultaneously. Untreated skin was used as control.

7.3 Results and discussion

7.3.1 Preparation and characterization of NLC

The composition and production conditions of NLC prepared by solvent emulsification-evaporation were based on previous works, taking SV loaded solid lipid nanoparticles as template, therefore tripalmitin as oil phase [5]. However, for the preparation of the OL-loaded NLC, due to the low OL solubility in tripalmitin (<12 mg/g) [2], fixed amounts of tripalmitin were replaced with oleic acid (Table 7.1).

Table 7.1 Optimization of the OL loaded NLC composition prepared by SE/E. Key: EE - entrapment efficiency; DL - drug loading; PI - polydispersity index. The results are expressed as mean ± SD (n=3).

Formulations OL amount and Oleic Acid:Tripalmitin ratio	Mean particle size (nm)	PI	Zeta potential (mV)	%EE	%DL
NLC (25:75)	227.±6	0.152	-35.7±0.4	-	-
OL5mg-NLC (25:75)	226.±6	0.130	-33.9±0.3	76.5±0.2	1.561±0.004
OL10mg-NLC (25:75)	229±10	0.193	-32.5±0.9	77.61±0.03	3.104±0.001
OL15mg-NLC (25:75)	226.±7	0.190	-27.3±0.6	79.5±0.2	4.80±0.01
NLC (35:65)	224.±4	0.121	-36.4±0.1	-	-
OL15mg-NLC (35:65)	226.±4	0.151	-31.8±0.5	84.2±0.2	5.05±0.01
NLC (50:50)	231.±4	0.103	-35.9±0.8	-	-
OL15mg-NLC (50:50)	226.±4	0.094	-34±3	91.±1	5.48±0.08

The OL entrapment efficiency (EE) increased with the oleic acid content (Table 7.1). The ratio 50:50 oleic acid:tripalmitin (OL15mg-NLC) was selected for the Combo-NLC formulation, since it allowed EE higher than 90% and low polydispersity index. For Combo-NLC, the same amount of OL and SV (15 mg each for SE/E and 80 mg in the case of HPH) was used. Physicochemical properties of Combo-NLC prepared by SE/E and HPH methods are presented in Table 7.2.

Table 7.2 Physicochemical properties of the optimized Combo-NLC formulation prepared according to SE/E and HPH methods. The results are expressed as mean ± SD (3≤n≤6).

Formulation code	Mean particle size (nm)	PI	Zeta potential (mV)	% EE	% DL
Combo-NLC SE/E	223.±4	0.122	-32.±3	**SV** 98.0±0.8 **OL** 92.8±0.9	**SV** 5.88±0.05 **OL** 5.57±0.05
Combo-NLC HPH[a]	149±18	0.271	-36.3 ±1.6	**SV** 99.72±0.05 **OL** 97.0±0.5	**SV** 10.637±0.005 **OL** 10.34±0.05

[a] Ref. [2]

Compared with the SE/E method, the Combo-NLC prepared by HPH displayed a lower mean particle size, a higher polydispersity, but similar zeta potential, which confers physical stability to NLC suspensions [15]. In addition, HPH led to an almost two-fold higher drug loading, associated to an entrapment efficiency exceeding 95% for both drugs.

Using the HPH method, the Combo-NLC presented an average particle size between OL-NLC and SV-NLC (Table 7.3), and a polydispersity index below 0.3. Zeta potential values were all below -30 mV, which warrantied NLC physical stability. With an entrapment efficiency higher than 95% for both drugs, NLC were found to be efficient carriers for co-encapsulation. The high EE obtained were confirmed by the DSC results (Figure 7.2). The thermograms of NLC did not display the melting transition peak of SV and OL, irrespective of the method of production, indicating that the drug is dissolved within the lipid matrix, without the presence of crystals in the external phase. Concerning the crystallinity degree of the NLC lipids, whatever the preparation method, NLC matrices presented a higher degree of disorder due to the presence of oleic acid, since a shift of the tripalmitin melting point towards lower temperatures was observed (Table 7.4). A less structured matrix seemed to be associated to the NLC prepared by SE/E, compared with NLC prepared by HPH, as evidenced by the broadness of the peak transitions and by the slight decrease in the enthalpy observed. In the case of NLC

prepared by HPH, the incorporation of the drugs also generally led to a decrease in the crystallinity of the lipid matrix, particularly when both drugs were entrapped (Table 7.4).

Table 7.3 Physicochemical properties of the optimized NLC prepared through the hot high pressure homogenization (HPH) technique: mean particle size, polydispersity index (PI), zeta potential, entrapment efficiency (EE) and drug loading (DL). The results are expressed as mean ± SD (3≤n≤6).

Physicochemical property	Formulation Code			
	NLC HPH	OL-NLC HPH	SV-NLC HPH	Combo-NLC HPH[a]
Particle size (nm)	152.±9	181±22	131±23	149±18
PI	0.278	0.199	0.212	0.271
Zeta potential (mV)	-37.±5	-36.±9	-36.±6	-36.3 ±1.6
%EE (OL)	-	96.±2	-	97.0±0.5
%EE (SV)	-	-	99.5±0.3	99.72±0.05
%DL (OL)	-	10.2±0.2	-	10.34±0.05
%DL (SV)	-	-	10.62±0.03	10.637±0.005

(a) Ref. [2]
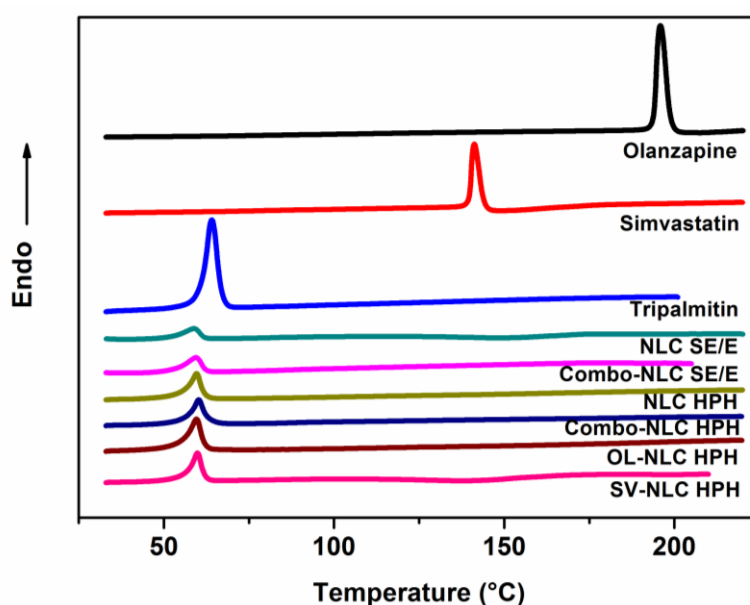
Figure 7.2 DSC thermograms of the pure compounds (drugs and tripalmitin) and of NLC prepared by SE/E or HPH.

Table 7.4 DSC melting characteristics of pure compounds and NLC formulations.

Pure compounds/ NLC formulations	T_{on} (ºC)	T_{peak} (ºC)	Enthalpy of fusion (J/g)
Olanzapine	193.93	195.86	-116.73
Simvastatin	139.93	141.28	-76.83
Tripalmitin	61.08	64.08	-171.35
NLC SE-E	52.02	58.83	-35.33
Combo-NLC SE-E	52.60	59.49	-41.17
NLC HPH	55.82	59.62	-58.14
Combo-NLC HPH	57.07	60.27	-33.54
OL-NLC HPH	56.54	59.60	-45.08
SV-NLC HPH	57.59	59.86	-36.61

The IR spectrum analysis from 1200 to 1400 cm^{-1} focused on the conformation of the CH$_2$ groups from the acyl chains (tripalmitin and oleic acid) (Figure 7.3A). Spectra of NLC prepared by HPH presented several regular bands, while spectra of NLC prepared by SE/E showed a significant convolution. The regular bands in the NLC prepared by HPH were ascribed to a tendency for a full-trans arrangement of the methylene groups, and the mutual coupling vibrations of the long chains of tripalmitin and oleic acid [16]. This order of the acyl chains was somewhat lost in the lipid matrix of the NLC prepared by SE/E, resulting in broader peaks, which suggests a less ordered structure or an amorphous state of the lipid matrix. These results correlated well with the DSC analysis (Table 3). In the spectra of NLC prepared by SE/E (Figure 7.3B), a broad peak was also present at around 3320 cm^{-1}, probably corresponding to the stretching of the PVA hydroxyl groups. Additionally, there was some evidence of the presence of olanzapine at the surface of the NLC prepared by HPH, as illustrated by the C=C stretching around 1587 cm^{-1} (Figure 7.3C), which could be ascribed to the high drug load.
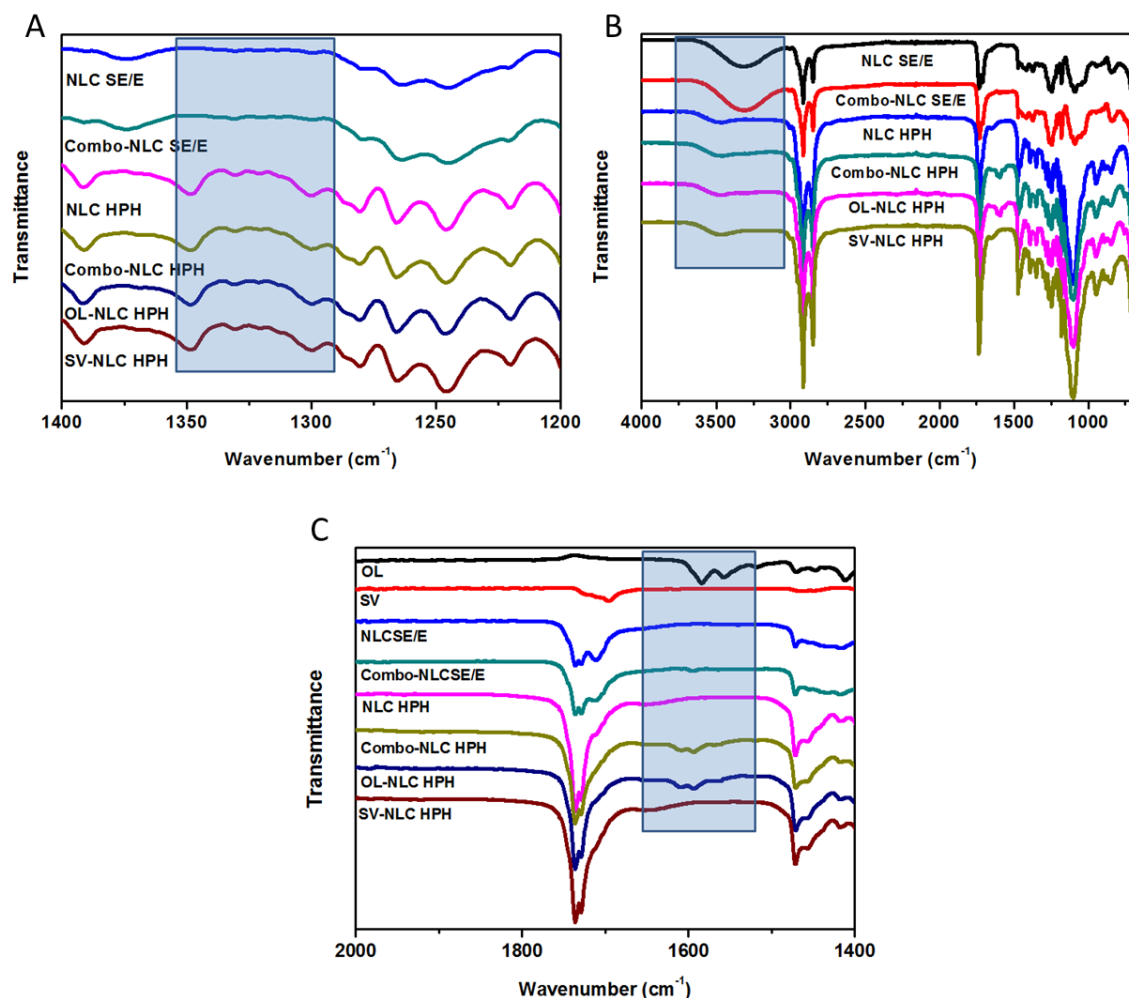
Figure 7.3 FTIR spectra of NLC prepared by SE/E or HPH: (A) 1400-1200 cm^{-1}, (B) 4000-650 cm^{-1} and (C) 2000-1400 cm^{-1}, the latter including OL and SV as pure compounds.

7.3.2 Release profiles from Combo-NLC dispersions

Figure 7.4 displays the release profiles of NLC formulations prepared by SE/E or HPH. It can be observed that olanzapine was released to a higher extent than simvastatin, irrespective of the method of preparation. This was ascribed to their differential solubility in tripalmitin and oleic acid, which, in turn, led to different drug distribution within NLC. Simvastatin exhibited a higher solubility in the solid lipid tripalmitin, leading to a higher control over the release. Conversely, olanzapine being more soluble in the liquid lipid oleic acid, the degree of retention was lower. NLC prepared by HPH tended to release drugs more slowly than the ones prepared by SE/E, which was ascribed to the less structured matrix of the latter (see DSC and FTIR analysis). The use of different emulsifiers, PVA in SE/E and Tween® 80 in HPH, may

also influence results. Release profiles obtained with Combo-NLC prepared with HPH were, however, comparable to those obtained with single-drug loaded NLC.
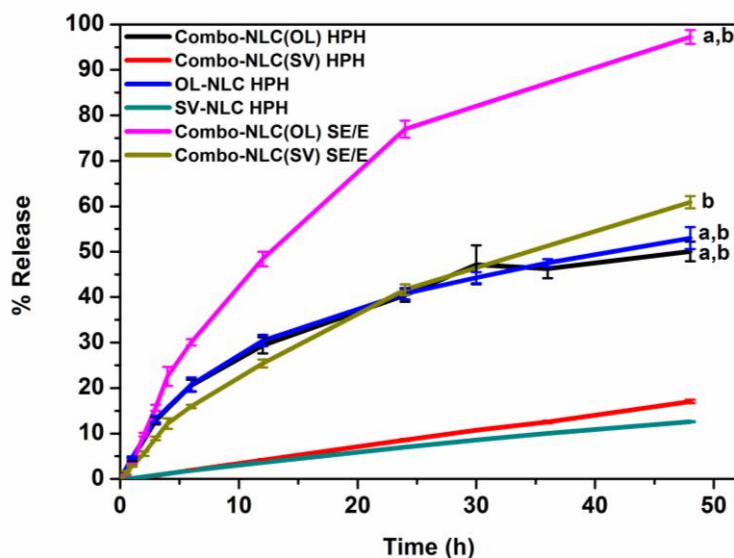
Figure 7.4 *In vitro* release profiles of the NLC prepared through the SE/E and HPH methods. (mean ± SEM, 3≤n≤ 6). [a] The mean OL percentage release (48 h) is statistically higher than the respective SV in both methods, for a $p < 0.05$. [b] The mean OL SE/E percentage release (48 h) is statistically higher than the respective OL HPH, for a $p < 0.05$.

Table 7.5 compiles the parameter values for different mathematical models used for regression of the release data. For the first-order and Weibull functions, one additional parameter, c_1, was introduced taking into account the predicted asymptotic value for release, which may differ from 100% [17]. It can be concluded that the Weibull function provided, in general, the best regression function, followed by the Korsmeyer-Peppas and first order models, of similar performance. Focusing on the Weibull model, it should be noted that the shape parameter (c_3) characterizes the curves as exponential (c_3=1), sigmoidal (c_3>1), i.e. S-shaped with an upward curvature followed by a turning point, or parabolic (c_3<1), with a higher initial slope and after that consistent with the exponential [18]. According to the results obtained, c_3 is systematically lower than 1 for OL HPH formulations, and slightly above unity for SV HPH formulations. However, low values of c_2, indicated that the formally first-order release approached in fact a zero order. In addition, with c_3 values above 1, the sigmoid shape of the Weibull function indicated that a complex mechanism governed the release process [19]. This seems to indicate that OL NLC formulations tended more rapidly to a steady state, corresponding to the drug with the highest release rate (Figure 7.5A) and B)). In the case of NLC prepared by SE/E, an exponential shape characterised the OL release profiles, and the SV release profiles were close to the ones found for the OL HPH profiles.

Table 7.5 Regression parameters resulting from the application of the different mathematical models to the experimental release data.

Function	Formulation	c_1	c_2	c_3	R^2
Zero order $c_1 t$	OL-NLC HPH	$1.35 \pm 1.27 \times 10^{-1}$	-	-	0.77572
	SV-NLC HPH	$2.76 \times 10^{-1} \pm 4.47 \times 10^{-3}$	-	-	0.99529
	Combo-NLC(OL) HPH	$1.32 \pm 1.33 \times 10^{-1}$	-	-	0.75038
	Combo-NLC(SV) HPH	$3.53 \times 10^{-1} \pm 2.25 \times 10^{-3}$	-	-	0.99931
	Combo-NLC(OL) SE/E	$2.41 \pm 2.39 \times 10^{-1}$	-	-	0.84403
	Combo-NLC(SV) SE/E	$1.43 \pm 1.05 \times 10^{-1}$	-	-	0.91322
First order $c_1(1-exp(-c_2 t))$	OL-NLC HPH	51.16 ± 1.85	$7.72 \times 10^{-2} \pm 8.39 \times 10^{-3}$	-	0.99022
	SV-NLC HPH	37.08 ± 4.23	$8.72 \times 10^{-3} \pm 1.17 \times 10^{-3}$	-	0.99951
	Combo-NLC(OL) HPH	49.96 ± 1.42	$8.03 \times 10^{-2} \pm 7.02 \times 10^{-3}$	-	0.99354
	Combo-NLC(SV) HPH	-*	-*	-	-
	Combo-NLC(OL) SE/E	$1.05 \times 10^{2} \pm 2.41$	$5.37 \times 10^{-2} \pm 2.59 \times 10^{-3}$	-	0.99817
	Combo-NLC(SV) SE/E	71.62 ± 2.88	$3.83 \times 10^{-2} \pm 2.87 \times 10^{-3}$	-	0.99703
Higuchi $c_1 t^{0.5}$	OL-NLC HPH	$7.99 \pm 1.50 \times 10^{-1}$	-	-	0.99051
	SV-NLC HPH	$1.55 \pm 1.15 \times 10^{-1}$	-	-	0.90594
	Combo-NLC(OL) HPH	$7.87 \pm 2.16 \times 10^{-1}$	-	-	0.97991
	Combo-NLC(SV) HPH	$1.97 \pm 1.74 \times 10^{-1}$	-	-	0.87482
	Combo-NLC(OL) SE/E	$13.8 \pm 7.32 \times 10^{-1}$	-	-	0.95252
	Combo-NLC(SV) SE/E	$8.00 \pm 4.35 \times 10^{-1}$	-	-	0.95185
Weibull $c_1(1-exp(-c_2 t^{c_3}))$	OL-NLC HPH	62.95 ± 4.74	$4.54 \times 10^{-2} \pm 8.99 \times 10^{-3}$	$7.35 \times 10^{-1} \pm 4.53 \times 10^{-2}$	0.99851
	SV-NLC HPH	24.91 ± 2.69	$1.51 \times 10^{-2} \pm 2.24 \times 10^{-3}$	$1.09 \pm 3.03 \times 10^{-2}$	0.99980
	Combo-NLC(OL) HPH	54.32 ± 3.27	$6.49 \times 10^{-2} \pm 1.05 \times 10^{-2}$	$8.34 \times 10^{-1} \pm 6.81 \times 10^{-2}$	0.99671
	Combo-NLC(SV) HPH	73.97 ± 38.69	$6.12 \times 10^{-3} \pm 3.62 \times 10^{-3}$	$1.10 \pm 4.88 \times 10^{-2}$	0.99962
	Combo-NLC(OL) SE/E	$1.05 \times 10^{2} \pm 3.76$	$5.48 \times 10^{-2} \pm 4.57 \times 10^{-3}$	$1.01 \pm 4.50 \times 10^{-2}$	0.99819
	Combo-NLC(SV) SE/E	89.52 ± 8.49	$2.42 \times 10^{-2} \pm 4.54 \times 10^{-3}$	$8.65 \times 10^{-1} \pm 3.40 \times 10^{-2}$	0.99912
Korsmeyer -Peppas $c_1 t^{c_2}$	OL-NLC HPH	$8.45 \pm 8.61 \times 10^{-1}$	$4.83 \times 10^{-1} \pm 2.99 \times 10^{-2}$	-	0.99091
	SV-NLC HPH	$3.90 \times 10^{-1} \pm 3.74 \times 10^{-2}$	$9.03 \times 10^{-1} \pm 2.68 \times 10^{-2}$	-	0.99829
	Combo-NLC(OL) HPH	8.53 ± 1.25	$4.76 \times 10^{-1} \pm 4.29 \times 10^{-2}$	-	0.98100
	Combo-NLC(SV) HPH	$3.28 \times 10^{-1} \pm 2.13 \times 10^{-2}$	$1.02 \pm 1.80 \times 10^{-2}$	-	0.99940
	Combo-NLC(OL) SE/E	$6.23 \pm 8.30 \times 10^{-1}$	$8.37 \times 10^{-1} \pm 6.18 \times 10^{-2}$	-	0.98382
	Combo-NLC(SV) SE/E	$4.00 \pm 2.69 \times 10^{-1}$	$7.40 \times 10^{-1} \pm 2.39 \times 10^{-2}$	-	0.99615

* For these profiles, the non-linear first order equation least-squares fitting did not converge.
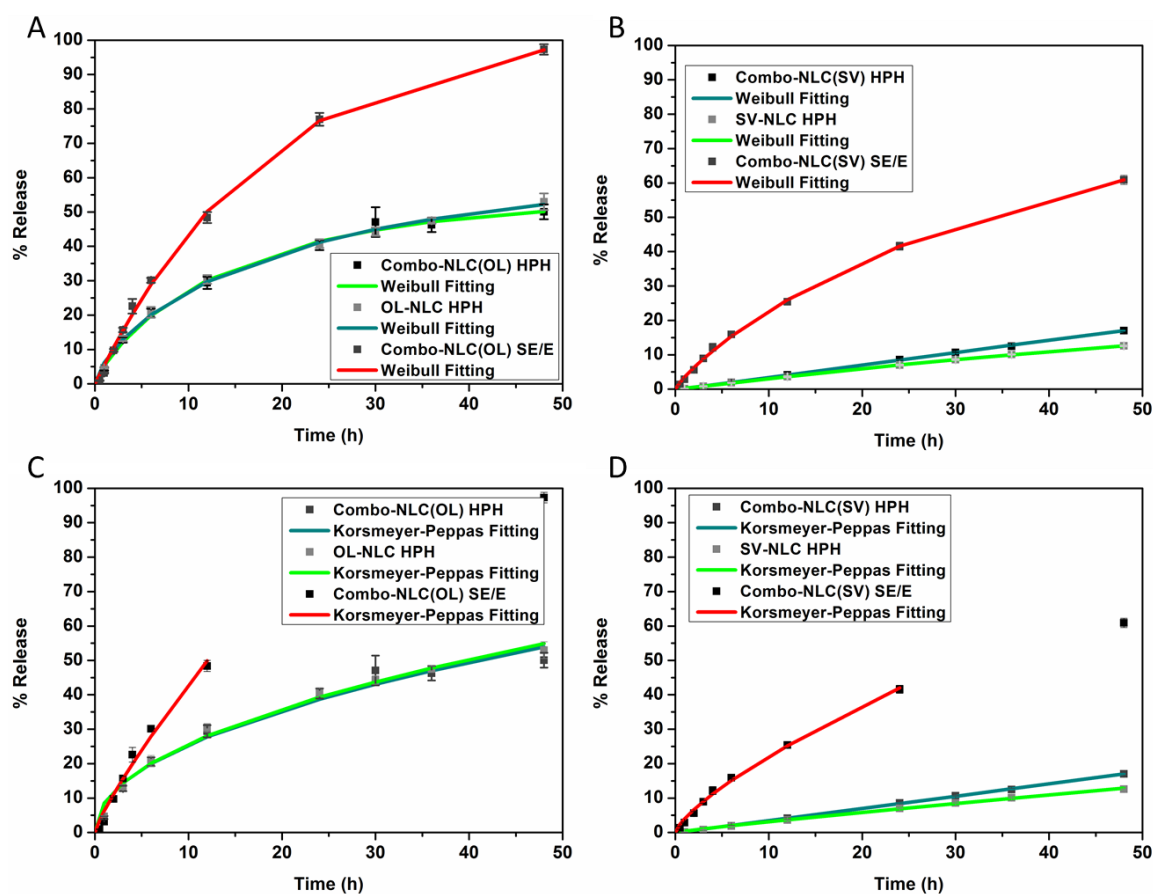
Figure 7.5 Representation of the least squares regression of the release profiles: (A) and (B) Weibull model; (C) and (D) Korsmeyer-Peppas model.

In the first order model the c_1 parameter corresponds to the asymptotic value predicted for each profile, and this value was higher for the OL-loaded NLC than for the SV-loaded NLC. The corresponding release rates were also larger, as extracted from the c_2 values. For Combo-NLC prepared by HPH, the SV profile followed very closely a zero-order release.

The value of the c_2 parameter in the Korsmeyer-Peppas model is important for the characterization of the drug transport mechanism. Thus, c_2 values close to 0.5 correspond to a Fickian diffusion process and values between 0.5 and 1.0 to an anomalous (non-Fickian) transport. With c_2 value of 1.0, a zero-order model applies. Note that for the estimation of this exponent, only the first 60% of the release are considered [20]. Transposing this classification to the results obtained, it is seen that the OL HPH formulations display a diffusionally controlled release ($c_2 \sim 0.5$), while the SV HPH are characterized by a zero-order release ($c_2 \sim 1$) [20]. For OL and SV SE/E

formulations, an anomalous transport is reported ($0.5 < c_2 < 1.0$), where diffusion is coupled with other mechanisms (Table 7.5 C) and D)).

7.3.3 *In vitro* permeation studies

NLC prepared by HPH promoted a higher permeation rate than NLC SE/E (Table 7.6). This can be attributed to the higher drug loading in HPH, in spite of the higher release rate observed in the SE/E formulations. On the other hand, differences between methods are less marked in the *Kp* values. This can be ascribed to the use of a majorant for C_0, Equation (2.12), based on the total drug content of the NLC, which is higher for the HPH method. Also, OL permeated in a higher degree than SV, as evidenced by the *Q24* and *Q48* parameters, which is compatible with the respective release rate.

Table 7.6 *In vitro* permeation parameters (human skin) of OL and SV released by Combo NLC prepared by SE/E or HPH. mean ± SEM ($3 \leq n \leq 6$).

Combo-NLC Preparation Method	Drugs	J_{ss} ($\mu g/cm^2/h$)	Kp (cm/h) (x 10^{-3})	Q24 ($\mu g/cm^2$)	Q48 ($\mu g/cm^2$)
SE/E	OL	0.09±0.03	0.17±0.05	0.9±0.4	2.5±0.4
	SV	0.19±0.01	0.38±0.02	1.7±0.3	6.4±0.5
HPH	OL	0.43±0.08	0.16±0.03	4.4±0.2	15.7±0.9
	SV	0.33±0.07	0.12±0.03	2.7±0.4	7.4±0.1

Taking into consideration the higher drug loading, the better permeation rate, and other advantages, such as the scale up feasibility, the avoidance of organic solvents and the shorter production process, NLC prepared by HPH were chosen to proceed into the *in vitro*/*in vivo* studies.

The effect of the permeation enhancers (ethanol and limonene) and of the vehicle viscosity on the permeation of the drugs formulated as NLC was subsequently investigated (see Table 7.7, which also gathers some previously obtained data, [2]). Due to the large number of experiments, the readily available newborn pig skin was used in place of human skin, since it gave similar results (see Combo-NLC data, Table 7.7). The addition of ethanol to the Combo-NLC dispersion medium increased the permeation rate, compared to the respective aqueous medium (Table 7.6). The skin-permeation-enhancing effect of ethanol is well-known [21]. Ethanol is reported to act by a dual mechanism: acting as a co-solvent, increasing permeant partitioning into and solubility within the stratum corneum, and acting as a permeation enhancer by extracting large amounts of stratum corneum lipids [21, 22]. Olanzapine tended to permeate to a higher

extent when alone than when in association with simvastatin (Table 7.7), while the opposite behaviour was observed for simvastatin. The addition of limonene, also a well-known permeation enhancer [23], at a previously optimized concentration [2] further increased permeation rates. Increasing the vehicle viscosity with carbomer had a negative effect on permeation rates. This behaviour has already been reported, and was attributed to the effect of the gel viscosity on the diffusion coefficient in the vehicle [24]. *Q24*, *Q48* and *Kp* corroborated this trend. In what follows, liquid and gel formulations including ethanol and limonene were used for the PK studies in rats.

Table 7.7 *In vitro* OL and SV permeation parameters for NLC prepared by the HPH method, in the presence of permeation enhancers, ethanol (Et) and/or limonene (L), (mean±SEM, 3≤n≤6).

Skin origin	Formulation	J_{ss} ($\mu g/cm^2/h$)		Kp (cm/h) ($\times 10^{-3}$)		$Q24$ ($\mu g/cm^2$)		$Q48$ ($\mu g/cm^2$)	
		OL	SV	OL	SV	OL	SV	OL	SV
Human	OL-NLC + Et	2.5±0.3	-	1.3±0.2	-	25.±4	-	83.±8	-
	SV-NLC + Et	-	0.59±0.04	-	0.32±0.02	-	9.±2	-	26.±2
	Combo-NLC + Et	1.9±0.7	0.8±0.1	1.0±0.4	0.43±0.07	12.±5	7.±3	55±17	21.±3
Newborn pig	Combo-NLC + Et[a]	1.9±0.4	0.74±0.08	1.2±0.2	0.42±0.05	29.±7	13.±3	79±18	31.±5
	Combo-NLC+Et+L[a]	15.±2	7.0±0.8	10.±1	3.9±0.5	261±51	82±19	534±33	249±36
	Combo-NLC+Et+L Gel[a]	7.5±0.3	3.6±0.3	4.8±0.2	2.1±0.2	145.±6	48.±5	314±10	133±12

[a] Ref. [2]

7.3.4 *In vivo* pharmacokinetic studies in rats

Transdermal administration

In order to evaluate the efficiency of Combo-NLC with permeation enhancers, either in the liquid dispersion (Combo-NLC+Et+L) or in the carbomer hydrogel (Combo-NLC+Et+L Gel), together with the effect of skin microneedle pretreatment *in vivo* pharmacokinetic studies were performed in rats (Figure 7.6). The 500 μm or 1500 μm-length microneedles gave similar increase in TEWL values, compared to control skin, in agreement with previous studies [25, 26]. Accordingly, the 500-μm-length microneedles were used for the *in vivo* PK studies.
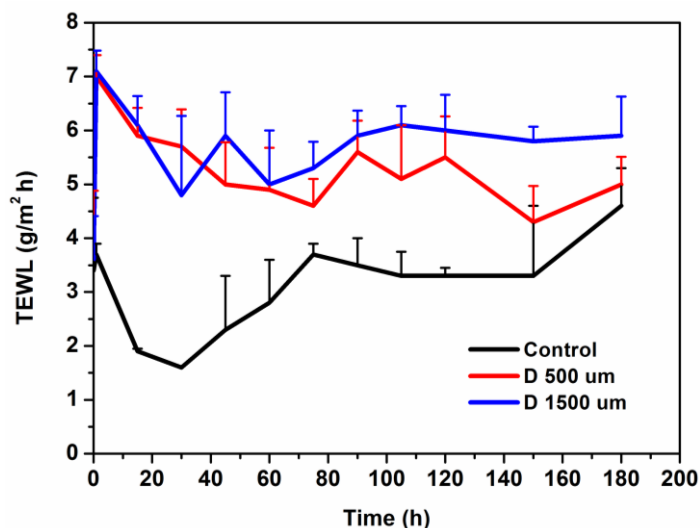
Figure 7.6 Dependence on time of TEWL determined on rat skin *in vivo*, with and without the application of Dermaroller® with microneedles length of 500 μm and 1500 μm. Results are expressed as mean ± SEM (n=3).

The application of the formulation had no visible impact on skin integrity, as observations showed after formulation removal.

The mean plasma concentration-time profiles for OL and SV after transdermal administration are depicted in Figure 7.7 and PK and permeation parameters are summarized in Table 7.8.
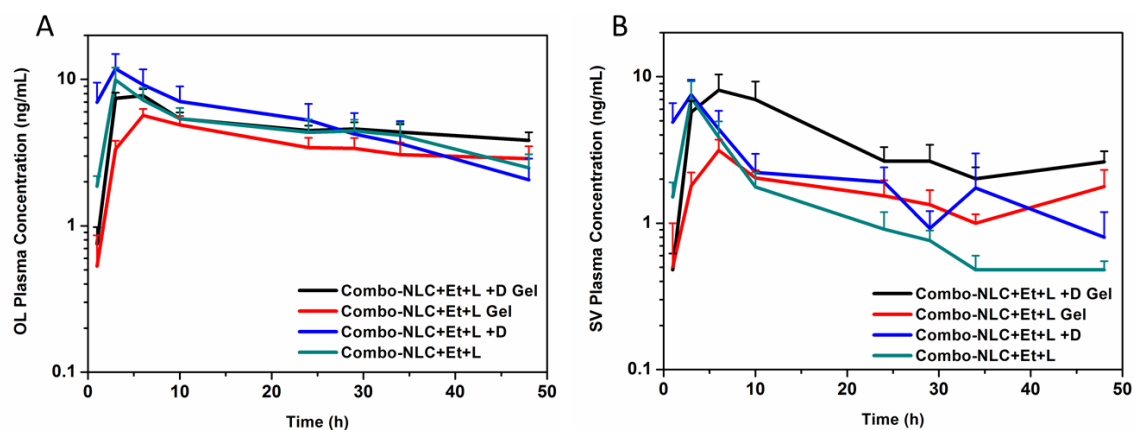
Figure 7.7 Plasma concentration-time curves of (a) OL and (b) SV after application of NLC plus permeation enhancers in the liquid dispersion (Combo-NLC+Et+L) or the gel (Combo-NLC+Et+L Gel) vehicle, with and without Dermaroller® (D) skin pretreatment, mean±SEM (n=6).

Table 7.8 Pharmacokinetic parameters of OL and SV after skin application of Combo-NLC formulations, in a liquid or gel permeation enhancer-containing vehicle. Results are expressed as mean±SD (n=6).

Formulation		Without microneedle skin pretreatment		With microneedle skin pretreatment	
		Combo-NLC+Et+L	Combo-NLC+Et+L Gel	Combo-NLC+Et+L	Combo-NLC+Et+L Gel
OL PK and skin permeation parameters	C_{max} (ng/mL)	10.1 ± 5.2^a	5.7 ± 1.5	11.6 ± 7.2	8.2 ± 1.7^b
	t_{max} (h)	5.0 ± 1.6^c	6.0 ± 0.0	2.3 ± 1.0	$4.5\pm1.6^{b,d}$
	AUC_{0-48} (ng h/mL)	214.9 ± 99.1	171.8 ± 66.1	220.3 ± 172.2	229.0 ± 52.8
	C_{ss} (ng/mL)	3.9 ± 2.0	3.2 ± 1.4	3.3 ± 3.1	4.3 ± 1.2
	J_{ss} (µg/cm²/h)	1.7 ± 0.8	1.4 ± 0.6	1.4 ± 1.2	1.9 ± 0.5
SV PK and skin permeation parameters	C_{max} (ng/mL)	7.2 ± 5.2	3.2 ± 1.4	8.9 ± 4.2	8.8 ± 5.5^b
	t_{max} (h)	3.0 ± 0.0	6.0 ± 0.0	2.5 ± 0.8	5.7 ± 2.6^d
	AUC_{0-48} (ng h/mL)	70.0 ± 41.2	78.0 ± 32.5	105.8 ± 56.8	182.3 ± 108.6^b
	C_{ss} (ng/mL)	0.7 ± 0.3	1.4 ± 0.8	1.4 ± 1.5	2.5 ± 1.3^b
	J_{ss} (µg/cm²/h)	0.3 ± 0.1	0.5 ± 0.3	0.7 ± 0.7	0.9 ± 0.5

Key: [a] Combo-NLC+Et+L > Combo-NLC+Et+L Gel,

[b] Combo-NLC+Et+L Gel+D > Combo-NLC+Et+L Gel,

[c] Combo-NLC+Et+L > Combo-NLC+Et+L+D,

[d] NLC+D > Gel+D, for $p<0.05$.

In general, plasma concentration reached a maximum 2 to 6 hours post skin application and then decreased to reach a plateau at around 10 h which was maintained for 48 h (Figure 7.7). The C_{max} and J_{ss} values for OL were higher than for SV, a result that is in agreement with the *in vitro* skin permeation studies conducted using newborn pig skin (Table 7.7). Microneedle pre-treatment generally resulted in earlier t_{max} and higher C_{max}. With the gel vehicle, the mean C_{max} values were approximately twice lower than with the liquid vehicle, and the t_{max} was delayed (Table 7.8). This trend is confirmed by the 2^2 full factorial planning (Table 7.9). A negative sign associated to β_1 indeed corresponded to a decrease in the PK parameters (e.g., C_{max} and AUC_{0-48h} for OL, and C_{max} for SV) when the gel is applied. In the case of OL, C_{ss} and J_{ss} were similar whatever experimental conditions, whereas with SV, gel vehicle and microneedle pretreatment resulted in an increase in C_{ss} and J_{ss} (see the values of β_2 coefficients). Moreover, the interaction term, β_{12}, has generally no significance.

Table 7.9 Estimated coefficient terms of the response surfaces for pharmacokinetic parameters obtained from the 2^2 factorial planning in the indicated formulations and Student's t-test analysis. ** p<0.01, *<0.05

Coefficient term	Response				
	C_{maxOL}	t_{maxOL}	AUC_{OL}	C_{ssOL}	J_{ssOL}
β_0	8.902**	4.458**	208.997**	3.658**	1.569**
β_1	-1.943*	0.792**	-8.613	0.094	0.040
β_2	1.018	-1.042**	15.652	0.123	0.053
β_{12}	0.263	0.292	12.979	0.442	0.190
Coefficient term	Response				
	C_{maxSV}	t_{maxSV}	AUC_{SV}	C_{ssSV}	J_{ssSV}
β_0	7.005**	4.292**	108.996**	1.494**	0.618**
β_1	-1.039	1.542**	21.115	0.457*	0.121
β_2	1.839*	-0.208	35.036*	0.445*	0.181
β_{12}	0.975	0.042	17.128	0.093	0.026

The *in vivo* flux for OL was 4.87 and 2.57 times higher than the corresponding to SV for NLC dispersion and hydrogel, respectively. This trend corroborates the results obtained from *in vitro* permeation fluxes. The skin perforation with the Dermaroller® produced a more marked enhancement of drug penetration and permeation for SV than for OL. The results showed that the use of a microneedles device pretreatment as an active enhancement strategy lead only to a slight increase in the permeation rate of both drugs, thus indicating that the formulation itself is the more relevant factor for skin permeation. Such effect could be attributed to short lifetime of the pores created following microneedle application, which limits the clinical utility of this approach [27].

The *in vitro* fluxes were 9.18 and 5.50 times (OL) and 20.49 and 6.71 (SV) higher than the respective *in vivo* fluxes, for the dispersion and hydrogel formulations, respectively. The differences found could be attributed to the skin model used, rat versus newborn pig epidermis.

Human skin was found to be generally less permeable (about 4 times,[28]) than rat skin, but considering an increase in the application from 3.8 cm^2 to 40 cm^2, we should expect human J_{ss} values ca. 2.6 times higher than those obtained in the present *in vivo* studies for the Combo-NLC gel formulation.

These values are in good agreement with previous estimates (cite previous paper) that report a human flow rate of 3.64 µg/cm^2/h for OL and 1.42 µg/cm^2/h for SV, thus suggesting a promising result for a possible clinical formulation development.

Subcutaneous administration

Subcutaneous administration of NLC was tested as an alternative route to the transdermal one. According to the PK parameters presented in Table 7.10, the half-life value ($t_{1/2}$) after NLC subcutaneous injection was clearly prolonged for both drugs, when compared with the IV solution, thus demonstrating the sustained release properties of Combo-NLC.

Table 7.10 Pharmacokinetic parameters of olanzapine (OL), simvastatin (SV) and its active form, simvastatin acid (SVA), after IV infusion (over 30 min) as solution of OL and SV in PEG 400 and subcutaneous administration of OL- and SV-loaded Combo-NLC. Dose of each drug: 1 mg per kg of body (IV infusion) or 5 mg per kg (SC).

	IV			Subcutaneous		
	OL	**SV**	**SVA**	**OL**	**SV**	**SVA**
C_{max} (ng/mL)	163.4±16.4	130.3±46.9	187.3±32.3	358.6±59.2	70.4±28.7	219.8±42.2
t_{max} (h)	-	-	-	1.0±0.0	1.4±0.8	1.4±0.8
Vd (mL/kg)	7419±417	11315±6059	-	-	-	-
AUC (ng/mL.h)	185.1±15.7	106.6±42.4	221.1±51.8	1647±282	392±263	1330±371
Cl_t (mL/h/kg)	5440±444	11031±4645	-	-	-	-
$t_{1/2}$ (h)	0.95±0.06	0.68±0.08	0.67±0.04	2.6±0.1	2.2±0.3	3.4±0.7

7.3.5 Confocal laser scanning microscopy

Confocal laser scanning microscopy (CLSM) was employed to visualize the distribution of Nile Red loaded-Combo-NLC within the skin, following the application of the liquid or the gel formulations, with or without skin-pretreatment with 500 μm-needle Dermaroller®. Results are illustrated in Figure 7.8. CLSM images showed that the nanoparticles were located on upper layers of epidermis and of hair follicles and did not penetrate beyond the superficial epidermis layers. At the skin surface, Nile Red was however released from NLC to some extent and diffused into deeper layers, as shown by the red fluorescence of the stratum corneum (SC). The fluorescence intensity in the deeper strata was higher at 48 h than at 24 h, and was apparently more important when the hydrogel was applied. The perforation caused by the Dermaroller® pretreatment seemed to induce some damages in the SC and upper epidermis. However, after 48 h the skin seemed to recover, due to its elastic and regenerative properties and injuries

were no longer visible [27]. In summary, the NLC showed some affinity for hair follicles, and released an associated "active" into the skin.
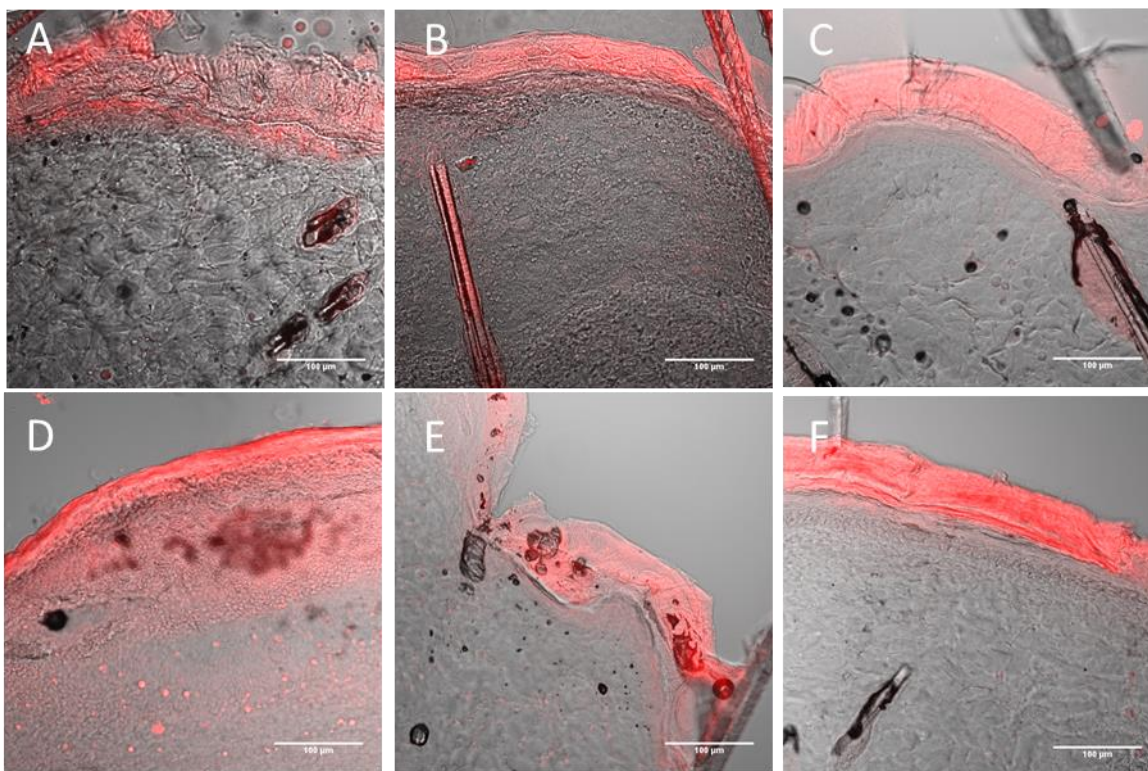
Figure 7.8 CLSM fluorescence micrographs revealing the penetration and distribution of the Nile Red marker within rat skin 1.5 h (a, c, e) or 48 h (b, d, f) after application of Nile-Red-loaded Combo-NLC formulation containing ethanol and limonene in the liquid (a, b) or gel (c, d, e, f) form. In (e) and (f), skin was pre-treated with 500-µm-needle Dermaroller®.

7.4 Conclusions

A NLC-based formulation for olanzapine and simvastatin co-encapsulation was successfully developed, with properties adequate for sustained drug transdermal delivery over 48 h. Except at the early times, the skin perforation by a 500 µm-needle Dermaroller® before formulation application had little or no impact on drug transdermal delivery. The transposition of the present results to human administration suggests the formulation as a promising transdermal delivery system for both co-encapsulated drugs. The subcutaneous injection in rats of NLC demonstrated clear sustained release effects, shown by the longer half-life of drugs, spreading the potential of Combo-NLC to deliver OL and through alternative routes of administration.

References

1. Alexander, A., S. Dwivedi, Ajazuddin, T.K. Giri, S. Saraf, S. Saraf, and D.K. Tripathi, Approaches for breaking the barriers of drug permeation through transdermal drug delivery. Journal of Controlled Release, 2012. 164(1): p. 26-40.

1. Vitorino, C., J. Almeida, L.M. Gonçalves, A.J. Almeida, J.J. Sousa, and A.A.C.C. Pais, Co-encapsulating nanostructured lipid carriers for transdermal application: From experimental design to the molecular detail. Journal of Controlled Release, 2013. 167(3): p. 301-314.

3. Coulman, S.A., A. Anstey, C. Gateley, A. Morrissey, P. McLoughlin, C. Allender, and J.C. Birchall, Microneedle mediated delivery of nanoparticles into human skin. International Journal of Pharmaceutics, 2009. 366(1–2): p. 190-200.

4. Kumar, A., X. Li, M.A. Sandoval, B.L. Rodriguez, B.R. Sloat, and Z. Cui, Permeation of antigen protein-conjugated nanoparticles and live bacteria through microneedle-treated mouse skin. International Journal of Nanomedicine, 2011. 6.

5. Vitorino, C., F.A. Carvalho, A.J. Almeida, J.J. Sousa, and A.A.C.C. Pais, The size of solid lipid nanoparticles: An interpretation from experimental design. Colloids and Surfaces B: Biointerfaces, 2011. 84(1): p. 117-130.

6. ISO13321, Methods for Determination of Particle Size Distribution Part 8: Photon Correlation Spectroscopy, International Organisation for Standardisaton (ISO). 1996.

7. ISO22412, Particle Size Analysis – Dynamic Light Scattering, International Organisation for Standardisation (ISO). 2008.

8. Lv, Q., A. Yu, Y. Xi, H. Li, Z. Song, J. Cui, F. Cao, and G. Zhai, Development and evaluation of penciclovir-loaded solid lipid nanoparticles for topical delivery. International Journal of Pharmaceutics, 2009. 372(1-2): p. 191-198.

9. Jemal, M., Z. Ouyang, and M.L. Powell, Direct-injection LC–MS–MS method for high-throughput simultaneous quantitation of simvastatin and simvastatin acid in human plasma. Journal of Pharmaceutical and Biomedical Analysis, 2000. 23(2–3): p. 323-340.

10. Mandawgade, S.D. and V.B. Patravale, Development of SLNs from natural lipids: Application to topical delivery of tretinoin. International Journal of Pharmaceutics, 2008. 363(1–2): p. 132-138.

11. Marchand, S., P. Gobin, J. Brillault, S. Baptista, C. Adier, J.-C. Olivier, O. Mimoz, and W. Couet, Aerosol Therapy with Colistin Methanesulfonate: a Biopharmaceutical Issue Illustrated in Rats. Antimicrobial Agents and Chemotherapy, 2010. 54(9): p. 3702-3707.

12. Darlenski, R., S. Sassning, N. Tsankov, and J.W. Fluhr, Non-invasive in vivo methods for investigation of the skin barrier physical properties. European Journal of Pharmaceutics and Biopharmaceutics, 2009. 72(2): p. 295-303.

13. Yang, A.Y., L. Sun, D.G. Musson, and J.J. Zhao, Application of a novel ultra-low elution volume 96-well solid-phase extraction method to the LC/MS/MS determination of simvastatin and simvastatin acid in human plasma. Journal of Pharmaceutical and Biomedical Analysis, 2005. 38(3): p. 521-527.

14. Valiveti, S., D.C. Hammell, K.S. Paudel, M.O. Hamad, P.A. Crooks, and A.L. Stinchcomb, In vivo evaluation of 3-O-alkyl ester transdermal prodrugs of naltrexone in hairless guinea pigs. Journal of Controlled Release, 2005. 102(2): p. 509-520.

15. Souto, E.B., S.A. Wissing, C.M. Barbosa, and R.H. Müller, Evaluation of the physical stability of SLN and NLC before and after incorporation into hydrogel formulations. European Journal of Pharmaceutics and Biopharmaceutics, 2004. 58(1): p. 83-90.

16. Lin, X., X. Li, L. Zheng, L. Yu, Q. Zhang, and W. Liu, Preparation and characterization of monocaprate nanostructured lipid carriers. Colloids and Surfaces A: Physicochemical and Engineering Aspects, 2007. 311(1-3): p. 106-111.

17. Costa, F.O., J.J.S. Sousa, A.A.C.C. Pais, and S.J. Formosinho, Comparison of dissolution profiles of Ibuprofen pellets. Journal of Controlled Release, 2003. 89(2): p. 199-212.

18. Costa, P. and J.M. Sousa Lobo, Modeling and comparison of dissolution profiles. European Journal of Pharmaceutical Sciences, 2001. 13(2): p. 123-133.

19. Papadopoulou, V., K. Kosmidis, M. Vlachou, and P. Macheras, On the use of the Weibull function for the discernment of drug release mechanisms. International Journal of Pharmaceutics, 2006. 309(1-2): p. 44-50.

20. Ritger, P.L. and N.A. Peppas, A simple equation for description of solute release I. Fickian and non-fickian release from non-swellable devices in the form of slabs, spheres, cylinders or discs. Journal of Controlled Release, 1987. 5(1): p. 23-36.

21. Sinha, V.R. and M.P. Kaur, Permeation enhancers for transdermal drug delivery. Drug Development and Industrial Pharmacy, 2000. 26(11): p. 1131-1140.

22. Heather, A.E.B., Transdermal Drug Delivery: Penetration Enhancement Techniques. Current Drug Delivery, 2005. 2(1): p. 23-33.

23. Sapra, B., S. Jain, and A. Tiwary, Percutaneous Permeation Enhancement by Terpenes: Mechanistic View. The AAPS Journal, 2008. 10(1): p. 120-132.

24. Bhaskar, K., C.K. Mohan, M. Lingam, S.J. Mohan, V. Venkateswarlu, Y.M. Rao, J. Anbu, and V. Ravichandran, Development of SLN and NLC Enriched Hydrogels for Transdermal Delivery of Nitrendipine: *In vitro* and *In vivo* Characteristics. Drug Development and Industrial Pharmacy, 2009. 35(1): p. 98-113.

25. Badran, M.M., J. Kuntsche, and A. Fahr, Skin penetration enhancement by a microneedle device (Dermaroller®) in vitro: Dependency on needle size and applied formulation. European Journal of Pharmaceutical Sciences, 2009. 36(4–5): p. 511-523.

26. Zhou, C.-P., Y.-L. Liu, H.-L. Wang, P.-X. Zhang, and J.-L. Zhang, Transdermal delivery of insulin using microneedle rollers *in vivo*. International Journal of Pharmaceutics, 2010. 392(1–2): p. 127-133.

27. Milewski, M., N.K. Brogden, and A.L. Stinchcomb, Current aspects of formulation efforts and pore lifetime related to microneedle treatment of skin. Expert Opinion on Drug Delivery, 2010. 7(5): p. 617-629.

28. Godin, B. and E. Touitou, Transdermal skin delivery: Predictions for humans from in vivo, ex vivo and animal models. Advanced Drug Delivery Reviews, 2007. 59(11): p. 1152-1161.

Chapter 8

Concluding remarks

The work contained in this dissertation aimed at developing a transdermal drug delivery system based on an innovative strategy which combined both passive and active methodologies. Passive strategies comprised the use of nanocarrier systems and chemical enhancers, while microneedle pretreatment was investigated as active approach.

Lipid nanoparticles, particularly nanostructured lipid carriers, were successfully assessed as potential nanocarriers for the co-encapsulation of drugs with different lipophilicity. The development of the NLC-based formulation included optimization procedures for composition, production conditions, *in vitro* release and permeation, physicochemical characteristics, cytotoxicity, compatibility and stability analyses and, finally, *in vivo* performance.

From a technological point of view, two different methods for the preparation of the NLC were compared, namely SE/E and HPH. HPH was selected on the basis of a better performance in terms of drug loading and *in vitro* permeation rate.

Factorial designs proved to be a powerful tool for the screening procedures, and system rationalization in every development step.

Several mathematical models were used to elucidate the release mechanisms from lipid nanoparticles. *In vitro* release kinetics was shown to be driven by diffusion, but other mechanisms were also present, and supported the feasibility of using NLC for sustained drug delivery.

In vitro versus in vivo and experimental *versus in silico* analyses of the strategies were pursued in order to strengthen the proposed mechanisms and interpretations.

The *in vitro* skin studies showed that the chemical penetration enhancers, limonene and ethanol, added to the NLC formulations, promoted a synergistic permeation enhancement of both drugs, with olanzapine exhibiting a higher permeation than simvastatin.

The *in vivo* experiments in rats well correlated with *in vitro* findings and revealed that the combined use of ethanol and limonene, incorporated in the NLC formulation provided the main driving force for drug permeation. The Dermaroller® pretreatment did not significantly enhance drug permeation, supporting the use of passive methods as suitable for a transdermal delivery system.

Furthermore, this work may provide a promising proof-of-concept for further clinical application in the treatment of schizophrenia and associated disorders, combined with dyslipidemia.

Finally, the subcutaneous injection of the NLC dispersion indicated clear sustained release effects, as extracted from the longer half-life of drugs, thus proving to be a useful alternative as route of administration. This highlights the versatility of NLC while drug carrier to be administered through different routes.

8.1 Future work

In the follow up of this work, supplementary *in vivo* experiments involving biodistribution studies and determination of drug concentration in target organs should be pursued, in order to prove the therapeutic efficacy of the plasma concentrations obtained when the drugs are delivered through the skin. This includes the development of the extraction and quantification procedures of olanzapine and simvastatin in brain and liver, respectively. Alternatively, bioluminescence imaging studies would be useful to elucidate the biodistribution of drugs after skin application.

Furthermore, since the skin may act as a drug reservoir, the quantification of olanzapine and simvastatin remaining in dermis and epidermis would provide useful complementary results. Microdialysis and tape stripping are available techniques that could give insight into drug located in the different skin layers, considering not only animal but also human skin sources.

Additionally, the analysis of the NLC system using X-rays diffraction and RMN techniques, as structural studies, would complement the physicochemical characterization.

The overall results from the present work indicate that the further development of a transdermal device including the NLC-based system into a reservoir patch would also be very promising. The optimal nanoparticulate formulation opens the way for the

investigation of new combinations of drugs, for different routes of administration, which is relevant from both the fundamental and application point of view.

Appendix 1

Method revalidation

A1.1 Introduction

In the present Appendix, a partial validation of the method developed in Chapter 5 is described for the determination of OL, SV and SVA in the release and permeation medium (PBS pH 7.4, containing 30% V/V). This procedure was conducted under Good Laboratory Practices.

A1.2 Materials and methods

A1.2.1 Materials

Simvastatin (99.4%) was kindly provided by Labesfal - Laboratórios Almiro, S.A. (Santiago de Besteiros, Portugal). Olanzapine (98.9%) was purchased from Zhejiang MYJOY Import & Export Co.,Ltd (Hangzhou, China). Phosphate buffer saline pH 7.4, was purchased from Sigma. All other reagents were from HPLC grade.

A1.2.2 Instrumentation and chromatographic conditions

See Section 5.2.2.

A1.2.3 Preparation of stock solutions, calibration standards and quality controls

A working standard solution containing OL, SV and SVA at a concentration of 50 µg/mL was prepared by further dilution of each stock solution with release medium, PBS pH 7.4 containing 30%(V/V) of ethanol. Eight standard solutions (0.25, 0.5, 1, 2.5,

5, 10, 25 and 50 µg/mL) were obtained by appropriate dilution of the working standard solution with release medium. As quality control (QC), six replicates of 0.25, 0.5, 5 and 50 µg/mL standards containing the three compounds were considered.

A1.2.4 Method validation

The HPLC method previously established was revalidated according to the US Food and Drug Administration (FDA) regulations [1].

Limits of detection and quantification

See Section 5.2.4.

Linearity

Calibration curves were constructed with eight standard solutions, containing the three compounds simultaneously, ranging from 0.25 to 50 µg/mL.

Accuracy and precision

Four standard solutions (quality controls), 0.25, 0.5, 5 and 50 µg/mL, respectively, were prepared six times each for the analyses of accuracy and (intra-day and inter-day) precision.

Specificity

See Section 5.2.4.

A1.3 Results and discussion

A1.3.1 Method revalidation of OL, SV and SVA simultaneous assay

See optimized chromatographic conditions in Section 5.3.1.

Limits of detection and quantitation

The estimated LD and LQ were 0.02 and 0.05 µg/mL for the three compounds, respectively.

Linearity

Linearity was evaluated over the concentration range of 0.25-50 µg/mL for the OL, SV and SVA by visual inspection (Figure A.1.1), estimating the regression equation and the determination coefficient (R^2) obtained from the least squares method (Table A1.1). The coefficient of determination for the calibration curves for the three compounds were higher than 0.999, thus indicating a good linearity over the concentration range proposed. Moreover, the analysis of the response factors (Figure A.1.1) show a slope close to zero (-0.0168, 0.0382 and -0.0220 , for OL, SV and SVA, respectively) and a residual standard deviation of 0.99%, 6.30% and 1.96%, thus confirming the method as linear [2, 3].
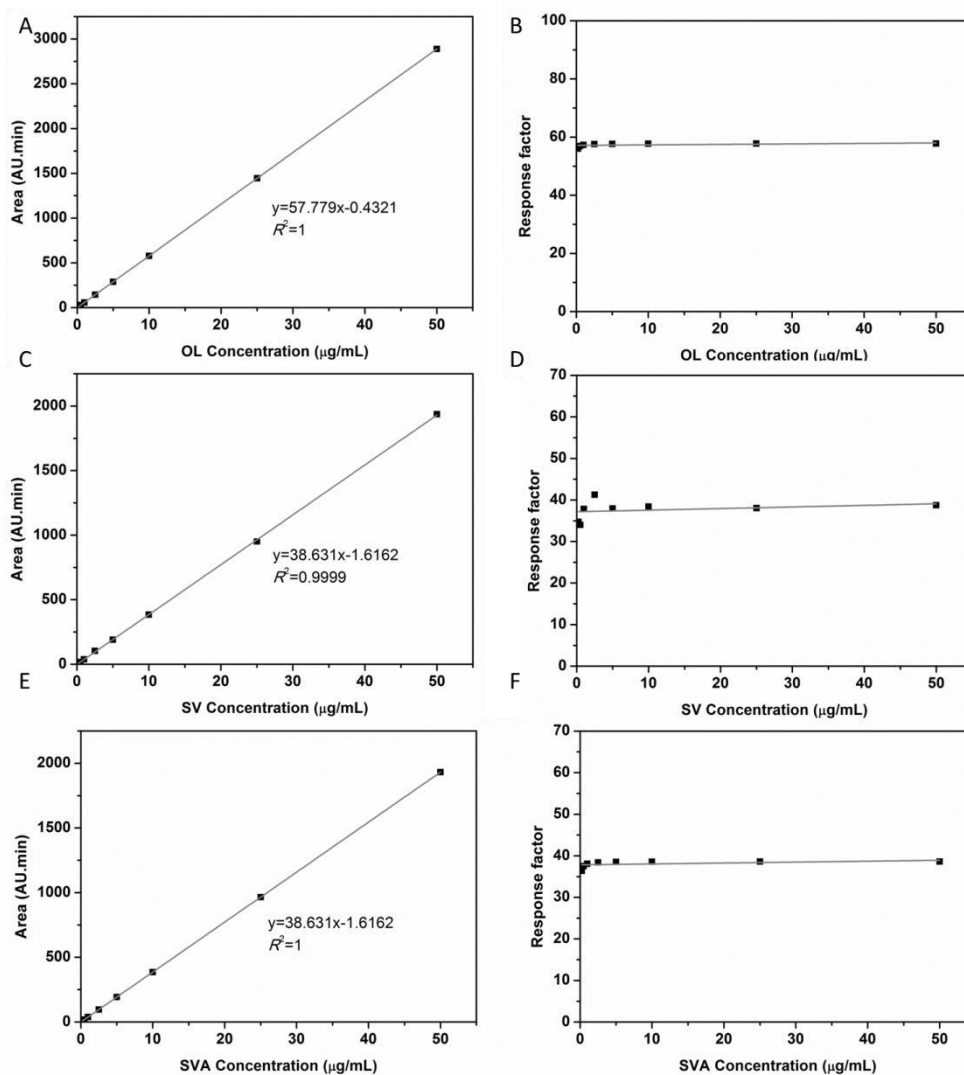
Figure A.1.1 Linearity studies for the developed HPLC method: calibration curves obtained with OL (A), SV (C) and SVA (E) standard solutions in PBS pH 7.4, containing 30% (V/V) of ethanol, and response factor *versus* OL (B), SV (D) and SVA (F) standard solutions concentrations, respectively.

Table A1.1 Results obtained from the regression analysis by the least squares method for OL, SV and SVA.

Analyte	Mean R^2 ± S.D.	Mean slope ± S.D. (n=6)	Mean intercept[a] ± S.D. (n=6)
OL	0.9997 ± 0.0005	54.3976 ± 6.2595	-1.2092 ± 1.6761
SV	0.99998 ± 0.00004	37.7859 ± 1.9928	-1.1480 ± 1.6794
SVA	0.99999 ± 0.00003	38.5094 ± 1.0002	-0.3341 ± 1.0558

[a] Intercept is expressed in µg/mL.

Accuracy and precision

Accuracy and precision for the quality controls in the intra-day and inter-day run are shown in Table A1.2. All the data fulfill the acceptance criteria. The intra- and inter-day RSD values did not exceed 9.014%. The intra- and inter-day bias values were found in the interval -2.11 to 3.08%, -1.429 to 7.575, and -4.15 to 1.91%, for OL, SV and SVA, respectively. These data indicate that the developed method is accurate, reliable and reproducible, since neither RSD nor bias exceeded 15%, which is in agreement with acceptance recommendations [1].

Table A1.2 Intra-day and inter-day precision and accuracy results for OL, SV and SVA. (n=6)

Nominal concentration (µg/mL)	Intraday (n=6)			Interday (n=18)		
	Measured Concentration (µg/mL) Mean±SD	Precision % CV	Accuracy % Bias	Measured Concentration (µg/mL) Mean±SD	Precision % CV	Accuracy % Bias
OL (0.25)	0.266±0.032	12.119	6.267	0.251±0.029	11.552	0.289
OL (0.5)	0.502±0.024	4.698	0.446	0.500±0.042	8.375	0.091
OL (5)	4.854±0.128	2.636	-2.922	4.944±0.389	7.870	-1.117
OL (50)	47.921±1.525	3.182	-4.158	49.847±3.270	6.560	-0.307
SV (0.25)	0.263±0.029	11.139	5.322	0.278±0.039	14.051	11.080
SV (0.5)	0.514±0.041	7.946	2.876	0.528±0.071	13.443	5.545
SV (5)	4.976±0.166	3.337	-0.471	4.954±0.122	2.456	-0.916
SV (50)	107.575±0.815	5.360	-6.939	47.153±2.234	4.739	-5.694
SVA (0.25)	0.257±0.026	9.951	2.885	0.260±0.035	13.312	3.803
SVA (0.5)	0.494±0.035	7.059	-1.131	0.494±0.058	11.666	-1.110
SVA (5)	4.893±0.128	2.621	-2.139	4.835±0.190	3.931	-3.305
SVA (50)	50.717±1.619	3.192	1.434	49.676±1.454	2.927	-0.647

Specificity

The specificity of the method was analyzed in the presence of Franz cells receptor medium (see chromatograms, Figure A1.2). As shown, the medium supernatant did not exhibit any peaks interfering with analytes retention times, thus indicating that the method is specific.
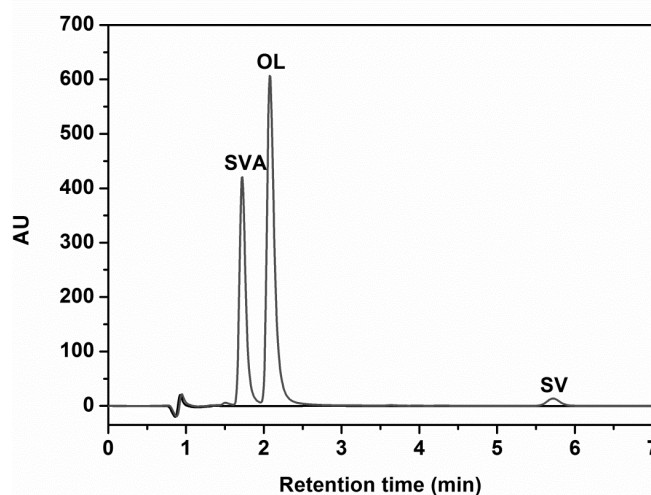
Figure A1.2 Chromatograms of medium (PBS pH7.4, containing 30% Ethanol) (black) and OL, SV and SVA determined in the receptor medium, released from Gel Combo-NLC+Et+Lim (red) formulation.

A1.3.2 Method applicability

The method partially revalidated was successfully used to determine the content of OL and SV (note that SV stands for both contributions of SV and SVA forms) in PBS pH7.4, containing 30% of ethanol, the medium for the release and permeation studies conducted in the Franz diffusion cells.

A1.4 Conclusion

This revalidation allowed to simultaneously determine the content of OL, SV and SVA in the medium of the release and permeation studies used for the screening of the optimal transdermal formulation.

References

1.   FDA, Guidance for Industry: Bioanalytical Method Validation.2001: US Department of Health and Human Services, Food and Drug Administration, Center for Drug Evaluation and Research and Center for Veterinary Medicine.

2.   das Neves, J., B. Sarmento, M.M. Amiji, and M.F. Bahia, Development and validation of a rapid reversed-phase HPLC method for the determination of the non-nucleoside reverse transcriptase inhibitor dapivirine from polymeric nanoparticles. Journal of Pharmaceutical and Biomedical Analysis, 2010. 52(2): p. 167-172.

3.	LoBrutto, R. and T. Patel, Method Validation, in HPLC for Pharmaceutical Scientists2006, John Wiley & Sons, Inc. p. 455-502.

Appendix 2

Method validation for the determination of olanzapine and simvastatin in rat plasma by liquid chromatography - tandem mass spectrometry (LC-MS/MS)

A2.1 Introduction

A transdermal drug delivery system based on a combination of nanostructured lipid carriers and chemical enhancers has been previously optimized in Chapter 4 supported on an *in vitro* permeation screening. In order to assess product performance, an *in vivo* approach in Sprague-Dawley rats was subsequently carried out. The study was performed throughout 48 h under a pre-established schedule of blood samplings. Rat plasma was obtained after centrifugation, extracted and analyzed according to the procedure described below in this Appendix.

A rapid and effective liquid chromatography tandem mass spectrometry method for the estimation of olanzapine, simvastatin, the inactive lactone form, and simvastatin acid, the active hydroxy acid form in human plasma, using deuterated olanzapine and mevastatin as internal standards, respectively, was developed and validated according to principles of Good Laboratory Practices. The validated method was successfully applied to determine the concentration of OL, SV and SVA in rat plasma to study the respective pharmacokinetic when administered via transdermal, subcutaneous and intravenous route. Note that human plasma was used for the validation procedure, since it is available in higher amount. The validation procedure was based on the FDA Guideline on bioanalytical method validation [1].

A2.2 Materials and methods

A2.2.1 Materials

Simvastatin (99.4%) was kindly provided by Labesfal - Laboratórios Almiro, S.A. (Santiago de Besteiros, Portugal). Olanzapine (98.9%) was purchased from Zhejiang Myjoy (Hangzhou, China). Simvastatin hydroxy acid ammonium salt (SVA-S) and olanzapine-D3 were purchased from @rtmolecule (Poitiers, France). Diethyl ether was acquired from JT Baker, ammonium Formate 97% from Acros, and Titrisol pH4 buffer from Merck. All chemicals used were of analytical grade, and solvents were of HPLC grade.

A2.2.2 Liquid chromatography - tandem mass spectrometry

The LC-MS/MS system consisted of an Agilent 1100 separation module equipped with a binary pump, an autosampler thermostated at 4°C, and an API 3000, Sciex tandem mass spectrometer with an electrospray ionization (ESI) interface. The ESI source was operated in the positive-ion mode. The multiple-reaction monitoring (MRM) transition ions were:

Transition (m/z)	Compound	Internal standard	Dwell time (ms)
316.2 → 256.1	Olanzapine D3		250
313.2 → 256.1	Olanzapine	Olanzapine D3	250
413.2 → 311.2	Mevastatine		250
441.2 → 325.3	Simvastatin	Mevastatine	250
459.5 → 343.3	Simvastatin acid	Mevastatine	250

The analysis was conducted under the following settings:

	Olanzapine	Olanzapine D3	Simvastatin	Simvastatin acid	Mevastatin
NEB	8	8	8	8	8
CUR	8	8	8	8	8
IS (V)	4000	4000	4000	4000	4000
Temperature (°C)	300	300	300	300	300
CAD (psi)	4	4	4	4	4
DP (V)	50	50	90	90	90
FP (V)	200	200	200	200	200
EP (V)	10	10	10	10	10
CE (V)	30	30	35	34	33
CXP(V)	10	10	10	10	10
Resolution Q1	Unit	Unit	Unit	Unit	Unit
Resolution Q3	Low	Low	Low	Low	Low
Ion Energie 2	2	2	2	2	2
Multiplier (V)	2000	2000	2000	2000	2000

Key: NEB=Nebulizer gas, CUR=Curtain gas, IS=Ion Spray voltage, CAD=collision-activated dissociation gas pressure; DP=declustering potential; FP=Focusing Potential; EP=entrance potential; CE=collision energy; CXP=collision cell exit potential

For the reversed-phase chromatography a Jupiter C18 column (5.0 µm, 50 mm x 2.1 m; Phenomenex, Le Pecq Cedex, France) was used. The mobile phase at a 0.2 mL/min flow rate was an ammonium formate (2 mM in water) and acetonitrile mixture, 25:75 (V/V). Injection volumes were of 20 µL for OL and 10 µL for SV and SVA quantitation. A run time of 3.5 min was established for the elution of the five compounds. Under these conditions OL and OL-D3 were eluted at 1.11 and 1.12 min, and SV, SVA and MEV at 2.13, 1.42, and 1.56 min, respectively

All data were processed using Analyst Version 4.1.2 software.

A2.2.3 Stock solutions

Five stock solutions of 1mg/mL of OL, SV, SVA-S and the respective IS, OL-D3 and MEV, were prepared by dissolving approximately 10 mg of each compound in 10 mL of methanol. Each solution was stored at -20ºC for a maximum period of 6 months.

A2.2.4 Preparation of the standards and quality controls (QC)

A working standard solution containing OL, SV and SVA at a concentration of 10 µg/mL was prepared by further dilution of each stock solution with methanol. Eight calibration standards (1, 2.5, 5, 10, 25, 50, 75 and 100 ng/mL) were obtained by appropriate spiking of blank plasma with the working standard solution.

Two working standard solutions of 10 µg/mL of mevastatin and olanzapine-D3 each in methanol were also considered to obtain the IS solutions of 200 ng/mL in Titrisol buffer pH4 for MEV and 20 ng/mL in water in the case of OL-D3.

Quality control (QC) samples (six replicates of each), including low QC, 1 ng/mL, two intermediate QC, 2.5 and 50 ng/mL and high QC, 100 ng/mL were prepared by spiking blank plasma with the drugs working standard solution.

A2.2.5 Sample preparation

A two-step liquid-liquid extraction from plasma was carried out for calibration standards, controls, and samples, in order to extract sequentially analytes, i.e. first SV and SVA at a pH 4.5, which is a pH shown to minimize conversion of SV into SVA [2], and second OL at pH 10. Briefly, 200 µL of Tritisol buffer, pH 4, and 50 µL of OL-D3 solution (20 ng/mL in water) were added to 100 µL plasma sample. After vortexing, 2 mL of diethyl ether were added. The mixture was vortexed for 1 min and then centrifuged at 3000 rpm for 10 min. The diethyl ether supernatant (containing mostly SV and SVA molecules) was then transferred to a glass tube and evaporated to dryness under a gentle stream of N_2 gas at 45 ºC. Dry residues were re-dissolved in 70 µL of mobile phase and 50 µL of mevastatin solution (200 ng/mL in Tritisol buffer at pH 4) by vortexing, centrifuged at 3000 rpm for 5 min and transferred to the LC-MS/MS vials.

After the first extraction procedure, 30 µL of NaOH 1.0 M were added to the plasma (final pH: 10) and vortexed for OL extraction. Two mL of diethyl ether were then added and the mixture was vortexed for 1 min and centrifuged at 3000 rpm for 10 min. The supernatant was transferred to a glass tube and evaporated as described above. Dry residues were finally re-dissolved with 120 µL by vortexing, centrifuged at 3000 rpm for 5 min, before filled in the vials.of mobile phase and transferred to the LC-MS/MS vials.

A2.3 Bioanalytical method validation

A2.3.1 System suitability

System suitability parameters were determined by injecting six extracted HLQ samples before the start of each analytical run.

A2.3.2 Selectivity

Double blanks, i.e. blank biological matrix processed without internal standard, were scrutinized throughout the different runs to check that eventual interfering component peak surface areas were below 20% of the analyte peak surface area at lower limit of quantification (LLOQ) and below 5% of the IS peak surface area [3].

A2.3.3 Precision and accuracy

Intra-day and inter-day precision and accuracy were evaluated by spiking known amounts of OL, SV and SVA-S and IS in plasma (QC) according to the procedure above described (n=6). The precision was expressed as % RSD (relative standard deviation) and accuracy by the % bias determined using the formula: measured concentration/nominal concentration x 100.

Intra-day precision and accuracy were assessed using replicate (n=6) determinations for each concentration of the spiked plasma samples analyzed each day, whereas inter-day precision and accuracy were evaluated throughout three days using replicated (n=6) for each concentration used.

Tables A2.1 and A2.2 shows a summary of intra and inter-day precision and accuracy for OL, SV and SVA in human plasma. The results obtained are below 15% [1], thus indicating that the method is precise and accurate.

Table A2.1 OL, SV and SVA repeatability assays. Within-run precision and bias of simvastatin human plasma measurements.

Nominal concentration (ng/mL)	Day 1 (n=6)			Day 2 (n=6)			Day 3 (n=6)		
	Measured Concentration (ng/mL) Mean±SD	Precision % RSD	Accuracy % Bias	Measured Concentration (ng/mL) Mean±SD	Precision % RSD	Accuracy % Bias	Measured Concentration (ng/mL) Mean±SD	Precision % RSD	Accuracy % Bias
OL (1)	0.902±0.033	3.71	-9.80	0.963±0.100	10.41	-3.72	1.050±0.043	4.05	4.97
OL (2.5)	2.235±0.033	1.46	-10.60	2.333±0.214	9.16	-6.67	2.473±0.070	2.83	-1.07
OL (50)	49.980±4.458	8.92	-0.04	49.483±1.348	2.72	-1.03	49.350±0.472	0.96	-1.30
OL (100)	107.500±3.619	3.37	7.50	94.967±2.683	2.83	-5.03	100.683±2.474	2.46	0.68
SV (1)	1.080±0.061	5.60	7.99	1.004±0.135	13.44	0.37	1.131±0.117	10.36	13.08
SV (2.5)	2.491±0.203	8.14	-0.34	2.389±0.277	11.58	-4.44	2.815±0.213	7.56	12.58
SV (50)	57.303±2.332	4.07	14.61	53.084±2.694	5.08	6.17	53.225±6.274	11.79	6.45
SV (100)	104.548±3.375	3.23	4.55	112.585±4.339	3.85	12.59	107.795±8.285	7.69	7.80
SVA (1)	1.057±0.095	8.94	5.71	0.931±0.057	6.13	-6.88	0.928±0.098	10.58	-7.23
SVA (2.5)	2.604±0.231	8.88	4.15	2.187±0.064	2.91	-12.50	2.273±0.256	11.24	-9.06
SVA (50)	54.120±4.981	9.20	8.24	51.028±1.176	2.30	2.06	49.370±2.978	6.03	-1.26
SVA (100)	109.418±9.838	8.99	9.42	98.772±2.941	2.98	-1.23	113.480±3.101	2.73	13.48

Table A2.2 Olanzapine repeatability assays. Between-run precision and bias of olanzapine human plasma measurements.

Nominal concentration (ng/mL)	Interday (n=18)		
	Measured Concentration (ng/mL) Mean±SD	Precision % RSD	Accuracy % Bias
OL (1)	0.972±0.036	3.73	-2.85
OL (2.5)	2.347±0.128	5.45	-6.11
OL (50)	49.582±2.095	4.22	-0.84
OL (100)	101.050±0.610	0.60	1.05
SV (1)	1.071±0.039	3.63	7.15
SV (2.5)	2.515±0.052	2.08	0.60
SV (50)	54.538±2.179	3.99	9.08
SV (100)	108.309±2.601	2.40	8.31
SVA (1)	0.972±0.023	2.34	-2.80
SVA (2.5)	2.355±0.119	5.03	-5.80
SVA (50)	51.506±1.903	3.70	3.01
SVA (100)	107.224±3.937	3.67	7.22

A2.3.4 Lower limit of quantification

The lower limit of quantification [1] for each compound analyzed by the developed method was found to be 1ng/mL and 0.25 ng/mL for human and rat, respectively.

A2.3.5 Goodness of fit

The best fit calibration curves of the ratio of OL, SV and SVA to IS peak area versus concentration of the calibration standards were determined by quadratic regression analysis ($y= a+bx+cx^2$) with a $1/x^2$ weighting factor. The R^2 were generally higher than 0.999 (Table A2.3) and %bias was below 15% for all calibration level (even

for LLOQ for which a %biais could be up to 20%) (Table A2.4), which is in accordance to US FDA/EMA recommendations for bioanalytical method validation [1, 3].

Table A2.3 Results obtained from the regression analysis by the least squares method for OL, SV and SVA.

Analyte	Mean R^2 ± SD	Mean c ± SD (n=4)	b ± SD (n=4)	a^a ± SD (n=4)
OL[b]	0.9995 ± 0.0003	0.00006±0.0001	0.1695 ± 0.0209	0.0213 ± 0.0517
SV[c]	0.9983 ± 0.0012	-1.64667±5.9862	6760 ± 632	1256 ± 884
SVA[c]	0.9993 ± 0.0004	-0.38467±1.4123	1957 ± 91	62.00 ± 198.4

[a] Intercept is expressed in ng/mL. [b] Independent variable is the ratio of analytes/IS peak area, [c] Independent variable is the analyte peak area.

Table A2.4 Summary of OL, SV and SVA human plasma back-calculated concentration (ng/mL) of calibration standards. Between-run precision and bias of the method.

Compounds	Calibration standards, ng/mL (n=4)									
	1	**2.5**	**5**	**10**	**25**	**50**	**75**	**100**
OL								
Mean±SD	1.009±0.010	2.448±0.109	4.943±0.159	10.053±0.233	25.675±0.275	49.700±1.663	75.375±2.333	99.400±2.022
RSD (%)	1.02	4.46	3.22	2.31	1.07	3.35	3.10	2.03
Bias (%)	0.88	-2.10	-1.15	0.53	2.70	-0.60	0.50	-0.60
SV								
Mean±SD	1.009±0.135	2.635±0.423	5.264±0.269	10.034±1.336	24.907±1.660	50.469±2.786	76.281±5.408	99.091±3.107
RSD (%)	13.43	16.04	5.11	13.32	6.66	5.52	7.09	3.14
Bias (%)	0.85	5.41	5.28	0.34	-0.37	0.94	1.71	-0.91
SVA								
Mean±SD	1.005±0.135	2.436±0.044	5.064±0.177	10.054±0.485	25.766±1.291	48.100±2.157	67.743±12.909	101.820±2.820
RSD (%)	13.47	1.80	3.50	4.83	5.01	4.48	19.06	2.77
Bias (%)	0.46	-2.58	1.28	0.54	3.06	-3.80	-9.68	1.82

A2.3.6 Recovery

The recovery of OL, SV and SVA from human plasma samples was determined at two concentration levels 2.5 and 100 ng/mL by repeated analysis (n = 6). The recovery of the analytes was calculated by comparing the analyte/IS peak area ratio of processed plasma samples with the corresponding ratio obtained from the processed aqueous solutions at the same concentrations.

The % recovery from the plasma samples was higher than 70% for all the three compounds. This indicates that the developed method is adequate to simultaneously quantify the three compounds.

Table A2.5 Overall recovery calculated from the results obtained after the replicate (n=6) analysis of a plasma extract and a non-processed standard spiked with 2.5 and 100 ng/mL of OL, SV and SVA.

% Recovery	Nominal concentration (ng/mL)					
	Olanzapine		Simvastatin		Simvastatin acid	
	2.5	100	2.5	100	2.5	100
	75.68	77.44	85.22	83.53	79.80	83.20
RSD (%)	7.39	2.17	6.75	4.28	12.04	3.43

A2.3.7 Dilution effect

The influence of the dilution was also assessed considering, since it was a procedure conducted with some plasma samples, in particular in intravenous and subcutaneous collects. The %RSD and %bias (**Table A2.6**) validate this procedure in what concerns treatment of plasma samples.

Table A2.6 Simvastatin repeatability assays - Within-run precision and bias of simvastatin human plasma measurements. Influence of the dilution.

Nominal concentration (ng/mL)	Dilution effect (n=6)		
	Measured Concentration (ng/mL) Mean±SD	Precision % RSD	Accuracy % Bias
OL (200)	209.13±6.884	3.29	4.57
SV (200)	230.88±12.337	5.34	15.44
SVA (200)	216.90±12.522	5.77	8.45

A2.4 Conclusion

The validated method revealed a routine sensitivity of 0.25 ng/mL in 0.1mL rat plasma, being reliable and accurate over the range of concentrations considered in the present pharmacokinetic study.

References

1.   FDA, Guidance for Industry: Bioanalytical Method Validation.2001: US Department of Health and Human Services, Food and Drug Administration, Center for Drug Evaluation and Research and Center for Veterinary Medicine.

2.   Yang, A.Y., L. Sun, D.G. Musson, and J.J. Zhao, Application of a novel ultra-low elution volume 96-well solid-phase extraction method to the LC/MS/MS determination of simvastatin and simvastatin acid in human plasma. Journal of Pharmaceutical and Biomedical Analysis, 2005. 38(3): p. 521-527.

3.   EMA, Guideline on bioanalytical method validation2011: European Medicines Agency.